University of Naples Federico II

PhD PROGRAM IN NEUROSCIENCE
XXXV CYCLE

Identification and pharmacological characterization of novel K_v7 potassium channels modulators for the treatment of hyperexcitability disorders

Coordinator: **Prof. Maurizio Taglialatela**

Tutor ***Candidate***

Prof. Maurizio Taglialatela **Dr Lidia Carotenuto**

ACADEMIC YEAR 2021-22

Index

Abbreviations

3D: three-dimensional

ACMG: American College of Medical Genetics

ADNFLE: autosomal dominant nocturnal frontal lobe epilepsy

AEDs: antiepileptic drugs

AHP: afterhyperpolarization

AIS: axon initial segment

AKAP: A-kinase anchoring protein

ankG: ankyrin G

AP: action potential

ASMs: antiseizures medications

BBR: Benzbromarone

BFNS: *Benign Familial Neonatal Seizures*

BHB: β-hydroxybutyric acid

Ca^{2+}: calcium ion

CaM: Calmodulin

CHO: Chinese Hamster Ovary

CHRNA4: cholinergic receptor nicotinic alpha 4 subunit

Cl^{-}: chloride ion

CMA: chromosomal microarray

CNS: central nervous system

CNVs: copy number variants

-COOH: carboxy

CryoEM: Cryo-electron microscopy

DAG: diacylglycerol

DEE: developmental and epileptic encephalopathies

DFNA2: deafness nonsyndromic autosomal dominant 2

DNA: Deoxyribonucleic acid

DRE: drug-resistant epilepsy

DRG: dorsal root ganglion

EC_{50}: half maximal effective concentration

EEG: electroencephalogram

EIMFS: Epilepsy of infancy with migrating focal seizures

EMA: European Medicines Agency

FDA: Food and Drug Administration

GABA: γ-amino-butyric acid

$GABA_A$: gamma-aminobutyric acid type A

GABOB: γ-amino-β-hydroxybutyric acid

GCs: granule cells

GoF: gain-of-function

GPCRs: G protein-coupled receptors

GSK: GlaxoSmithKline

GWAS: genome-wide association study

H^+: hydrogen ion

HBA: hydrogen bond acceptor

HBD: hydrogen bond donor

hERG: human Ether-à-go-go-Related Gene

HTS: high throughput screening

IC_{50}: half maximal inhibitory concentration

ID: intellectual disability

I_{KM}: M-current

I_{Ks}: delayed rectifying K^+ current

ILAE: International League Against Epilepsy

IP_3: inositol triphosphate

iPSCs: Induced pluripotent stem cells

IVA: isovaleric acid

K^+: potassium ion

K_{2P}: tandem pore domain potassium channel

K_{Ca} Ca^{2+}-activated K^+ channels

KCC2: potassium-chloride co-transporter 2

K_{ir} inward-rectifier K^+ channels

K_{Na}: Na^+-activated K^+ channels

K_v: voltage-gated K^+-channels

LBDD: ligand-based drug design

LoF: loss-of-function

LQTS: long QT syndrome

LZ: leucine zipper

MD: Molecular Dynamics

MEA: microelecrode array

MES: maximal electroshock seizures

MiRPs: MinK-related peptides

MS: Mass spectrometry

MTX: mallotoxin

Na^+: sodium ion

nAChR: nicotinic acetylcholine receptor

Nedd4-2: neuronal precursor cell-expressed developmentally downregulated

NGS: next-generation sequencing

$-NH_2$: amino

NKCC1: sodium-potassium-chloride co-transporter 1

NMD: non-sense mediated mRNA decay

NMDA: N-methyl-D-aspartate

OHCs: outer hair cells

PB: PiggyBac

PCR: Polymerase Chain Reaction

PD: pore domain

PDB: Protein Data Bank

Pen/strep: penicillin/streptomycin

PIP_2: Phosphatidylinositol 4,5-bisphosphate

PKA: cAMP-dependent protein kinase A

PKC: protein kinase C

PLC: phospholipase C

P_o: maximal probability of opening

PRE: pharmacoresistant epilepsy

PTZ: pentylenetetrazole

Rs: arginine residues

SAR: structure–activity relationship

SBDD: structure-based drug design

Sec1 or STXBP1: syntaxin binding protein 1

SeLFIS*: Self-limited Familial Infantile Seizures*

SeLFNE *self-limited Familial Neonatal Epilepsy*

SeLFNIS: *Self-limited Familial Neonatal-Infantile Seizures*

SID: subunit interaction domain

SQTS: short QT syndrome

SUDEP: sudden unexpected death in epilepsy patients

syx-1A: syntaxin-1A

TEA: tetraethylammonium

Tl^+: thallium ion

TM: Transmembrane

UHPLC: Ultra High Performance Liquid Chromatography

$V_{1/2}$: half-activation potential

VSD: Voltage Sensing Domain

VUS: variant of unknown significance

WES: whole-exome sequencing

WGS: whole-genome sequencing

WHO: World Health Organization

WT: wild type

ZnPy: Zinc Pyrithione

Amino acids

Alanine	Ala	A	Leucine	Leu	L
Arginine	Arg	R	Lysine	Lys	K
Asparagine	Asn	N	Methionine	Met	M
Aspartic acid	Asp	D	Phenylalanine	Phe	F
Cysteine	Cys	C	Proline	Pro	P
Glutamic acid	Glu	E	Serine	Ser	S
Glutamine	Gln	Q	Threonine	Thr	T
Glycine	Gly	G	Tryptophan	Trp	W
Histidine	His	H	Tyrosine	Tyr	Y
Isoleucine	Ile	I	Valine	Val	V

Abstract

The K_v7 subfamily of voltage-gated potassium (K^+) channels includes 5 members ($K_v7.1$-$K_v7.5$) having distinct expression patterns and physiological roles. In neurons, $K_v7.2$, $K_v7.3$ and $K_v7.5$ subunits underlie the so-called M-current (I_{KM}), a sub-threshold K^+ current playing a critical role in the control of neuronal excitability. Mutations in the genes encoding for $K_v7.2$, $K_v7.3$ and $K_v7.5$ are responsible for a wide spectrum of early-onset epilepsies.

Retigabine is the first antiepileptic drug acting on K_v7 channels. It was approved for clinical use in 2011 as an adjunctive therapy in adults showing drug-resistant partial onset seizures. Retigabine suppresses neuronal hyperexcitability by shifting the $K_v7.2/7.3$ activation threshold toward more hyperpolarized potentials, thereby increasing their participation to the stabilization of the membrane potential. Unfortunately, retigabine suffers from considerable drawbacks including photo instability: light exposure causes retigabine photodegradation and oxidation, leading to the formation of dimers. Upon long-term use, retigabine dimers accumulate into light-exposed tissues, thus inducing retinal and mucocutaneous blue-gray discoloration in patients. This led to a progressively reduced use of retigabine, until the manufacturing company (GSK) has decided to withdraw the drug from the market in 2017. Since then, no K_v7 activator is clinically available as anticonvulsant.

The present work originates from our effort to identify novel and safer K_v7 channels activators to be used as new antiseizures medication. For this purpose, we developed a cellular fluorescence-based assay to rapidly evaluate the effect of K_v7 modulators, suitable for both small-scale and large-scale high throughput screening (HTS). The assay was exploit for two different drug discovery approaches:

1. **Structure-based Drug Design**: retigabine structure-activity relationship (SAR) and the molecular determinants responsible for its photo-induced dimerization were combined to guide the design of novel analogues. The new-synthesized retigabine derivatives were screened for their K_v7 opening ability using the fluoresce-based assay. Among them, **compound 60** was unable to form photo-induced dimers, was more potent and effective than retigabine in activating $K_v7.2/7.3$ currents *in vitro* and *in vivo* as anticonvulsant in an acute epilepsy animal model.

2. **Drug Repurposing**: the Fraunhofer repurposing library, containing more than 5600 bioactive compounds already tested in preclinical and clinical studies, was screened in search of new K_v7 channel openers using the fluoresce-based assay adapted to a large-scale HTS. From the screening, **C4** emerged as the most potent and effective newly

identified K_v7 channel opener; further *in vitro* characterization of **C4** revealed an efficacy and potency comparable to retigabine in activating $K_v7.2/7.3$ currents.

1. Introduction

1.1 Epilepsy: definition and classification

With an incidence ranging from 50.4 to 81.7 per 100,000 people per year and 50 million people affected worldwide (WHO 2019), epilepsy is one of the most common contributors to the global burden of neurological disorders, together with Alzheimer's disease, stroke and migraine (Beghi et al., 2019). It affects people across all ages and sexes, albeit with a higher prevalence at the very early and late developmental stages in males over females (Fiest et al., 2017).

The International League Against Epilepsy (ILAE) founded in 1909 with the aim of improving the lives of people with epilepsy through research, works on defining and classifying epilepsy to provide key concepts and clear terminology. In 2005 epilepsy was conceptually defined as "a disorder of the brain characterized by an enduring predisposition to generate epileptic seizures" (Fisher et al., 2005). Later in 2014 the definition was amended and expanded (Fisher et al., 2014) and epilepsy was defined as "a disease of the brain defined by any of the following conditions: (1) at least two unprovoked seizures occurring more than 24 hours apart; (2) one unprovoked seizure and a probability of further seizures similar to the general recurrence risk (at least 60%) after two unprovoked seizures, occurring over the next 10 years; (3) diagnosis of an epilepsy syndrome".

Noteworthy, in this new definition epilepsy was defined as a disease instead of a disorder, to make patients better understand the gravity of this condition, and the concept of "resolved epilepsy" was added: according to the 2014 definition, epilepsy is considered resolved if (1) no seizures have occurred for at least 10 years and (2) no medications have been taken to treat epilepsy for at least the past 5 years (3) and/or if one had an age-dependent epilepsy syndrome, and one is older than the age above which it resolves.

The latest classification of epilepsy was published by ILAE in 2017 (Scheffer et al., 2017) and it is based on three elements: seizure type, epilepsy type and epileptic syndrome (Figure 1.1).

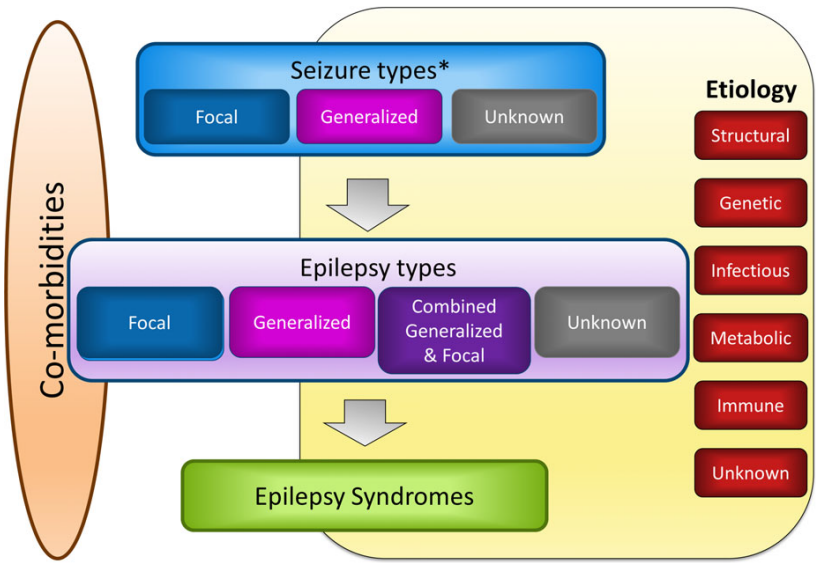

Figure 1.1 Framework for classification of the epilepsies. *Denotes onset of seizure (from *Sheffer et al., 2017*)

An epileptic seizure is defined as “a transient occurrence of signs and/or symptoms due to abnormal excessive or synchronous neuronal activity in the brain” (Fisher et al., 2005).
To identify a seizure type, ILAE provided an Operational classification (Fisher et al., 2017) that considers the onset, the awareness status (weather is impaired or not) and the motor symptoms caused by seizures (Figure 1.2).

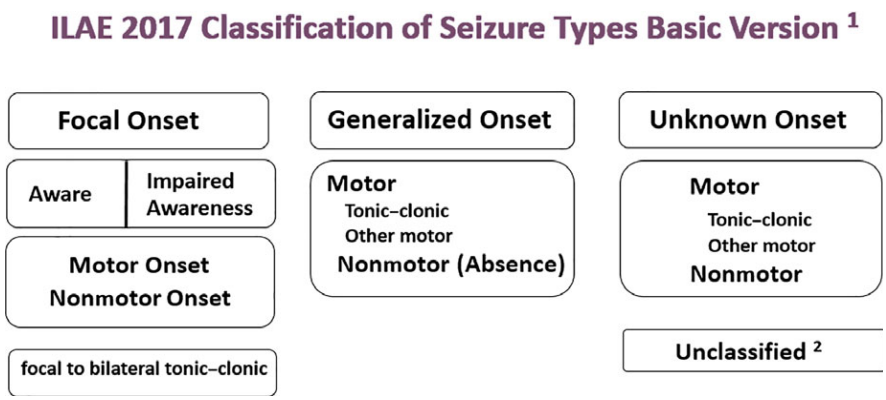

Figure 1.2. The basic ILAE 2017 operational classification of seizure types (from *Fisher et al., 2017*)

Based on their onset, seizures are classified into focal, generalized, and unknown, the latter also called “unclassified”.

Focal seizures (previously namely partial seizures) originate within networks limited to one hemisphere. During a focal seizure awareness of self and environment can be retained or impaired. Focal aware or impaired awareness seizures are further distinguished according to the manifestation of motor or nonmotor symptoms and they are classified by the earliest prominent feature.
Seizure activity propagates through brain networks, so focal epileptic seizures may evolve to bilateral tonic-clonic seizures (previously called secondarily generalized seizures) and present with multiple clinical manifestations as a result of propagation. Propagation sometimes leads to uncertainty about whether an event is a unitary seizure or a series of multiple seizures starting from different networks, in such cases, they are called “multifocal seizures”. The term “bilateral” is used to describe a propagation pattern of a focal-onset seizure, while “generalized” means seizures that engage bilateral networks from onset.

Generalized seizures affect both cerebral hemispheres; manifestations can be asymmetrical, rendering difficult the distinction from focal-onset seizures. Generalized seizures are divided into motor (tonic-clonic, clonic, myoclonic, atonic, etc.) and nonmotor (typical or atypical absences, absences with myoclons) seizures and are associated with impairment of awareness or complete loss of consciousness.

After diagnosis of the seizure type, the second level to classify epilepsy is the definition of the epilepsy type. Considering the type of epileptic seizures manifested by the patient, epilepsy can be classified in four main classes: focal, generalized, mixed (generalized and focal epilepsy), and unknown epilepsy, when there is insufficient information available.

Finally, the third level is represented by the delineation of the epilepsy syndrome. An epilepsy syndrome refers to a collection of features including seizure types, EEG, and imaging features that tend to occur together. Often it has age-dependent features such as age at onset and remission, seizure triggers, diurnal variation, and sometimes prognosis. It may also have distinctive comorbidities such as intellectual and psychiatric dysfunction, together with specific findings on EEG and imaging studies. Epileptic syndromes are therefore defined by a set of elements (clinical characteristics of the patient, EEG features, type of epileptic seizures, etiology, comorbidities, etc.) that constitute and define a particular clinical condition; their correct classification allows to use of a more targeted treatment and define with more precision the prognosis. The epilepsy type may also be the final level of diagnosis achievable when the clinician is unable to make an epilepsy syndrome diagnosis.

Once the epilepsy type has been defined, then the etiology should be determined. Etiological categories in the ILAE classification (Figure 1.1): include (1) structural: a structural finding (for example stroke, trauma etc.) is the likely cause of the epilepsy; (2) genetic: a known or presumed genetic defect is the principal contributor to the epileptic seizures, although environmental factors may contribute to the expression of the disease; (3) infectious: this etiology occurs when a patient who previously had an infection of the brain develops epilepsy and continues to have seizures after the acute phase of the infection; (4) metabolic: epilepsy is the result of metabolic conditions or diseases that may also be of genetic origin, in this case epilepsy has both a metabolic and a genetic etiology; (5) immune: immunological causes of epilepsy, include autoimmune diseases, can be recognized; (6) unknown: there is no clear etiology for epilepsy. It is important to note that epilepsy etiology is unknown in approximately 50% of cases in both children and adults (Falco-walter, 2020).

Differences in etiology of epilepsy are observed amongst different age groups: in children, the most common causes of seizures are genetic, injury due to perinatal insults, and malformations of cortical development (Sokka, 2016; Aaberg, 2017). In adults without a genetic predisposition to epilepsy, common etiologies for seizures include encephalitis/meningitis, traumatic brain injury, and brain tumors (Bosak, 2019). In elderly

patients, epilepsy is usually the result of primary neurodegenerative disorders, head trauma, and brain tumours (Liu, 2019).

1.2 Genetic epilepsies

It has been estimated that about 20% of epilepsy cases are genetically determined (Syvertsen et al. 2015).

The first epilepsy-associated gene to be discovered was CHRNA4, encoding for the α4-subunit of the neuronal nicotinic acetylcholine receptor nAChR. In this gene a S248F amino-acid exchange was found in a patient with autosomal dominant nocturnal frontal lobe epilepsy (ADNFLE) (Steinlein et al., 1995).

Since the identification of the first epilepsy-associated gene in 1995, the history of gene discovery in epilepsy went through three phases (1) the pioneer era of gene discovery in monogenic familial epilepsy syndromes; (2) a period of relative stagnation where very few novel genes were identified; and, finally, (3) the genome-wide era in which the information about the genetic basis of epilepsy syndromes has grown exponentially, thanks to the revolution in next-generation sequencing (NGS) that has accelerated novel gene discovery (Figure 1.3) (Helbig et al., 2016).

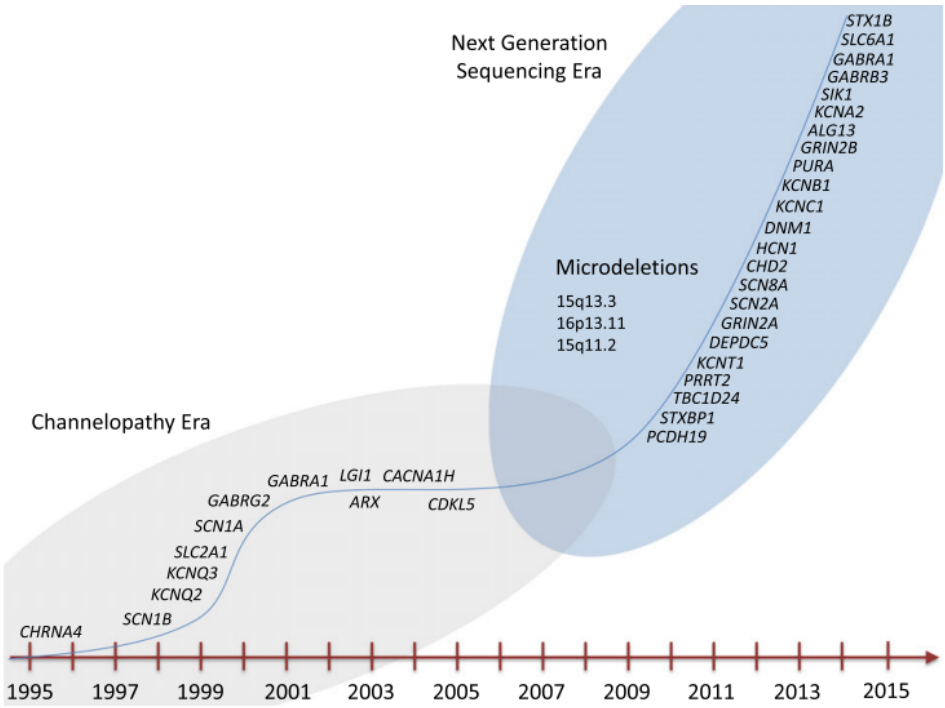

Figure 1.3 The history of epilepsy genetics (from Helbig et al., 2016)

The NGS technology, also known as “massively parallel sequencing”, has largely replaced traditional Sanger sequencing in the research and clinical laboratories, allowing the simultaneous sequencing of millions of short fragments of DNA.

It is applied in “Sequencing-Based Gene and Variant Discovery Approaches” such as targeted sequencing (focused on specific regions of interest in the genome), whole-exome sequencing (WES), and whole-genome sequencing (WGS).

Sequencing-Based approaches allow *de novo* mutation discovery through the powerful parent–child trio design (the genomes of the affected individual and their parents are analysed through WES in order to identify and report any variants relating to the affected individuals disease and determine whether the disease-causing variant is inherited) (McTague et al. 2016) and larger cohort-based variant analysis such as a WES study of 9,000 individuals with epilepsy published in 2019 where ultra-rare, deleterious variants were identified in patients, compared with controls (Feng et al. 2018).

With the new technologies available, genome-wide association studies (GWAS) can be performed. In 2018, the ILAE Consortium on Complex Epilepsies published the results from a GWAS involving 15,212 cases and 29,677 controls, revealing 16 genome-wide significant loci for epilepsy, of which 11 were novel (Abou-Khalil et al., 2018).

To date, more than 140 epilepsy-associated genes or loci are listed in the Online Mendelian Inheritance in Man database. Pathogenic variants predisposing to epilepsies may range from changes in single base pairs, to small deletions or insertions of genomic material (microdeletions/microduplications), to chromosomal rearrangements, up to chromosomal abnormalities/monosomy or trisomy (Sorge G. and Sorge A., 2010). If the structural variants are larger than 1 kb (1,000 base pairs), they are referred to as copy number variants (CNVs) (Coppola et al., 2019).

Genetic variants contributing to epilepsy etiology can be common or rare, defined by whether they are present in ≥1% or <1% the population, respectively, and are classified into five different categories: benign, likely benign, variant of unknown significance (VUS), likely pathogenic, and pathogenic, according to the American College of Medical Genetics (ACMG) guidelines (Richard et al., 2015).

Both monogenic and polygenic mutations can lead to epilepsy (Poduri and Lowenstein, 2011). Monogenic variants are usually rare or unique (absent in healthy populations) and have been identified in a large number of epilepsy genes, even though only a minority of epilepsies overall has a monogenic etiology. Although a single gene is affected, phenotype-genotype correlation can be challenging in monogenic epilepsy.

Common epilepsies, such as the genetic generalized epilepsies and focal epilepsies, follow complex inheritance with a polygenic basis, where multiple gene variants contribute to the disorder, with or without an effect from environmental factors. Each variant may

have a weak effect size, but when combined their interaction reduces seizure threshold and results in epilepsy, with mechanisms difficult to investigate (Poduri and Lowenstein, 2011).

An increasingly important issue in the genetics of the epilepsies is the role of somatic mosaicism (Yew et al., 2019). Mosaicism arises when an individual has two populations of cells: one wild-type and one pathogenic, because the variant occurs in post-egging developmental stages. The pathogenic variant may be confined to one tissue (somatic mutation), if the patient has gonadal mosaicism the mutation may be transmitted to the patient's offspring.

Identification of a genetic etiology in epilepsy is important to guide management and pharmacological treatment. Genetic variations can affect treatment response through pharmacokinetic and pharmacodynamic mechanisms or produce idiosyncratic adverse drug reactions (Balestrini et al., 2018). Furthermore, information about the functional alteration due to a genetic mutation could lead intervention of "precision medicine" (Striano et al., 2020). Genetic diagnosis could be helpful in guiding the selection of suitable candidates for invasive intracranial monitoring and resective surgery (Sanders et al., 2019). Finally, genetic etiology provides additional prognostic information, for example a higher risk of sudden unexpected death in epilepsy (SUDEP) present in some genetic epilepsies, such as sodium channelopathies (Matthews et al. 2020).

Genetics plays a major role particularly in patients with refractory epilepsy. When the clinical diagnosis suggests a possible genetic etiology, the patient is suggested to undergo a genetic testing: karyotype, chromosomal microarray (CMA), epilepsy gene panels, WGS, WES (Poduri A. 2017; Bayat et al. 2021).

Gene panels utilize NGS technology to analyse multiple genes known to be associated with epilepsy simultaneously. They provide a higher sequencing depth and lower cost when compared to WES and WGS but restrict the diagnosis to specific genes in the panel.

Although several genes encoding for proteins other than ion channels have been recently identified and added to the gene panels, the majority of the genes causing epilepsy listed in gene panels encode components of neuronal ion channels, in which pathological mutations lead to neuronal hyperexcitability or depletion of inhibitory mechanisms (Herrab and Mefford, 2020). Variants in KCNQ2, KCNQ3 and KCNQ5 genes, encoding for potassium channels belonging to the family of our interest K_v7, figure as responsible of a range of epileptic syndromes that will be discussed in more detail in the next sections.

1.3 Potassium channels

Potassium (K^+) channels represent the broadest and the most functionally heterogeneous class of ion channels present in both eukaryotic and prokaryotic cells. They are located in cell membranes and control the K^+ ions efflux from cells.

In excitable and non-excitable cells, K^+ channels are involved in the control of cell volume, proliferation, differentiation, and survival.

In excitable cells, these channels play an important role in in controlling and stabilizing the membrane potential: inward potassium current push the membrane voltage toward the potassium equilibrium potential (−84 mV) and away from the threshold potential for action potential (AP). Therefore, the activation of potassium channels reduces the frequency and the duration of the AP, as well decreases the susceptibility of the cell to excitatory stimuli.

In humans, more than 70 genes encoding proteins serving as K^+ channel subunits have been identified. They share a highly conserved selectivity filter for K^+ ions within the pore but show different gating mechanisms adapted for their function and respond to diverse physicochemical stimuli. K^+ channels can be activated by voltage changes (K_v), intracellular calcium (Ca^{2+}) (K_{Ca}) or sodium (Na^+) oscillations (K_{Na}), cellular mediators (K_{ir}), or temperature (K_{2P}). Based on their different gating mechanism, they can be classified in different subfamilies (Figure 1.4):

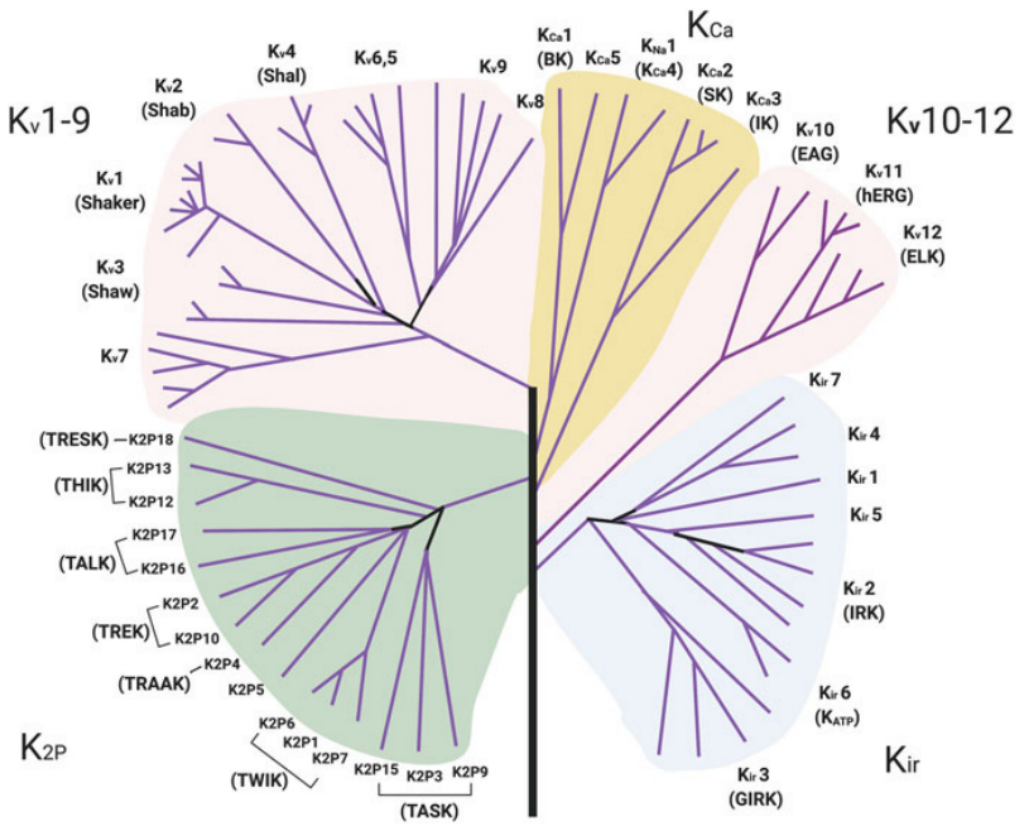

Figure 1.4 Dendrogram of the different families of potassium channels

All K^+ channels are formed by subunits assembling into a tetrameric (K_v, K_{Ca}, K_{Na} and K_{IR} channels) or tetramer-like (K_{2P} channels) architecture. Subunits forming K^+ channels can either be the same (homomers) or different (heteromers), conferring great diversity to these channels. Based on transmembrane topology of their subunits, K^+ channels could be classified in three main families:

I) *Channels with six transmembrane segments subunits* (6TM): includes voltage-gated K^+ channels (K_v channels; K_v1–K_v12), small conductance Ca^{2+}-dependent K^+ channels (K_{Ca}) and Na^+-dependent K^+ channels (K_{Na}).

II) *Channels with two transmembrane segments subunits* (2TM): composed by the inward-rectifier channels ($K_{IR}1$–$K_{IR}7$), structurally homologous to the S5 –S6 segments of K_v channels and voltage-independent as they lack the voltage-sensing domain (VSD).

III) *Channels with four transmembrane segments subunits* (4TM): includes at least 15 different genes ($K_{2P}1$–$K_{2P}17$), topologically characterized by the tandem repetition of two pore domains.

However, structural, and functional heterogeneity of K^+ channels is not restricted to these three groups. For example, large-conductance Ca^{2+}-dependent K^+ channels assemble as tetramers of subunits containing seven transmembrane segments, which differ from K_v subunits for an extra transmembrane segment (S0) at the N-terminus.

1.3.1 K_v7 potassium channels

The K_v7 subfamily comprises five members of volage-gated potassium channels ($K_v7.1$ – 7.5) encoded by the KCNQ genes (KCNQ1–5).

K_v7 channels underlie voltage-activated K^+ currents characterized by slow activation, slow deactivation and no inactivation and by a rather negative activation threshold (~60 mV). These features make these channels crucial in controlling cellular excitability in neurons and muscle cells (Delmas and Brown 2005; Du et al. 2018; Gamper and Shapiro 2015).

K_v7 currents were recorded and studied in neuronal, cardiac and epithelial cells before the KCNQ genes were identified: first, in bullfrog sympathetic neurons a slow, non-inactivating K^+ current fraction was identified, and from the observation that muscarinic acetylcholine receptor agonist, muscarine, inhibited this voltage-sensitive K^+ currents, derived its name “M-current” (I_{KM}) (Brown and Adams 1980); later, a K^+ current mediating the late repolarization of the cardiac action potential, with even slower kinetics than I_{KM}, was identified in the heart and called “I_{Ks}” (Walsh and Kass 1988); finally, a small-conductance

K^+ current was identified in the basolateral membrane of some epithelial cells, where it provides the driving force for electrogenic Cl^- secretion (Lohrmann et al. 1995; Warth et al. 1996).

With the advent of new genetic and cloning techniques the ion channels producing these currents were identified as belonging to the same protein family: the K_v7 channel subfamily.

1.3.1.1 Structure of K_v7 channels

Structurally, K_v7 channels are organized in tetramers in which each α-subunit shows a common architecture, with six transmembrane domains (from S1 to S6), and intracellular amino ($-NH_2$) and carboxy (-COOH) termini. The region encompassing S1-S4 segments forms the *Voltage Sensing Domain* (VSD), whereas the S5 and S6 segments and the interconnecting loop (P region) forms the *Pore Domain* (PD) (Figure 1.5).

The VSD plays a crucial role in switching the channel from a resting to an activated configuration in response to changes in membrane potential. In particular, the S4 segment, which contains from four ($K_v7.1$) to six ($K_v7.2$-5) positively charged arginine (Rs) separated by uncharged residues, plays a key role in voltage-sensitivity (Robbins J. 2001).

The P region consists of about 20 amino acids representing the molecular determinants of the so-called *selectivity filter:* a glycine-tyrosine-glycine-aspartate (GYGD) sequence, essential for discrimination between K^+ and other ionic species.

Recently, the structure of $K_v7.1$ was solved using cryoelectron microscopy (Cryo-EM) techniques: Sun and MacKinnon first published in 2017 a construct of *Xenopus laevis* $K_v7.1$, (which shares 78% sequence with human $K_v7.1$) in complex with calmodulin (CaM) and in absence of phosphatidylinositol-(4,5)-bisphosphate (PIP_2); later in 2020 the same authors published a Cryo-EM structures of the human $K_v7.1$ in complex with its ancillary subunit KCNE3 (see below) and in the presence or absence of the PIP_2. These works revealed important structural insights for regulatory interactions between CaM, PIP_2 and K_v7 channels (see section 1.4.3); furthermore, the available Cryo-EM structures reveal a *domain-swapped architecture*, which is typical of many K_v channels families, in which the VSD of each subunit interacts with the PD of the adjacent subunit.

Subsequently, two more human K_v7 Cryo-EM structures, the $K_v7.2$ and $K_v7.4$ structures respectively, were solved: $K_v7.2$ structure was determined in complex with two activators, ztz240 or retigabine, to study their binding modes and mechanisms of action (Li X. et al.,

2021); $K_v7.4$ structure was first solved in complex with the opener retigabine or the blocker linopirdine (Li T. et al 2021), and later in complex with the activator ML213 in the absence or presence of PIP_2 (Zheng et al. 2022). These studies allowed a deeper understanding of the structure of K_v7 channels, provided insights into the mechanism of action of synthetic modulators and of how K_v7 channels are regulated by PIP_2 (Cooper et al. 2022).

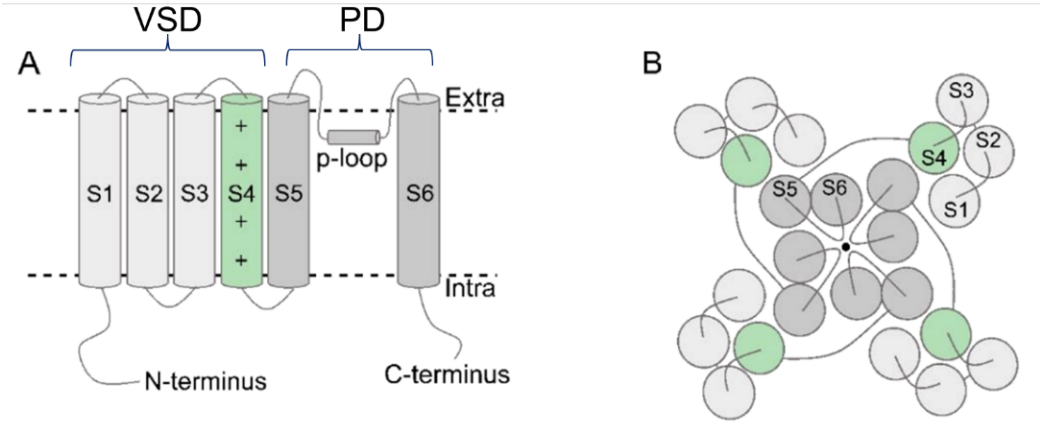

Figure 1.5 A) Schematic architecture of one α K_v7 channel subunit of the tetrameric channel (side view). Cylinders are helical segments. Transmembrane helices S1-S4 assemble into a voltage-sensing domain. "+"-signs in S4 represent the positive charges of arginine. The ion-conducting pore is formed by S5-p-loop-S6 (dark gray), with the p-loop harboring the selectivity filter. VSD: voltage sensing domain; PD: pore domain **B)** Schematic representation of the assembled tetrameric K_v7 channel in a domain-swapped fashion (top view)

The properties of K_v7 channels can be modified through the association of K_v7 α-subunits with five β-subunits called MinK-related peptides (MiRPs) encoded by KCNE1–5 genes. Structurally, MiRPs are single-transmembrane-spanning segment with extracellular NH_2-terminus and intracellular COOH-terminus (Figure 1.6). While four K_v7 α-subunits are necessary and sufficient to form a functional tetrameric voltage-gated channel, MiRPs subunits cannot form functional channels alone, therefore they are considered auxiliary β-subunits. Although the properties of all K_v7 channels are modified to some extent when they are co-expressed with MiRPs, the best-studied associations are those involving $K_v7.1$: when co-expressed in heterologous systems, each MiRP exerts a different effect and drastically modifies biophysical characteristics and pharmacology of $K_v7.1$ channel (see section 1.4.3) (Melman et al. 2004; Wrobel, Tapken and Seebohm 2012; Abbott 2016; Abbott et al. 2021).

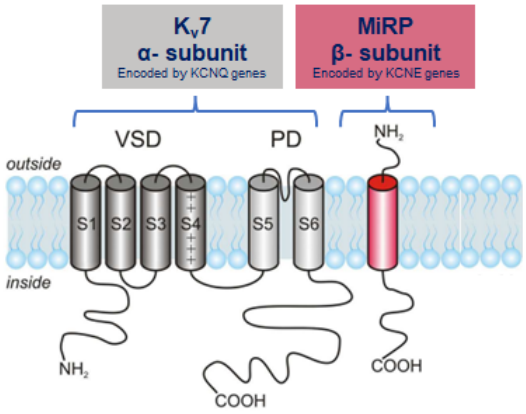

Figure 1.6. Topology of a Kv7.x/KCNEx subunit (adapted from Wrobel, Tapken and Seebohm 2012)

K_v7 channels assembly in tetramers composed of identical or compatible subunits. Two domains in the COOH-terminus called "subunit interaction domains" (SID) are responsible for coiled-coil interactions among subunits and determine the subunit-specific assembly (Schwake et al. 2003) (Figure 1.8). The SID may also act as a platform for K_v7 interactions with accessory MiRP subunits (Haitin et al. 2009), although additional sites in S6 and in the VSD also have been implicated (Lundby et al. 2010).

K_v7 channels assembly in heteromeric tetramers with specific patterns: $K_v7.3$ co-assembles with either $K_v7.2$ (Shapiro et al. 2000), $K_v7.4$ (Bal et al. 2008) or $K_v7.5$ (Lerche et al. 2000); $K_v7.4$ and $K_v7.5$ also form heteromeric channels with each other (Brueggemann et al. 2014); $K_v7.2$ does not multimerize with $K_v7.4$ (Sogaard et al. 2001), and although initial studies suggested that $K_v7.2$ was not to be able to co-assembly with $K_v7.5$ (Lerche et al. 2000), in a more recent study the heteromeric configuration $K_v7.2/7.5$ was found to be possible (Soh et al. 2022); $K_v7.1$ was initially considered unable to co-assemble with any other K_v7 subunits (Schwake et al. 2006) but later it was found that $K_v7.1$ and $K_v7.5$ form heterotetrameric channels in smooth muscle cells (Oliveras et al. 2014).

1.3.1.2 Voltage gating of K_v7 channels

K_v channels are gated through changes in the voltage across the cell membrane which induces a conformational change of the VSD coupled to the opening of the pore.

During depolarization, the positively-charged S4 segment in the VSD follows the electrostatic force and moves through the membrane, making the VSD pass from its *resting downward position* to an *activated outward position*. This movement is mediated by positive charged Rs in S4 (numbered from the outer side of the cell membrane to the inner

cytoplasmic side, see Figure 1.7) and pulls the intracellular S4-S5 linker, which in turn transfers these mechanical forces to the distal region of S6 of a neighbour subunit, leading to pore opening. When the membrane potential returns to its resting potential, the channel returns to the resting state. In some K_v channels an inactivated state following the open state is also present, this is not the case for K_v7 channels that are non-inactivating channels.

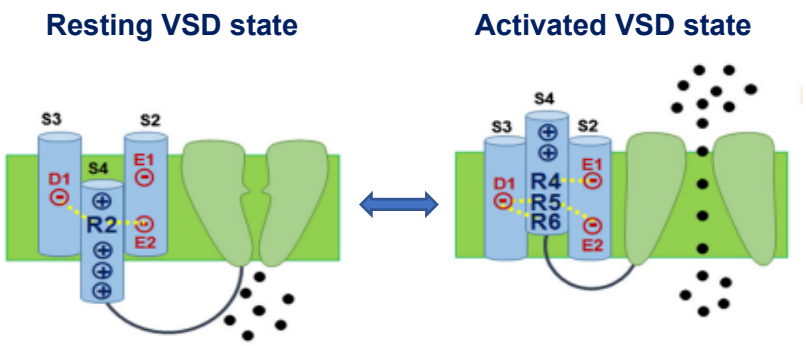

Figure 1.7. Representation of the differential role of ionized hydrogen bonds involving arginines (R) in the proximal (R2) and distal (R4, R5, R6) portions of the S4 transmembrane segment on VSD movement during K_v7 channel gating (adapted from Nappi et al. 2020)

The precise rearrangements occurring in the VSD during activation are not fully understood yet, the hypotheses indicate that resting and activated states are stabilized by ionized hydrogen bonds occurring between the positive Rs in S4 and clusters of highly conserved negatively charged residues in the neighbouring segments (Tao et al. 2010). In a recent paper published by our research group about the molecular basis of $K_v7.2$, $K_v7.3$ and $K_v7.5$ channels defects, it was hypotesized that the *activated VSD configuration* is stabilized by hydrogen bonds established between arginine residues R4, R5, R6 and an internal negative amino acid cluster mostly provided by E1 and E2 in S2 and D1 in S3, wheras R2 residue stabilizes the *resting VSD states* by forming an intricate network of electrostatic interactions with neighboring negatively charged residues (Figure 1.7) (Long et al., 2007; Miceli et al., 2015a; Nappi et al. 2020).

Direct contacts between the S4-S5 linker and the terminal region of S6 is required for efficient electromechanical coupling between VSD dislocation and pore opening during depolarization, but this is not sufficient: K_v7 are indeed considered both voltage and PIP_2 dependent (see section 1.3.1.3).

K_v7 channels have a bundle crossing at the level of the COOH-terminal region of S6 that functions as a pore gate thanks to a hinges proline-adenine-glycine (PAG) motif (Sun and MacKinnon 2017). In particular, the PAG sequence of each subunit creates a bundle of four flexible helices that dislocate radially during pore opening and converge centrally during the closing, thereby interrupting ion flux (Seebohm et al. 2006).

1.3.1.3 Regulation of K_v7 channels

K_v7 channels exhibit a very long intracellular COOH-terminal tail, organized into four α-helical regions (called A-D helices), which are conserved in all K_v7 family members (Yus-Najera et al., 2002). The COOH-terminus presents the binding sites for different molecules and proteins playing a crucial role for K_v7 channel function and regulation (Figure 1.8).

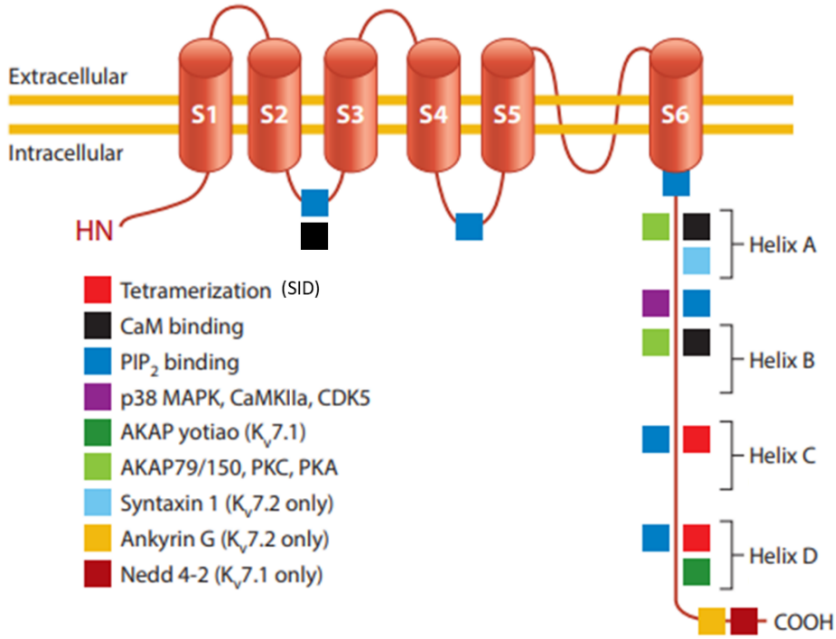

Figure 1.8. Schematic representation of a K_v7 subunit and COOH-terminus. The long COOH-terminal domain is organized in four helices (A–D) and contains most of the binding sites for regulatory proteins as well as the regions responsible for channel tetramerization, indicated with different colours. (Modified from Barrese et al. 2017)

Subunit interaction domains

The regions involved in multimerization and subunit-specific heteromerization, called subunit interaction domains (SID), were identified in helices C and D. They are responsible for coiled-coil interactions among subunits and determine the subunit-specific assembly (Schwake et al. 2003).

Phosphatidylinositol-(4,5)-bisphosphate

PIP_2 is a negatively charged phospholipid present in the inner leaflet of the cell plasma membrane. It is essential for the activation of all K_v7 channels: without PIP_2, VSD activation does not itself cause pore opening (Zaydman et al. 2013). All the homomeric and heteromeric K_v7 channels studied have been found to be highly sensitive to PIP_2, and differences in the single-channel open probability (P_o) are dependent on their intrinsic affinities for intracellular PIP_2 (Hernandez et al. 2009).

The earliest study identified an interaction site of PIP_2 in $K_v7.2$ in the junction between S6 and the A helix, the so call the S6Jx domain. The replacement of a histidine in this region (at position 328 in $K_v7.2$) with a cysteine reduced the sensitivity of the channel to PIP_2 (Zhang et al. 2003).

Later, in both $K_v7.2$ and $K_v7.3$, a cationic cluster identified in in the A-B helix linker was suggested to interact with negatively charged phosphate headgroups of PIP_2 molecules (Hernandez et al. 2009).

Lastly, two binding sites have been detected in the S2-S3 and in the S4-S5 loop, respectively. Particularly, PIP_2 binds the S2-S3 loop in the closed state in $K_v7.2$, whereas, upon channel activation, PIP_2 interacts with the S4-S5 loop, modulating the gating of the channel (Zhang et al. 2013).

PIP_2 binds to S2-S3 loop, the S4-S5 loop and S6 also in $K_v7.1$, as first hypothesized through molecular dynamics simulations (Kasimova et al. 2015) and later found in the cryo-EM structures of $K_v7.1$ in complex with the KCNE3 β-subunit, CaM and PIP_2 (Sun and MacKinnon 2020). Homomeric $K_v7.1$ channel shows a low PIP_2 sensitivity that is increased by several orders of magnitude when $K_v7.1$ α-subunits are co-expressed with KCNE1 β-subunits (Li et al. 2011).

The mechanism underlying K_v7 regulation by PIP_2 is not completely unveiled. In the $K_v7.4$ cryo-EM structure solved in the absence or presence of PIP_2, the authors identified two bound PIP_2 molecules per subunit (one bound at the S4-S5 linker and the other at the cytosolic half of S6) mediating the interaction between the VSD and PD (Zheng et al. 2022). Moreover, molecular dynamic simulations performed with the PIP_2-bound and PIP_2-free $K_v7.4$ structures showed that PIP_2 induces a dramatic conformational reorganization of each K_v7 subunit's intracellular C-terminal region, leading to an expansion of the inner gate and the opening of the K_v7 channel pore (Zheng et al. 2022).

Calmodulin

All members of K_v7 subfamily interact with Calmodulin (or calcium-modulated protein, CaM) (Gamper and Shapiro, 2005). CaM is a small, soluble, ubiquitous and thermostable protein able to bind calcium (Ca^{2+}) ions, switching from an apo state to a Ca^{2+}/CaM state based on the in intracellular Ca^{2+} concentration. Structurally, CaM presents two globular domains, the N-lobe and the C-lobe, and each lobe is composed of two EF-hands, which are responsible for the binding of up to four Ca^{2+} ions per CaM molecule.

CaM binds different sites in the COOH-terminus of K_v7 channels: the first one is in helix A and is formed by an IQ-binding motif (IQXXXRXXXXR); the second is in helix B and displays two overlapping consensus 1-5-10 CaM-binding motifs (Yus-Näjera et al., 2002). Apo-CaM binds both helices A and B, whereas Ca^{2+}/CaM forms binds to helix B only. A new site was found in the VSD through the Cryo-EM structure of $K_v7.1$ in complex with CaM: a nine-amino-acid sequence in the S2-S3 loop, partially conserved among the K_v7 but not present in the other K_v channels. This newly identified binding site led to the hypothesis that interaction of CaM with both the VSD and the helices A and B could provide an alternative functional linkage between VSD and the pore of $K_v7.1$ separate from the S4-S5 linker (Sun and MacKinnon 2017). This hypothesis was corroborated by evidence that CaM regulates also $K_v7.4$ activation binding to its S2-S3 loop (Zhuang and Yan 2021).

CaM functions as a regulator of channel gating: in response to increased intracellular Ca^{2+}, CaM is converted to Ca^{2+}/CaM that binds K_v7 channels causing suppression of $K_v7.2$, $K_v7.4$ and $K_v7.5$ currents, through decrease of channels PIP_2 affinity (Gamper and Shapiro 2003) whereas Ca^{2+}/CaM augments the $K_v7.1$/KCNE1 channel current (Shamgar et al. 2006).

CaM contributes to channel assembly (Ghosh et al. 2006) and plays an important role in surface trafficking: in hippocampal neurons, CaM regulates the trafficking and the enrichment of $K_v7.2/7.3$ channels at the axonal initial segment (AIS) (Liu and Devaux 2014); in heterologous-expression systems, CaM binding to $K_v7.1$ COOH-terminus was found to be essential for proper channel folding, assembly and expression (Shamgar et al. 2006) while mutations in $K_v7.2$ CaM-binding sites can reduce the export from the endoplasmic reticulum to the plasma membrane (Exteberria et al. 2008).

Phosphorylation and muscarinic acetylcholine receptors stimulation

The COOH-terminus region of K_v7 channels presents different sites amenable to be phosphorylated, but the consequences of phosphorylation are still being investigated and not completely clarified.

First a binding site for the A-kinase anchoring protein **AKAP79/150** was found in $K_v7.2$ subunits. AKAP79/150 forms a trimeric complex with **protein kinase C (PKC)**. Activation of PKC leads to phosphorylation of serine residues located in helix B (S541 in $K_v7.2$), which suppress $K_v7.2$ currents via M1 muscarinic acetylcholine receptor activation (see below) (Kosenko et al. 2012). This effect is largely prevented by removing two putative

PKC phosphorylation sites in helix B (Hoshi et al., 2003). PKC activation was found to suppress K_v7.4/7.5 currents expressed in murine aortic smooth muscle cells (Brueggemann et al. 2014) and to decrease K_v7.1 subunit membrane localization and K_v7.1/KCNE1 channel activity (Xu Parks et al. 2020).

Many other phosphorylation sites were identified in K_v7.2 and *in vitro* and *in vivo* studies suggested these could be phosphorylated by enzymes such as CDK5, PKCα, PKA, p38 MAPK, CamKIIα, and GSK3β (Erdem et al. 2017). Five specific serine residues (S427, S436, S438, S446, S455 in K_v7.2) substrate for **CDK5, p38 MAPK, CaMKIIα** and **PKA** enzymes, were found to be important for K_v7.2 PIP_2 sensitivity (Salzer et al. 2017).

A leucine zipper (LZ) motif in the K_v7.1 COOH-terminus is the substrate for the A-kinase anchoring protein **AKAP9**, also called Yotiao, that recruits the cAMP-dependent protein kinase A (PKA) and phosphatase 1 (Marx et al. 2002). Phosphorylation of K_v7.1 at S27 residue via the PKA pathway enhances K_v7.1/KCNE1 (Kurokawa et al. 2003) and K_v7.1/KCNE2 channel activity but not K_v7.1/KCNE3 channel activity (Kurokawa et al. 2009).

AKAP9 also binds K_v7.1 NH_2-terminus and was suggested to have a PKA-independent role in regulating K_v7.1 channel (Kurokawa et al. 2004).

As previously mentioned, the current underlying by K_v7 channels is called M-current (I_{KM}) because it is suppressed upon stimulation of several muscarinic acetylcholine receptors linked to G proteins of the G_q/11 family, like M1, M3, and M5. Stimulation of the M receptors triggers the G_q pathway: activation of phospholipase C (PLC) causes hydrolysis of PIP_2 into diacylglycerol (DAG) and inositol triphosphate (IP_3), leading to the activation of PKC. These events cause three phenomena that negatively modulate the I_M (Figure 1.9):

I) the depletion of PIP_2 by PLC prevents the opening of channels;

II) the activation of PKC, which anchors the K_v7 complex through AKAP79/150, phosphorylates the COOH-terminus of the K_v7.2 subunit, which overlaps with the CaM binding site in helix B. Phosphorylation of the K_v7.2 subunit leads to dissociation of CaM and destabilizes PIP_2 interaction (Kosenko et al. 2012);

III) the production of the second messenger IP_3 triggers Ca^{2+} release from the endoplasmic reticulum. The Ca^{2+}/CaM complex binding sites overlap the putative binding site for PIP_2, reducing the interaction of PIP_2 with the channel (Gamper and Shapiro 2003).

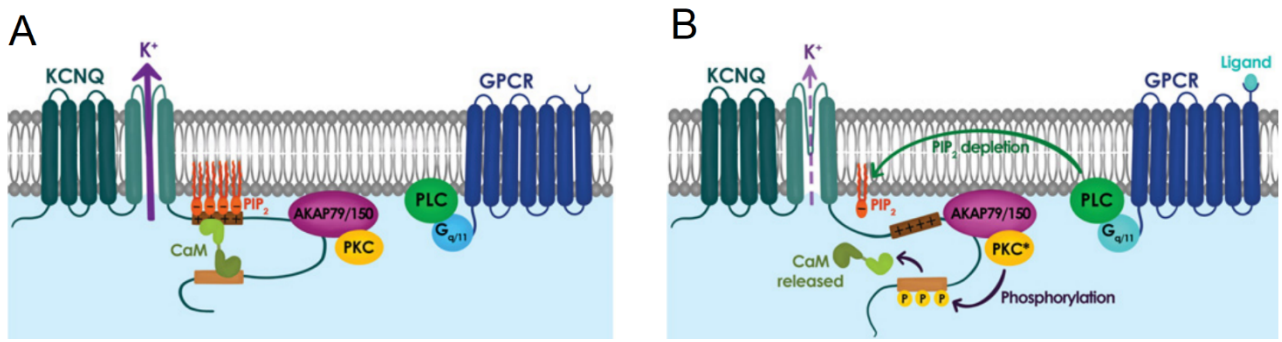

Figure 1.9 Signal transduction mechanisms controlling M-current activity. **A**) M-current activity when G-protein coupled receptor (GPCR) is inactive. **B**) M-current activity is suppressed when GPCR is active (from Weckhuysen and George, 2022).

Ankyrin-G

In the distal end of the helix-D of $K_v7.2$ and $K_v7.3$ COOH-termini (but not in other K_v7 subunits), an interaction domain for the protein Ankyrin-G (AnkG) has been identified. AnkG is an adaptor protein that allows localizing $K_v7.2$ and $K_v7.3$ subunits at the axon initial segment and in nodes of Ranvier, two neuronal sites crucially involved in the generation and propagation of action potentials (Devaux et al. 2004; Pan et al. 2006).

Ubiquitination

In $K_v7.1$ a proline-tyrosine motif (PY) at the COOH-terminal responsible for the interaction with the ubiquitylating enzymes **Nedd4-2** (neuronal precursor cell-expressed developmentally downregulated) was identified, whereas the role of the same region in other K_v7 subunits is less defined. Nedd4-2 is a ubiquitin-protein ligase that regulates the plasma membrane expression of $K_v7.2/7.3$, $K_v7.3/7.5$ channels (Ekberg et al. 2007) and $K_v7.1$/KCNE1 heteromultimers (Jespersen et al. 2007). The protein reduces the current generated by these channels, probably by promoting their ubiquitination, internalization, and degradation (Krzystanek et al 2012).

Syntaxin-1A

In both $K_v7.2$ and $K_v7.3$ subunits, the protein **syntaxin-1A (syx-1A),** a major component of the exocytotic SNARE complex, interacts with the helix A. Syx-1A is a plasma membrane protein that regulates neurotransmitter release; when N-terminal of syx-1A interacts with the neuronal syntaxin binding protein 1 (Sec1 or STXBP1), establishes a core complex involved in membrane fusion and neurotransmitters release (Misura et al. 2002).

Syx-1A binds $K_v7.2$ and $K_v7.3$ subunits producing different effects: it decreases currents mediated by $K_v7.2$ or $K_v7.2/7.3$ channels, while it fails to inhibit the $K_v7.3$ currents. This

could be due to the presence of additional binding sites for syx-1A in the $K_v7.2$ channel, which may not be present in $K_v7.3$ (Regev et al. 2009). STXBP1 has no direct effects on K_v7 current but dampens the inhibition produced by Syn-1A by abrogating Syn-1A binding to K_v7 channels (Devaux et al. 2017).

1.3.1.4 Distribution and physiological role of K_v7 channels

K_v7 channels are not uniformly expressed across the body. Since they were first discovered in neurones and cardiac myocytes, K_v7 channels are referred to as "cardiac" K_v7 channel ($K_v7.1$) and "neuronal" K_v7 channels ($K_v7.2$-7.5) but the more their physiological and pathological roles are studied, the more it becomes clear that this classification is reductive and that K_v7 channels play important physiological roles in many different cell types.

The **$K_v7.1$** subunit, encoded by KCNQ1 gene, is mainly expressed in cardiomyocytes, where, together with KCNE1 β-subunits, underlies the slow component of *delayed rectifying K^+ current* (I_{KS}) involved in the repolarization of the cardiac action potential (Sanguinetti et al. 1996). The pathophysiological importance of I_{Ks} in the heart electrical activity is demonstrated by the fact that mutations in the KCNQ1 and KCNE genes are responsible for cardiac diseases characterized by severe arrhythmias, syncopal episodes, and sudden death. Most $K_v7.1$ loss-of-function variants reduce the amplitude of the repolarizing outward I_{Ks} current and thus increase the ventricular action potential duration causing the long QT syndrome (LQTS); conversely, rare severe gain-of-function mutations in $K_v7.1$ channels cause short QT syndrome (SQTS) and atrial fibrillation by increasing I_{Ks} channel activity thereby shortening the ventricular action potential duration (Dvir et al. 2014).

$K_v7.1$ subunits are localized also in non-cardiac tissues, such as the inner ear, gastrointestinal tract, thyroid gland and pancreas. In the apical membrane of strial marginal cells and dark cells, $K_v7.1$/KCNE1 channel provides a conduit for K^+ secretion, thus recycling K^+ in the endolymph of the inner ear. In the human ear, loss of this recycling is sufficient to cause bilateral sensorineural deafness.

Contrary to $K_v7.1$/KCNE1 heteromers, $K_v7.1$/KCNE2 and $K_v7.1$/KCNE3 complexes generate channels that are constitutively open in the voltage range between -80 to +80 mV (Abbott 2015; Abbott 2016a). In gastric parietal cells, $K_v7.1$/KCNE2 channels are involved in the apical K^+ recycling coupled to the H^+-K^+-ATPase, essential for acid secretion, while in thyrocytes they regulate the synthesis of thyroid hormones (Roepke et al., 2006). In the

intestine, $K_v7.1$/KCNE3 channels are located on the basolateral membrane of colonic crypt cells where their constitutive activation and lack of inactivation enable them to provide a K^+ recycling conduit that facilitates electrogenic intestinal Cl^- secretion (Preston et al. 2010).

Although the activity of $K_v7.1$ channel is modulated by all five KCNEs proteins, the roles of KCNE4 and KCNE5 β-subunits *in vivo* are still being studied (Abbott 2016b). *In vitro* studies showed that co-expression of KCNE4 suppress $K_v7.1$ channel activity through a shift in the voltage sensitivity toward positive membrane values (Grunnet et al. 2002); KCNE5 shifts the voltage dependence of $K_v7.1$ and in addiction it exerts a temperature-dependent modulation on $K_v7.1$ activation and deactivation (Angelo et al. 2002).

The **$K_v7.2$** and **$K_v7.3$** subunits, encoded by KCNQ2 and KCNQ3 genes respectively, are highly expressed in both the central and peripheral nervous systems. In neuronal cells, $K_v7.2$ and $K_v7.3$ are localized at subcellular sites that play key roles in the regulation of neuronal transmission, such as the perisomatic region, the AIS, nodes of Ranvier, and synaptic terminals (Soldovieri et al., 2011). The currently most accepted hypothesis is that $K_v7.2$ and $K_v7.3$ channels are mainly present in adult neurons assembled in the heteromeric $K_v7.2/7.3$ channel that underlies the I_{KM} current, crucial in controlling neuronal excitability (as described in the next section). This viewpoint is supported by various findings:

1) in heterologous cells, heteromeric $K_v7.2/7.3$ channel shows biophysical and pharmacological properties that best resemble those of the native I_{KM} current (Wang et al., 1998; Shapiro et al., 2000; Hadley et al., 2003);

2) in heterologous cells and in neurons as well, $K_v7.2$ or $K_v7.3$ homomers generate rather small currents, while co-expression of $K_v7.2$ with $K_v7.3$ leads to a larger current density than expression of $K_v7.2$ or $K_v7.3$ channel alone (Schwake et al., 2000);

3) co-expression of $K_v7.3$ with $K_v7.2$ leads to increased trafficking to the membrane of $K_v7.3$ channel that is otherwise retained in the endoplasmic reticulum (Schwake et al., 2000) and to a stabilization of $K_v7.3$ pore residues that are instable and in a quiescent silent conformation in the homomeric $K_v7.3$ channel (Shapiro et al., 2000).

However, recent fundings suggest that $K_v7.2$ and $K_v7.3$ channels composition likely differs during development, nervous system region, and from cell type to cell type, supporting the possible expression of homomeric $K_v7.2$ and $K_v7.3$ channels in neurons.

$K_v7.2$ and $K_v7.3$ channels show a different age-dependent expression. In the mouse brain, $K_v7.2$ is already present 3 days after birth, increases one week after birth and remaining

stable until the adult stage; conversely, $K_v7.3$ expression is very low at day 3 but increases continuously until the adult stage (Tinel et al., 1998). In human hippocampus, temporal lobe, cerebellum and medulla oblongata, high $K_v7.2$ expression in pre-natal period was revealed, with levels decreasing after birth; in contrast, the expression of $K_v7.3$ increased from late fetal life to infancy (Kanaumi et al., 2007). Different expression levels for $K_v7.2$ and $K_v7.3$ in the pre- and post-natal period reflect a different role for the two channel, as proven by the fact the the *Kcnq2* homozygous knockout mice initiate breathing but die within an hour due to pulmonary atelectasis (i.e., lungs are deflated) (Watanabe et al, 2000), while *Kcnq3* knockout mice survive to adulthood (Tzingounis et al, 2008). In accordance with mouse studies, a recent work in humans identified epilepsy patients who lack both copies of functional $K_v7.3$ channels (Lauritano et al., 2019), while, until know, no patients with homozygous $K_v7.2$ variants have been identified.

In the brain, $K_v7.2$ and $K_v7.3$ have been detected in different areas, including the dentate gyrus and CA1-3 regions of the hippocampus, the subiculum, all layers of the neocortex, and in the reticular nucleus of the thalamus (Cooper et al. 2001; Tzingounis et al. 2010; Weber et al. 2006; Geiger et al. 2006). In the hippocampus and cortex, $K_v7.2$ and $K_v7.3$ colocalize in excitatory and inhibitory cells, with the exception of the vasoactive intestinal polypeptide (VIP) interneurons GABAergic cell, a cell type that controls the activity of interneuron networks. VIP interneurons express $K_v7.2$ but very limited number of $K_v7.3$ channels (Tasic et al., 2016; Goff and Goldberg, 2019). Although the majority of cells in the forebrain and thalamus express both $K_v7.2$ and $K_v7.3$ channels (Saganich et al, 2001), this trend may not occur in subcortical regions, and different evidence support the notion that $K_v7.2$ channels may be expressed at much higher levels in the brainstem and spinal cord (Verneuil et al., 2020) than $K_v7.3$ channels. Other neuronal populations, for instance, a subpopulation of dorsal root ganglion neurons (King et al., 2014), large sciatic nerve axons (Schwarz et al., 2006) have been found to express $K_v7.2$ but not $K_v7.3$; while in vagal bronchopulmonary neurons $K_v7.3$ mRNA was detected but was not so for $K_v7.2$ mRNA (Sun et al., 2019).

All together these studies support the hypothesis that homomeric $K_v7.2$ and $K_v7.3$ channels are expressed in the neuronal membrane in various areas and in different developmental stages, playing individually different roles.

Furthermore, the concept that I_{KM} current is mainly mediated by the heteromeric $K_v7.2/7.3$ channel formed by 2 $K_v7.2$ subunits and 2 $K_v7.3$ subunits (Hadley et al., 2003) has recently

been expanded, including the possibility of a stoichiometry for $K_v7.2$ and $K_v7.3$ subunits different from 2:2, or considering the participation of the $K_v7.5$ subunit.

In a conditional mouse model the deletion of $K_v7.2$ from granule cells (GCs) of the dentate gyrus diminished the I_{KM} current by only 50%, due to compensation through increased expression of $K_v7.3$ channels, which led to the formation of $K_v7.3$ homomers or $K_v7.2/7.3$ heteromers with a 1:3 $K_v7.2$:$K_v7.3$ channel stoichiometry (Carver and Shapiro, 2019).

In a recent work, Soh and colleagues demonstrated that $K_v7.2$, contrary to what was believed, is able to assemble and form heteromeric channels with $K_v7.5$ in heterologous cells and in the brain. Moreover, the $K_v7.2/7.3/7.5$ channel composition, that was already hypnotized to be possible according to what observed using super-resolution microscopy (Zhang at al., 2016) was detected in a heterologous expression system and functionally characterized, resulting in a channel with unique biophysical properties (Soh et al., 2022). These evidence, together with the fact that brain and subcellular expression of $K_v7.5$ overlaps with those of $K_v7.2$ and $K_v7.3$ subunits (Figure 1.10), strongly support the hypothesis that $K_v7.5$ participates to the molecular component of I_{KM}, together with $K_v7.2$ and $K_v7.3$ subunits (Lerche et al., 2000; Schroeder et al., 2000).

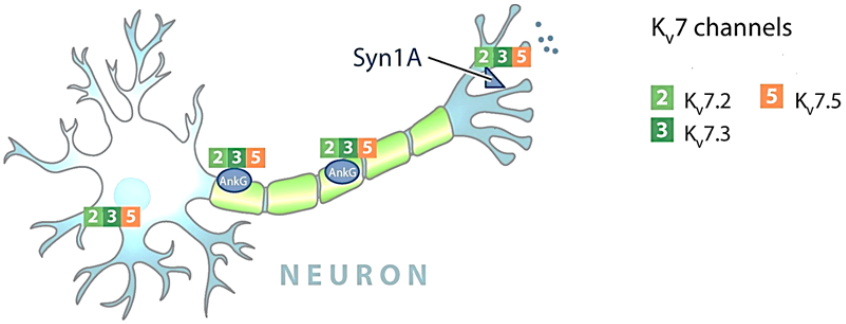

Figure 1.10 Schematic representation of the distribution of K_v7 channels in the different compartments of a myelinated axon. The $K_v7.2$, $K_v7.3$ and $K_v7.5$ subunits were detected at the AIS, nodes of Ranvier and presynaptic terminals (adapted from Barrese et al., 2017)

The **$K_v7.4$** subunit, encoded by KCNQ4 gene, is highly expressed in sensory outer hair cells (OHCs) of the cochlea, where it is involved in the regulation of their intrinsic excitability (Housley and Ashmore 1992) and, at a lower level, in inner hair cells (IHCs) (Kimitsuki et al. 2010). Loss-of-function mutations in the KCNQ4 gene result in autosomal-dominant non-syndromic deafness (DFNA2), a rare condition in which hearing loss is caused by a slow degeneration of OHCs induced by their chronic depolarization (Kubisch et al.,1999).

$K_v7.4$ subunits have also been detected in vascular and visceral smooth muscle, where they are involved in the control of basal tone and in response to myogenic stimuli (Ipavec

et al.,2011; Jepps et al.,2011; Svalø et al., 2013), and in skeletal muscle cells, where they regulate proliferation, differentiation, and response to myotoxic stimuli (Iannotti et al. 2010; 2013)

K_v7.5, encoded by the KCNQ5 gene, was the last subunit member of the K_v7 family to be identified. As mentioned above, K_v7.5 subunit shows an overlapping cellular pattern of expression with K_v7.2 and K_v7.3 subunits in brain areas (Lerche et al., 2000) and in neuronal cells (Soldovieri et al., 2011) being localized at perisomatic region, the AIS, the nodes of Ranvier, and synaptic terminals of neurons. K_v7.5 subunit can form heteromeric channel with K_v7.2 (Soh et al., 2022) and with K_v7.3 (Lerche et al., 2000) subunits and has been proposed to participate in I_{KM} molecular heterogeneity (Lerche et al., 2000; Schroeder et al., 2000). Moreover, K_v7.5 has been found to be important in regulating excitability especially in the hippocampus where it contributes to the afterhyperpolarization currents (Tzingounis et al., 2010). This subunit was also found in non-neuronal tissue, like skeletal and smooth muscle cells where K_v7.4/7.5 heteromeric channels may contribute to the hyperpolarizing K^+ current in as vascular smooth muscle cells that promotes vasodilation by preventing Ca^{2+}-dependent contraction (Stott et al., 2014).
Recently, both gain-of-function and loss-of-function mutations in the KCNQ5 gene have been discovered in patients affected with severe epilepsy conditions (Lehman et al., 2017; Wei et al., 2022), constituting further evidence for K_v7.5 crucial participation in regulating neuronal excitability.

1.3.1.5 The roles of the M-current

In 1980, Brown and Adams recorded in bullfrog sympathetic neurons a slow-activating voltage-gated potassium current that was blocked by muscarine, therefore they termed it the “M-current” (I_{KM}) (Brown and Adams 1980).

About two decades later the molecular component underlying I_{KM} current was identified in K_v7.2 and K_v7.3 potassium channel subunits (Wang et al., 1998) which were previously identified through positional cloning in patients experiencing self-limiting familial neonatal seizures (Singh NA et al., 1998; Charlier C et al., 1998). Currently, more and more evidence supports K_v7.5 subunit participation to I_{KM} (Lerche et al., 2000; Schroeder et al., 2000, Soh et al., 2022).

I_{KM} was recorded in almost all regions of the central and peripheral nervous system (Green and Hoshi, 2017) and it is characterized by slow activation, slow deactivation and no inactivation and triggered by a rather negative activation threshold (~60 mV) (Gamper and

Shapiro 2015). These features lend it to various roles associated with controlling excitability in the brain that are summarized in Figure 1.11.

In the AIS and in the nodes of Ranvier, K_v7 channels are involved in the control of the **resting membrane potential**, a key parameter to regulate AP generation. The AP is biological signalling provided by a transient change in the membrane potential. It is triggered by a stimulus inducing a gradual depolarization toward threshold values, beyond which there is a rapid rising phase, an overshoot, and a repolarization phase (Figure 1.11, panel A). Membrane potential modification are induced by the flow of ions inside/outside the cell: the depolarization upstroke of the action potential spike is mediated by an increase in inward Na^+ conductance and, instead, the repolarization downstroke is mediated by the inactivation of some of voltage-gated Na^+ channels (Na_v) and an increase of K^+ efflux.

At the AIS, K_v7 channel activation at a subthreshold potential induces hyperpolarization of the membrane, setting the neuronal resting potential, shaping the action potential profile and promotes the recovery of inactivated Na_v channels (Battefeld et al., 2014).

During the repolarization phase, the membrane potential goes below the resting membrane potential. Hence, there is an undershoot or hyperpolarization phase, termed **afterhyperpolarization** (AHP) (Figure 1.11, panel B), where K^+ channels remain open. AHP persists until the membrane potassium permeability returns to its usual value, restoring the membrane potential to the resting state. AHP is divided into three phases:

I) a fast one, namely fAHP, lasting 1-5 ms, largely mediated by Ca^{2+} - and voltage-dependent BK channels;

II) a medium one called mAHP, lasting 50-200 ms, mediated by K_v7 and HCN channels;

III) and a slow one the sAHP, lasting from about 0.5 s to several seconds, mediated by K_v7 and SK Ca^{2+} channels.

The M-current contributes to the medium (mAHP), and the slow components (sAHP) of the afterhyperpolarization current determining the refractory period and the discharge frequency on neurons (Tzingounis and Nicoll, 2008).

A neuron that emits an action potential is often said to “fire”. Action potentials in neurons are also known as “spikes”, and the temporal sequence of action potentials generated by a neuron is called its “spike train”. I_{KM} contributes to **spike-frequency adaptation** by reducing the frequency of neuronal firing in response to sustained stimuli (Figure 1.11,

panel C). When I_{KM} is inhibited (e.g., by channel blockers like linopirdine or XE991), the neuron remains depolarized for a long period, during which it may generate multiple spikes (Yue and Yaari, 2004).

In individual neurons, or in a neuronal population, rhythmic patterns of AP can be observed, these are called “neural oscillation”. When the oscillation amplitude increases in response to stimuli at a specific frequency, this is called “resonance”. In pyramidal neurons in the hippocampus, somatic K_v7 channels in conjunction with dendritic HCN channels facilitate neuronal responsiveness to oscillating subthreshold membrane potential within theta frequencies (2–7 Hz) (Hu et al., 2002), therefore this **theta-resonance** is also called M-resonance (Figure 1.11, panel D).

Network oscillations at the theta frequency have been shown to be important for hippocampal function, such as exploration and working memory (Sarnthein et al., 1998). As such, disruption of M-channel activity, such as conditional knockout of $K_v7.2$ subunits, reduces hippocampal theta resonance and consequently impairs animal performance in spatial memory tasks (Peters et al., 2005).

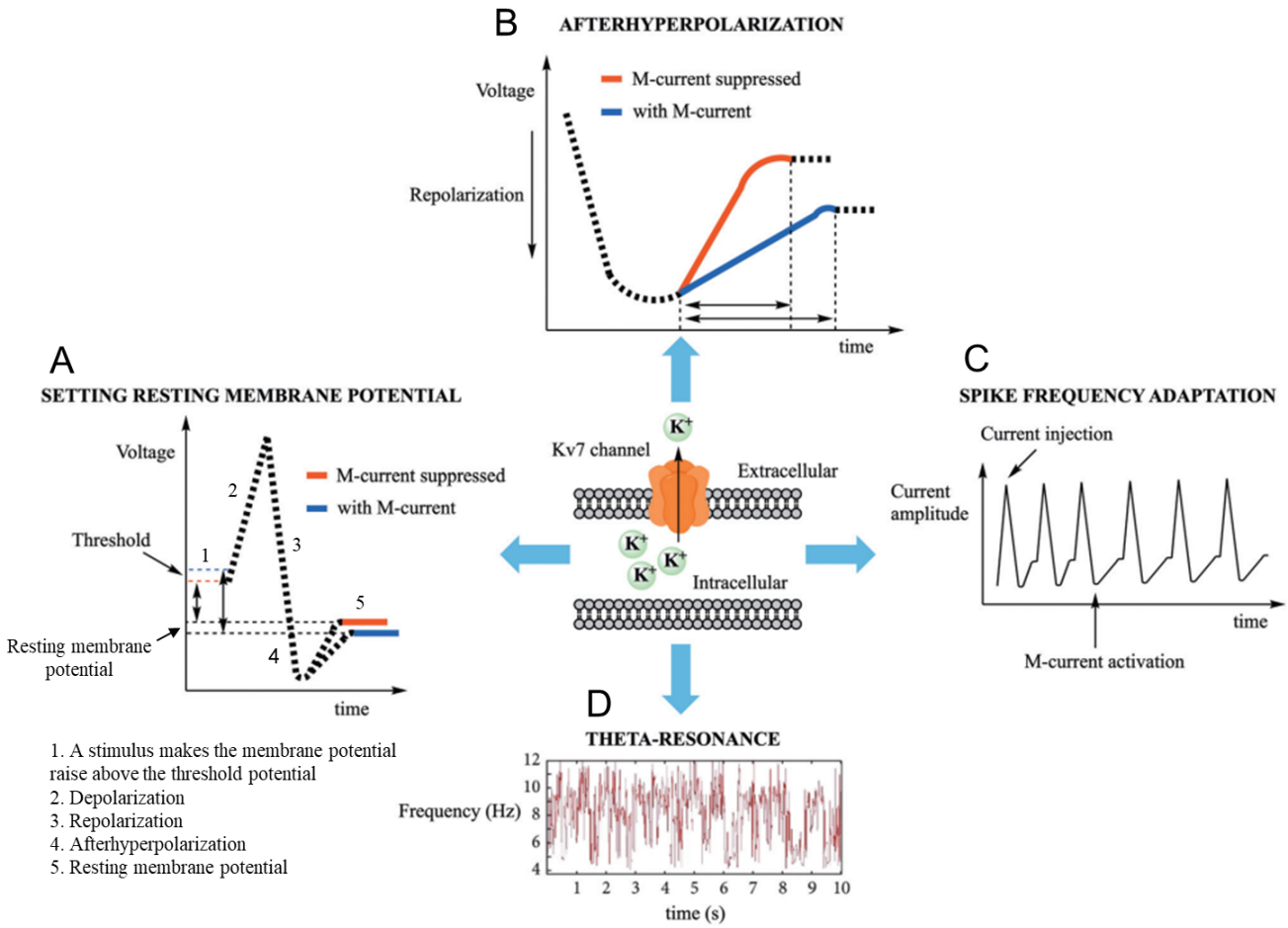

Figure 1.11 Summary of I_{KM} current electrophysiological effects in neurons. **A)** Following K_v7 channel opening, the outward K^+ flow hyperpolarizes the cellular membrane, setting the resting potential, thus a

greater stimulus is required to trigger an AP. **B)** K_v7 channel opening contributes to the afterhyperpolarization phase following an AP. **C)** Spike frequency adaptation was observed after train of action potentials were induced by depolarizing current injection, limiting the ability of the neurons to fire repetitively. **D)** Theta waves were recorded in CA1 pyramidal neurons in the hippocampus and were noted to disappear after M-current suppression. (Adapted from Borgini et al., 2021)

Finally, K_v7 channels are express in the presynaptic terminal and can modulate the **release of the neurotransmitter**. In 2003 Martire and co-workers, have demonstrated that activation of presynaptic I_{KM} may hyperpolarize hippocampal nerve endings, reducing Ca^{2+} influx through voltage-gated Ca^{2+} channels resulting in a reduction of norepinephrine GABA and D-aspartate release (Martire et al., 2004). The same authors in 2007 also described the involvement of $K_v7.2$ subunits in dopamine release from rat striatal synaptosome, showing that [^{3}H] dopamine release is inhibited by the I_{KM} activator retigabine while the I_{KM} blockers TEA and XE991 enhanced [^{3}H] dopamine release and prevented retigabine induced inhibition (Martire et al., 2007).

1.3.1.6 KCNQ2, KCNQ3 and KCNQ5-related channelopathies

The KCNQ2 and KCNQ3 genes were identified through positional cloning in patients experiencing self-limiting familial neonatal seizures (Singh et al., 1998; Charlier et al., 1998). Indeed, mutations in the KCNQ2, KCNQ3, and also KCNQ5 genes, encoding for $K_v7.2$, $K_v7.3$ and $K_v7.5$ subunits, respectively, are responsible for a wide spectrum of human neuronal pathologies in which epilepsy is often (but not always) present, consistent with the crucial role of I_{KM} in the control of neuronal excitability.

Diseases caused by the dysfunction of ion channel subunits are referred to as *channelopathies*, and so are the pathological conditions due to mutations that alter the K_v7 functions. Mutation-induced alteration of K_v7 currents can be investigated through functional *in vitro* analysis. In particular, electrophysiological whole-cell patch clamp recordings of currents generated upon heterologous expression of wild-type (WT) and mutant subunits allow to analyse the consequences of the inserted mutation: a mutation that reduces the WT ionic current exerts a Loss-of-function (LoF) effect, conversly gain-of-function (GoF) effect is observed for a mutation enhancing the WT current.

KCNQ2-related channelopathies

Mutations in **KCNQ2** are responsible for highly heterogenous epileptic and neurodevelopmental phenotypes ranging from more benign forms like *self-limited familial*

neonatal epilepsy (SeLFNE, previously called Benign Familial Neonatal Seizures, BFNS) to more severe phenotype, such as *developmental and epileptic encephalopathy* (DEE).

Among the benign forms, two genetic conditions similar to SeLFNE have also been described: The *Self-limited Familial Infantile Seizures* (SeLFIS) or *Self-limited Familial Neonatal-Infantile Seizures* (SeLFNIS) (Zhou et al. 2006, Zara et al. 2013).

The term self-limited was recently proposed by the ILAE to replace the more confusing term “Benign” and indicates that epileptic seizures resolve in patients within the first few months or years of life (Scheffer et al., 2017). Indeed, SeLFNE is characterized by multifocal seizures starting around the third day of life and disappearing within a few weeks or months; however, 10-15% of affected children show seizures later in life. Seizures are generally brief, lasting one to two minutes, and the motor activity may be confined to one body part, migrate to other body regions, or generalize. The patient’s neuropsychological development is usually normal (Miceli et al., 2018).

In SeLFNE, KCNQ2 mutations are transmitted from affected parents following a classical autosomal dominant inheritance mode. Mostly missense and frameshift/deletion variants have been identified in patients, but also splice variants, nonsense mutations, exon and whole-gene deletions were identified.

Mutations found in SeLFNE appear to be spread along the entire $K_v7.2$ sequence, frequently localized in the VSD between the S2 and S3 segments and cause a mild LoF, that cannot be compensated by the wild type allele, thus resulting in haploinsufficiency. Functional studies suggested that in most cases a decrease of I_{KM} of only 25% is sufficient to cause SeLFNE (Schroeder et al., 1998).

Several molecular mechanisms appear responsible for the mutation-induced LoF: mutations in residues located the PD can alter the K^+ ion permeation; variants affecting the VSD may reduce sensitivity to changes in membrane potential (Dedek et al 2001, Castaldo et al 2002, Miceli et al 2013); mutations affecting the C-terminus can alter the affinity and/or functional regulation mediated by modulators like calmodulin or syntaxin-1A (Alaimo et al., 2009; Soldovieri et al., 2014). In case of frameshift/deletion variants, the nonsense-mediated RNA decay (NMD) of the transcript, and enhanced subunit turnover are the two molecular mechanisms responsible for decreased levels of functional subunits.

As mentioned above, mutations in KCNQ2 gene can also cause DEE. “*Developmental and epileptic encephalopathies*” is the more recent definition introduced by the ILAE to designate a heterogeneous group of disorders characterized by early-onset, often severe

epileptic seizures and EEG abnormalities on a background of developmental impairment that tends to worsen as a consequence of epilepsy (Specchio et al. 2022). KCNQ2-related DEE are characterized by pharmacoresistant seizures that begin in the first week of life and remit between nine months and four years of age. Patients show moderate to severe developmental impairment (Weckhuysen and George, 2022). Additionally, KCNQ2 mutations have been identified in several individuals with Ohtahara syndrome (Saitsu et al., 2012), the most severe and the earliest developing age-related epileptic encephalopathy, characterized by tonic seizures occurring within the first three months of life, often within the first two weeks.

Mutations found in KCNQ2-related DEE are all missense *de novo* pathogenic variants (except 2 variants causing an in-frame deletion of a single amino acid); however, few children with KCNQ2-DEE were born from mosaic parents (Milh et al., 2015; Kato et al., 2013; Mulky et al., 2017).

DEE-associated mutations appear to be concentrated in channel sites critical for the activity, such as: the S4 in VSD, the proximal C-terminal segment which binds PIP_2 and CaM, the B helix also involved in CaM-binding (Millichap et al., 2016), the PD, the S6 and the intracellular S6-helix A linker (Goto et al., 2019). Consistent with their localization at crucial channel sites, pathogenic variants causing KCNQ2-DEE exert more severe functional defects than haploinsufficiency, with more than a 25% function impairment resulting in a profound LoF (Orhan et al., 2014). However, in addition to LoF variants, *de novo* missense variants causing GoF effects on the I_{KM} were found in DEE-affected patients (Miceli et al., 2015a; Mulkey et al., 2017).

In addition to epileptic syndromes, mutations in the KCNQ2 gene have also been recently associated with severe, non-epileptic neurodevelopmental diseases, specifically 10 patients carrying a KCNQ2-R201C or KCNQ2-R201H missense variant showed neonatal encephalopathy without seizures, burst suppression EEG, profound developmental delay, and early mortality (Mulky et al., 2017).

KCNQ3-related channelopathies

Although less frequently (Miceli et al., 2017) mutations in the **KCNQ3** gene are identified in patients with different neurological phenotypes. KCNQ3 variants have been found in patients with SeLFNE or SeLFIS, with clinical characteristics indistinguishable from $K_v7.2$-related self-limited syndromes. Patients usually present a normal psychomotor development, although some individuals showed some degree of intellectual disability (ID)

(Soldovieri et al., 2014; Miceli et al., 2015b). KCNQ3 mutations causing SeLFNE are inherited in an autosomal dominant manner, are mostly missense, and cause LoF effect *in vitro*.

Additionally, more severe phenotypes have been associated with de novo KCNQ3 variants: pathogenic LoF variants have been described in few patients with DEE (Ambrosino et al., 2018), ID apparently without epilepsy (McRae et al., 2017), cortical visual impairment (Bosch et al., 2016) and ID with autism spectrum disorder (Sands et al., 2019).

Contrary to KCNQ2, KCNQ3 homozygous variants are compatible with life, indeed two frameshift variants causing LoF effect, were found in homozygosity in patients with developmental delay and neonatal seizures (Kothur et al., 2018. Lauritano et al., 2019). In addition, in both families described, heterozygous carrier parents of the KCNQ3 frameshift variant were unaffected. In general, the ability of KCNQ3 to tolerate mutations better than KCNQ2 may contribute to the lower incidence of epilepsy-associated variants described for KCNQ3 when compared with KCNQ2.

In addition to LoFs, recently, KCNQ3 de novo missense mutations producing a GoF effect have been found in children with global developmental delay, autism spectrum disorder ASD, frequent sleep-activated multifocal epileptiform discharges. These mutations are located in the VSD at the two outermost arginines of the $K_v7.3$ S4 segment, R1 and R2, and resulted in GoF (Sands et al., 2019).

Interestingly, corresponding mutations found in KCNQ2 R1 and R2 arginine residues, also resulted in GoF (Millichap et al., 2017; Mulkey et al., 2017). Although the *in vitro* functional characterization revealed a GoF effect for both $K_v7.3$ and $K_v7.2$ mutated channels, the clinical picture of patients carrying KCNQ2 or KCNQ3 variants at these positions was different (Millichap et al., 2017; Mulkey et al., 2017). A possible explanation of the different phenotypes between KCNQ2 and KCNQ3 variants at homologous positions can be given to the distinct expression pattern during ontogenesis and a distinct functional role of KCNQ2 and KCNQ3 genes.

KCNQ5-related channelopathies

While several hundred disease-causing variants are known in KCNQ2 and a few tens in KCNQ3, only twelve **KCNQ5** variants are currently known to be associated with distinct human phenotypes. In particular, four patients with ID with or without seizures carried

KCNQ5 de novo heterozygous missense mutations causing LoF or GoF (Lehman et al., 2017). Another patient affected by mild ID with history of absence epilepsy in adolescence and no EEG nor MRI alterations carried an intragenic duplication of the KCNQ5 gene in heterozygosity (Rosti et al., 2019). Recently, our research group functional characterized two de novo heterozygous variants found in two patients affected by DEE or ID without seizures, both resulted strong GoF (Nappi et al., 2022).

Moreover, in a large WES study three deleterious heterozygous missense variants, one truncation and one splice site alteration were identified in ten individuals from five independent families affected by genetic generalized epilepsy (GGE). Two identified variants were *de novo,* one was inherited from an unaffected parent, one from a parent suffering from absence seizures and one from a parent affected by ID. The five new variants identified were functionally characterized as strong LoF (Krüger et al., 2022).

Although *in vitro* functional studies performed in heterologous cells do not completely reproduce the complexity of the *in vivo* phenotypes, the identification and quantification of a LoF or a GoF channel effect allows to delineate genotype-phenotype correlations: more severe phenotypes are correlated to more drastic alterations of K_v7 channel function, such as strong GoF or LoF, while milder phenotypes results from smaller alterations (Nappi et al., 2020). This is particularly clear for KCNQ2-related disorders, because several KCNQ2 mutations have been identified and functionally characterized and more and more are identified every year, thanks to NGS techniques. Given the fewer number of KCNQ3 variants described until now when compared with KCNQ2, genotype-phenotype correlations are not so clear for this gene, and for KCNQ5 it is currently impossible to draw genotype-phenotype correlations due to the very small number of variants identified until now.

1.3.1.7 Pharmacology of K_v7 neuronal channels

Given the prominent role in human physiology and pathology of I_{KM}, it is not surprising that neuronal K_v7 potassium channels represent an attractive pharmacological target for several neurologic disorder (Barrese et al., 2010).

Compounds acting on neuronal K_v7 channels include both *activators* and *blockers*. Historically, *blockers* were developed for treatment of learning and memory disorder while application of *activators* appears as a rational approach to treat epileptic disorders as well as other pathological conditions in which neuronal hyperexcitability plays a critical role such as neuropathic pain (Liu et al., 2021), ischemic stroke (Bierbower et al., 2015) and

amyotrophic lateral sclerosis (Wainger et al., 2021) (figure 1.13). Moreover, activation of K_v7 channel has been proposed as pharmacological intervention to treat migraine, anxiety (Korsgaard et al.,2005), mania (Dencker et al., 2008), attention deficit hyperactivity disorder (Hansen et al., 2008) addiction to psychostimulants (Hansen et al., 2007) and depression (Friedman et al., 2016).

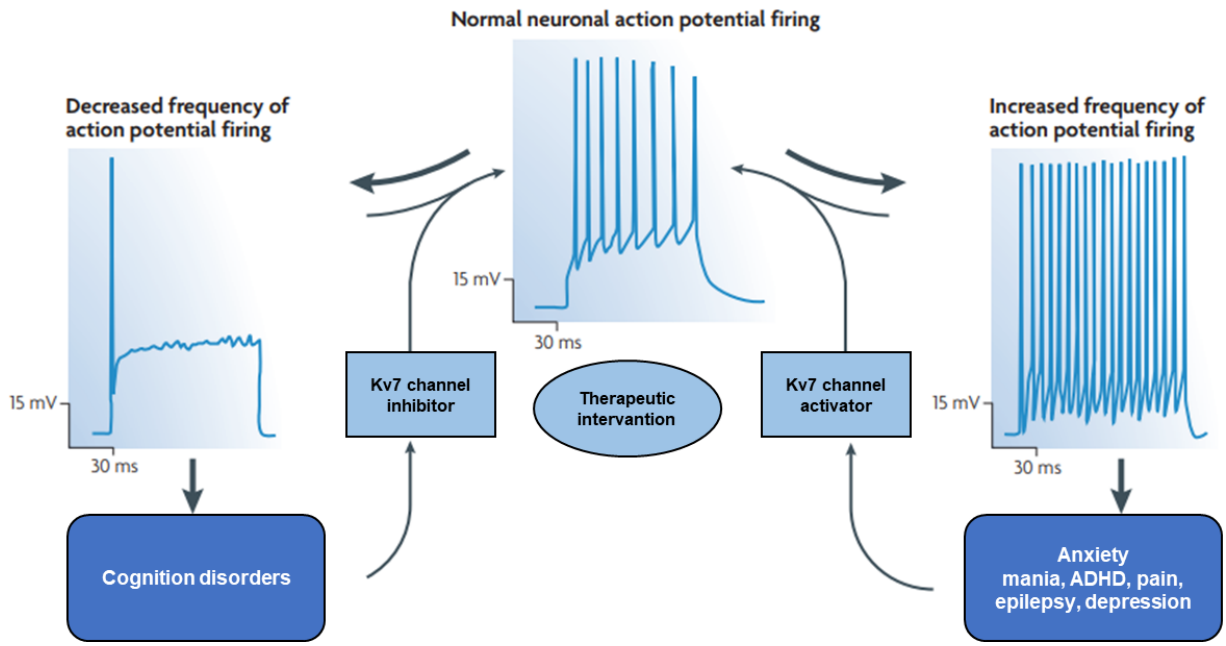

Figure 1.13 Effects of K_v7 channel inhibitors and activators on pathologically altered neuronal activity (adapted from Wulff et al., 2009).

1.3.1.8 I_{KM} blockers

K_v7 blockers promote a reduction of outward K^+ current, and, consequently, shift the cellular membrane potential to more positive values.

The first selective K_v7 blocker has been the phenyl indolinone derivative **linopirdine** (*for all structure molecules see Table 1.1*), synthesized in 1980s. Linopirdine is a non-selective K_v7 blocker, being active also on cardiac $K_v7.1$ channels, although with a lower potency when this channel co-assembles with KCNE1 accessory subunits (Aiken et al., 1995), and a cryo-EM structure revealed its binding site in a cytosolic pocket underneath the inner gate in $K_v7.4$ (Li T. et al., 2021). Linopiridine was able to release acetylcholine in rat hippocampus, cortex and caudate nucleus slices, in addition to causing increased dopamine, glutamate, aspartate, GABA, and serotonin levels (Zaczek et al., 1993). Because of its ability to increases the performance in learning and memory in several animal models (Brioni et al.,1993) Linopiridine has been proposed for the treatment of neurodegenerative conditions like Alzheimer's disease. Nevertheless, clinical trials did not

show a clear effectiveness of linopiridine on Alzheimer's patients, and finally it failed in phase III clinical trials due to undesired pro-epileptic side effects (Rockwood et al., 1997). Possible reasons for the lack of effect of linopiridine in ameliorating the cognitive state in humans might be its low brain penetration and short half-life. To address these drawbacks, many linopirdine analogues were synthesized. Among these, the **XE-991** showed an increased potency in blocking K_v7 currents, improved brain-plasma ration and longer half-life. Like linopirdine, also XE991 is unable to discriminate among K_v7 subunits (Wang et al., 2000). The absence of seizures in an animal model after XE991 and linopirdine treatment and their neuroprotective properties could be explained by their slow binding kinetics to the active conformation of K_v7 channels, mainly exerting their inhibition in hyperexcited neurons (Greene and Hoshi, 2017).

Differently from non-selective K_v7 blockers linopiridine and its derivatives **UCL2077** inhibits K_v7 channels in a subtype-selective manner, acting mainly on $K_v7.1$ and $K_v7.2$ channels. Moreover, this compound increases $K_v7.3$ currents at negative membrane potentials, while inhibits them at more depolarized values. UCL2077 was able to suppress slow afterhyperpolarization (sAHP) at low micromolar concentration, without affecting medium afterhyperpolarization (Soh and Tzingounis, 2010). This property is probably derived from a combination of UCL-2077's inhibitory effects on a wide variety of channels, not only a selective $K_v7.1$ and $K_v7.2$ inhibition, but also hERG current suppression, inhibition of intermediate-conductance Ca^{2+}-activated K^+ (IK_{Ca}) channels, and a weak effect against the large-conductance Ca^{2+}- activated K^+ (BK_{Ca}) channels (Hsu et al., 2020).

Another potent K_v7 inhibitor recently described is **ML252**. This molecule, unlike other K_v7 channel blockers (XE991, linopiridine), exerts an inhibitory action at very low concentrations, proving to be very potent. Furthermore, it appears to be more selective than other inhibitors in blocking specifically $K_v7.2$ isoforms: in fact, the inhibitory action on $K_v7.2$ currents is about 40 times greater than that shown on $K_v7.1$ cardiac isoform. The ML252 shows reduced selectivity for $K_v7.2/7.3$ heteromeric channels or $K_v7.4$ channels (Cheung et al., 2012). Interestingly, SAR studies revealed that small structural changes of ML-252 (substitution of the ethyl group with a hydrogen) are sufficient to cause a functional switch of its activity from an antagonist to an agonist.

During a screening for new retigabine analogues, a K_v7 antagonist was identified and subsequently modified to improve its properties; the results was the compound **HN38**, a K_v7 blocker 7-times more potent than XE991 in inhibiting $K_v7.2$ channels (Hu et al., 2013).

In addition another bloker, the fenamets **NH17** has been described as a $K_v7.2$ channel inhibitor, although its subtype selectivity for other K_v7 family members is unknown (Peretz et al., 2007).

Recently, **fangchinoline**, an natural alkaloid isolate from *Stephania tetrandra* that exerts anticancer, anti-inflammatory, and antihypertension effects, has been described as a K_v7 blocker. It inhibited K_v7 currents in heterologous expression without selectivity among the different member of the family. Furthermore, fangchinoline slowed the activation of $K_v7.1$-7.5 channels and inhibited native M-channel currents of DRG neurons (Li H et al., 2022).

Table 1.1. K_v7 channel inhibitors.

Compound Name	Structure
Linopirdine	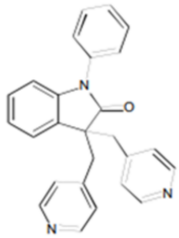
XE991	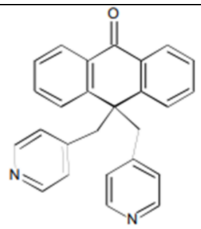
UCL-2077	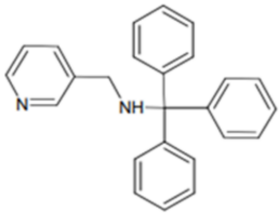
ML252	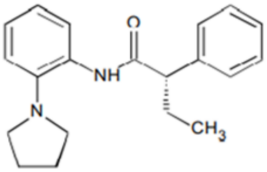
HN38	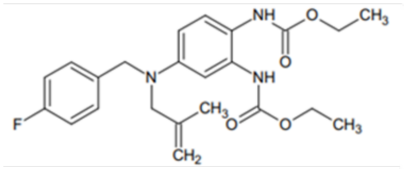

NH17	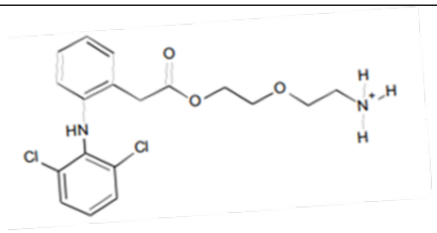
Fangchinoline	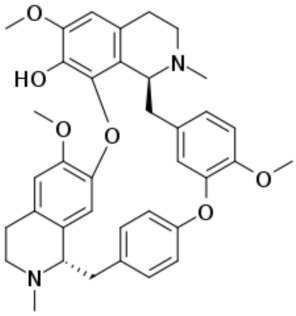

1.3.1.9 I_{KM} activators

1.3.1.9.1 Flupirtine, Retigabine and Derivatives

Flupirtine was the first compound identified as a K_v7 activator, even though its development predates the discovery of these channels. The drug was initially introduced as a non-opioid nonsteroidal antinflammatory analgesic in the 1980's by the German pharmaceutical company Chemiewerk Homburg and became the first clinically approved K_v7 channel agonist in 1984 in Europe on the basis of its unique analgesic and muscle relaxation properties compared to opioids and other non-steroidal anti-inflammatory drugs.

The analgesic action of flupirtine has been initially ascribed to its ability to acts as an antagonist of N-methyl-D-aspartate (NMDA) receptors or an agonist of γ-amino-butyric acid ($GABA_A$) receptors (Szelenyi et al., 2013), but further studies have demonstrated that flupirtine enhanced the activity of I_{KM}, acting on homomeric $K_v7.2$ channels at concentrations close to those achieved during standard therapy with this drug (Martire et al., 2004). Flupirtine is a pan-$K_v7.2$–7.5 agonist, sharing the same binding site than retigabine and other K_v7 openers in the pore channel region (Kim et al., 2015; Bock, et al., 2019).

In addition to analgesia, flupirtine displays neuroprotective effects (Boscia et al., 2006) and anticonvulsant activity, both in in pentylenetetrazol-induced seizures (PTZ) mice models and in kainic acid model of neonatal seizures (Raol et al., 2009). Flupirtine was effective as anticonvulsant in patients with pharmacoresistant epilepsy, but at ten-times higher than that producing analgesia (Rostock et al., 1996).

Because of its severe liver toxicity, flupirtine use was first limited to short-term pain management in 2013, and later in 2018 its marketing authorization was withdrawn by EMA (see European Medicines Agency, Withdrawal of pain medicine flupirtine endorsed, www.ema.europa.eu/docs/enGB/documentlibrary/Pressrelease/2018/03/WC500246353.pdf). Despite this significant setback, flupirtine remained a compound of great interest for its potential therapeutic properties and as a starting point for the development of more potent and selective K_v7 activators.

To separate the analgesic action from the anticonvulsant activity, molecular modelling studies have been carried out. Analyses of pharmacophoric region suggested that the phenyl ring and the basic nitrogen atom in the pyridine put at a specific distance from this ring, is essential for the analgesic activity. The absence of this basic nitrogen atom enhanced the antiepileptic activity, reducing at the same time analgesic activity (Figure 1.14).

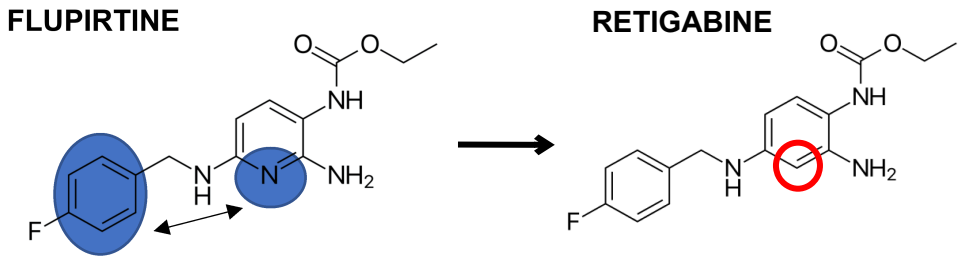

Figure 1.14 Pharmacophore modification of flupirtine and development of retigabine**.**

Based on these observations a synthesis program began and resulted in the development of several desazaflupirtine derivatives. Among this new class of anticonvulsants, the most potent obtained has been the **retigabine**. Retigabine represent the first approved anticonvulsant drug acting on K_v7 potassium channel, it was indicated adjunctive therapy for partial-onset seizures in patients aged 18 years or older and commercialized by GSK in 2011 as Trobalt® in Europe and Potiga® in the US. The drug has also shown to be effective in the treatment of KCNQ2 LoF mutations, representing an option for personalized therapy approach (Millichap et al., 2016).

Retigabine is a pan $K_v7.2$-7.5 activator, while the cardiac $K_v7.1$ channel is completely insensitive to this drug. The principal effect of retigabine is a hyperpolarizing shift in channel activation, together with an acceleration in channel activation and a slowing down of its deactivation (Main et al., 2000). Its effect on the channel voltage-sensitivity depends on the K_v7 channel subtype: on $K_v7.3$ homomers the effect on voltage sensitivity is maximal (maximal shift of -43mV), intermediate for $K_v7.2/7.3$ heteromers (-30 mV) and

$K_v7.2$ homomers (-24 mV) and very small for $K_v7.4$ homomers (Tatulian et al., 2001) (Table 1.2).

In $K_v7.5$ homomers retigabine does not change voltage sensitivity, but increases current amplitude (Dupuis et al., 2002). Finally, on $K_v7.2/7.3$ heteromers retigabine increases the single channel open probability by stabilizing the open conformation, without any significant change in channel conductance (Tatulian and Brown 2003).

Table 1.2. Potency of retigabine against $K_v7.1$, $K_v7.2$, $K_v7.3$, $K_v7.4$, and $K_v7.2/7.3$. (From Tatulian et al., 2001)

	Maximum shift in $V_{1/2}$ (mV)	**Retigabine EC_{50} (μM)**
$K_v7.2/7.3$	-30.4	1.9 ± 0.2 (n=5)
$K_v7.1$	-0.7	100.1 ± 6.5 (n=5)
$K_v7.2$	-24.2	2.5 ± 0.6 (n=5)
$K_v7.3$	-42.8	0.6 ± 0.3 (n=5)
$K_v7.4$	-24.6	5.2 ± 0.9 (n=5)

Anticonvulsant activity of retigabine has been also demonstrated in a broad spectrum of animal model. In 1996 Rostock and collaborators demonstrated that retigabine was effective in reducing seizure induced electrically (MES) or chemically by PTZ, picrotoxin and NMDA. The drug has been also effective in genetic animal model like the DBA/2 mouse in which showed an additive effect when co-administered diazepam, phenobarbital, phenytoin, and valproate (Rostock et al., 1996; de Sarro et al., 2001) or epilepsy-prone rats (GEPR-3 and GEPR-9) (Dailey et al., 1995). Moreover, in the amygdala kindling model, retigabine was able to reduce seizure severity and duration, total duration of behavioral changes, and after discharge duration showing higher potency compare to valproate (Tober et al., 1996). The drug also exhibited anticonvulsant activity in two pharmacoresistant epilepsy models; lamotrigine-resistant kindled rats (Postma et al., 2000) and in the 6 Hz psychomotor mouse model (Barton et al., 2001).

More recently, retigabine has been test in two heterozygous knock-in mice carrying BFNS causing mutations Y284C, A306T in KCNQ2 ($KCNQ2^{Y284C/+}$ and $KCNQ2^{A306T/+.}$ Here, after intraperitoneal injection of kainic acid, retigabine mitigated induced seizure activities in

both mice models, more significantly than phenobarbital (Ihara et al., 2016). However, retigabine has some known pharmacologic actions distinct from its effects on K_v7 channels; most notably, *in vitro* it potentiates $GABA_A$ receptor responses at similar or perhaps slightly higher concentrations than are effective on potassium channels (Otto et al., 2002).

In neuronal K_v7, retigabine recognizes an intracellular hydrophobic pocket located between the segments S5 and S6 in the pore domain (Main et al 2000). Within this cavity, a residue of tryptophan (W236 in $K_v7.2$. W265 in $K_v7.3$), present at the end of the S5 helix, was found to be crucial for the retigabine effect. Beside this residue, also other amino acids are involved in the binding of retigabine, like L243 in S5, L275 in the pore, L299/ and Gly301 in the S6 (according to $K_v7.2$ sequence); however, none of them seems to be critical as the tryptophan.

The key-role of this residue was confirmed by site-specific mutagenesis experiments; substitution of this residue with a leucine, resulted in a completely loss ability of retigabine to activate $K_v7.2$ currents (Schenzer et al., 2005; Wuttke et al., 2005).

In 2009 Lange and co-authors, hypothesized a generic hydrophobic interaction between the fluorophenyl ring of retigabine and the conserved tryptophan residue therefore (Lange et al., 2009). The binding mode involving this tryptophan residue and retigabine was fully elucidated by Kim and collaborators, using unnatural amino acid. They demonstrated that an H-bond interaction occurs between the carbamate group of retigabine, that acts as a H-bond acceptor (HBA) and the amino group of the tryptophan residue, that acts as a H-bond donor (HBD). This evidence suggested a “flip” conformation compared to the original proposed by Lange (Kim et al., 2015).

This binding mode was also observed in molecular docking and MD studies using a $K_v7.2$ pore homology model (Shi et al., 2020) and it was recently validated by MD studies using the publish Cryo-EM structures of the human $K_v7.2$ and $K_v7.4$ in complex with retigabine (Li X et al., 2021; Li T et al., 2021). Interestingly, in these models, further interaction sites were described: in both cases an H-bond interaction occurred between the aniline group of retigabine and the side chain of serine. Electrophysiological experiments showed a decreased activity of retigabine in the $K_v7.2$ S303A mutant (Li X et al., 2021) while the in $K_v7.4$ S309H retigabine activity was completely lost (Li T et al., 2021).

Moreover, in $K_v7.4$ MD simulations a π-π stacking contact was observed between fluorophenyl group of retigabine and the aromatic ring of F246 (F240 on $K_v7.2$); mutation of F246 to alanine partially abrogated the retigabine effect (Li T et al., 2021).

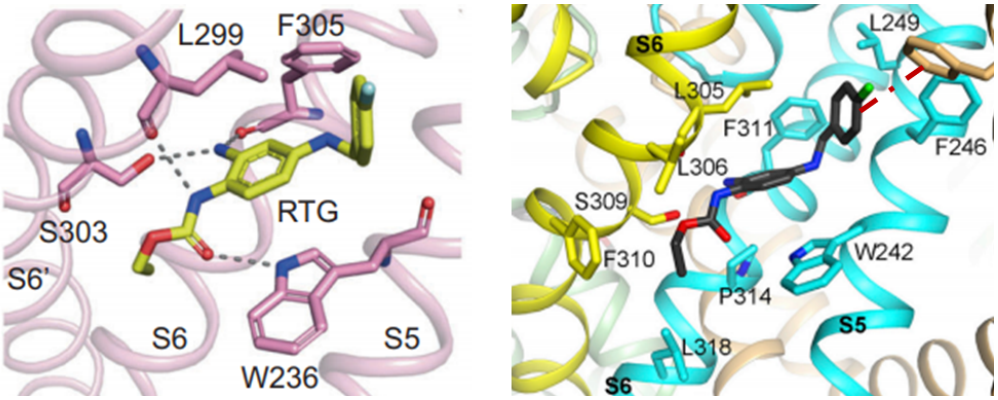

Figure 1.15. Localization of retigabine in $K_v7.2$ (left, from Li X et al., 2021) and $K_v7.4$ (right, from Li T et al., 2021)

Nevertheless, the precise structural basis for the activation mode remains enigmatic. Homology models of the closed and open conformations of the $K_v7.3$ PD suggested that π–π interactions of W265 in S5 and F343 in S6 were determinant for the stability of the PD closed conformation and that retigabine binding destabilized this π–π interaction in favor of the open channel conformation (Syeda et al., 2016). Alignment of the apo structure of $K_v7.2$ (without the ligand) and $K_v7.2$-retigabine, revealed that retigabine binding causes conformational changes mainly in the PD. By contrast, the VSD in $K_v7.2$-retigabine structure remained almost unchanged but displayed increased mobility upon retigabine binding (Li X et al., 2021). According, alignment of the apo structure of $K_v7.4$ and $K_v7.4$-retigabine revealed displacement of residues that are involved in ligand binding, as well as the movement of S5, that was transduced to the whole VSD through the S4-S5 linker (Li T et al., 2021). These conformational changes caused by the binding of retigabine provide a possible explanation for the activation mechanism on $K_v7.2$-5 channels, suggesting that retigabine acted as an allosteric modulator.

Despite its efficacy as anticonvulsant, retigabine clinical use was limited such that the company decide to discontinue its marked distribution in 2017. The limitations causing retigabine unfavourable risk/benefit ratio were:

I) *poor selectivity for K_v7 subtypes*. Indeed, activation of $K_v7.4$ and $K_v7.5$ channels expressed in genitourinary smooth muscle caused urinary retention (Brickel et al., 2012; Malysz and Petkov, 2020). Recently, this hypothesis has been questioned by Tykocki and colleagues which suggest that urological side effects of retigabine are due to activation of K_v7 channels in sensory nerves which decreases sensory outflow in the mouse urinary bladder (Tykocki et al., 2019).

II) *Short half-life*. The rapid metabolism by phase-II enzymes (acetylation and N-glucuronidation), leading to the requirement of a three-times-a-day dosing regimen (Barrese et al., 2010).

III) *Poor brain penetration.* Due to the limited lipophilicity (log P = 3.08) (Zhou et al., 2015)

IV) *Photo-induced dimers formation*. In 2013, the Food and Drug Administration (FDA) issued an alert that retigabine could induce retinal and muco-cutaneous blue-gray discoloration upon long-term use. This off-target effect was observed in patients treated for at least four years (Clark et al., 2015) with unclear consequences on vision and no information about the permanency of these alterations (Brickel et al., 2020). A proposed mechanism for formation of the phenazinium dimers, hypothesized by our research group, is depicted in figure 4.16 in chapter 4.

In animal models, considering pigmented (Long Evans) and albino (Wistar Han) rats, dimers have been detected only the eye tissues from the pigmented rats while they were absent non-melanin containing ocular tissues from the albino rats, demonstrating a high affinity of these by products to tissue containing melanin (Groseclose and Castellino, 2019).

Since retigabine has been discontinued, no drug acting on K_v7 channels is clinically available, therefore several companies and academic groups are pursuing the synthesis of novel retigabine derivatives with improved physico-chemical, pharmacokinetic, or pharmacodynamic properties (Bock and Link, 2019).

Retigabine and flupirtine derivatives

In 2015 Kalappa and colleagues, synthetized the fluroanilinic retigabine derivative **SF0034** (*for all structure molecules see Table 1.3*), obtained by introducing a fluorine atom at the 3-position of the aniline ring of retigabine. The compound appeared 5-times more potent than retigabine on $K_v7.2/7.3$ channels. Moreover, SF0034 showed reduced affinity for the channels associated with urinary retention side effect, such as $K_v7.4/7.5$ and more chemical stability compared to retigabine. In fact, incorporation of an electron-withdrawing atom on the aniline ring of retigabine reduce the oxidation and the consequent dimers formation. Considering *in vivo* model, in the MES and corneal kindled seizure models SF0034 was significantly more potent than retigabine (Kalappa et al., 2015)

Considering the structure of SF0034, in 2016 by Kumar and collaborators synthetized the **RL-81**, characterized by a CF3-group at the 4-position of the benzylamine moiety,

combined with the fluorine atom on the aniline ring. Compered to SF0034, RL-81 has been reported to be 3- times more potent in activating K_v7.2/7.3 channels. As well as SF0034, RL-81 appears to preferentially target K_v7.2/7.3 channels over K_v7.4/7.5 channels, thus obtaining a compound more potent, selective, and stable than retigabine (Kumar et al., 2016). Similarly, to retigabine, conserved residue W236 is necessary for SF0034, and RL-81 activity. In both cases, gating effect on K_v7.2 channels are abolished upon substitution of W236 to L (leucine) suggesting that these analogues share the same binding site.

Starting from the RL-81 as new lead compound, Liu and co-authors synthetized 19 newly analogues. Several molecules exhibited an improved selectivity on K_v7.2/7.3 over the other tested channels (e.g., K_v7.3/7.5, K_v7.4, and K_v7.4/7.5) specifically, **RL-36** and **RL-12** resulted more potent on K_v7.2/7.3 than K_v7.3/7.5, K_v7.4 and K_v7.4/7.5. The authors also identified an analogue of RL-81, **RL-56**, remarkably potent on K_v7.2/7.3 compared to lead compound (Liu et al., 2019).

As reported previously, one of the limits of retigabine is our poor brain penetration, lead to the limited lipophilicity. To overcome them, by introducing a propargyl group at the N4 position of the retigabine linker, the so-called **P-retigabine** has been developed. The compound showed an increased brain-to-plasma ratio equal to 2.30 versus 0.16 for retigabine, while electrophysiological experiment demonstrated that P-retigabine was more potent than retigabine on K_v7.2. In *in vivo* models, P-retigabine exhibits an improved antiepileptic activity anticonvulsant less toxicity when compared to retigabine (Zhou et al., 2015). Upon deleting the ortho liable −NH2 group and installing two adjacent methyl groups to the carbamate motif of P-retigabine, the same group generated the **HN37** (pynegabine), which exhibited enhanced activation potency toward neuronal K_v7 channels and high *in vivo* efficacy in a range of pre-clinical seizure models, including the maximal electroshock test and a 6 Hz model of pharmacoresistant limbic seizures. With its improved chemical stability, strong efficacy, and better safety margin, HN37 has progressed to clinical trial in China for epilepsy treatment (Zhang et al., 2021).

Based on P-retigabine structure, the N-3 tertiary butyl substituted compound has been synthesized. The so-called **compound 10g**, exhibited a highly selectivity to K_v7.4 and K_v7.5 channels without potentiating the other subtypes of the family. Mainly, the compound increased current the current amplitude, with no effect on the voltage-dependent activation curves probably because, according to authors, G-V shift should be sensitive to N3 structure alterations (Wang et al., 2018a).

To obtain more stable compounds another strategy has been to replace the secondary amine linker by a sulphur atom. With this approach Bock and colleagues have produced a series flupirtine/retigabine derivatives which showed a strong less oxidative behaviour and a pharmacological activity retained or even increased. For example, flupirtine analogue **compound 48**, showed an enhanced potency on K_v7.2/7.3, improved toxicity/activity ratio and the same efficacy as retigabine while **compound 36** showed the same potency and efficacy as flupirtine but less toxicity (Bock et al., 2019).

Another flupirtine/retigabine chemical analogue is **NS15370**, a potent K_v7.2-K_v7.5 channels activator. NS15370 is effective in rodent models of partial epilepsy the 6 Hz seizures and rat amygdala kindling providing full protection against discharges (Dalby-Brown et al., 2013).

To remove the aniline ring of the retigabine, responsible for dimers formation, a series of dimethoxy-pyrimidines have been synthesized by Davoren and colleagues. Among them the lead compound **PF-05020182**, in which the aniline structure and carbamate at the 5-position have been replaced with a 4,6-dimethoxypyrimidine and an amide respectively, showed: potent K_v7.2/7.3 channel opener activity, no effect over the cardiac K_v7.1/KCNE1 channels and anticonvulsant activity in the MES model (Davoren et al., 2015).

Based on the structure of retigabine and PF-05020182, using a hybridization drug design strategy, a novel series of substituted piperidine derivatives were obtained by replacing the carbamate group with an amide group and two methyl groups into the core phenyl scaffold. Between these, **compound 11** displayed a better activity than retigabine on K_v7.2, a slightly higher potency *in vitro* and a good pharmacokinetic profile in rat (Yang et al., 2018a). Piperidine derivatives were subsequently optimized by the authors who synthesized a novel series of N-phenylbutanamide derivatives. Several molecules were found to be potent K_v7 openers in Rb^+ flow assay, in particular **compound 1** emerged for its higher potency than retigabine in Rb^+ flow assay. Subsequently tested by patch-clamp, compound 1 showed higher efficacy in leftward shifting the $V_{1/2}$ compared to retigabine. A significant anticonvulsant activity in MES model with no adverse effects and good brain permeability was also exhibit (Yang et al., 2018b).

To reduce the formation of dimers responsible for the mucocutaneous discoloration induced by long-term use of retigabine, Surur and colleagues applied a retro-metabolic drug design strategy; starting for the dimers structure, they synthesized a series of 43 compounds were the amino groups supposed to be involved in the dimerization reaction are modified. Two derivatives emerged: the **compound 22d** was more potent that

retigabine in activating K_v7.2/7.3 channels, but it displayed limited aqueous solubility; the **compound 25b** was less potent than compound 22d but more soluble in aqueous solutions and showed a safe hepatoxicity profiles *in vitro* (Surur et al., 2019). The same research group also tried a ligand-based design strategy, replacing amino substituents of the triaminoaryl core with alkyl substituents, generating led carba analogues of flupirtine and retigabine with improved oxidation resistance and negligible risk of quinoid metabolite formation, as observed the N-1/3 dicarba analogues **35a** and **43b**, displaying a good submicromolar K_v7.2/7.3 opening activity, no critical toxicity *in vitro and* improved oxidation stability (Wurm et al., 2022a). The author further attempted to separate retigabine and flupirtine activity from toxicity by employing a drug design strategy to avoid the detrimental oxidation of the central aromatic ring. The inversion of the amide group (forming a nicotinamide central scaffold) together with an additional methil group in ortho position respect to the amide group, resulted in **compound 36b**, a flupirtine analogue showed potent K_v7.2/7.3 opening activity, being six times as active as flupirtine itself, and by design is devoid of the potential for azaquinone diimine formation (Wurm et al., 2022b). A further attempt to increase K_v7.2/7.3 opening ability was made by introducing a morpholino substituent and a 2,2,2-trifluoroethoxy group in the structure of compound 36b. The resulting **compound 18c** was 150 times more potent than flupirtine and 20 times more potent than retigabine in activating K_v7.2/7.3 channel in a fluorescence-based assay. Compound 18c also showed a superior toxicity/activity ratio, but also a low water solubility (Wurm et al., 2023).

A different strategy to improved chemical stability was explored by Ostacolo and collaborators who synthesized three different series of conformationally restricted retigabine analogues. Among 42 tested compounds, the two selected **compounds 23a** and **24a** were able to increase K_v7.2 currents more than retigabine at −40 mV and at 0 mV. Compared to the reference compound, compounds 23a and 24a exhibited slow ON/OFF kinetics due to their increased hydrophobicity, a very important aspect since, as report previously, one limit of retigabine is its poor brain penetration, a pharmacokinetic drawback that might be improved by the increased hydrophobicity. Additionally, compared to retigabine compound 23a showed higher potency on K_v7.2 channels, whereas no change in potency was observed for 24a. Furthermore, both derivatives showed higher potency in activating heteromeric K_v7.2/7.3 and homomeric K_v7.4 channels (Ostacolo et al., 2020).

Lately, Xenon Pharma has developed the **XEN1101,** a K_v7 potassium channel modulator, chemically designed to improve potency, selectivity, pharmacokinetics, and chemical stability of retigabine. Currently Xenon has initiated a Phase IIb clinical trial with XEN1101. Moreover, Xenon has initiated a Phase III randomized, double-blind, placebo-controlled, parallel group, multicenter clinical trial, called the "EPIK" study, evaluating the efficacy, safety, and tolerability of **XEN496,** a pediatric formulation of retigabine, administered as adjunctive treatment in approximately 40 pediatric patients aged one month to less than 6 years with KCNQ2-DEE.

Table 1.3. Flupirtine, Retigabine and Derivatives

Compound Name	Structure
Flupirtine	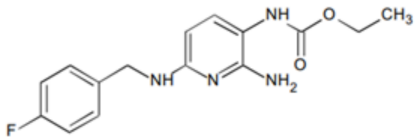
Retigabine	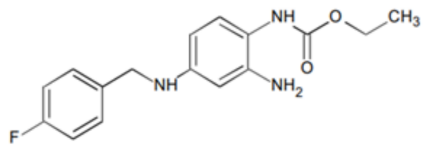
SF0034	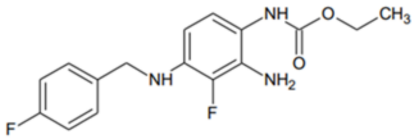
RL-81	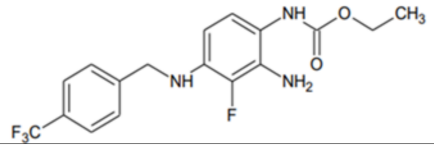
RL-12	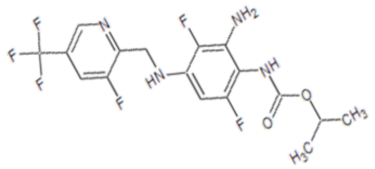
RL-36	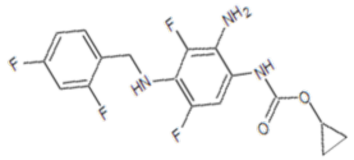
RL-56	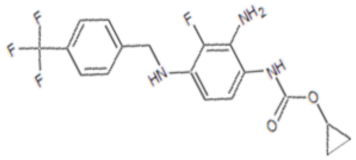

P-Retigabine	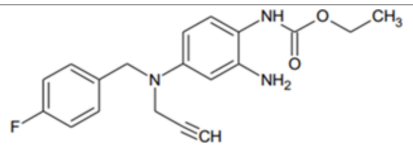
HN37 (pyne-retigabine)	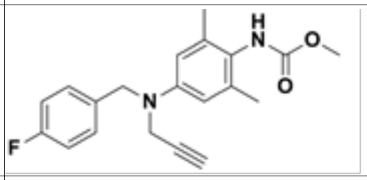
Compound 10g	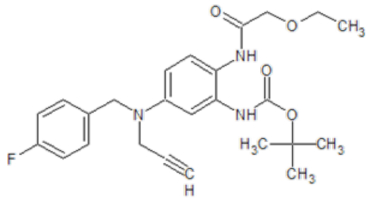
Compound 48	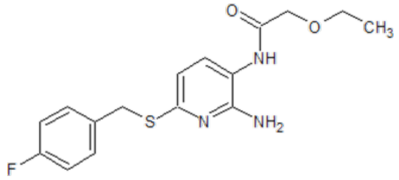
Compound 36	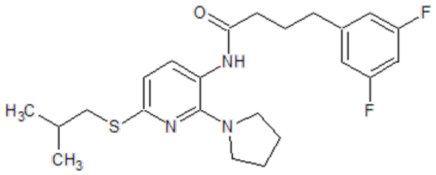
NS15370	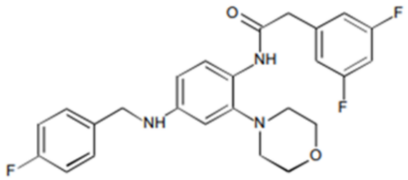
PF-05020182	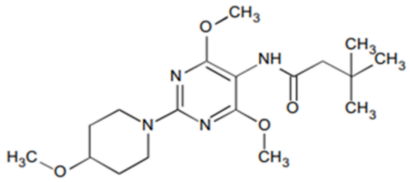
Compound 11	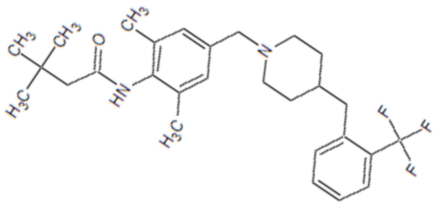
Compound 1	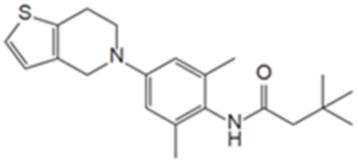

Compound 22d	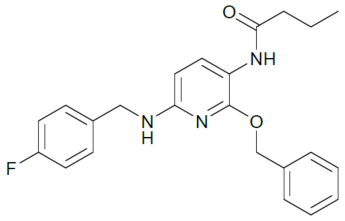
Compound 25b	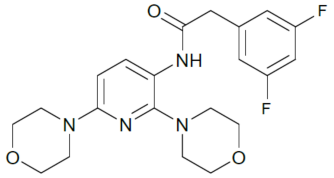
Compound 35a	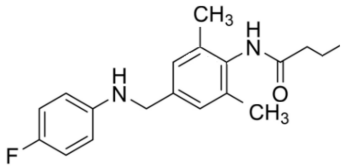
Compound 43b	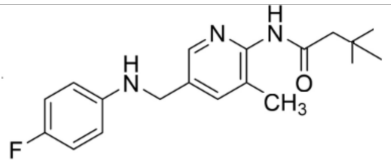
Compound 36b	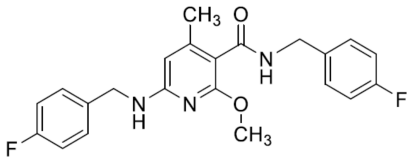
Compound 18c	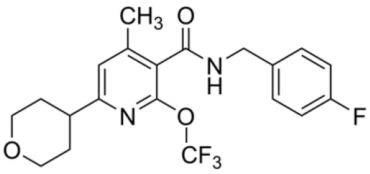
Compound 23a	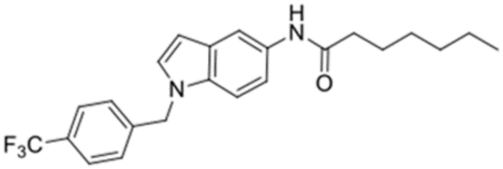
Compound 24a	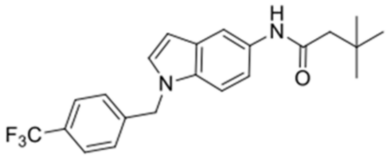
XEN1101	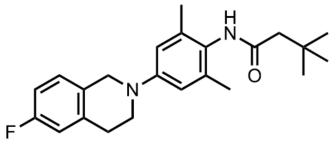

1.3.1.9.2 Acrylamides

Besides flupirtine and retigabine, other molecules act as potent K_v7 channels activators, like compounds belonging to the class of the acrylamide. Developed by the Bristol-Myers Squibb Pharmaceutical Research Institute, the fluoro-oxindoles **BMS-204352** (*for all structure molecules see Table 1.4*) represent the first acrylamide synthetized. Originally described as an agonist of calcium-activated potassium channels (BK channels) indicated for the treatment of ischemic stroke (Gribkoff et al., 2000), BMS- 204352 was also active on $K_v7.4$ channels, producing a leftward shift of the activation curve and an increase in the maximal current, with a potency similar to retigabine (Schroder et al., 2001).

Later, the Bristol-Myers Squibb, synthesized the so called **(S)-1** compound, a $K_v7.2$ opener with excellent oral bioavailability, showing positive effect in a cortical spreading depression model of migraine (Wu et al., 2003a) (S)-1 exhibited opposite effect on cardiac and neuronal K_v7 channels, acting as a blocker of $K_v7.1$ and $K_v7.1$/KCNE1 current whereas enhancing $K_v7.4$ and $K_v7.5$ maximal current amplitude at all potentials, contrary to $K_v7.2$ and $K_v7.2/7.3$, in which the activation/block of was strongly voltage-dependent (Bentzen et al., 2006).

Since (S)-1 compound leading to the formation of a reactive intermediate found to be responsible for CYP3A4 metabolism-dependent inhibition, subsequent structural optimization yielded to the **BMS-568274**, a difluoro analogue which does not alter CYP3A4 metabolism, thus showing lesser potential for pharmacokinetic interactions (Wu et al., 2003b).

In the search for more powerful compounds, the **(S)-2** compound was developed. (S)-2 displayed a profound hyperpolarizing shift in the voltage-dependence of activation of $K_v7.2$; also, it was able to reduces spontaneous neuronal discharges in rat hippocampal slices (Wu et al., 2004a). Following structure modification of (S)-2 lead to identification **(S)-3, (S)-4,** and **(S)-5** derivatives. Notably, (S)-3 was most potent but less efficacious compared to (S)-2, while (S)-4 and (S)-5 showed moderate potency but improved efficacy over (S)-2, (S)-3 and retigabine. Moreover, is important to underling that the (R)-enantiomers of these compounds did not show any opener activity on $K_v7.2$, thus suggesting a strong stereoselectivity (Wu et al., 2004b).

Two biaryl ether acrylamides, **(S)-6**, and **(S)-7**, have been later synthetized: the (S)-6 derivative, in particular, is a strong $K_v7.2$ and shown significant efficacy in the treatment of neuropathic pain (Wu et al., 2013).

Finally, an analogue of acrylamide (S)-2, called **SMB-1**, showed a unique profile of action on K_v7 channels; inhibiting $K_v7.2$ and activating $K_v7.4$ channels (Blom et al., 2014). According to acrylamides binding site, (S)-1 and SMB-1 binds within the same pocket as retigabine; in both case the activity on $K_v7.4$ was critically dependent on the tryptophan residue in S5 (Bentzen et al., 2006).

Table 1.4. Acrylamides structures

Compound Name	Structure
BMS- 204352	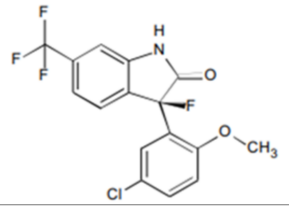
(S)-1	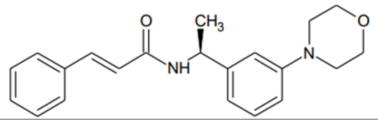
BMS-568274	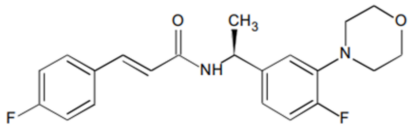
(S)-2	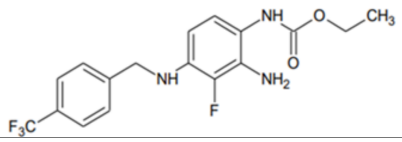
(S)-3	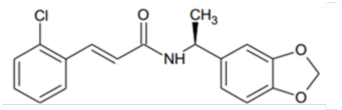
(S)-4	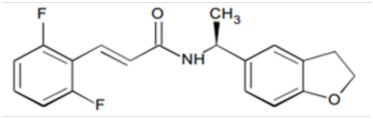
(S)-5	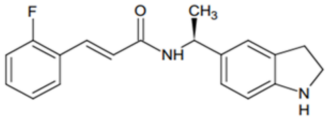
(S)-6	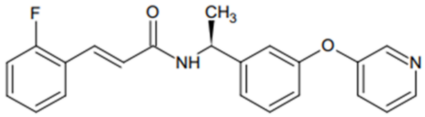
(S)-7	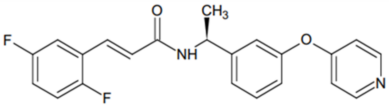

SBM-1	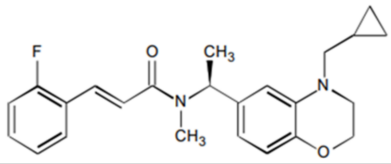

1.3.1.9.3 Benzamides

Belonging the class of benzamides the compound **ICA-27243** (*for all structure molecules see Table 1.5*), represent the first benzamide described as a strong K_v7 activator. It caused a strong hyperpolarizing shift in the voltage-dependence of activation in $K_v7.2/7.3$ channel, but was less active on $K_v7.4$ and $K_v7.3/7.5$ channels. No effect on GABA-activated chloride channels, Na_v 1.2 or voltage-gated calcium channels have been reported. In addition, ICA-27243 suppresses seizure-like activity in an *ex vivo* hippocampal slice model and exhibits anticonvulsant activity in a broad spectrum of seizure animal models such as MES, PTZ-induced seizures, amygdala kindling model of partial seizures and in the 6-Hz model of psychomotor seizures (Wickenden et al., 2008; Roeffols et al., 2008). For these reasons, **ICA-27243** represented a good antiepileptic candidate, even though toxicity studies showed that repetitive dosages of the drug-induced non hemolytic anemia in animal models.

Therefore, novel N-pyridyl benzamides derivatives were synthesized, like the **ICA-069673**, an orally active compound effective in several animal models of epilepsy, with good pharmacokinetic properties and higher selectivity on $K_v7.2/7.3$ over $K_v7.3/7.5$ (Amato et al., 2011).

Another compound belonging to the class of benzamides is **ICA-110381** which predominantly activates $K_v7.2$ causing a hyperpolarizing shift in channel activation and a slowing of channel deactivation. ICA-110381 showed anticonvulsant activity in the amygdala kindling model by reducing seizure severity and duration (Boehlen et al., 2013).

A HTS of ChemBridge Diverset™ library composed by 20,000 compounds allowed the identification of the benzamide **ztz240**, structurally similar to ICA-27243. On $K_v7.2$ ztz240 produced a significant increase in outward current amplitude, a slowing in deactivation kinetics, and a marked left-shift on the voltage activation curve. On the other hand, ztz240 potentiates $K_v7.4$ and $K_v7.5$ more than $K_v7.2$, in terms of current amplitude whereas, the left shift of activation was similar. Finally, $K_v7.3$ and $K_v7.1$ were insensitive to the compound (Gao et al., 2010).

Compared to retigabine and acrylamides, the compounds belonging to the class of benzamides show a different binding site. While retigabine binds in a hydrophobic pocket in the PD, benzamides bind to the VSD (Padilla et al., 2009), indeed the K_v7.2 W236L mutant channel was sensitive to both ICA compounds and ztz240 (Padilla et al., 2009; Gao et al., 2010; Boehlen et al., 2013). Recently it has been demonstrated that these compounds not only differ for the binding site but also for the subunit stoichiometry needed to evoke their effects, indeed, while for retigabine a single subunit is sufficient to produce the near-maximal effect (Yau et al., 2018), all four subunits are required for maximal sensitivity to ICA-069673 and even a single insensitive subunit leads to significantly diminished effects (Wang et al., 2018b).

To understand which residues in VDS are involved in the binding of these compounds mutagenesis experiments were conducted. Considering the ztz240, the phenylalanine in position 137 (highly conserved in the family of K_v channels) was found to be critical for the activity of the compound, and when mutated with an alanine (F137A) dramatically reduced the effect of ztz240 on K_v7.2. Also, other residues seemed important like E130, I134, G138, R207 (Li P et al., 2013). Regarding ICA-069673, Wang and co-workers demonstrated that the two residues F168 and A181 in the S3 segment appear essential for its activity (Wang et al., 2017). More recently, cryo-EM structures of the human K_v7.2 in complex with ztz240 has been obtained (Li X et al., 2020), confirming that the binding site is located between the S3 and S4 segments in the VSD and residues F137, I171, D172, R207, R210 are involved in ztz240 binding. Indeed, electrophysiology experiments performed on F137A, D172A, and R210Q mutants, in presence of ztz240, revealed a reduced increase of outward current amplitude ratio and prevented or attenuated the left-shift of the curve. Furthermore, R207Q attenuated the left-shift of the curve without changing the outward current amplitude whereas mutation I171A decreased the outward current amplitude with no effect on the voltage activation. It is important to note that residues involved in the interactions with the ztz240 are less conserved in K_v7.1 or K_v7.3. This could explain the lesser sensitivity of these two K_v7 family subtypes to ztz240 (Li X et al., 2020).

Table 1.5. Benzamides structure

Compound Name	Structure

ICA-27243	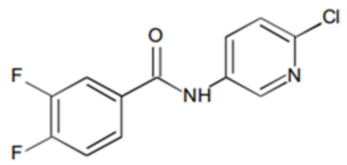
ICA-069673	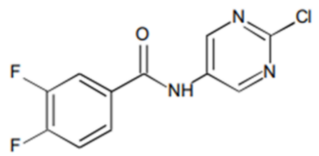
ICA-110381	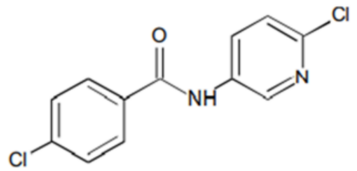
ztz240	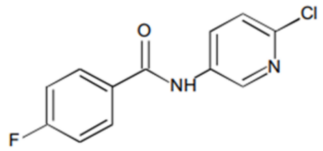

1.3.1.9.4 Fenamates

Belonging to the family of fenamates, **meclofenamic acid** (*for all structure molecules see Table 1.6)* and **diclofenac**, two well-known nonsteroidal anti-inflammatory drugs acting as non-selective inhibitors of the COX-1 and COX-2 cyclooxygenases, activate K_v7 potassium channel. Mainly these two compounds activate $K_v7.2/7.3$ channels, by causing a leftward shift in the voltage-dependent gating of the channel and slowing the deactivation kinetics while no effects are elicited on cardiac $K_v7.1$ channel (Peretz et al., 2005). Moreover, diclofenac also exhibits anticonvulsant activity in MES model.

To separate the I_{KM}-opening property from COX inhibition activity, several derivatives have been developed. Among them, the diclofenac derivative **NH6** was obtained by adding a diethylene glycol tail to the carboxylic acid group of the molecule. On $K_v7.2/7.3$ channels, NH6 caused a hyperpolarizing shift of the voltage activation curve and markedly slowing of the deactivation kinetics whereas it did not affect homomeric $K_v7.1$ and heteromeric $K_v7.1$/KCNE1 currents. In cortical, hippocampal, and dorsal root ganglion (DRG) neurons the compounds strongly reduced the number of evoked and spontaneous action potentials while in hippocampal slices it decreased somatically evoked spike afterdepolarization of CA1 pyramidal neurons. By activating K_v7 channels, NH6 decreased the frequency of

miniature excitatory (mEPSC) and inhibitory (mIPSC) postsynaptic currents with no modification in their amplitude and waveform (Peretz et al., 2007).

The second derivative of diclofenac called **NH29** was able to increase $K_v7.2$ currents, produced a hyperpolarizing shift in the gating of the channel, and significantly enhanced both activation and deactivation kinetics of $K_v7.2$ channels, whereas like the other members of the family it failed to activate homomeric $K_v7.1$. In DRG neurons and primary cultures of hippocampal neurons **NH29** reduced the number of evoked spikes and depressed synaptic transmission, respectively. NH29 was active in retigabine-insensitive $K_v7.2$ W236L channels suggesting that did not interact with the retigabine binding site on $K_v7.2$. Docking studies have demonstrated that NH29 binds a pocket in the VSD formed by K120 in the S1-S2 loop, Y127 and E130 in helix S2, and L200 and R207 in S4. Here, the nitro group of one aromatic ring of NH29 forms a hydrogen bond with the guanidinium group of R207 and the carboxylate of E130 (Peretz et al., 2007).

Table 1.6. Fenamates structure

Compound Name	Structure
Diclofenac	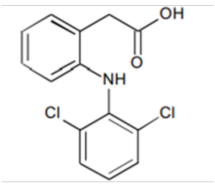
Meclofenamic acid	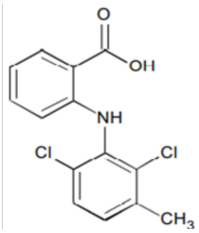
NH6	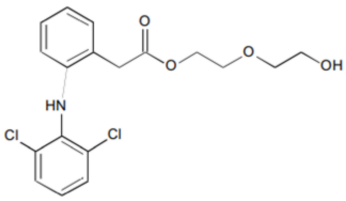
NH29	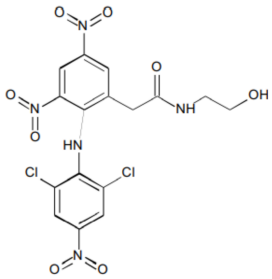

1.3.1.9.5 Other chemotypes of neuronal K_v7 activators

In 2011 Yu and co-workers screening the NIH Molecular Libraries Small Molecule Repository (MLSMR) containing 300, 000 molecules, identified the compound **ML-213** (*for all structure molecules see Table 1.7*). The authors reported that this molecule activated preferentially $K_v7.2$ and $K_v7.4$ channels (Yu et al., 2011), although it was later found to be a pan $K_v7.2$-7.5 activator (Kanyo et al., 2020). Subsequent studies performed in A7r5 vascular smooth muscle cell line, have shown that ML-213, was a potent and effective activator of homomeric $K_v7.5$ and heteromeric $K_v7.4/7.5$ channels and was able to increase the maximum conductance, to negatively shift of their activation curves and to decrease the current deactivation rates. Substitution of the tryptophan residue at position 235 of $K_v7.5$ and 242 of $K_v7.4$ to leucine (W235L/W242L), abolished the effects of ML-213 on $K_v7.5$ and $K_v7.4$ demonstrating that the compound recognized the same binding site of retigabine (Brueggemann et al., 2014).

Zinc Pyrithione (ZnPy), a compound used for the treatment of psoriasis and dandruff control, has been demonstrated to be a potent activator of K_v7 channels, except for $K_v7.3$ and $K_v7.1$/KCNE1 subunits. This molecule produced an increase in open probability, a leftward shift in the activation process and a reduction in the deactivation rate (Xiong et al., 2007). The binding site is located within the pore, but unlike retigabine ZnPy is active in retigabine-insensitive $K_v7.2$ W236L channels suggesting that this residue is not essential for the activity. Moreover, mutagenesis studies based on $K_v7.2$ channels have revealed that residues L249 in S5, L275 between S5 and the pore region, and A306 in segment S6 play an important role (Xiong et al., 2008).

A HTS of a library of 80,000 compounds enabled the identification of two novel $K_v7.2$ activators, the amide **ZG1732** and the benzothiophene **ZG2083**. The two selected compounds increased the outward $K_v7.2$ currents and left shifted the activation curve, at micromolar concentrations (Yue et al., 2016).

The compound **NS1643**, reported as an opener of K_v11 channels, is also a K_v7 channel activator; in fact, NS1643 potentiated homomeric $K_v7.2$, $K_v7.4$, and heteromeric $K_v7.2/7.3$, but not cardiac $K_v7.1$ channel. When tested on $K_v7.2$ channels, NS1643 left shifted the activation curve and slowed deactivation (Li et al., 2014).

Benzbromarone (BBR), an inhibitor of urate transporters, has been recently demonstrated to activate K_v7 channels. BBR shows promising antinociceptive effects,

consistently attenuating bradikinin-, formalin-, or monosodium urate-induced inflammatory pain in rat and mouse models (Zheng et al., 2015).

At the American Epilepsy Society's 2019 meeting, Knopp Biosciences presented a new K_v7 channel activator, compound **KB-3061**, described as a potent $K_v7.2/7.3$ channel activator studied for the treatment of KCNQ2-Neonatal Epileptic Encephalopathy (Picchione et al., 2019).

The 4- aminotetrahydroquinoline **ZK-21** is a potent $K_v7.2$ activator. Its structure represented a novel K_v7 activator chemotype identified by Hernandez and colleagues screening an in-house library of compounds through an electrophysiological HTS. Since ZK-21 lost activity in the $K_v7.2$W236L mutant, this new lead structure is likely to occupy the same pore region S5 binding site as retigabine and the RL-series of compounds (Hernandez et al., 2022).

Compound **GRT-X** was synthesized during a search for novel analgesics acting on K_v7 channels (Kühnert et al., 2012). This K_v7 allosteric modulator lacks a GABAergic component (Bloms-Funke et al., 2022a). In a receptor and ion channel screen, the mitochondrial translocator protein 18 kDa (TSPO) receptor was identified as the only other target of GRT-X in addition to K_v7 potassium channels. Subsequent *in vitro* and *in vivo* experiments showed that GRT-X acts as an activator at the TSPO receptor, stimulating the synthesis of GABAmimetic neurosteroids such as allopregnanolone in the rat brain (Bloms-Funke et al., 2022a). GRT-X is the first drug combining an agonistic effect at K_v7 and TSPO receptors. When its antiseizure efficacy was compared to that of retigabine in six different rodent epilepsy models, GRT-X was more effective than retigabine in three of the tested models, the most important difference being the high efficacy in the 6-Hz seizure model in mice (Bloms-Funke et al., 2022b).

Table 1.7. Structure of other chemotypes of neuronal K_v7 activators

Compound Name	Structure
ML213	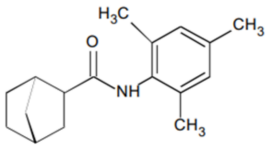
ZnPy	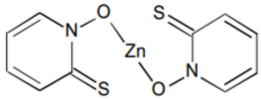

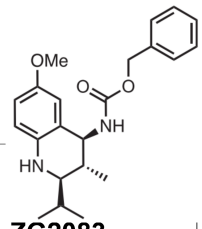	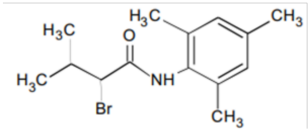
ZG2083	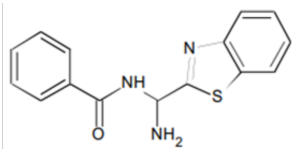
NS1643	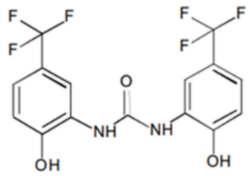
Benzbromarone	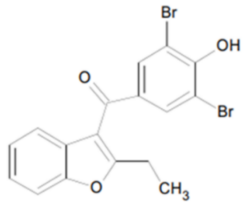
KB-3061	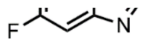
GRT-X	
ZK-21	

1.3.1.9.6 Gaba, gabapentinoids, and ketogenic diet

The hypothesis that endogenous ligand, with similar chemical properties to retigabine, were able to bind the conserved tryptophane residue in S5 of K_v7 channels was pursued for the first time by Manville and colleagues. The authors found that the primary inhibitory neurotransmitter **GABA**, containing a negative electrostatic surface potential cantered on a carbonyl group (like retigabine), interacted with $K_v7.2$–5 tryptophane; electrophysiological recordings showed that $K_v7.3$, $K_v7.5$ and $K_v7.2/7.3$ channels, were activated by GABA, which caused a negative-shifts in the voltage activation current (Manville et al., 2018b).

Because of the structural similarities with GABA, the authors, hypothesized that **gabapentin** and **pregabalin** could modulate K_v7 channels. The results obtained showed that gabapentin, but not pregabalin, was a potent activator of the heteromeric $K_v7.2/7.3$ and homomeric $K_v7.3$, $K_v7.5$ channels, exhibiting nanomolar potency (Manville et al., 2018c) But was ineffective in $K_v7.2$ and $K_v7.4$ channels. Gabapentin activation of $K_v7.2/7.3$ or homomeric $K_v7.3$ channels requires $K_v7.3$-W265 residue, the conserved tryptophan in segment S5. Pregabalin failed to activate $K_v7.2/7.3$ because it lacks of the negative electrostatic surface potential close to carbonyl group (Manville et al., 2018). More recently, gabapentin has been used for the first time as a precision treatment in a DEE-affected child carrying a *de novo* LoF in KCNQ2 (Soldovieri et al, 2020).

Two related endogenous metabolites of GABA, **β-hydroxybutyric acid (BHB)** and **γ-amino-β-hydroxybutyric acid (GABOB)** have been reported to activate $K_v7.2/7.3$. BHB, the primary ketone body generated by ketosis, directly activated $K_v7.2/7.3$ channels and exhibited an anticonvulsant activity in the PTZ seizure assay in mice. Also, GABOB activated $K_v7.2/7.3$ channels with high affinity and lower efficacy than GABA or BHB. In addition, GABOB acted as a partial agonist and competed with GABA, retigabine and BHB for the same binding site (Manville et al., 2020). Among non-pharmacological therapies, the ketogenic diet has been shown to be particularly effective in children with DEE caused by KCNQ2 variants (Ko et al., 2018). More recently, Miceli and co-authors have demonstrated that BHB was able to reverse channel dysfunction induced by the $K_v7.3$-M240R variant identified in a SeLFNS family (Miceli et al., 2020).

1.3.1.9.7 Polyunsaturated fatty acids (PUFA) and endocannabinoids

Polyunsaturated fatty acids (PUFAs) are naturally occurring lipids formed by a carboxyl head group and an unbranched hydrocarbon tail, that contains two or more double bonds in *cis* conformation. PUFA are part of the human diet and cannot be formed de novo in the human body, but they can be transformed in the body to generate other desired PUFA species, such as triacylglycerols and phospholipids.

PUFA, generated from the hydrolysis of phospholipids by phospholipases, can interact with membrane proteins, such as ionic channels. It was observed that PUFA can potentiate K_v channels (Borjesson et al. 2008). In particular, **PUFAs** can activate $K_v7.1$ (Liin et al 2015), $K_v7.2/7.3$ (Liin et al., 2016) and $K_v7.5$ (Frampton et al., 2022) inducing a shift in the voltage dependence of the channels and an increase of the maximum conductance observed at the most positive voltages. The molecular hypothesis for K_v7 PUFAs activation involved electrostatic interactions between positively charged arginine in

the upper half of S4 of the VSD and the negatively charged head group on PUFAs (and their analogues) (Yadzi et al., 2021; Liin et al., 2018).

Interestingly, PUFAs showed an opposite effect in $K_v7.4$, where they inhibit activation of the channel by shifting the voltage dependence toward more positive voltages. In $K_v7.4$ PUFAs bind to a different region compared to the other K_v7 channels (Frampton et al., 2022) and this is a possible explanation for their different mechanism of action in this channel.

Endocannabinoids are a class of bioactive lipids that bind to cannabinoid receptors. The endocannabinoids are PUFA-related substances and recently they have been described as K_v7 channels activators.

Arachidonoyl-L-Serine (**ARA-S**), an arachidonic acid–based endocannabinoids, was identified as a potent activator of $K_v7.2/7.3$, $K_v7.1$ and $K_v7.5$ but not $K_v7.4$, which instead was inhibited. Interestingly, Larson and colleagues found that co-application of ARA-S and retigabine allowed to use lower concentrations of both drugs to still observe a $K_v7.2/7.3$ channel opening effect, without activation of other K_v7 subtypes (Larson et al., 2020).

Other endocannabinoids, as well as the cannabidiol (**CBD**) were also recently reported to act as agonists for K_v7 channels in heterologous CHO cells, as well as in superior cervical ganglion, and hippocampal neurons (Incontro et al., 2021; Zhang et al., 2022).

1.3.1.9.8 Traditional medicine

In recent years, several plant compounds have proven effective in activating K_v7 potassium channels. Two components of *M. oppositifolius* leaf extract, **mallotoxin (MTX)** and **isovaleric acid (IVA)** have been reported to be potent activator of $K_v7.2$ channels, synergistically activate $K_v7.2/7.3$ and protect against tonic seizures and associated mortality in PTZ mouse model. MTX and IVA bind the same binding pocket of retigabine, but mutagenesis results indicate a differential requirement of W236/W265. The presence of these residues was not required for MTX binding, by contrast, was essential for IVA on activating $K_v7.2/7.3$. Retigabine might synergize with MTX and/or IVA, converting $K_v7.2/7.3$ it into a voltage-independent channel (Manville et al., 2018a). The compound **E-2-dodecenal** contained in methanolic cilantro leaf extracts (*Coriandrum sativum*) activated preferentially $K_v7.2$ and $K_v7.5$ while lesser effects were produced on $K_v7.1$ and $K_v7.4$ and no effect on $K_v7.3$. Finally.$K_v7.2/7.3$ channels were highly sensitive. Consistent with docking studies, mutagenesis experiments confirmed that $K_v7.2$–W236 residue in S5 and $K_v7.2$–R213 in the S4–S5 were both required for E-2-dodecenal effects in $K_v7.2/7.3$

channels (Manville et al., 2019a). Additionally, E-2-dodecenal showed anticonvulsant activity in PTZ model. **Aloperine**, extracted from the *Sophora flavescens* specifically activated $K_v7.5$ channel with nanomolar potency and required $K_v7.5$–R212 residue for both binding and activation. In the vasculature, channels formed by $K_v7.5$ alone or complex with $K_v7.4$ are a potential target for blood pressure control medications (Manville et al., 2019b).

Quercitin, a flavonoid present in the *Capparis spinosa* extract, was found to potentiate $K_v7.1$/KCNE1, $K_v7.2/7.3$ and $K_v7.4$ currents but not $K_v7.5$. Strikingly, quercetin augmented both activation and inactivation of $K_v7.1$ via a unique $K_v7.1$ activation mechanism involving sites atop the voltage sensor and in the pore (Redford and Abbott, 2020).
Abbott and colleagues tested the effect of five plant-extracts derived from Native American traditional medicine as analgesics and gastrointestinal therapeutics (*A. menziesii, A. glandulosa, U. dioica, P. munitum,* and *H. maximum*) on $K_v7.2/7.3$ channels. They found that **tannic acid**, **gallic acid** and quercetin were the principal K_v7 active compounds in the extracts. In particular, tannic acid increased $K_v7.2/7.3$ current at hyperpolarized potentials, and gallic acid to a lesser extent. Moreover, while tannic acid also activated $K_v7.1$ and $K_v7.1$/KCNE1 at hyperpolarized, negative membrane potentials, it inhibited $K_v7.1$-KCNE3 at both negative and positive membrane potentials (Abbott et al., 2021).

1.4 The need for new antiseizures medications

Epilepsy is most commonly treated with antiseizures medications (ASMs), also called anti-epileptic drugs (AEDs), administered chronically with the intent of preventing the occurrence of epileptic seizures.

From the first reported use of bromide for seizure control in 1850s, more than 20 ASMs have been introduced with the aim of providing better efficacy or safety profile than the previous drugs.

ASMs approved prior to 1989 are generally referred to as “first-generation”, those introduced after as “second-generation”. The more recently approved agents that either represent improvement on a classic drug family or have new mechanisms of action, are often considered as “third-generation” ASMs. Compared to the first-generation ASMs, some of the second and third generation ASMs demonstrated similar efficacy in seizure control while having more favourable pharmacokinetics and drug interaction profiles (Chen, Brodie and Kwan, 2020) (Figure 1.16).

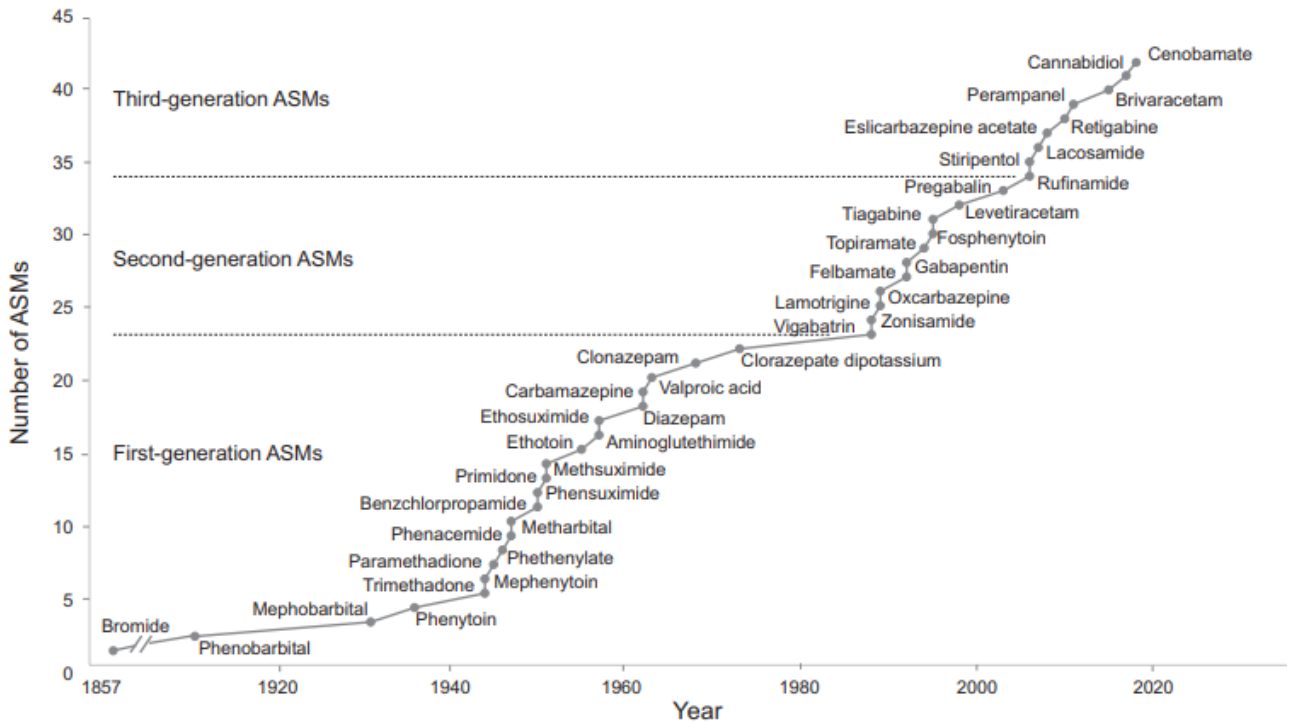

Figure 1.16 Chronological development of antiseizure medications (ASMs) according to the year they were first approved. (From *Chen, Brodie and Kwan, 2020*)

ASMs mechanisms of action can be classified into four basic subdivisions:

1) regulation of voltage-gated sodium channels (e.g., phenytoin, carbamazepine), voltage-gated calcium channels (e.g., ethosuximide), or voltage-gated potassium channels (e.g., retigabine);

2) augmentation of inhibitory neurotransmission through gamma-aminobutyric acid type A ($GABA_A$) receptors (e.g., benzodiazepines, tiagabine);

3) reducing excitatory neurotransmission through glutamate receptors (e.g., perampanel);

4) regulating neurotransmitter release through alterations at the presynaptic terminal (e.g., levetiracetam, gabapentin) (Sills and Rogawski, 2020).

These actions reduce the probability of seizure occurrence by modifying the bursting properties of neurons, reducing synchronization in localized neuronal ensembles, and inhibiting the spread of abnormal firing to adjacent and distant brain sites.

Despite such variety of mechanisms, studies have shown that ASMs fail to control seizures in more than 30% of clinical cases (Pohlmann-Eden and Weaver, 2013), resulting in the development of pharmacoresistant epilepsy (PRE) also referred to as drug-resistant epilepsy (DRE).

According to the ILAE, a patient is deemed to suffer from PRE when ≥2 ASMs are incompetent in seizure control, even after being appropriately selected based on the patient's history and subject to sufficient drug usage (Kwan et al., 2010).

PRE is likely due to several, multifactorial mechanisms, which may even occur together in the same patient. Current hypotheses about the mechanisms underlying PRE can be broadly categorized into three groups: disease-related mechanisms, drug-related mechanisms, and genetic mechanism (Löscher et al., 2020).

Long-term outcome studies suggested that, after failure of two well-tolerated ASM schedules appropriately chosen for the seizure type(s), the chance of success with further drug manipulation becomes progressively less likely (Chen et al., 2018).

Lack of seizure control is inversely associated with a higher risk of SUDEP (Langan et al., 2005). Studies also observed that children diagnosed with PRE are more prone to the risk of developing ID (Cormack et al., 2007).

Studies of PRE may be complicated by unexplained temporal dynamics: the same person may have prolonged periods of seizure freedom, with intervals during which seizures cannot be controlled (Berg et al., 2003). In theory, at least four clinical patterns of drug resistance can be observed:

1) *de novo* (or *ab initio*) PRE, whereby the patient never enters a useful period of seizure freedom from the onset of the epilepsy;

2) delayed resistance, which is when the patient initially becomes seizure-free but seizures recur and become uncontrollable;

3) a waxing-and-waning (or fluctuating) pattern, which occurs when the epilepsy alternates between being controlled and uncontrolled;

4) the epilepsy is initially drug-resistant but with time responds to treatment (Schmidt and Löscher, 2005).

Patients with PRE often undergo presurgical evaluation as resective surgery has been shown to offer a better chance of controlling seizures (Anyanwu and Motamedi, 2018). Resective surgery involves the removal of a small portion of brain tissue where seizures occur, such as the site of a tumor, brain injury or malformation. However, not all patients qualify for surgery. As a management alternative, patients with PRE who do not qualify for resective surgery are often instructed to follow dietary therapies. The ketogenic diet is the most widely used and best validated such treatment approach and consists in a special high-fat, low-carbohydrate diet that helps to control seizures in some people with epilepsy.

(Goswami and Sharma, 2019). However, due to its unappetizing and restrictive characteristics, the ketogenic diet is often discontinued by patients (D'Andrea Meira et al., 2019). Moreover, side effects such as hypercholesterolemia, as well as bone, growth and cardiac impairments are reported in children long-term exposed to this diet (Wells et al., 2020).

Although new ASMs are being designed every year, still 30% of people with epilepsy have seizures that remain drug-resistant, even if ASMs with different mechanisms of action are combined (Chen, Brodie and Kwan, 2020).

Thus, there is an urgent need to design newer and more effective anti-seizures drugs and to identify new molecular targets.

1.5 Drug discovery

Drug discovery is the first phase in the process of developing a new drug.

Drug development is very complex, expensive, and time-consuming process: it comprises all the activities involved in transforming a newly identified bioactive molecule (the end-product of the discovery phase) to a product approved for marketing by the appropriate regulatory authorities. Developing a drug from the identification of a new candidate to the launch of a finished product can take 12–15 years and cost about 1-2 billion euro for each new drug to be approved for clinical use and marketed (Hughes et al., 2011).

Typically, drug development can be divided into four main stages with different aims (Figure 1.17):

1. *Drug Discovery process*: aims to find potential new molecules (called *leads*) active in a specific disease-related target.

2. *Pre-Clinical Phase*: points to characterize the leads for their safety and efficacy. Data collected in this phase are necessary to authorize investigation in humans.

3. *Clinical Phases*: the drug candidates resulted safe in the preclinical studies are tested in humans. In *phase I*, the safety, pharmacokinetics, best dose, timing, and route of administration of a new treatment are evaluated in healthy volunteers; in *phase II* the effectiveness and possible side effects of the new treatment are tested in patients; in *phase III* the treatment is tested in a larger number of patients through randomized controlled multicentre trials to better asses its value in clinical practice.

4. *Regulatory Approval*: agencies in charge of the evaluation and supervision of pharmaceutical products review and approve, or do not approve, the drug application

submitted by the development company. In Europe this task is assigned to the European Medicines Agency (EMA), in the United States of America the federal agency Food and Drug Administration (FDA) is responsible for controlling and supervision of drugs, dietary supplements and food safety.

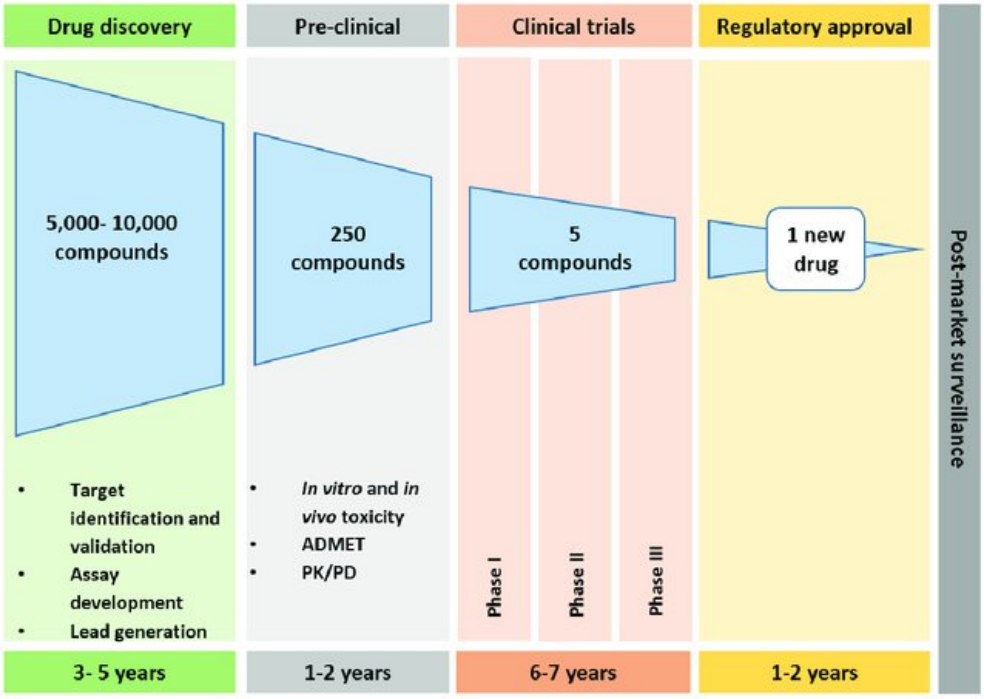

Figure 1.17 Drug discovery and development timeline. The current drug approval pipeline can take ~15 years. It is estimated that from 5,000-10,000 compounds only one new drug reaches the market.

An unmet clinical need is the underlying driving motivation to start a program to develop a new drug, therefore the first and most important step in the drug discovery process is the identification of a biological target (e.g., a gene, an enzyme, an ion channel, or a receptor) and its validation as pathogenically relevant and druggable.

This phase is influenced by a complex balance of scientific, medical, and strategical considerations and needs strong experimental evidence: *in vitro* tools, animal models and modulation of a desired target in disease patients are combined in a multi-validation approach to demonstrate that I) the target plays a crucial role in the pathogenetic mechanism and II) pharmacological actions on the target significantly modify the consequences of the disease.

Once the target has been identified and validated, different approaches can be used to identify new molecules acting on it and called *lead compounds.* Traditional approaches to identify new *leads* active on the target of interest rely on a stepwise synthesis and *in vitro* testing of large number of compounds to identify a potential candidate. In comparison to traditional methods, rational drug design methods used to identify new *lead compounds* or

during the lead-optimization stages bring down the time and cost involved in the drug development process and has become an essential part of drug discovery projects.

1.5.1 Structure-based drug design

Drug design, often referred to as *rational drug design*, is the inventive process of finding new medications based on the knowledge of a biological target. Based on available information, two different drug design approaches can be used: *structure-based drug design* (SBDD), used when the three-dimensional (3D) structure of the target is known and is exploited to develop new modulators; *ligand-based drug design* (LBDD), used in the absence of the receptor 3D information, and relying on the molecular structure of known ligands of the biological target. These methods are also referred to as “computer aided” (*in silico*) drug design.

The 3D structures required for SBDD are determined by experimental techniques such as *X-ray crystallography*, *NMR spectroscopy* and Cryo-EM and collected in the Protein Data Bank (PDB). Compared to X-ray crystallography, cryo-EM specimen is made by fast freezing biological samples in liquid nitrogen temperature directly from the solution, therefore maintaining the macromolecules in their soluble states in comparison with a state in the crystal packing constraint. This lends cryo-EM the advantage to reveal structures in more close-to-native state than X-ray crystallography (Wang et al., 2017).

If the structure of the protein drug target is not available, protein structure can be predicted by computational methods like threading and homology modelling.

The 3D structure of a target is studied using software allowing molecular docking and molecular dynamics (MD) analysis. These techniques are not only able to predict if and where a ligand interacts with a target, but also which type of interaction occur between the ligand and the target, thus, helping in the definition of the relationship between chemical-physical properties and the pharmacological activity of the molecule.

In the first part of the present work, a SBDD study was carried out using the $K_v7.2$ CryoEM structure in complex with retigabine (Li X. et al., 2021) to analyse the chemical space in the retigabine binding pocket. This knowledge has guided the synthesis of novel retigabine analogues designed to find new ligand-target interactions increasing the retigabine K_v7 opening ability, as described in section 4.2.

1.5.2 Drug repurposing

Drug repurposing (also named drug repositioning, reprofiling, redirecting or re-tasking) is a strategy for identifying new uses for approved or investigational drugs that are outside the scope of the original medical indication. It is also called “drug rescue” when a new use for a developmental drug, that failed for its primary intended purpose, is successfully identified.

Drug repurposing offers various advantages over developing an entirely new drug for a given indication, such as lower failure risk, reduced time frame and less economic investment. These advantages are greater the more preclinical and clinical phases (preclinical testing, safety assessment in human, formulation development) have been completed for the drug. Although the regulatory and phase III costs may remain more or less the same for a repurposed drug as for a new drug in the same indication, it was estimated that the costs of bringing a repurposed drug to market is around 300 million euro, compared with an estimated 1–2 billion for a new chemical entity.

Historically, drug repurposing has been largely opportunistic and serendipitous: once a drug was found to have an off-target effect or a newly recognized on-target effect, it was taken forward for commercial exploitation. A classic example is thalidomide, a sedative marketed in some countries in 1957 but withdrawn within 4 years owing to its teratogenic effects in children born to mothers who had taken the drug during the first trimester of their pregnancies. Thalidomide was first serendipitously found to be effective in the treatment of erythema nodosum laprosum (Opromolla et al., 1966), decades later in multiple myeloma (Singhal et al., 1999) and the research about its possible repurposed uses is still on-going (Teng and Siegel, 2022), even going so far as to test a possible use against SARS-CoV-2 infections (Sundaresan et al., 2021).

Typically, a drug repurposing strategy consists of three steps: 1) identification of the right drug for an indication of interest with a high level of confidence (hypothesis generation); 2) mechanistic assessment of the drug effect in preclinical models; 3) evaluation of efficacy in phase II clinical trials (assuming there is sufficient safety data from phase I studies undertaken as part of the original indication).

Early serendipitous successes have encouraged the development of more systematic approaches to aid drug repurposing, especially for the first crucial step of generating a new hypothesis of use. These systematic approaches can be subdivided into experimental approaches and computational (*in silico*) approaches.

Among the experimental approaches there is the *phenotypic screening*. In the world of drug discovery and development, the term *phenotyping screening* is used to describe the techniques adopted to identify the biological effects of a drug directly or indirectly linked to a disease. Drugs candidates are tested in cell-based or whole organism HTS assays to evaluate their possible effect on cell viability, cell apoptosis, infection, cell motility, cell cycle, signalling pathways or disease-related mechanisms.

In the second part of the present work an assay called FluxOR was optimized using K_v7-expressing cells as a phenotypic screening to measure the K_v7 opening ability of compounds. This experimental paradigm was used to screen the Fraunhofer repurposing library with the aim to repurpose already approved or tested drugs as new ASM acting as K_v7 channels activators, as described in the section 4.3.

Drug Repurposing and rare diseases

Rare diseases, also called “orphan diseases”, are defined by WHO as diseases with a prevalence of less than 6.5–10 in 10,000 (Aronson et al., 2006). It is estimated that more than 7,000 rare diseases exist and over 95% of them lack an approved therapeutic agent.

It is very challenging to develop new drugs for the treatment of rare diseases for different reasons: 1) the number of patients suffering from these diseases is very limited; 2) often there is high variability among patients since rare diseases are mostly influenced by genetic factors; 3) financially, the development and subsequent production of these drugs to treat rare disease is not viable for the pharmaceutical companies. Therefore, drug repurposing is a particularly attractive approach for rare diseases for both scientific and commercial reasons (Pushpakom et al., 2019).

Commercially, there are specific regulatory measures that are meant to encourage research into rare diseases, e.g., commercial exclusivity in situations where repurposed products cannot be protected by a patent or if that patent is weak.

Scientifically, these conditions are often poorly patho-physiologically characterized, therefore computational techniques for predictive repurposing offer a relatively quick method to identify testable hypotheses that may be translated into the clinic.

The drug repurposing approach to find treatments for rare diseases often leads to an “off-label" drug use. *Off-label* refers to the practice of prescribing a drug for a different indication than what approved, or for a different dosage form, dose strength, route of administration or in that patient age group which are not approved. To be used in this way,

proofs of drug efficacy and safeness in preclinical as well as clinical studies are needed. Off-label drug use is being extensively practiced by physicians to treat any life-threatening condition where no treatment is available and there is strong evidence that off-label use of a drug may be helpful for the patient.

Rare diseases include various forms of epilepsy, especially severe early-onset genetic epilepsies that are often drug-resistant and affect patient's neurocognitive development. In such cases a quick identification of a treatment option, such as the off-label use of a repositioned drug, is crucial.

There are many examples of drugs which have been first prescribed as “off-label” in a patient with a rare disease and then the encouraging results paved the way for its use in a larger number of patients. One of this is the case of quinidine repurposed to treat seizure disorders caused by mutations in the $K_{Na}1.1$ potassium channel (Liu et al., 2022).

Pathogenic $K_{Na}1.1$ variants prompting GoF effects cause a range of rare infant-onset epilepsy syndromes frequently associated with developmental delay and characterized by drug-resistant seizures (Bonardi et al., 2021).

Quinidine, a class I antiarrhythmic agent blocking Na^+ channels (Grace and Camm, 1998) also inhibits $K_{Na}1.1$ channels (Yang et al., 2006), including those carrying GoF mutations causing epilepsy (Rizzo et al., 2016; Dilena et al., 2018). Based on this evidence, quinidine was tested as off-label treatment in a patient affected by a $K_{Na}1.1$-related pharmacoresistant epileptic syndrome and it was found to reduce seizure frequency (Bearden et al. 2014). This result prompted other clinical trials of quinidine for treatment of $K_{Na}1.1$-related epilepsies, with different outcomes (Fitzgerald et al., 2019; Xu et al., 2022). Although not effective in all patients in controlling seizures, and despite its clinical use is limited due to the adverse effect of QT prolongation (Mullen et al., 2018) quinidine is nevertheless a therapeutic option to be explored for severe $K_{Na}1.1$-related epilepsies otherwise resistant to common ASM, therefore representing an example of how drug repurposing can be helpful to find treatments for rare diseases.

1.5.3 Ion channels high-throughput screening (HTS) techniques

Given the variety of fundamental physiological processes in which they are involved, ion channels represent a class of attractive drug targets for *in vitro* pharmacological profiling. Traditionally, patch clamp electrophysiology is the gold standard for ion channel studies. However, the method is time-consuming with a low throughput and requires highly trained staff to perform the experiments.

One of the *in vitro* technologies developed in the 1990s that enable a rapid evaluation of thousands of chemical compounds in biologic assays is the HTS, consisting of highly automated screening systems to record a biological activity at the model organism, cellular, pathway, or molecular level. Cell based assays involve cell lines derived from human or animals, immortalized cell lines or induced pluripotent cells lines (iPSCs).

Evaluation of molecule collections using these automated systems increases the chance to find active compounds, the so-called *"hits"* compounds, that represent the basic structures on which pharmaceutical chemists and biologists will focus to identify the prototype molecule, the *"lead"* compound. HTS can also be performed using libraries of known bioactive molecules/already tested drugs to explore drug repurposing opportunities.

In the past decades, the rapid progress in developing functional assays and instrumentation has enabled HTS campaigns on an expanding list of ion channel types (Yu et al. 2016). The HTS methodologies for studying ion channels can be divided into non-electrophysiological and electrophysiological methods and include the *ligand binding assay*, *flux-based assay*, *fluorescence-based assay*, and *automated electrophysiological assay*.

Non-electrophysiological ion channels HTS methods

Ligand binding assays was extensively used, in the past, to screen channel modulators. This assay requires previous knowledge of I) target binding sites and II) a radio-labeled ligand. It is useful to determine the affinity of a given compound (without distinguishing between an agonist or an antagonist) but not its ability to alter the functionality of ion channels.

Because of its intrinsic limits, ligand binding assays have been replaced by *Flux-based assay,* even if radiolabelled [^{3}H]-astemizole, [^{3}H]-dofetilide and [^{125}I]-BeKm are still today regularly used to assess K_v11.1 (hERG) channel pharmacology or to investigate new potential modulators (Finlayson et al., 2001). Flux-based assay has been successfully applied to detect the functional change of ion channel activity. For this purpose, radioactive isotopes like $^{22}Na^+$, $^{45}Ca^{2+}$ and $^{86}Rb^+$ have been used to trace the cellular influx or efflux of specific ions, such as Na^+, Ca^{2+}, and K^+ channels, respectively.

However, the inconvenience and cost associated with the handling of radioactive materials, radioactive flux-based assay have been substituted by *non-radioactive fluorescence-based assay* or considering the radioactive Rb^+, this has been replaced by unlabelled Rb^+ detected by atomic absorption spectroscopy (Wang et al.,2004).

Fluorescence-based methods can measure the membrane-potential dependent- or ion concentration-dependent changes of fluorescence signals by using voltage-sensitive dye or ion-specific fluorescent probes, respectively.

Fluorescent reports of membrane potential are lipophilic compounds containing a delocalized charge (oxonols) that respond to variation in membrane potential with changes in intramolecular charge distribution or by plasma membrane association/dissociation, which causes a change in their fluorescent emission. To date, these are being overcome by genetically encoded indicators (e.g., GECIs) (Wu et al., 2019).

Ion-specific fluorescent reporters commonly used are fura-2, fluo-3, fluo-4, for calcium channels, PBFI for potassium and SBFI indicators for sodium. When the intracellular concentration of the specific ion increases, a binding event occurs between the dye and the ion, leading to an increase in fluorescence or a change in spectral properties of the dye. The relatively small changes in the intracellular concentrations of Na^+ and K^+ under normal physiological conditions can make Na^+ and K^+ indicators challenging to use, particularly for HTS applications. In many instances, thallium (Tl^+) flux assays offer an outstanding alternative to fluorescent potassium and sodium indicators. They take advantage of Tl^+-selective fluorescent indicators, such as FluxOR or Thallos, and the fact that potassium and sodium channels are permeable to Tl^+. When Tl^+ is added to the outside of cells loaded with Tl^+-selective fluorescent indicators, Tl^+ entering cells through ion channels permeable to Na^+ or K^+ results in a dramatic increase in fluorescence. An example of the application of a fluorescence-based HTS using Tl^+-sensitive indicators is offered by the work of Spitznagel and colleagues that used the Thallos assay in HEK293 cells engineered to express $K_{Na}1.1$ potassium channels and screened a 100,000 compounds library, identifying a new $K_{Na}1.1$ channel blocker, namely VU0606170 (Spitznagel et al. 2020).

Electrophysiological ion channels HTS methods

Electrophysiological techniques range from the classical patch-clamp to multielectrode arrays (MEA). Conventional patch-clamp represents the gold standard to directly record ion channel activity but suffers from low throughput and is labor-intensive, requiring highly skilled and trained personnel. To overcome these limits, *Automated electrophysiological assays* have been developed and to date, many automated platforms are commercially available (PatchXpress, IonFlux, Qpatch, Patchliner, SyncroPatch, IonWorks ecc). Compared to traditional patch, glass pipettes are replaced by a planar substrate

characterized by openings where the single cell is placed. This removes the physical technicalities and allows for parallel experimentation. These technologies have been profitably used to identify new potassium channels modulators within small collections of compounds, as described by Hernandez and colleagues that used the SyncroPatch to screen an in-house library of 22 compounds and identified the compound ZK-21 representing a new $K_v7.2$ channel agonist chemotype (Hernandez et al., 2022).

Conversely, MEA is characterized by multi-well plate with multiple electrodes at the bottom of each well, allowing for real-time spontaneous activity measurement from hundreds of neurons simultaneously under normal culture conditions. This device is suitable, for example, to observe the response of iPSC-derived neurons to compounds added to the well. Recently, Hirose et al. have reported that using inhibitor and excitatory neurons differentiated from Dravet syndrome iPSCs in MEA, they identified among 13 million drugs, two AED candidate compounds that mitigated deficient electrophysiological activity in inhibitory neurons, the core pathogenic mechanism of $Na_v1.1$ haploinsufficiency Dravet syndrome (Hirose et al., 2020)

Different HTS approaches can be combined to screen large libraries of molecules, validate hits, and successfully identify new leads compounds. An examples of the application of these techniques in the discovery of new potassium channels modulators is offered by the works of Yue and colleagues: they demonstrated that the use of a fluorescence-based Tl^+-flux HTS (FluxOR) in combination with an automated patch-clamp technology (IonWorks) enhanced the chance to identify new $K_v7.2$ activators in a library of thousands of compounds and reduced the false positive hit rate previously observed in other screening campaigns. In their work the FluxOR assay was used in a $K_v7.2$-expressing cell line to primary screen a library of 80,000 compounds, identifying the 565 primary hits. They were subsequently screened using the IonWorks automated patch-clamp technology, this validation phase led to the identification of compounds ZG1732 and ZG2083, showing higher potency in activating $K_v7.2$ compared to the reference compound ztz240 (Yue et al. 2016).

1.5.4 Libraries of compounds

The outcome of a HTS depend on three major factors: the chosen target, the screening assay, and the quality of the compound library. Many virtual and physical libraries of compounds, with different properties, are commercially available. The choice of the library

to be used is important whether the screening to perform is virtual or experimental, for repurposing or *de novo* drug discovery (Gribbon and Sewing, 2005).

The whole concept of “compound library” came into play with the introduction of combinatorial synthesis and HTS. Combinatorial chemistry, born in the early 1980, is an approach increasing the speed of the production of several hundreds of compounds, thus forming compound libraries, known as combinatorial libraries. Combinatorial libraries are simply collections of chemical compounds, small molecules, or macromolecules, usually represented by one structure with a small number of R-group positions for each of which there is a list of alternative groups. Since the introduction of HTS techniques in early 1990s, compound libraries used in drug screening projects were usually assembled randomly: they were typically collections of companies compounds previously created during drug-discovery programmes. From around 1990 to present, the trend in library design was to reduce size and increase quality and diversity of screened compounds, to improve hit rates and reduce the attrition rates found during hit triage and the subsequent phases of drug development (Spears and Brown, 2017).

Initially, the *chemical diversity* of the compounds was the parameter most focused on to improve the quality of the libraries. Soon, however, it was realised that chemical diversity may not necessarily overlap with biological activity, and the concept of “*drug-like molecule*” was introduced. Drug-likeness is a term used to rationalize how physicochemical properties influence the molecular behaviour *in vivo* and especially the oral bioavailability of a compound. Most models for drug-likeness use physicochemical properties calculated from the molecular structure of a compound to predict its cell and tissues permeability and correlate them against orally administered drugs (Zuegg and Cooper, 2012). One of the first of such rules, the Rule of Five described by Lipinski et al., is to limit the size (molecular weight ≤500), the hydrophobicity (logP ≤5) and polarity (hydrogen-bond acceptors ≤10 and donors ≤5) of compounds, sticking to values found in compounds with good oral bioavailability (Lipinski et al., 2001). The drug-likeness concept was extended to include “*lead-like properties*” of compounds. One of the current lead-likeness models proposed by Oprea et al. follows the concept of drug-likeness, but applying more stringent criteria, limiting the size (molecular weight ≤ 450), hydrophobicity (log ≤4.5), and polarity (hydrogen-bond acceptors ≤8 and donors ≤5) (Oprea et al., 2001).

The main aim of the various drug-likeness and lead-likeness rules is to give researchers, as early as possible in the drug discovery process, a tool to eliminate compounds with potentially low cell and tissue permeability and therefore a high risk of failure. Additional

chemistry-based rules are used to eliminate compounds with chemically reactive groups, toxicophores or promiscuous binders.

However, although over 10^{63} drug-like molecules do currently exist, only a tiny fraction of these molecules is likely to be therapeutically relevant and may generate successful leads. To improve the effectiveness of an *in silico* on *in vitro* HTS, compound libraries must be rational designed. *Diversity-based libraries,* designed to maximize structural diversity, are usually used for targets with few known active chemotypes, to provide multiple starting points for further development. Contrary to diversity-based libraries, *focused screening libraries* are often designed for well-studied targets, such as GPCRs, kinases and, in some cases, ion channels, and revolve around active known chemotypes.

However, *focused libraries* are not necessarily a replacement for *diversity-based libraries*, even for well-studied target classes, and many other compounds features can be taken in account, such as novelty or repurposing, route of administration, a specific therapeutic area or combinations.

The library design must be addressed based on the chemical, biological and medical data available, given that screening the right set of compounds enhances the success rate in any drug-discovery programme (Paricharak et al., 2018).

2. Aim of the work

K_v7 potassium channels represent an attractive pharmacological target for several neurologic disorder, including epilepsy (Barrese et al., 2018).

Retigabine was the first approved antiepileptic drug targeting K_v7 channels; unfortunately, this molecule presents some drawback such as poor selectivity for K_v7 subtypes, short half-life, poor brain penetration and chemical instability. For these reasons retigabine was withdrew from the market in 2017 and currently no K_v7 activator is clinically available as anticonvulsant drug, making necessary the identification of novel I_{KM} modulators.

According to these premises, the aim of this work was to identify novel and safer $K_v7.2/7.3$ activators. Two different approaches were explored:

1) A rational *structure-based drug design* strategy was used to design, synthesize, and screen novel retigabine analogues overcoming some limitations of the lead compound. This part of our work involved the collaboration of the *Department of Pharmacy, University of Naples Federico II*, for the synthesis of novel retigabine analogues, and the *Department of Chemical, Biological, Pharmaceutical and Environmental Sciences, University of Messina*, for the *in silico* analyses. To facilitate the screening of newly synthesized derivatives, I have generated stable cell lines expressing $K_v7.2/7.3$, $K_v7.2$ and, $K_v7.3$ A315T channels and I have used these cell lines in a fluorescence-based assay called FluxOR Green Potassium Ion Channel. Then I evaluated the effect of known K_v7 activators and inhibitors to assess the sensibility and the feasibility of the assay on $K_v7.2/7.3$ channels. Finally, I used this assay to evaluate the ability of the newly synthesized retigabine derivatives to activate $K_v7.2/7.3$ channels.

2) A *drug repurposing* strategy was exploited to identify new K_v7 activators among drugs already tested in preclinical and clinical phases, in order to shorten the time and cost of developing a new molecule and bring it more quickly to clinical use. This work originates from the collaboration with the Screening-Port of the Fraunhofer Institute for Translational Medicine and Pharmacology ITMP, where I spent a period of time to adapt the lab-scale FluxOR assay to a large scale HTS, suitable to screen the Fraunhofer Library. These research activities were carried out within the framework of the project “TreatKCNQ”, a four-years project with the aim to develop improved therapies for KCNQ-associated encephalopathies, funded by the European Joint Programme for Rare diseases.

3. Materials and methods

3.1 Plasmids: site-directed mutagenesis

Each mutation was engineered by using the Quick-change Site-Directed Mutagenesis (Agilent Technologies, figure 3.1). The mutations were insert in each plasmid by Polymerase Chain Reaction (PCR), using a pair of primers (forward and reverse) (Table 3.1), incorporating the nucleotide mutation of interest.

Table 3.1. Mutations engineered in the K_v7-templates vector and nucleotide sequences of primers used for PCR.

Mutation	Primers
$K_v7.2$-NheI	F 5' - GGGAGACCCAAGCTAGCTTGTTC - 3' R 5' - GAACAAGCTAGCTTGGGTCTCCC - 3'
$K_v7.3$-XhoI	F 5' – ATGGATCCGCGGCCTCGAGGATCTGCGATCG – 3' R 5' – CGATCGCAGATCCTCGAGGCCGCGGATCCAT – 3'

The amplification reaction was performed in a final volume of 50 µL containing the following components: 50 ηg of plasmid, 125 ηg primer forward, 125 ηg primer reverse, 5% DMSO, 2.5U Pfu DNA Polymerase, 1X buffer Pfu, 1 µl dNTP mix. The PCR consisted of 18 cycles, with each cycle consisting of three temperature steps, that allow the denaturation of the DNA Double Helix (95°C for 30''), the annealing of the primers to the single strand of DNA (55°C for 1') and the extension of the primers (68°C for 10'). After the amplification reaction, the volume of the reaction contained both methylated (parental) and unmethylated (neo-synthesized) DNA. Therefore, to remove the parental DNA, enzymatic digestion was performed with 1 µl DpnI enzyme (10 U/ µl) able to digest only methylated DNA. Afterwards, the *DpnI*-treated and untreated samples were analyzed by agarose gel electrophoresis to confirm the presence of the mutated vector.

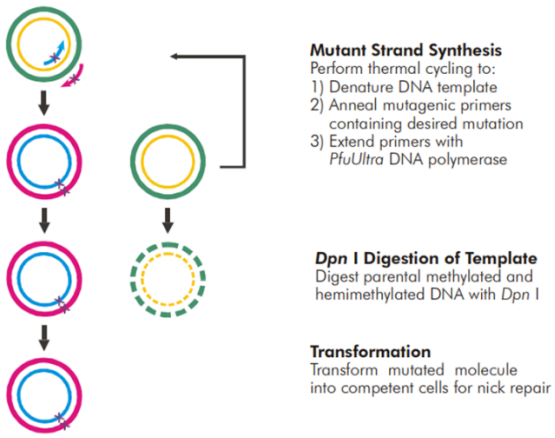

Figure 3.1 Overview of the QuikChange II site-directed mutagenesis method.

3.2 Bacterial transformation and plasmidic DNA preparation

Subsequently, the DpnI-treated sample was transformed into 100 µl of competent E. coli DH5α cells according to the heat-shock transformation protocol (30' at 4°C, heat shock step at 42°C for 45'' followed by 3' at 4°C), resuspended in 200 µl SOC medium (2% tryptone, 0.5% yeast extract, 10 mM NaCl, 2.5 mM KCl, 10 mM MgCl2, 10 mM MgSO4, 20 mM glucose) and then incubated at 37°C for 45'. Afterwards, the transformed product was plated on Ampicillin-containing (50 µm/ml) LB-Agar plates (10 g/L tryptone, 5 g/L yeast extract, 5 g/L di NaCl, agar 15 g/L) and incubated upside down at 37°C overnight. Single colonies were inoculated in 5ml of LB medium containing ampicillin (50 µg/ml) and incubated at 37°C/220 rpm overnight. DNA plasmid was extracted from bacteria cultures by using a commercially available kit (*QIAprep Spin Miniprep*, QIAGEN). Positive vectors were identified by using enzymatic digestion followed by DNA sequencing (Eurofins Genomics, Italy). To obtain DNA in large amount, one of the positive clones was amplified on a large scale and plasmidic DNA was extracted by using a commercially available kit (*Plasmid Plus Maxi*, QIAGEN). The cDNA was sequenced again, to confirm the presence of the mutation of interest and to exclude additional mutations in the entire coding sequence.

3.3 Cell cultures

Chinese Hamster Ovary (CHO) cells were grown in plastic Petri dishes (100 mm, 60 mm, or 40 mm, according to the different experimental needs) in DMEM (*Dulbecco's Minimum Eagle Medium*) supplemented with 10% Fetal Bovine Serum, 1% L-glutamine (2 mM in 0.85% NaCl), 1% penicillin (50 U/mL) and 1% streptomycin (50 µg/mL) in a humidified atmosphere at 37°C with 5% CO_2. Every time cells became confluent within the dishes (about every 2 days), they were split by using 1% trypsin solution and collected in novel dishes with a 1:3 dilution.

3.4 Generation of stable cell lines

3.4.1 PiggyBac Transposon system and PB-RedPuro-K_v7 plasmids cloning

SBI's PiggyBac (PB) Transposon System consists of a PiggyBac Vector and the Super PiggyBac Transposase; the PB-CMV-MCS-EF1α-RedPuro PiggyBac cDNA Cloning and Expression Vector (Cat# PB514B-1 is characterized by the CMV promoter and the site of multiple cloning (MCS) in which, using appropriate enzymes, allows the insertion of the gene of interest. Downstream the EF1α promoter, two selection markers are express: an RFP reporter and the gene encoding the Puromycin N-acetyltransferase. Inverted terminal repeat sequences (ITRs) are located on both ends of the cassette of gene expression that

are recognized by the transposase, encoded by the Super PiggyBac Transposase, which efficiently integrates the ITRs and intervening DNA into the genome at TTAA sites. The Super PiggyBac Transposase is delivered to the cell via the Super PiggyBac Transposase Expression Vector, which is co-transfected with one or more PiggyBac Vectors (Figure 3.2 and 3.3).

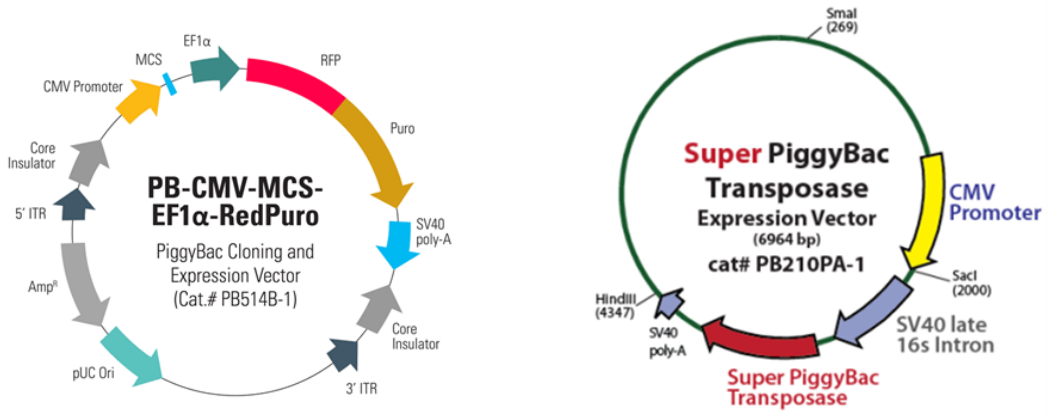

Figure 3.2 Structure of the PB-CMV-MCS-EF1α-RedPuro PiggyBac Vector and the Super PiggyBac Transposase

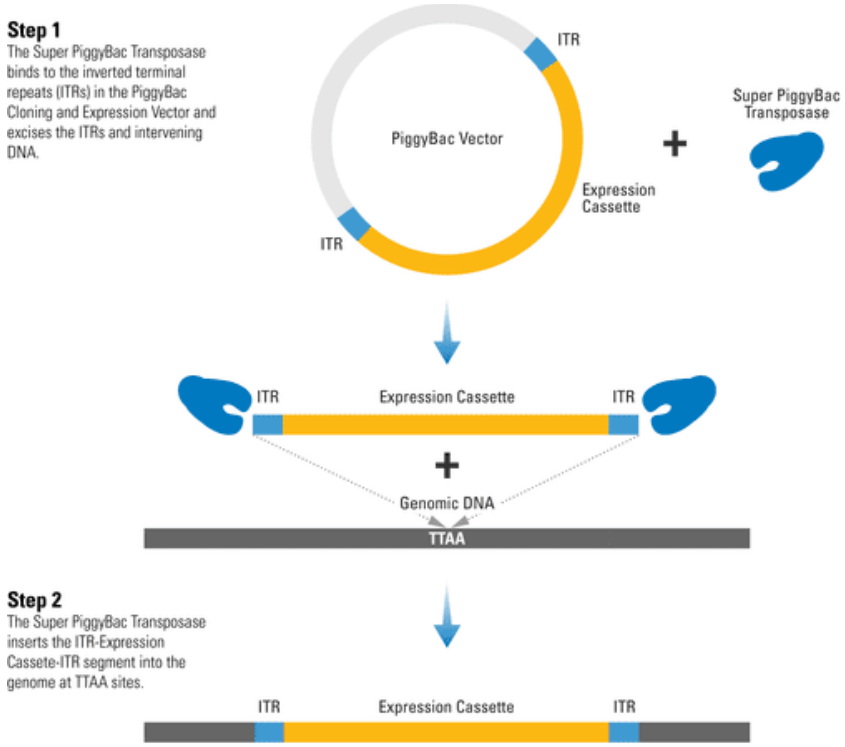

Figure 3.3 The PiggyBac Transposon System's cut-and-paste mechanism.

Generation of PB-RedPuro-K_v7.2

The pcDNA$_3$-KCNQ2-NheI vector was subcloned into the pB-CMV-MCS-EF1-RedPuro obtained from System Biosciences, LLC (Palo Alto, USA). Each vector was digested with 1U of NheI restriction enzyme and incubated at 37°C for 1h. Subsequently, the enzyme was inactivated incubating the mix at 65°C for 20' and then incubated with 1U of EcoRI enzyme for 1h. After the double digestion, in order to remove phosphate groups and prevent a possible closure, the pB-CMV-MCS-EF1-RedPuro vector was treataed with 1U of CIP (Calf Intestinal Phosphatase) at 37°C for 1h. Subsequently, pcDNA3-KCNQ2-NheI and the pB-CMV-MCS-EF1-RedPuro vectors were analyzed by Agarose gel electrophoresis. The band corresponding to the KCNQ2 cDNA and the band corresponding to the pB-CMV-MCS-EF1-RedPuro backbone were extracted from the gel using the GEL EXTRACTION KIT according to the manufacturer protocol.

Finally, 8µL of KCNQ2 fragment was inserted by ligation into 4µl of pB-CMV-MCS-EF1-RedPuro using 1U of T4 Ligase and incubated at 16°C overnight to obtain the final PB-RedPuro- K_v7.2 vector. The ligation product was transformed into One Shot® TOP10 Chemically Competent E. coli from Invitrogen and the right-ligated vector was selected as previously mentioned. All the sequences were validated by DNA sequencing.

Generation of PB-RedPuro-K_v7.3

The pcDNA$_3$-KCNQ3-XhoI vector was subcloned into the pB-CMV-MCS-EF1-RedPuro obtained from System Biosciences, LLC (Palo Alto, USA). Each vector was digested with 1U of NheI restriction enzyme and incubated at 37°C for 1h. Subsequently, the enzyme was inactivated incubating the mix at 65°C for 20' and then incubated with 1U of BamHI enzyme for 1h. After the double digestion, in order to remove phosphate groups and prevent a possible closure, the pB-CMV-MCS-EF1-RedPuro vector was treated with 1U of CIP (Calf Intestinal Phosphatase) at 37°C for 1h. Subsequently the pcDNA3-KCNQ3-XhoI and the pB-CMV-MCS-EF1-RedPuro vectors were analyzed by Agarose gel electrophoresis. The band corresponding to the KCNQ2 cDNA and the band corresponding to the pB-CMV-MCS-EF1-RedPuro backbone were extracted from the gel using the GEL EXTRACTION KIT according to the manufacturer protocol.

Finally, 6 µl of KCNQ3 fragment was inserted by ligation into 4 µl pB-CMV-MCS-EF1-RedPuro using 1U of T4 Ligase and incubated at 16°C overnight to obtain the final PB-RedPuro- K_v7.3 vector. The ligation product was transformed into One Shot® TOP10

Chemically Competent E. coli from Invitrogen and the right-ligated vector was selected as previously mentioned. All the sequences were validated by DNA sequencing.

Generation of PB-RedPuro-K_v7.3 A315T

The pcDNA3-KCNQ3 A315T vector was subcloned into the PB-RedPuro-K_v7.3 vector, previously obtained. Each vector was digested with 1U of KpnI restriction enzyme and incubated at 37°C for 1h. The pcDNA3-KCNQ3 A315T and the pB-RFPPuro- K_v7.3 vector were analyzed by Agarose gel electrophoresis and the band corresponding to the KCNQ3 A315TcDNA and the band corresponding to the pB-RFPPuro- K_v7.3 vector were extracted from the gel using the GEL EXTRACTION KIT according to the manufacturer protocol. Subsequently, each extract product was digested with 1U of NotI restriction enzyme and incubated at 37°C for 1h. The pcDNA3-KCNQ3 A315T and the pB-RFPPuro- K_v7.3 vector were analyzed by Agarose gel electrophoresis. The band corresponding to the pcDNA3-KCNQ3 A315T and the band corresponding to the pB-CMV-MCS-EF1-RedPuro backbone were extracted from the gel using the GEL EXTRACTION KIT according to the manufacturer protocol.

Finally, 5 µl of KCNQ3 A315T fragment was inserted by ligation into 4 µl pB-CMV-MCS-EF1-RedPuro using 1U of T4 Ligase and incubated at 16°C overnight to obtain the final PB-RedPuro- K_v7.3 vector. The ligation product was transformed into One Shot® TOP10 Chemically Competent E. coli from Invitrogen and the right-ligated vector was selected as previously mentioned. All the sequences were validated by DNA sequencing.

3.4.2 Cell cultures and stable transfection with Lipofectamine

CHO cell line was used to create the stably transfected cell line expressing the pB-RedPuro-K_v7 vector. CHO cells were plated into 60mm cell plate and transfected at a confluence of 80%. The transfection mix containing 3 µg of pB-RedPuro- K_v7 vector, 1 µg of Super PiggyBac Transposase Expression Vector (System Biosciences, Palo Alto, USA), 20 µl of Lipofectamine (Themofisher, Italy) and 500 ul of DMEM (*Dulbecco's Minimum Eagle Medium*) was incubated for 15 minutes according to the manufacturer protocol. The mix was added to the CHO cell plate and incubated at 37°C for 24h. The conditioned medium was replaced with fresh growing medium treated with 4µg/µl of Puromycin. After 7 days only the cells that had correctly internalized the expression vector and expressed the antibiotic resistance was detectable in the cell plate. Subsequently, for 3 to 8 small cell aggregates were isolated and amplified separately to obtain different stably transfected clones.

3.5 CHO cells preparation and whole-cell electrophysiology

For electrophysiological experiments, CHO cells were seeded on glass coverslips, heat-sterilized and pre-coated with poly L-lysine, in 35 mm dishes. After 24h, CHO cells were transfected using Lipofectamine 2000, according to the manufacturer protocol (Themofisher, Italy). In each transfection mixture, a plasmid encoding for an Enhanced Green Fluorescent Protein (pEGFP; *Clontech*, Palo Alto, CA) was used as transfection marker (3 µg of plasmids encoding for K_v7 cDNA + 1 µg di pEGFP).

Macroscopic currents were recorded, after 1 day, using patch-clamp technique in the whole-cell configuration with glass micropipettes of 3–5 MΩ resistance. No compensation was performed for pipette resistance and cell capacitance. During patch clamp recordings, cells were perfused with an extracellular solution containing (in mM): 138 NaCl, 5.4 KCl, 2 $CaCl_2$, 1 $MgCl_2$, 10 glucose, 10 HEPES, pH 7.4 (adjusted with NaOH). The pipettes used for recordings were filled with an intracellular solution containing (in mM): 140 KCl, 2 $MgCl_2$, 10 EGTA, 10 HEPES, 5 Mg-ATP, pH 7.4 (adjusted with KOH). Current was recorded using an Axopatch-200A amplifier, filtered at 5 kHz, and digitized using a DigiData 1440A (Molecular Devices). The pCLAMP software (version 10.2) was used for data acquisition and analysis (Molecular Devices).

To generate conductance/voltage curves, cells were held at -80 mV, then depolarized for 1.5 s from -80 mV to +20 mV in 10 mV increments, followed by an isopotential pulse at 0 mV (Figure 3.4). Current values recorded at the beginning of the 0mV pulse were measured, normalized, and expressed as a function of the preceding voltage. The data obtained were then fit to a Boltzmann distribution of the following form:

$$y = max / [1 + exp (V_{1/2} – V)/k]$$

where V is the test potential, $V_{1/2}$ indicate the half-activation potential, and k the slope factor (Figure 3.4). Current densities (expressed in picoamperes per picofarad, pA/pF) were calculated as peak K^+ currents (pA) measured at 0 mV divided by the capacitance of the same cell (expressed in pF) (Figure 3.4).

To evaluate the effects of drugs on K_v7, cells were clamped at - 80 mV and currents were elicited by 3-s voltage ramps from -80 mV to +20 mV in the presence and absence of each compound.

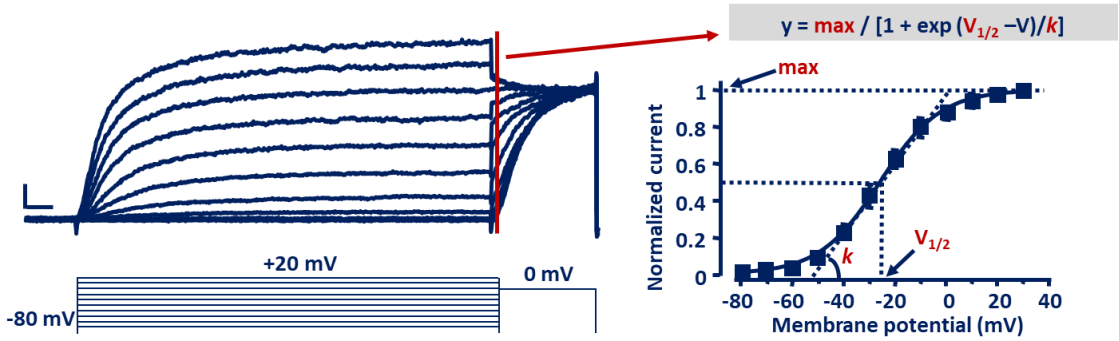

Figure 3.4. Whole-cell configuration of patch-clamp tecnique. On the left, representative trace obtained by application the voltage protocol in the bottom. On the right, conductance/voltage curve obtained fitting to a Boltzman distribution the data.

3.6 96-well format FluxOR II Green Potassium Ion Channel Assay

Screening of retigabine derivatives have been performed on stable CHO cell lines co-expressing K_v7 channel subunits of interest by using a fluorescence based (FluxOR Green Potassium Ion Channel Assay). Briefly, the assay is based on the uses of Thallium (Tl^+) as a surrogate for K^+ ions and a fluorescent Tl^+-sensitive dye called FluxOR™. The dye is loaded into cells as a membrane-permeable aminomethyl (AM) ester and its permeation is facilitated by the presence of the surfactant PowerLoad™. Once in the cytosol, AM ester dye is cleaved by endogenous esterase to obtain fluorogenic thallium-sensitive form and its cell extrusion is inhibited by the presence of probenecid, a blocker of the organic anion transporter. During the assay, a small amount of thallium is added to the cells with a stimulus to open channels. Thallium then passes into cells through open potassium channels according to a strong inward driving force. Upon binding cytosolic thallium, the de-esterified FluxOR™ dye exhibits a strong increase in fluorescence intensity at its peak emission of 525 nm (Figure 3.5 panel A)

CHO cells that stably expressed $K_v7.2/7.3$ channels were resuspend to 2×10^5 cells/ mL in complete growth medium, and 80 µL/well were plated into a Biocoat Poly-D-Lysine Celleware 96-well plates (Corning,USA) and incubated overnight at 37 °C in a 5% CO_2 incubator. The next day, the assay was performed using the “Wash method” as described by the manufacturer: after manual removal of the medium, 80 µL of 1X Loading Buffer (PowerLoad™ Concentrate 100X 100µL/10ml, FluxOR™ II Reagent 10 µL/ 10ml, deionized water 8.8 mL/10ml, FluxOR™ II Assay Buffer, 10X 1 mL/10ml and probenecid 100µL/10ml) were manually added into the cell plate, and then incubated in the dark at room temperature for 60 minutes. Subsequently the Loading Buffer was removed and replace with 70 µL/well of Assay Buffer (Deionized water 8.9mL/10mL, FluxOR™ II Assay Buffer 10X 1 mL/10mL, Probenecid 100 µL/10mL). Additionally, 10µl/well of the test compounds were manually added into the plate. Cell plates were loaded onto an FLUOstar

OPTIMA microplate reader (BMG LABTECH) Set up the instrument with standard FITC green filters or set the excitation wavelength to 485 nm and the emission wavelength to 520 nm. After 5 seconds of recording, 20 µL/well of stimulus buffer (Chloride-free Stimulus Buffer 2 mL/10mL, thallium Sulfate (Tl_2SO_4) 1 mL/10mL, deionized water 7 mL/10mL) were added and each well were read every second for 50 seconds. The OPTIMA data Analytics software was used for data acquisition.

To evaluate the effect of retigabine derivatives, two different parameters have been calculated; the ratio between the maximal fluorescent signal and the fluorescent signal at time 0 (F_{max}/F_0) and the slope of the fluorescent curve calculated between 5" and 15" (Figure 3.5 panel B)

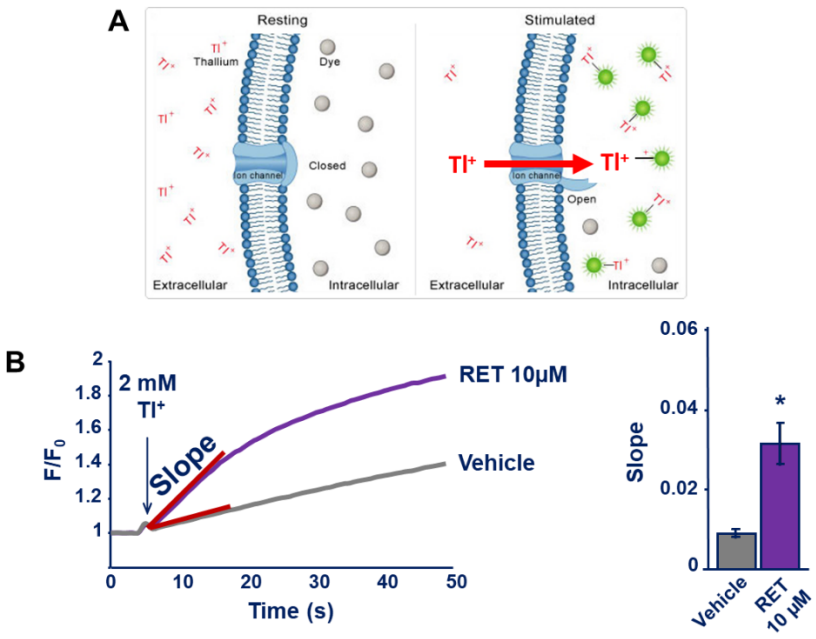

Figure 3.5. The FluxOR™ assay. A) Low basal fluorescence from cells loaded with FluxOR™ dye until potassium channels stimulation (left panel). Subsequently the addition of the stimulus, thallium flows down its concentration gradient into the cells, activating the dye (right panel). B) Representative fluorescent curve recoded on $K_v7.2/7.3$ in presence of 10µM RET (activator) and 1% DMSO (vehicle).

The normalized slope values were plotted versus log(concentration) of the compound, fitted to a four-parameter logistic equation, and EC_{50} values were calculated with SigmaPlot (version 12.3). Indicated EC_{50} values are the mean of at least three independent experiments ± standard deviation (SD).

3.7 384-well format FluxOR II Green Potassium Ion Channel Assay

CHO cells stably expressing $K_v7.3$ A315T channels were resuspended in complete growth medium, 4.000 cells/well were seeded in 50 µl growth medium in black transparent 384-welll plates (Greiner Cellstar, M1937-32A) and incubated overnight at 37 °C in a 5% CO_2 incubator. The next day the culture medium was replaced by 15 µl loading buffer plus

backdrop reagent (BackDrop™, B10512), cells were loaded for 30-60. Following, a “Direct” method was used: the loading buffer was not replace with assay buffer, as in the “wash method”, conversely the next assay steps were performed adding the compounds solution directly in the wells containing the loading buffer. Compounds to test were dissolved in 100 % DMSO, 15 nl of each solution was transferred to a single well using the EchoTM-compound transfer-system (Echo 550, Labcyte Inc.), resulting in a final concentration of 10 µM for each compound, or for the control retigabine. The vehicle was represented by DMSO 0.1%. The assay plate was immediately transferred to the Plate reader (Enivion 2103 multilabel Reader, PerkinElmer) to acquire a pre-stimulus scan: 2 scans were acquired using the FI bottom read protocol (sequential scan of all 394 wells with 45 sec (~ 0.12 sec per well). After the pre-stimulus scan 5 µl of Stimulus Buffer (containing Thallium) was added manually to each well using a multichannel pipette (16 channels). For a kinetic reading, multiple scans were recorded up to 5 min (45 sec per 384 well plate scan) using FI bottom read protocol.

To screen the Fraunhofer library, an endpoint measurement at 50 sec were performed. The tested compounds fluorescent signal was expressed as the ratio F_0/F_{50}, was normalized to the positive control retigabine, and expressed as relative percentage of activation.

3.8 Photochemical Stability Assay

Compounds were dissolved in DMSO and then diluted in buffered aqueous solutions at pH 7.4 to a final concentration of 10 µM. 1cm quartz cells, filled with the above-mentioned solutions were irradiated by an UV lamp (UV Consulting TQ 150 equipped with duran 50 sleeve and 150W power supply unit, Peschl, Germany) at a fixed distance of 20 cm from the UV source. Control samples were maintained at 37°C and wrapped by aluminium foils to avoid light exposure. At predetermined intervals aliquots were withdrawn and analysed by HPLC in order to assess the concentration decrease of the starting materials and the presence of the dimers usually formed by retigabine. UHPLC analyses were performed on a Nexera UHPLC system (Shimadzu, Kyoto, Japan) consisting of a CBM-20A controller, two LC-30AD pumps, a DGU-20 A5R degasser, an SPD-M20A photo diode array detector, a CTO-20AC column oven, a SIL-30AC autosampler.

The separation was carried out on a KinetexTM C18 150 × 2.1 mm × 2.6 µm (100 Å) column (Phenomenex, Bologna, Italy). The optimal mobile phase consisted of 0.1% TFA/H2O v/v (A) and 0.1% TFA/ACN v/v (B). Analysis was performed in gradient elution as follows: 0–13.0 min, 5–65% B; 13–14.0 min, 65–95% B; 14–15.0 min, isocratic to 95%

B; 15–15.01 min, 95–5% B; then three minutes for column re-equilibration. Flow rate was 0.5 mL min-1. Column oven temperature was set to 45°C. Injection volume was 7 µL of sample. The following PDA parameters were applied: sampling rate, 12.5 Hz; detector time constant, 0.160 s; cell temperature, 40°C. Data acquisition was set in the range 190–800 nm and chromatograms were monitored at 224 nm to assess the decrease in concentration of the starting material, while a wavelength of 550 nm was used to eventually detect dimerization.

3.9 *In vivo* experiments

Animals. Male C57Bl/6 mice (Charles River Laboratories, Italy) arrived in the animal facility at 21 days of age, and they were housed in groups of three per cage under controlled conditions (temperature 21 ± 1 °C, 60 ± 10% relative humidity and 12/12 h light cycle with lights on at 07:00 a.m.). Food and water were available ad libitum. Animals were experimentally naive and were used only once. Sample size (n) is indicated in the figure legends. The experiments were approved by the Italian Ministry of Health (n. 246/2019-PR) and performed in agreement with the ARRIVE (Animals in Research: Reporting *In Vivo* Experiments) guidelines,66 with the guidelines released by the Italian Ministry of Health (D.L. 26/14) and the European Community Directive 2010/63/EU.

Drugs. Retigabine (Valeant), compound 60 and XE-991 (Tocris) were dissolved in saline containing 2% Tween-20 and 2% PEG-400. Retigabine was administered in doses of 1 and 3mg/kg at concentrations of 0.1 and 0.3 mg/ml; compound 60 was administered in doses of 0.1, 0.3 and 1mg/kg at concentrations of 0.01, 0.03 and 0.1 mg/ml and XE-991 was administered in dose of 3mg/kg at concentrations of 0.3 mg/ml. Thus, each dose was dissolved to allow injection of 0.01 ml/g, i.p. Control group was represented by mice injected only with vehicle solution (saline containing 2% Tween-20 and 2% PEG-400). Retigabine, compound 60 and vehicle solution were administered 30 min prior to induction of seizures based on pharmacokinetics data published in a previous paper of retigabine efficacy against pentylenetetrazole (PTZ) induced seizures;67 XE-991 was administered 15 min before the retigabine or compound 60 or vehicle injection.

Seizure testing. PTZ (P6500-25G, Sigma, USA) (100 mg/kg, s.c.) was dissolved in saline and administered in doses of 10 mg/ml, thus it was dissolved to allow injection of 0.01 ml/g, s.c. Animals were removed from their home cage, weighed, numbered, and treated with vehicle, retigabine or compound 60 30 min prior to PTZ administration. PTZ was injected, and animals were placed in clear plexiglass boxes for observation of seizure activity. The severity of convulsions (from minimal “clonic” to maximal “generalized tonic-

clonic") as well as the latency to onset of maximal seizure was recorded. Animals were observed for 30 min following PTZ injection. The experiment was repeated upon pre-treatment with XE-991 15 min before vehicle, retigabine or compound 60 injection.

Seizure scoring. Seizures were scored using an 9-point scoring system modified from Lüttjohann's scale (Lüttjohann et al, 2009). 0= Wisker trembling, 1= Sudden behavioural arrest, 2= Facial jerking, 3= Neck jerks, 4= Clonic seizures (sitting), 5= Tonic Clonic seizures (lying on belly), 6= Clonic seizures (lying on side), 7= Tonic clonic seizures (lying on side), 8= Wild jumping. The behavioural assessments described above were performed in a blind manner and the observers had to reach a unanimous agreement regarding the scoring of the behaviour.

3.10 Statistical Analysis

Whole-cell electrophysiology. Statistically, significant differences in electrophysiological data were evaluated with the Student t-test, or with ANOVA followed by the Student-Newman−Keuls test when multiple groups were compared, with the threshold set at $p < 0.05$. Data were analyzed using the SigmaPlot 12.3 for Windows (Systat Software Inc, San Jose, CA). Values are expressed as the mean ± SD of at least three cells recorded in at least two independent transfections as the mean ± standard error of the mean (SEM) of at least three cells recorded in at least three independent transfections.

Fluorencence-based assay. Assay robustness was determined according to the Z' factor (Zhang et al., 1999).

$$Z' = 1 - \frac{3(SD_{RET} + SD_{VEHICLE})}{¿AV_{RET} - AV_{VEHICLE} \vee ¿¿}$$

SD: standard deviation of triplicate in a single experiment, AV: average of triplicate in a single experiment, RET: retigabine at concentration of 10 μM; Vehicle: Assay buffer prepared as indicated in the FluxOR protocol + 0.1% DMSO.

Only experiments resulting in a Z'>0.5 were considered for the retigabine analogues screening. For the Fraunhofer Library screening, also plates showing a Z'≥0.4 were considered. Data shown were obtained from at least three independent experiments. Slope of the fluorescent curves was calculated from point at second 5 to point at second 15 in Microsoft Excel. Values are expressed as the mean ± SEM.

Data were analyzed using the GraphPad Prism 8.0.2 (GraphPad Software, LaJolla, CA). Statistically, significant differences in the initial slope of the curves were evaluated through ordinary one-way ANOVA, multiple comparisons were corrected with the Tukey test. The

threshold of $p<0.01$ is indicated in figures as asterisk. The slope values of the curves, were plotted versus log(concentration) of the compound, fitted to a four-parameter logistic equation and EC_{50} values were calculated with SigmaPlot (version 12.3). Indicated EC_{50} values are the mean of at least three independent experiments ± standard error of the mean (SEM).

In vivo experiments. The number of animals needed for the experiment was determined using the power analysis software GPower version 3.1.92. The require minimum sample size resulted in 8 mice per each group. Statistical analyses were performed using GraphPad Prism (GraphPad Software, LaJolla, CA) using a one-way analysis of variance with Tukey post hoc test. P-value of <0.05 was accepted as indicative of a statistically significant difference.

4. Results

4.1 Development of a fluorescence-based assay to evaluate the activity of K_v7 channel modulators.

The first step of our work was to establish an *in vitro* model suitable to evaluate the activity of K_v7 modulators and to screen several compounds in a short time, therefore different Chinese Hamster Ovary (CHO) cell lines expressing the K_v7 channels were generated and a fluorescence-based thallium-flux assay was implemented.

4.1.1 Electrophysiological characterization of CHO cell lines stably expressing $K_v7.2$, $K_v7.2/7.3$ and $K_v7.3$ A315T potassium channels.

CHO cells transfected with cDNA encoding for ion channels are a cellular model widely used to study these proteins, especially in electrophysiological analyses, because CHO cells do not show spontaneous ionic currents, therefore, upon transfection, the only recorded currents are due to the expression in cellular membrane of the transfected ion channel (Gamper et al., 2005).

With the aim to establish a cellular model to be used in a fluorescence-based assay to study K_v7 channels modulators, we generated CHO cell lines stably expressing $K_v7.2$, $K_v7.2/7.3$ or $K_v7.3$ A315T channels by the means of PiggyBAC transposon system that ensures higher transfection efficiency and more long-lasting protein expression than traditional stable clone generation systems (Matasci et al., 2011).

After transfection and clone selection (described in section 3.1 of *Materials and Methods*), the stable clones were further characterized using the patch-clamp electrophysiological technique. Patch-clamp recordings were performed in CHO stable cell lines and in CHO cells transiently transfected with the cDNAs of interest, representing the control group. To generate conductance-voltage curves, the cells were held at −80 mV, then depolarized for 1.5 s from −80 mV to +20 in 10-mV increments, followed by an isopotential pulse at 0 mV. All electrophysiological results are summarised in table 4.1. Cells transiently transfected with $K_v7.2$ generate a K^+ selective currents showing a current density of 22.9 ± 4.5 pA/pF and exhibit a half-activation potential of -25.2±1.5 mV. Among 4 generated clones, clone number 1 showed $V_{1/2}$ and current density comparable to the control group ($V_{1/2}$=-29.2 ± 3.4 mV; current density= 13.7 ± 3.8 pA/pF) and was selected for further experiments (Figure 4.1, Table 4.1).

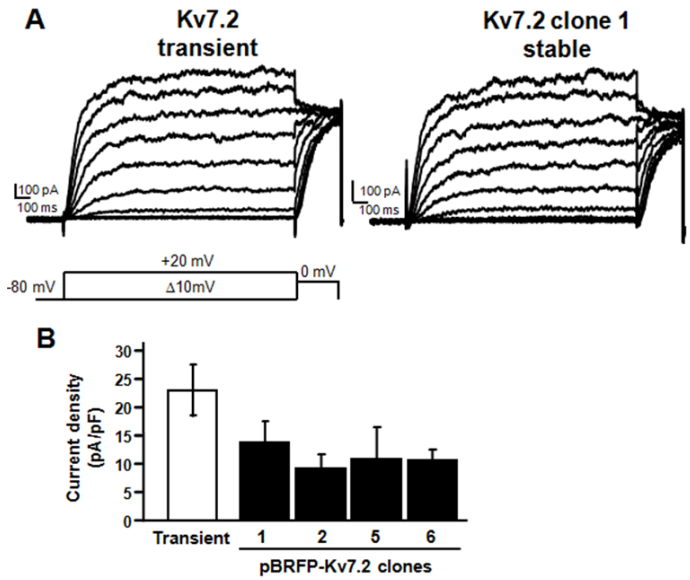

Figure 4.1 Functional characterization of $K_v7.2$ stable cell lines. Representative current traces recorded in CHO cells expressing, stably or transiently, the indicated subunits, in response to the voltage protocol shown in bottom part. Current scale, 100 pA; time scale, 0.1 s.

Cells transiently transfected with the cDNAs encoding for $K_v7.2$ and $K_v7.3$ generated a voltage-dependent K^+ selective current with a current density of 119.7 ± 13.2 pA/pF and a half-activation potential ($V_{1/2}$) of -35.1 ± 1.6. Among the selected 7 clones, clone number 5 exhibited biophysical properties similar to the control group with a calculated $V_{1/2}$ of -32.2 ± 1.7 mV and a current density at 0 mV of 71.1 ± 17.4 pA/pF (Figure 4.2, Table 4.1), therefore clone number 5 was chosen for the subsequent experiments.

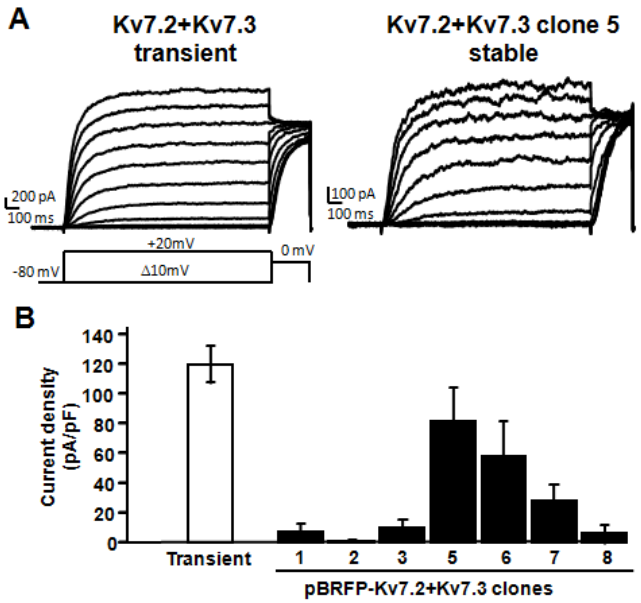

Figure 4.2 Functional characterization of $K_v7.2/7.3$ stable cell lines. A. Representative current traces recorded in CHO cells expressing, stably or transiently, the $K_v7.2/7.3$ subunits, in response to the voltage protocol shown in bottom part. Current scale, 200 pA (for stable) 100 pA (for transient); time scale, 0.1 s. **B.** Screening of 7 $K_v7.2/7.3$ stable clones based on their current density.

To ensure that both $K_v7.2$ and $K_v7.3$ subunits were expressed in the selected clone and formed heteromeric channels, pharmacological experiments with the K_v7 channel blocker tetraethylammonium (TEA) were performed. These experiments are based on the known differential TEA sensitivity existing between homomeric $K_v7.2$, homomeric $K_v7.3$ channels and heteromeric $K_v7.2/7.3$ channels: $K_v7.2$ is highly sensitive to TEA (IC_{50}= 0.3 mM), $K_v7.3$ is TEA-insensitive (IC_{50}= 30 mM), and the heteromeric $K_v7.2/7.3$ channel shows an intermediate sensitivity (IC_{50}= 3 mM) (Hadley et al. 2000). The high TEA sensitivity of $K_v7.2$ might result from the presence of a tyrosine residue in the pore loop of the channel (Kavanaugh et al. 1991), by contrast this residue is replaced by a threonine in $K_v7.3$ which may confers low sensitivity to TEA (MacKinnon et Yellen 1990).

The effect of TEA blockade on $K_v7.2/7.3$ currents of the selected clone was compared to that of the blockade exerted on the control group, represented by CHO cells transiently transfected with $K_v7.2/7.3$ channels. The effect of the TEA blockade was investigated using a ramp protocol in which $K_v7.2/7.3$ currents were activated by 3 s voltage ramps from −80 to +20 mV (Figure 4.3, panel A). Perfusion with 3 mM TEA in the control group induced a current inhibition of about 55% while in the selected clone, the inhibition was about 35%, suggesting that both $K_v7.2$ and $K_v7.3$ subunits are likely expressed, possibly with a slightly higher participation of $K_v7.3$ subunits (Figure 4.3 panel B, Table 4.1).

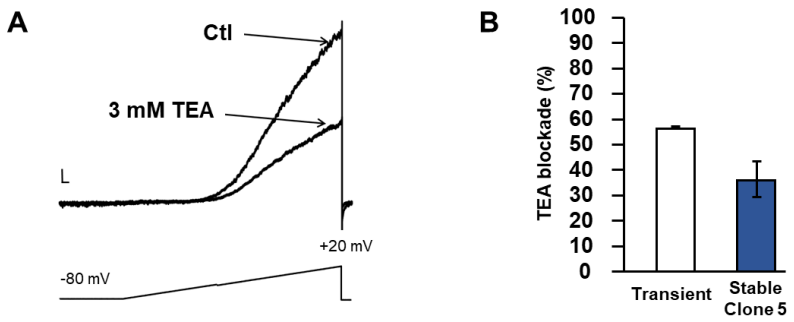

Figure 4.3 Effects of TEA on ramp-evoked $K_v7.2/7.3$ current. **A**. Representative current traces from CHO cells transiently expressing $K_v7.2/7.3$ subunits in response to the indicated voltage ramp protocol before TEA exposure (CTL, control), and during TEA exposure (TEA, 3 mM). Current scale, 100 pA; time scale, 0.1 s. **B.** TEA Blockade percentage in transiently (white) and stably-expressing (blue) $K_v7.2/7.3$ CHO cells.

Compared with other members of the family, $K_v7.3$ homomeric channels yield very small macroscopic currents; indeed, CHO cells transiently transfected with $K_v7.3$ WT showed current density at 0 mV of 17.2 ± 6.1 pA/pF.

Since the FluxOR fluorescence signal intensity is proportional to the flow of ions throw the channel pore, the low current density of $K_v7.3$ channels may represent a hurdle for the

generation of an HTS-compatible cellular model. For this reason, we decided to generate a stable cell line expressing the mutant K_v7.3 A315T.

The introduction of a single point mutation in the inner pore at the 315-position of K_v7.3 channels, changing an alanine with a hydrophilic threonine residue (A315T), is a tool experimentally used to increase the current density of K_v7.3 and enhance macroscopic current size (Etxeberria et al., 2004). It is suggested that this mutation stabilizes the selectivity filter of K_v7.3 homomers in an open conductive configuration through a network of interactions between the lower part of the selectivity filter and the pore helix (Choveau et al. 2012) that results in an increased conduction (Zaika et al. 2008) and perhaps an increase in membrane expression (Gomez-Posada et al. 2010) compared to K_v7.3 WT channel, without altering other important channel characteristics, such as voltage dependence of activation, maximal open probability or PIP_2 affinity (Zaika et al., 2008; Hernandez et al., 2009). Different studies showed that K_v7.3 A315T channel generates a potassium current with higher current density than K_v7.2/7.3 channel (Zaika et al., 2008; Choveau et al., 2012).

In our experiments, CHO cells transiently transfected with K_v7.3 WT showed current density at 0 mV of 17.2 ± 6.1 pA/pF and a $V_{1/2}$ of -36.4 ± 2.3 mV while CHO cells transiently transfected with K_v7.3 A315T showed a current density at 0 mV of 132.3 ± 50.5 pA/pF and a $V_{1/2}$ of -39.3 ± 3.0 mV (Table 4.1).

The K_v7.3* stable clones showed similar current density and $V_{1/2}$ values when compared to those measured in CHO cells transiently transfected with K_v7.3* (Figure 4.4, Table 4.1); among the 3 clones, clone number 1 was selected for the subsequent experiments.

Notably, the current density measured for the selected CHO-K_v7.2/7.3 clone was 71.1 ± 16.9 mV, while the CHO-K_v7.3 A315T clone exhibited a much higher current density of 179.2 ± 31.6 mV (Table 4.1), in accordance with the literature (Zaika et al. 2008; Choveau et al. 2012).

For simplicity, in the next sections, the cell lines stably expressing K_v7.2, K_v7.2/7.3 and K_v7.3 A315T will be named CHO-K_v7.2 CHO-K_v7.2/7.3 and CHO-K_v7.3*, respectively.

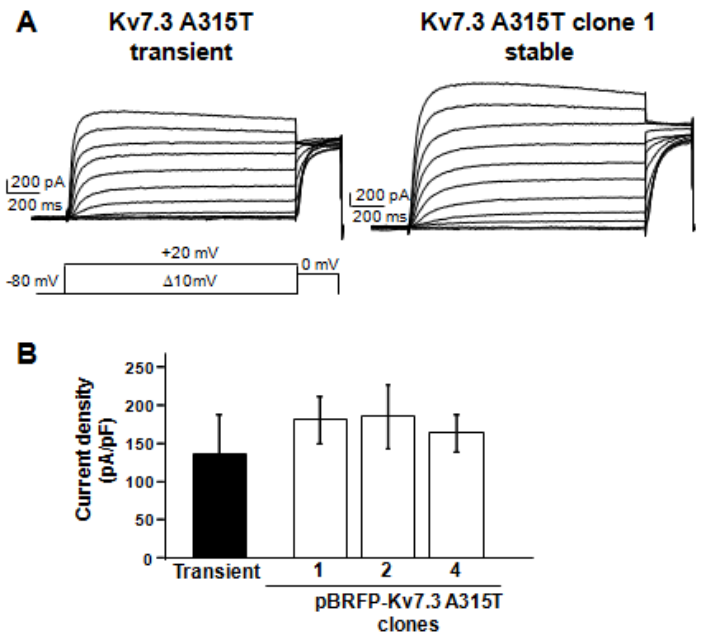

Figure 4.4. Functional characterization of K_v7.3 stable cell lines. **A.** Representative current traces recorded in CHO cells expressing, stably or transiently, the indicated subunits, in response to the voltage protocol shown in bottom part. Current scale, 200 pA; time scale, 0.2 s. **B.** Screening of 3 K_v7.3* stable clones based on their current density.

Table 4.1. Functional and pharmacological characteristic of stable and transient K_v7 cell lines. TEA: tetraethylammonium. Each data is the mean±SEM of cells recorded in at least three separate experimental sessions.

Cell lines	n	$V_{½}$ (mV)	k (mV/efold)	Current density (pA/pF at 0 mV)	Blockade by 3mM TEA (%)
pcDNA3-K_v7.2 transient	13	-25.2±1.5	13.3±1.5	22.9±4.5	
pBRFP-K_v7.2 clone 1	7	-29.2±3.4	10.4±0.6	13.7±3.8	
pcDNA3-K_v7.2/7.3 transient	16	-35.1 ± 1.6	13.0 ±0.7	119.7 ± 13.2	56.1 ± 0.06
pBRFP-K_v7.2/7.3 clone 5	12	-32.2 ± 1.7	9.4 ± 1.7	71.1 ± 16.9	36.0 ± 7.0
pcDNA3-K_v7.3 transient	5-7	-36.4 ± 2.3	8.2 ± 0.6	17.2 ± 6.1	
pcDNA3-K_v7.3 A315T transient	5-7	-39.3 ± 3.0	8.9 ± 0.8	132.3 ± 50.5	
pBRFP-K_v7.3 A315T clone 1	3-4	-41.1 ± 4.0	9.6 ± 1.6	179.2 ± 31.6	

4.1.2 Optimization of FluxOR assay using K_v7.2/7.3 and K_v7.3 A315T-expressing CHO cells

The current gold standard to measure ion channel activity and modulation are the electrophysiological techniques, however they are expensive, time-consuming and their

automated applications are limited.

Therefore, to test the activity of several K_v7 modulators, the fluorescence-based thallium-flux assay FluxOR™ (Thermo Fisher Scientific) was selected and the assay conditions were optimized using the cell lines described in section 4.1.1. Fluorescence-based thallium-flux assays have been widely used in drug discovery campaigns to identify new K_v7 modulators (Beachman et al., 2010; Li et al., 2011; Yue et al., 2016). Given the well-known permeability of potassium (K^+) channels to thallium (Tl^+), these assays exploit Tl^+ as surrogate for potassium K^+ and Tl^+-sensitive dyes, such as FluxOR, that are incubated in cell lines stably expressing the ion channel of interest. When Tl^+ is added to the external cellular solution, this flows through the open channels into the cytoplasm where it binds the Tl^+-sensitive dye, and this interaction generates a cytoplasmatic fluorescent signal proportional to the Tl^+ influx and therefore to the channels opening.

For the following experiments, the K_v7-expressing cells were seeded in 96-well plates, the "Wash method" was used and the addition of thallium solution to the wells was automated by an internal dispenser in the plate reader (detailed protocol is described in section 3.6.1 of *Materials and Methods.*)

Immediately after the drugs to test were added to the cells, the plate was inserted in the plate reader and the base-line fluorescent signal was recorded for 5 seconds (F_0). Then, the thallium solution was added automatically to the external cellular solution, the thallium influx through potassium channels resulted in a cytosolic fluorescent signal increasing over time that was measured for 45 seconds (F_t), obtaining fluorescence curves. Two different parameters were calculated: the ratio between the maximal fluorescent signal and the signal at time 0 before thallium was added (**F_{MAX}/F_0**) and the **slope** of the fluorescent curve between 5 and 15 seconds.

The K_v7 activator retigabine and of the inhibitor XE991 were used in CHO-$K_v7.2/7.3$ and in the parental cell line rapresented by non-transfected CHO cells to exclude off-target interferences with the thallium influx (Yu et al. 2016). In these experiments vehicle consists of Assay Buffer/0.1% DMSO (see section 3.6.1). In non-transfected CHO cells both retigabine (10 μM) and XE991(10 μM) did not modify the fluorescent signal or the slope of the curves (Figure 4.8, panles A and B). By contrast, in CHO-$K_v7.2/7.3$ cells retigabine increased both the F_{MAX}/F_0 and the initial slope of the fluorescent signal; this effects were abolished in presence of XE991 (10 μM) (Figure 4.8, panels C and D).

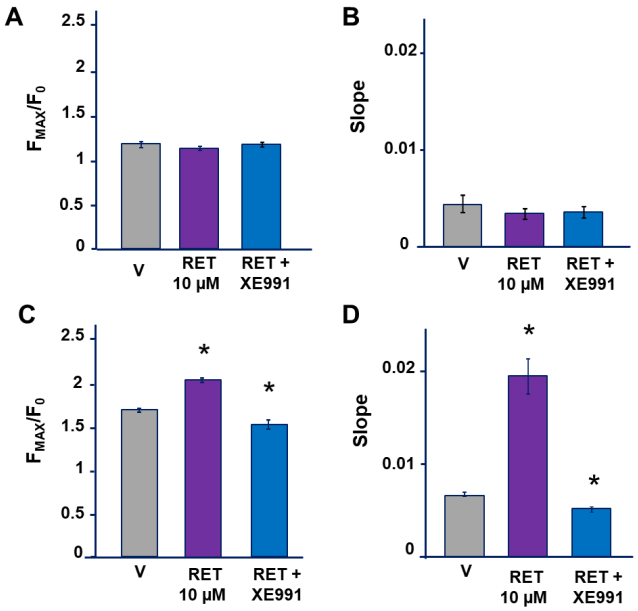

Figure 4.8 Effect of vehicle (V), Retigabine (RET) and XE991 on F_{MAX}/F_0 and slope generated by non-transfected CHO cells (panels A and B) and CHO-K_v7.2/7.3 cells (panels C and D) in the FluxOR assay; (*p < 0.01 vs vehicle)

Retigabine (1-100 µM) increased the fluorescent signal in CHO-K_v7.2/7.3 in a dose-dependent manner with an EC_{50} calculated on the normalized slope of 11.6 ± 1.6 µM, a value slightly higher than that calculated by electrophysiological techniques ($\Delta V_{1/2}$ EC_{50} was 2.5 ± 1.8 µM, see section 4.2.5) (Figure 4.9)

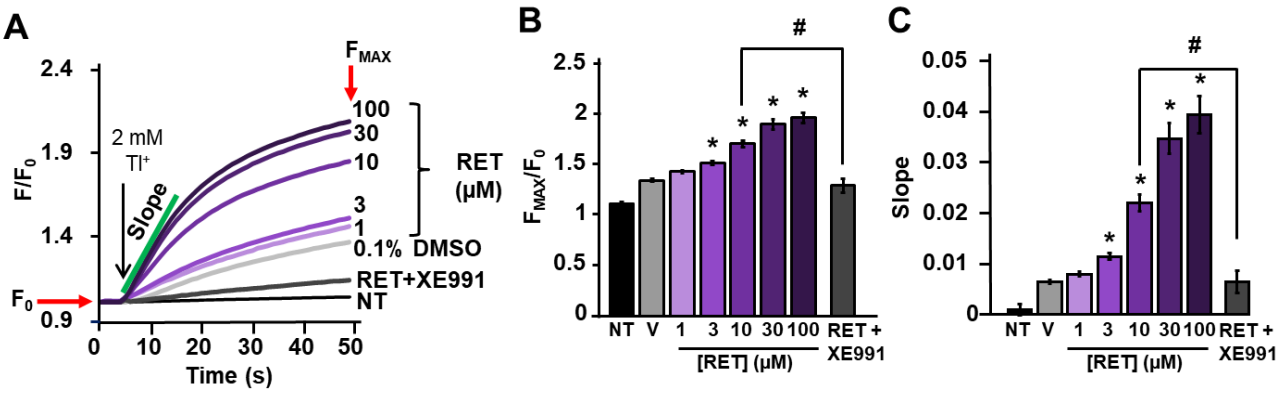

Figure 4.9 A) FluxOR fluorescence curves generated in CHO-K_v7.2/7.3 cells by the following: vehicle DMSO 0.1% (gray curve), retigabine (RET, purple curves), and retigabine + XE991 10 µM co-administrated (black curve). Non-transfected cell (NT) signal is also shown. **(B, C)** Average value of maximal fluorescence (F_{MAX}/F_0 **B)** and initial slope **(C)** of the FluxOR fluorescence signal calculated between 5 and 15 s. (* indicates p < 0.01 vs vehicle; **#** indicates p<0.01 for RET 10 µM vs RET 10 µM + XE991 10 µM)

To evaluate the ability of the assay to distinguish among compounds with different potency, we use the K_v7 activator RL-81 which has been described as a more potent K_v7.2/7.3 activator when compared to retigabine (Kumar et al. 2016). RL-81 (0.01-100 µM) dose-dependently increased both slope and maximal fluorescence, and resulted more

potent that retigabine, with a EC_{50} calculated on the normalized slope of 4.0 ± 1.0 μM, a value lower than that calculated for retigabine ($p<0.05$ vs retigabine, n=5) (Figure 4.10).

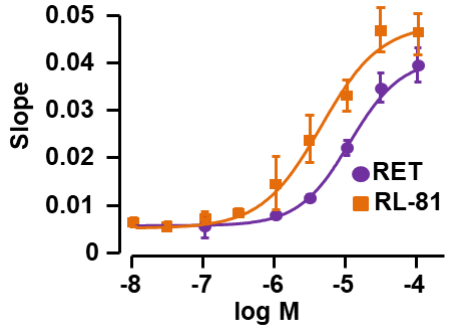

Figure 4.10 Dose−response curves of RET (purple) and RL-81 (yellow) in CHO-K_v7.2/7.3 cells. Solid lines represent fits of the experimental data to the four-parameter logistic equation used to estimate EC_{50} values.

The dynamic range calculated as ratio between F_{MAX}/F_0 induced by retigabine and vehicle in CHO-K_v7.2/7.3 cells was 1.35. An even higher dynamic range (2.09), resulting in a larger signal window, was obtained using CHO-K_v7.3* cells, in which retigabine (10 μM) induced higher F_{MAX}/F_0 and slope than those reached in CHO-K_v7.2/7.3 cells ($p<0.05$): F_{MAX}/F_0 and slope induced by 10 μM retigabine were 1.78 ± 0.02 and 0.02 ± 0.001 for CHO-K_v7.2/7.3 and 2.74 ± 0.14 and 0.08 ± 0.002 for CHO-K_v7.3* (Figure 4.11).

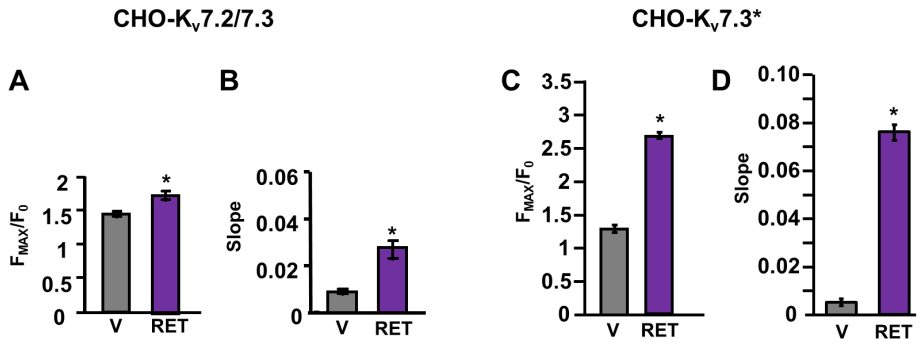

Figure 4.11 Average value of maximal fluorescence (F_{MAX}/F_0) and initial slope of the FluxOR fluorescence signal calculated between 5 and 15 s in CHO-K_v7.2/7.3 stable clone **(A, B)** or in in CHO-K_v7.3* stable clone **(C, D).** V: Vehicle; RET: 10 μM Retigabine (*$p < 0.05$)

Retigabine (1-100 μM) dose-dependent increased the fluorescent signal in CHO-K_v7.3* cells with an EC_{50} calculated on the normalized slope of 3.6 ± 1.5 μM (Figure 4.12). The lower retigabine EC_{50} measured for CHO-K_v7.3* compared to CHO-K_v7.2/7.3 was in line with our electrophysiological experiments performed in transiently transfected CHO cells, where retigabine showed an EC_{50} calculated on $\Delta V_{1/2}$ of 2.5 ± 1.8 μM for K_v7.2/7.3 (see section 4.2.6) and 0.6 ± 0.1 μM for K_v7.3* (see section 4.3.3). These data are in accordance with the higher sensitivity to retigabine described for K_v7.3 channel compared to K_v7.2/7.3 (Tatulian et al. 2001).

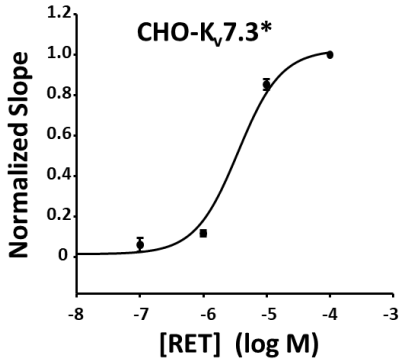

Figure 4.12 Dose-response curves of retigabine (RET) in CHO-K_v7.3* cells. Solid lines represent fits of the experimental data to the four-parameter logistic equation used to estimate EC_{50} values.

Assay robustness was measured using the Z' factor as described in the literature (Zhang et al. 1999) (see *Materials and Methods*): for both CHO-K_v7.2/7.3 and CHO-K_v7.3* cell lines a Z' factor ≥0.5 was calculated, indicating a robust assay, suitable to study K_v7 channels modulators. When the FluxOR assay was performed in CHO-K_v7.2 cells, the calculated Z' factor was <0.5 because of an unfavourable signal-to-noise ratio, therefore this cellular model was not pursued any further (data not shown).

The generated cellular models and the optimized FluxOR assay were used to test the K_v7 opening activity of new molecules in the search for new K_v7 activators, as described in the next sections.

4.2 Identification of novel K_v7 modulators using a Structure-based Drug Design Strategy

One of the strategies we applied to identify novel K_v7.2/7.3 channel activators was a rational *structure-based drug design* to develop novel retigabine analogues overcoming some retigabine limits. It is possible to apply this strategy when the three-dimensional structure of the drug target of interest is available. In our study, the retigabine structure-activity relationship (SAR) was studied exploring its binding site in K_v7.2-5 channels through *in silico* analysis and *in vitro* testing of newly synthesized retigabine analogues. A further effort was made to design molecules that would overcome some limitations of retigabine, such as the possibility of forming photo-induced dimers.

The experiments described in the section 4.2 were performed in collaboration with Dr. Carmine Ostacolo (Department of Pharmacy, University of Naples Federico II) who performed the synthesis of novel retigabine analogues and Dr. Nunzio Iraci (Department of Chemical, Biological, Pharmaceutical and Environmental Sciences, University of Messina) who performed the *in silico* analyses.

4.2.1 *In silico*-guided synthetic strategy of new retigabine analogues

To design novel retigabine analogues overcoming some retigabine limitations, the binding site, the structure-activity relations of retigabine and the structural determinants leading to photo-induced dimers formation were studied.

To investigate the features of the retigabine binding site and to explore the chemical space available in the retigabine binding pocket, molecular docking, and molecular dynamics (MD) experiments were performed.

Two retigabine analogues, namely compounds 23a and 24a, recently describe by Ostacolo and colleagues as more potent than retigabine in activating K_v7.2 channels, were the starting point for the study of the retigabine binding site. 23a and 24a harboured larger substituents at the carbamate region compared to retigabine. Molecular docking simulations performed using the K_v7.2 channel structure, generated by homology modelling starting from Kv1.2/2.1 paddle chimera, suggested that these substituents were accommodated in a plastic binding pocket lined by residues L221, V225, L232, F304, L307, I311 and L312 that is not occupied by retigabine (Figure 4.5). Moreover, electrophysiological experiments showed that 23a and 24a activities were abolished in the K_v7.2 W236L mutant channel, confirming that these analogues maintained the general binding orientation of the parental molecule (Ostacolo et al. 2020).

In this work, 23a and 24a were used to further investigate retigabine binding site in K_v7.2 using the cryo-EM structure of K_v7.2 in complex with retigabine (Li X. et al. 2021). Molecular docking and MD experiments confirmed that the larger substituents of both 23a and 24a specifically interact with residues V225, F304, and L312 lining a region defined as pocket 1 (Figure 4.6, panel B); these interactions are less pronounced in retigabine, given the smaller size of its amide carbonyl substituent.

In addition, MD simulations gave insight into the interaction of retigabine, 23a and 24a with two additional regions in K_v7.2, one contributed by S303 (pocket 2) forming an H-bond with the NH_2 at position 2 of retigabine (area 2) and flanking a small hydrophobic pocket lined by T276, L299, V302, S303, F305 and A306, and another formed by F240, L243, L268, L272, L275 and F305 (pocket 3), where F305 and F240 may interact with the fluorophenyl ring of retigabine (area 3) (Figure 4.6).

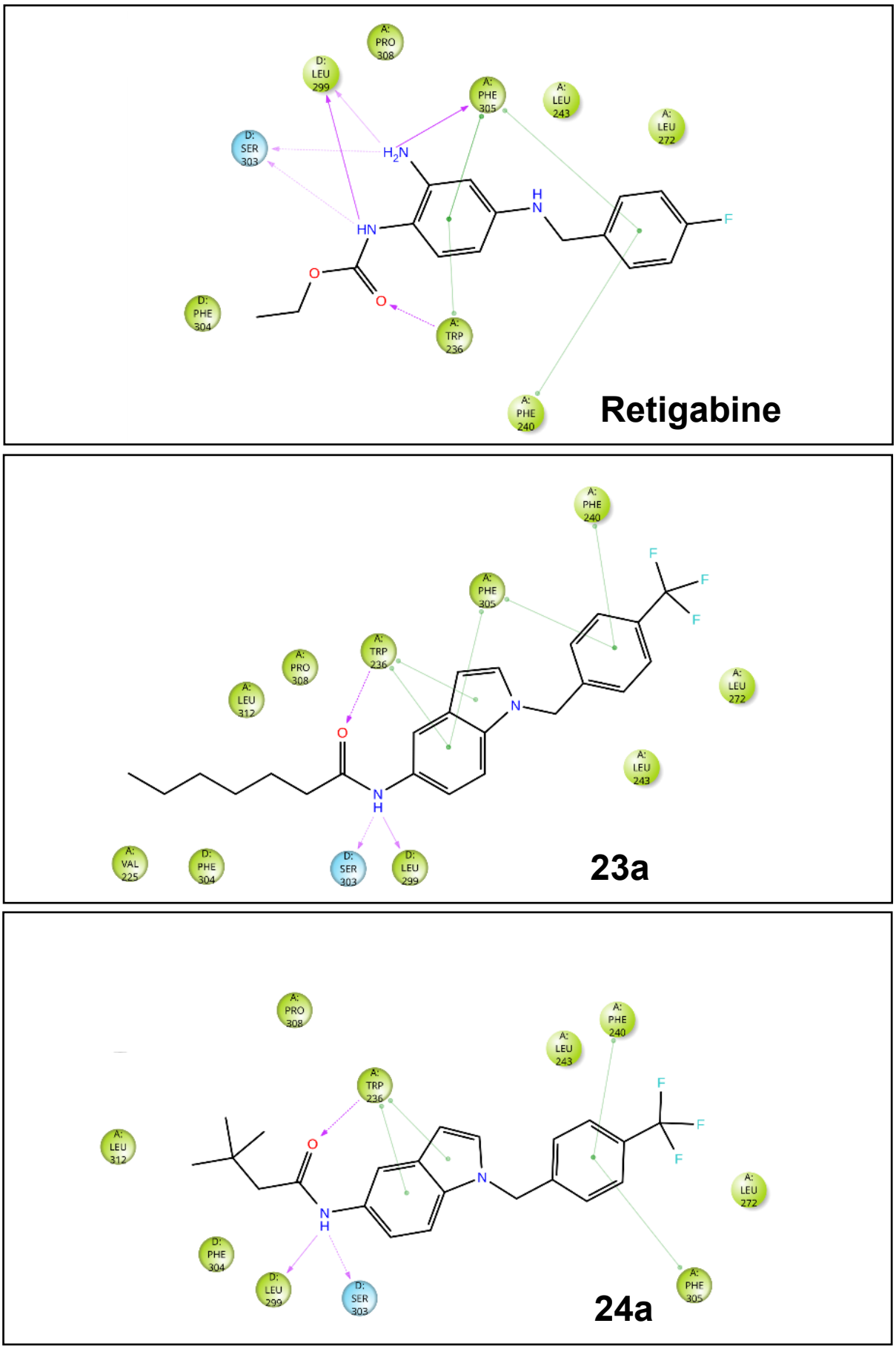

Figure 4.5 Ligand interaction diagram of 120ns-long MD simulations of $K_v7.2$ in complex with retigabine (Li X. et al. 2021) and with the previously-described indole derivatives 23a and 24a (Ostacolo et al. 2020). Only residues interacting with the ligand for at least 12ns out of 120ns of MD simulation time are shown. Hydrophobic residues are depicted in green, polar ones in cyan. H-bonds are represented by magenta arrows (dashed when side chain atoms are involved); green solid lines represent π-π

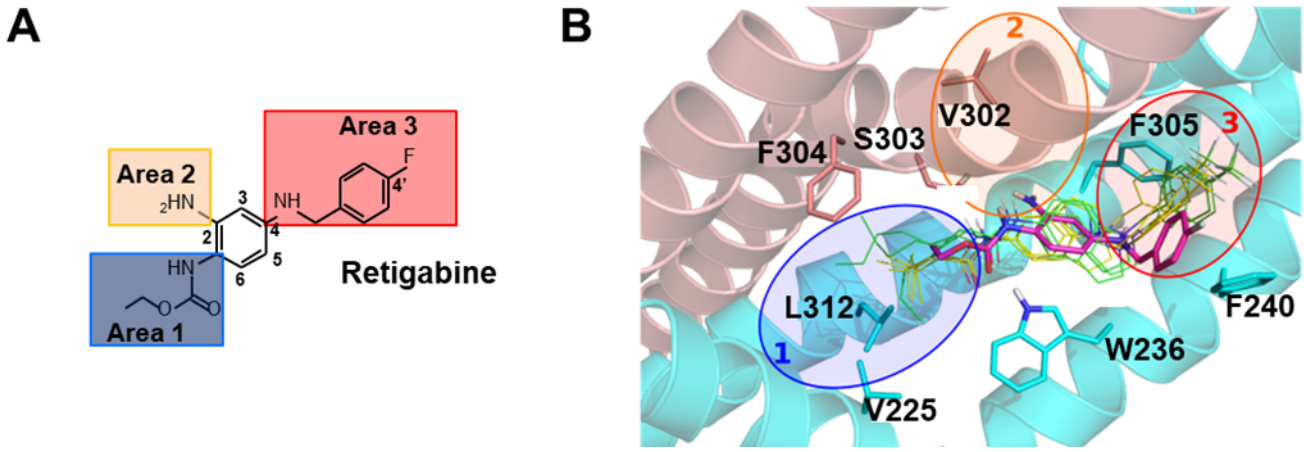

Figure 4.6 A) Retigabine structure with the three different areas investigated by structure-based approach. Highlighted: area 1 in blue, area 2 in orange, and area 3 in red. **B)** The retigabine binding pocket in $K_v7.2$ channels. The two $K_v7.2$ subunits shown are coloured in cyan and salmon. Bound conformations of retigabine (magenta), 23a (yellow) and 24a (green) are shown in thin solid sticks. For each ligand, three bound conformations (sampled at 0, 60 and 120 ns) from 120ns-long MD simulations of the ligand/$K_v7.2$ complex) are shown. Experimentally solved bound conformation of retigabine (PDB ID: 7CR2) is shown in magenta thick transparent sticks

These three pockets identified in $K_v7.2$ (Figure 4.6) also exist in other retigabine-sensitive K_v7 subunits, as revealed by the recent cryo-EM structure of $K_v7.4$ in complex with retigabine (Li T. et al. 2021). Moreover, the high primary sequence similarity among retigabine-sensitive subunits at the level of the residues contributing to these pockets also suggests that the indicated interactions may also occur in $K_v7.3$ and $K_v7.5$ subunits (Figure 4.7).

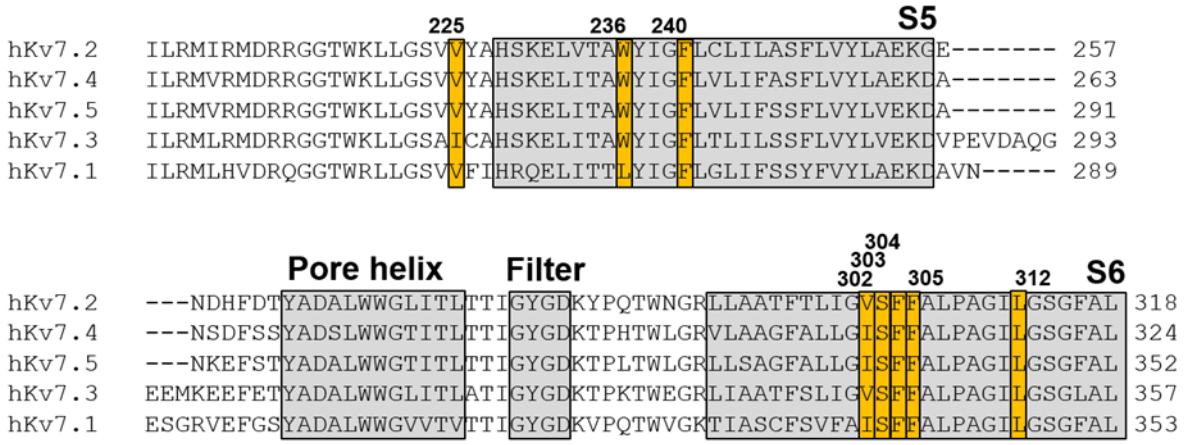

Figure 4.7 Sequence alignment of the S5, S6 and the S5-S6 intervening linker forming the pore domain of the indicated K_v subunits (www.ebi.ac.uk/Tools/psa/). Numbers above the sequences indicate the residues interacting with retigabine, 23a and 24a.

To investigate the structure-activity relations of retigabine, novel retigabine analogues were designed based on the in-silico hypothesis concerning the chemical space at the retigabine binding site: systematic modifications in each of the three areas of retigabine (Figure 4.6) were pursued, and a small library of retigabine derivatives was synthesized. Structures of the newly-synthesized retigabine analogues are depicted in table 4.2, blue

names are used to indicate modifications inserted in area 1, yellow names for modifications in area 2 and red names for modifications in area 3.

4.2.2 Structure-activity relationship study of newly synthesized retigabine analogues

To screen the library of the newly synthesized retigabine analogues, and to investigate the pharmacological consequences of the structural modifications introduced in the retigabine molecule, the fluorescence-based assay described in section 4.1.2 was used in CHO-K_v7.2/7.3 cells. The initial slope of the fluorescent signal produced by 10 μM of each newly-synthesized retigabine analogue was used to study their effect in opening K_v7.2/7.3 channels and was compared to that of 10 μM retigabine (or other compounds used as reference for each sub-series). Results are shown in figure 4.13 and summarized in table 4.2

Table 4.2 Chemical structures and K_v7 opening activity of synthesized compounds

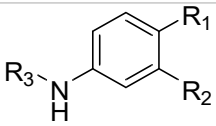

Compound	R_1	R_2	R_3	Slope of the fluorescent signal at 10 μM
RET	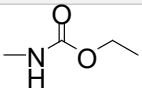	NH_2	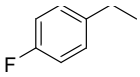	0.0270 ± 0.0052
13	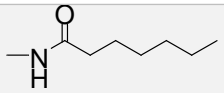	NH_2	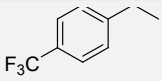	0.0443 ± 0.0049
14	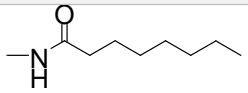	NH_2	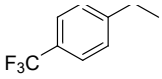	0.0563 ± 0.0039
15	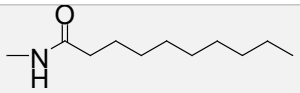	NH_2	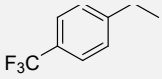	0.0261 ± 0.0030
16	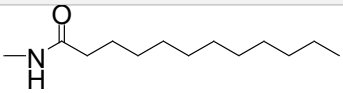	NH_2	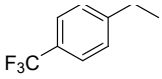	0.0084 ± 0.0004
17	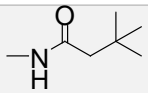	NH_2	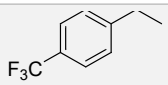	0.0512 ± 0.0040

18	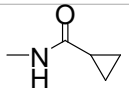	NH_2	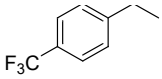	0.0346 ± 0.0078
19	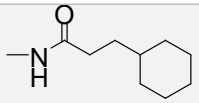	NH_2	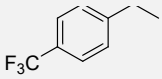	0.0452 ± 0.0077
20	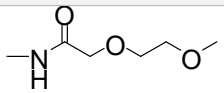	NH_2	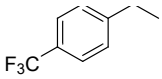	0.0062 ± 0.0005
71	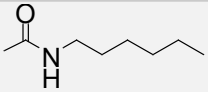	NH_2	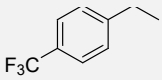	0.0066 ± 0.0006
2	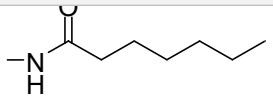	H	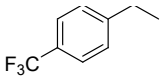	0.0326 ± 0.0063
23	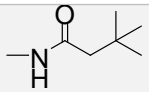		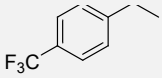	0.0772 ± 0.0036
24	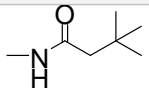		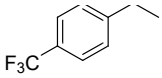	0.0591 ± 0.0043
41	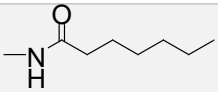	NH_2	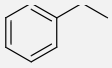	0.0476 ± 0.0030
42	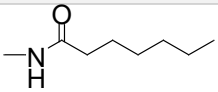	NH_2	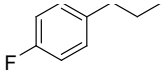	0.0098 ± 0.0010
43	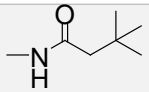	NH_2	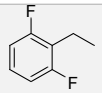	0.0534 ± 0.0028
47	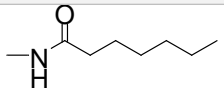	NH_2	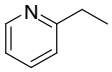	0.0071 ± 0.0004
51	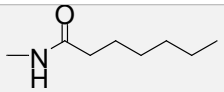	NH_2	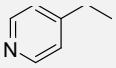	0.0063 ± 0.0002
52	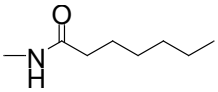	NH_2	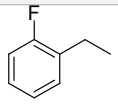	0.0448 ± 0.0035
57	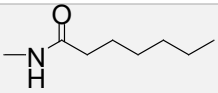	NH_2	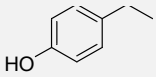	0.0068 ± 0.0003

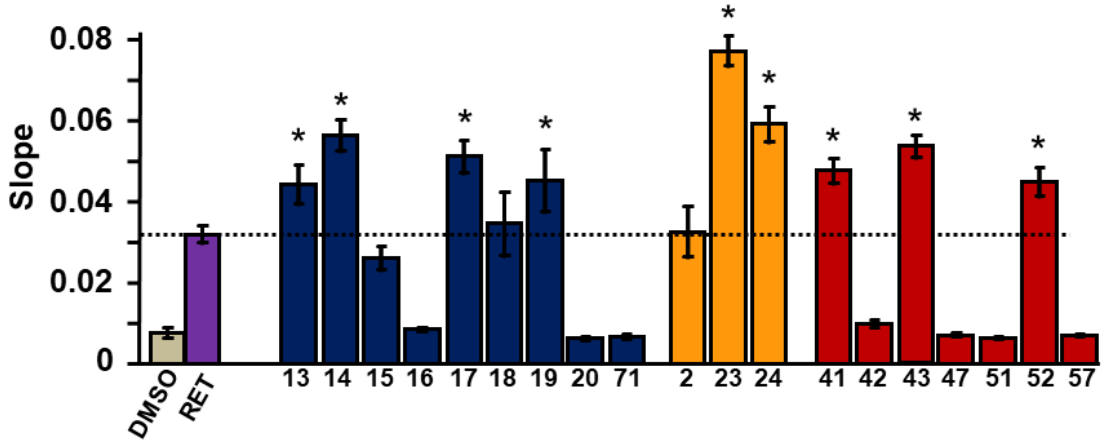

Figure 4.13 Average FluxOR flurescence signals obtained in K_v7.2/7.3-transfected cells upon exposure to the synthesized compounds exploring the chemical space at area 1 (blue bars), area 2 (orange bars) and area 3 (red bars) at a concentration of 10 μM in comparison with retigabine (purple bar). *p < 0.05 vs retigabine 10 μM.

Exploration of the lipophilic pocket 1 (Figure 4.6 panel B) was performed with compounds indicated as **13-20** and **71** carrying substitutions at R1 in area 1 (Figure 4.13, blue bars; Table 4.2). For this sub-series, compound **13** was considered as the reference compound, since a (4-(trifluoromethyl)benzyl group at R3 responsible for a marked improvement in agonist activity (i.e. RL-81) (Kumar et al. 2016; Ostacolo et al. 2020) was present in all these derivatives. The results obtained confirm the presence of a lipophilic pocket in which linear (compounds **13**, **14**), branched (compound **17**), or cyclic (compounds **18**, **19**) substituents are well accommodated when up to 7 carbon atoms are present at R1 (Table 4.2, Figure 4.6 panel A). Instead, at least for linear chains, beyond this optimal length, a progressive decrease in K_v7 opening ability was observed (compounds **15** and **16**); consistent with this are the results of MD simulations showing the escape from the binding pocket of the longer side chains of compounds **15** and **16** (Figure 4.14).

In addition, given the hydrophobic nature of pocket 1, hydrophilic substituents at R1 are poorly tolerated, as for the ethylene glycol chain of compound **20** showing a complete loss of activity.

The observation that the inversion of the amide group in derivative **71** abolished completely the K_v7 opening activity because of the loss of H-bonding between the carbamate group and the indole nitrogen atom of the W236 was in line with literature (Kim et al. 2015) and confirmed the constraints imposed by the specific orientation of the hydrogen bond donor (HBD)-hydrogen bond acceptor (HBA) pattern at W236 for the K_v7 opening.

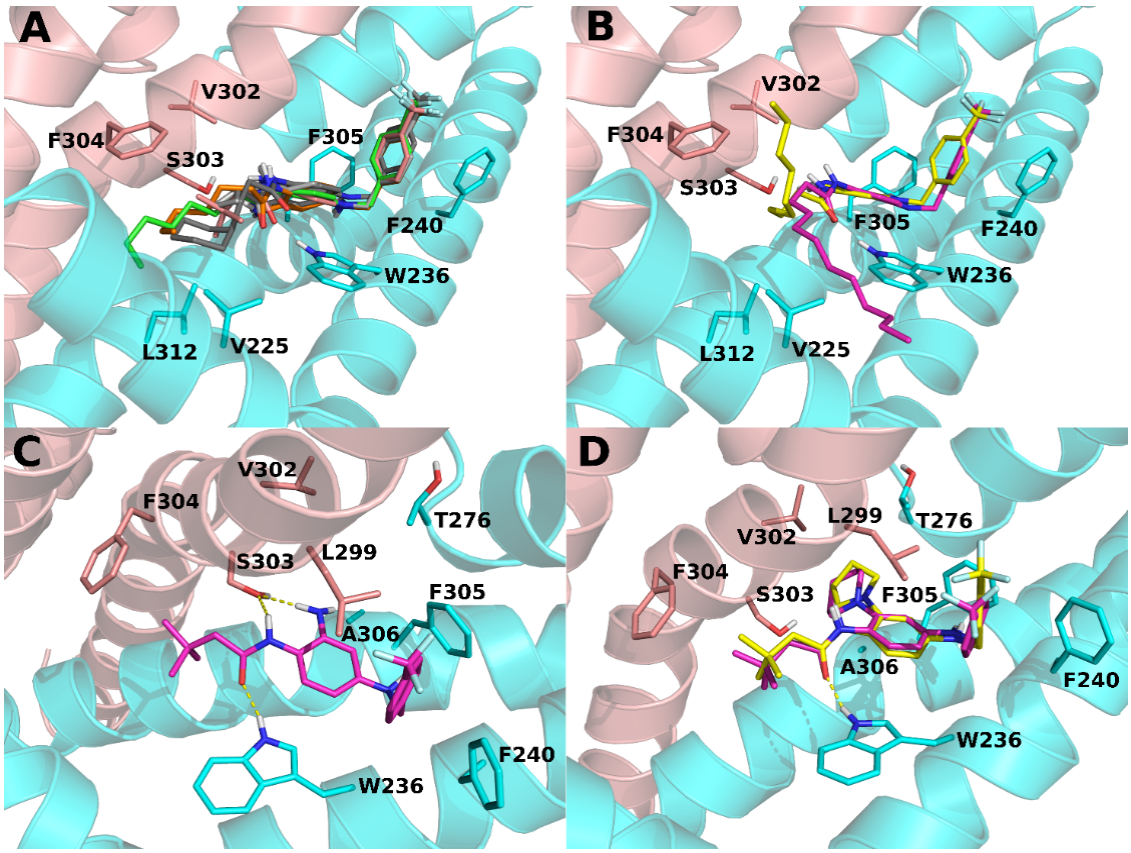

Figure 4.14 Molecular Dynamics (MD) simulations of retigabine analogues. (A) Predicted bound conformations of **13** (orange), **14** (green), **17** (pink), **18** (light gray) and **19** (dark gray) at 60 ns of MD simulations are depicted in sticks. B) Bound conformations of **15** (yellow) and **16** (magenta) at 60 ns of MD simulations are depicted in sticks. C) Predicted bound conformation of **17** (magenta sticks) at 60 ns of MD simulations. (D) Predicted bound conformations of **23** (yellow sticks) and **24** (magenta sticks). In all panels, the two different $K_v7.2$ monomers are depicted in sticks and cartoons and coloured in cyan and salmon. H-bonds are represented by yellow dashed lines.

To explore the lipophilic pocket 2, compounds **2, 23** and **24** were synthesized and the role of H-bond between $-NH_2$ in R2 and S303 side chain was investigated (Table 4.2). Compound **2**, in which the $-NH_2$ is replaced by a hydrogen atom, was still active although with slightly lower efficacy when compared to the structurally similar compound **13** (Figure 4.13, yellow bars).

Moreover, replacement of the NH_2 with larger substituents unable to act as HBDs such as pyrrolidin-1-yl and piperidin-1-yl groups (compounds **23** and **24**, respectively) resulted in K_v7 opening ability comparable to that of the reference compound **17**, with **23** being even more active (Figure 1G). Altogether these results suggested that H-bond interaction with S303 is not essential for K_v7 opening ability and that lipophilic interactions can occur within pocket 2; molecular modelling studies suggested that residues T276, L299, V302, S303, F305, and A306 might act as possible contributors to such interactions (Figures 4.14 panel C and D).

Within area 3 our MD simulations suggested that two phenylalanines (F305 and F240) are close enough to π-π stack with the retigabine benzyl ring.

In the attempt to probe the interactions of the terminal phenyl ring of retigabine with pocket 3, a series analogues carrying modifications at R3 in area 3 was synthesized (Table 4.2) and tested (Figure 4.13; red bars). Moving the fluorine atom in position 2 of the phenyl ring (compound **52**) or its removal (compound **41**) resulted in no change in activity when compared to reference compound **13**, thus ruling out any specific halogen bond involving this fluorine atom; in addition, the 2,6-difluoro analogue of compound **17** (compound **43**) designed to help the ligand phenyl ring to assume an optimal orientation for edge-to-face and/or face-to-face interactions with phenylalanines 240 and 305, still displayed strong activity. Altogether, these results confirm the critical functional role of the previously-mentioned π-π stacking interactions for K_v7 opening. Moreover, replacement of the fluorobenzyl group with hydrophilic hydroxybenzyl (compound **57**) or pyridine (compounds **47** and **51**) groups led to a complete loss of activity, despite their ability to form π-π stacking interactions; these results suggest that a critical degree of hydrophobicity at this region is required for K_v7 opening. Finally, increasing the length of the linker between the fluorobenzyl ring and the amino group at N4 of retigabine with an extra $-CH_2-$ led to a complete loss of activity (compound **42**), likely because this substitution impedes the interaction of the terminal phenyl ring of retigabine with pocket 3 residues L272 and F305 (Figure 4.15).

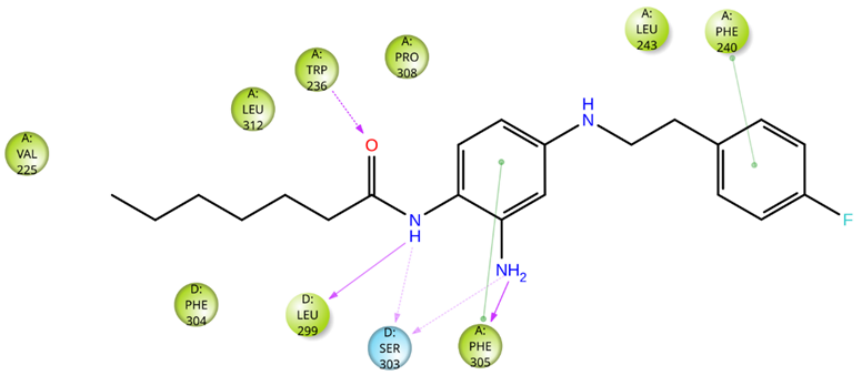

Figure 4.15 Ligand interaction diagram of 120ns-long MD simulations of $K_v7.2$ in complex with **42**. Only residues interacting with the ligand for at least 12ns out of 120ns of MD simulation time are shown. Hydrophobic residues are depicted in green, polar ones in cyan. H-bonds are represented by magenta arrows (dashed when side chain atoms are involved); green solid lines represent π-π interactions.

4.2.3 Photostability of newly synthesized retigabine analogues

One of the main clinical concerns over retigabine observed upon long-term treatment in patients is a retinal and muco-cutaneous blue-gray discoloration due to the formation and accumulations of photo-induced dimers into tissues. Identifying the structural determinants leading to retigabine photo-induced dimers formation is essential to design novel analogues less prone to this chemical reaction and therefore safer for a long-term use in patients.

A proposed mechanism leading to dimers formation is illustrated in figure 4.16, consisting of four reactions:

- Reaction 1 and 2: the first step of retigabine photooxidation is the cleavage of the C-N bond in the linker between the two phenyl groups, leading to the formation of 4-fluorobenzaldehyde and ethyl (2,4-diaminophenyl)carbamate; notably, ethyl (2,4-diaminophenyl)carbamate has been consistently detected as one of the four process-related impurities in several batches of retigabine (Wang et al. 2012); moreover, 4-fluorobenzaldehyde is formed upon UV-visible light irradiation of retigabine solution (Ostacolo et al. 2020).

- Reaction 3: Reaction of the aldehyde intermediate with an intact retigabine molecule leads to the formation of ethyl (2,4-bis((4-fluorobenzyl)amino)phenyl)carbamate, detected following UV-visible light irradiation of retigabine solution (Ostacolo et al. 2020).

- Reaction 4: reaction of the ethyl (2,4-bis((4-fluorobenzyl)amino)phenyl)carbamate with ethyl (2,4-diaminophenyl)carbamate, most likely in the imino tautomeric form, drives to the formation of phenazine and phenazinium dimers, such as those detected in melanin-rich eye tissues upon long-term treatment with retigabine (Groseclose et Castellino 2019).

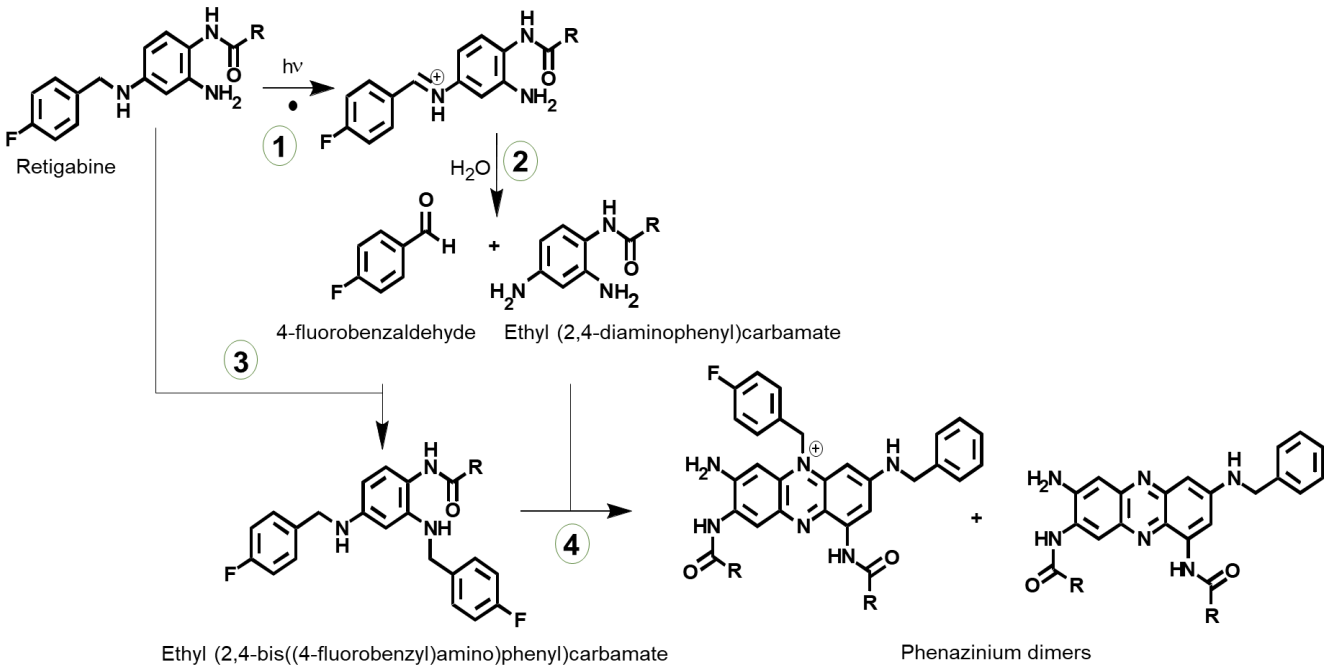

Figure 4.16 Proposed mechanism for retigabine photooxidation.

Among the compounds described in the previously section, **13**, **14**, **17**, **19**, **23, 24, 41**, **43,** and **52** showed higher efficacy compared to retigabine when tested at 10 μM ($p<0.05$). In order to assess their photostability and dimer-forming ability, each molecule was dissolved

in a saline solution at 10 μM, exposed for 3 hours to UV-visible light, and the reaction products were detected through HPLC analysis.

Two different HPLC wavelengths were utilized: a) 220 nm to evaluate the decreased concentration of the starting molecule (photodegradation); b) 550 nm to investigate the formation of phenazine/phenazonium dimers, as previously described (Groseclose et Castellino 2019). Unfortunately, dimer formation was detected for all tested compounds, except for **23** and **24**. However, these two compounds showed an enhanced degradation when compared to retigabine (Table 4.3).

Table 4.3 Photoinduced degradation of retigabine (RET) and its analogues under UV Lighting. Results are expressed as percentage of degradation ± SD.

Compound	% Degradation (3h, UV)	Dimers Formation
RET	61.3 ± 0.1	Yes
13	30.6 ± 2.2	Yes
14	73.2 ± 0.4	Yes
17	79.8 ± 4.2	Yes
19	64.8 ± 0.9	Yes
23	97.7 ± 1.0	**No**
24	79.8 ± 4.2	**No**
41	19.5 ± 4.7	Yes
43	98.4 ± 0.2	Yes
52	74.9 ± 0.1	Yes

The inability of compounds **23** and **24** to form dimers is likely due to the lack of the free amino group in position 2 required for reaction 4 to occur (Figure 4.16).

4.2.4 Synthesis of a second series of retigabine derivatives with improved photostability

With the aim to minimize dimer formation and, at the same time, retain the optimal pharmacological activity revealed by previously-described structure-activity studies, three additional groups of retigabine analogues were designed, synthesized (Table 4.4), and their effect in opening K_v7.2/7.3 channels was tested using the previously described the fluorescence-based assay (Figure 4.17). For the more active compounds, the photostability and dimer-forming ability were tested as described for the previously series of compounds (Table 4.5).

Table 4.4 Chemical structures and K_v7 opening activity of photostable retigabine derivatives.

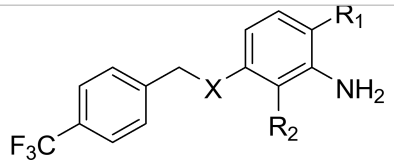

Compound	R_1	R_2	X	Slope of the fluorescent signal at 10 µM
RET	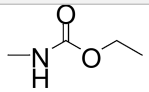	H	NH	0.0270 ± 0.0052
25	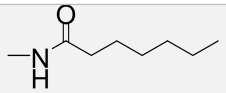	H	NCH_3	0.0637 ± 0.0033
26	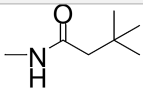	H	NCH_3	0.0721 ± 0.0034
27	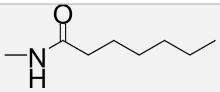	H	NCH_2CH_3	0.0363 ± 0.0052
28	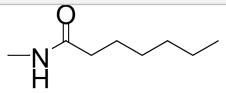	H	$NCOCH_3$	0.0138 ± 0.0024
31	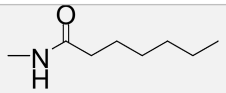	H	O	0.0057 ± 0.0005
59	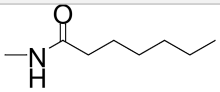		NH	0.0345 ± 0.0026
60	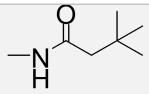		NH	0.0594 ± 0.0026
67	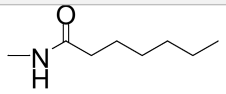	H	CH_2	0.0087±0.0002
68	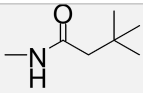	H	CH_2	0.0073±0.0005

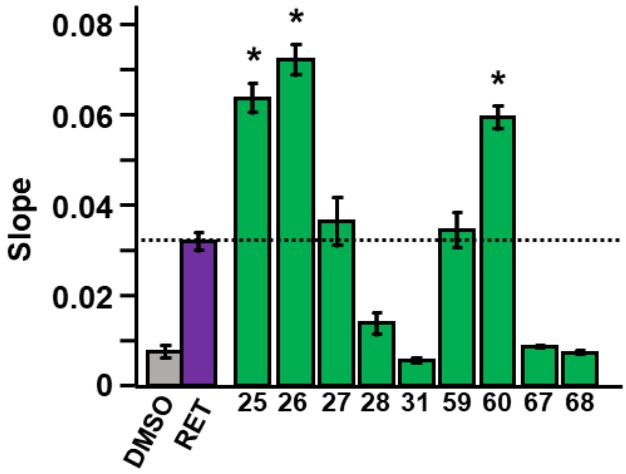

Figure 4.17 Average FluxOR flurescence signals obtained in K_v7.2/7.3-transfected cells upon exposure to the indicated compounds each used at a concentration of 10 μM in comparison with retigabine (RET 10 μM; purple bar). * indicates values significantly different ($p < 0.05$) from RET 10 μM.

The first group of retigabine analogues consisted of N4 (-X- in Table 2) substituted analogues, in which the tertiary amine is unavailable to form phenazine dimers (reaction 4 in figure 4.16) (compounds **25-28**).

Small lipophilic substituents at N4, such as the methyl groups of **25** and **26** improved agonist activity, whereas longer lipophilic substituents, such as a propyl group of **27** did not improve activity, finally, rigid substituents, such as the acetyl group of **28** markedly reduced activity. These observations suggested that pocket 3 displays a limited degree of plasticity, accommodating only small lipophilic substituents.

Since the first step of retigabine photooxidation is the cleavage of the C-N bond in the linker between the two phenyl groups, a second group of molecules designed to prevent C-N bond photooxidative cleavage was synthesized replacing the -NH- in position 4 with oxygen (**31**) or methylene groups (**67-68**). Unfortunately, none of these compounds were able to activate K_v7.2/7.3 channels.

The third group included derivatives replacing hydrogen atoms with electron-withdrawing fluorine atoms at position R2 of the benzene-1,2,4-triamine core scaffold (compounds **59, 60**), a strategy likely reducing the reactivity of N2 and N4. This latter approach has been profitably used before to develop potent and metabolically stable K_v7.2 activators such as RL-81 (Kumar et al. 2016) Within this series, when compared to retigabine, K_v7 opening activity was similar for **59**, and enhanced for **60**.

Overall, within this novel series of molecules, three compounds (**25**, **26**, **60**) displayed efficacy as K_v7.2/7.3 channel activators higher than that of retigabine, therefore their photostability and dimer-forming ability were tested as described above.

Intriguingly, while compounds **25** and **26** did not form dimers but underwent extensive photodegradation (Table 4.5), compound **60** was both more photostable than retigabine and failed to dimerize, as indicated by the absence of the peaks at 550nm in the HPLC spectrum (Figure 4.18). These results are consistent with the proposed mechanism for retigabine photodegradation and dimer formation shown in Figure 4.26. In fact, the tertiary amine in position 4 of **25** and **26,** although preventing phenazine dimers occurrence, remained prone to C-N photooxidative cleavage. The reduced electron availability at N2 and N4 due to the presence of fluorine atom in position 3 of compound **60** strongly reduces also the first photooxidative step, thus conferring remarkable photostability.

Table 4.5 Photoinduced degradation of retigabine (RET) and its analogues under UV Lighting. Results are expressed as percentage of degradation ± SD.

Compound	% Degradation (3h, UV)	Dimers Formation
RET	61.3 ± 0.1	Yes
25	63.3 ± 2.8	**No**
26	99.5 ± 0.1	**No**
60	34.8 ± 1.8	**No**

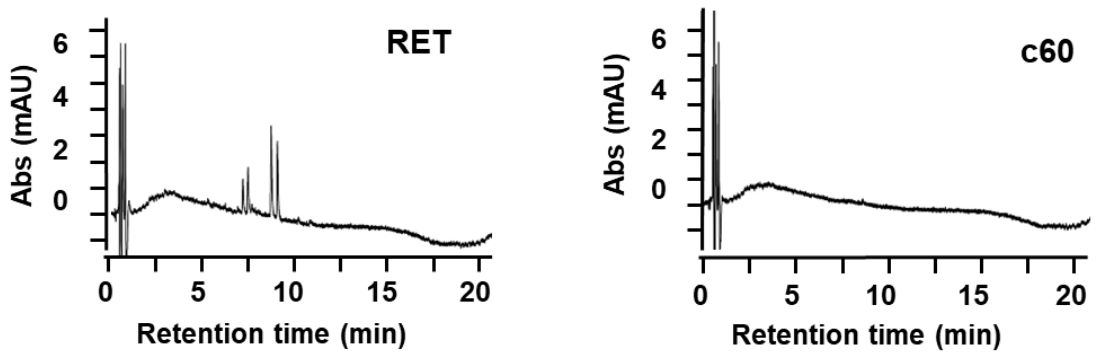

Figure 4.18 HPLC traces of retigabine (RET) and compound 60 at 550 nm after 3h exposure to UV-visible light.

4.2.5 *In vitro* metabolism of photostable retigabine derivatives

To further explore the metabolic stability of compounds **25**, **26**, and **60** in a biologically-relevant model, they were tested in an *in vitro* metabolism assay (S9 fraction of human liver microsomes) using retigabine as a comparator. In this assay, a very small extent (4.7 ± 0.5%) of retigabine undergoes phase I metabolism, whereas a larger fraction (17.4 ± 1.2%) was metabolized in phase II reactions, as previously reported (Hiller et al. 1999,

Hempel et al. 1999, Borlak et al. 2006). Such metabolic profile largely overlaps that of compound **60**, whereas larger fractions of both compounds **25** and **26** underwent *in vitro* metabolism via both pathways; indeed, compounds **60**, **25** and **26** showed a phase I turnover metabolism of 8.2±2.7%, 20.6±1.4% and 32.1±1.2, respectively, and a phase II turnover metabolism of 15.6±0.3, 33.2±1.0% and 32.7±0.3, respectively.

4.2.6 Electrophysiological assessment of compound 60 as K_v7 opener: comparison with retigabine and RL-81

Given the higher efficacy as $K_v7.2/7.3$ activator showed by compound **60** in the FluxOR assay and considering its improved photostability and *in vitro* metabolic profile when compared to retigabine, a further characterization of compound **60** was performed using the whole-cell patch-clamp electrophysiological technique, the gold-standard assay for a detailed evaluation of ion channel modulators.

Electrophysiological experiments were performed in mammalian CHO cells transiently transfected with $K_v7.2/7.3$ cDNA. Cells were held at -80 mV, then depolarized for 1.5 s from -120 mV to +20 mV in 10 mV increments, followed by an isopotential pulse at 0 mV (protocol depicted in figure 4.19).

$K_v7.2/7.3$ channels expressed in CHO cells generated voltage-dependent K^+-selective currents characterized by a slow time course of activation and deactivation, a threshold for current activation around -40 mV, and a half activation potential ($V_{1/2}$) of -30.2 ± 0.7 mV (Figure 4.19, control).

The effect of compound 60 was compared to retigabine and its more potent analogue RL-81 (Kumar et al. 2016). Perfusion with 1 μM retigabine induced a leftward shift in $V_{1/2}$ ($\Delta V_{1/2}$) of about 10 mV; the same concentration of RL-81 or compound **60** caused a leftward shift of about 40 mV and 50 mV, respectively.

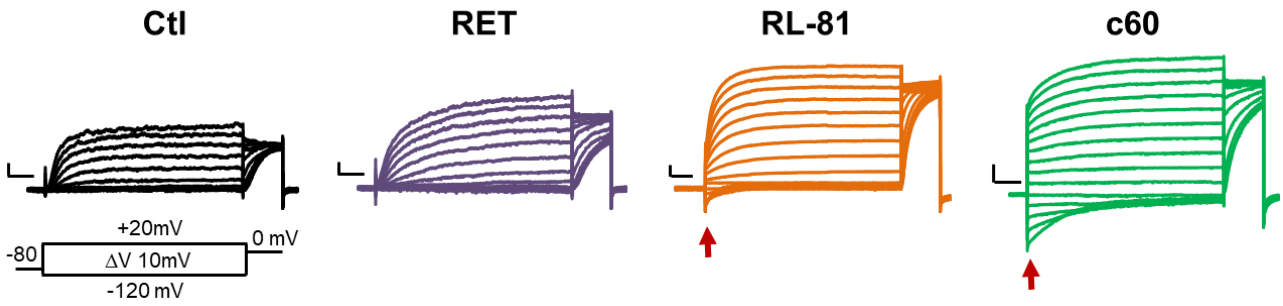

Figure 4.19 Effect of retigabine (RET), RL-81 and compound **60** on $K_v7.2/7.3$ currents. (A) Representative macroscopic current traces recorded from CHO cell expressing $K_v7.2/7.3$ channels in response to the indicated voltage protocol before (Ctl) and after application of 1 μM RET, RL-81 and compound **60**, as indicated. Current scale, 200 pA; time scale, 200 ms.

The negative shift in the activation voltage triggered by RL-81 and, more so, compound **60** in K_v7.2/7.3 channels caused a significant fraction of channels to be open at the holding voltage of -80 mV; most of those open channels were closed upon membrane hyperpolarization to -120 mV, leading to the appearance of deactivating inward currents (red arrows in Figure 4.19).

To better assess the quantitative differences occurring in K_v7-opening ability between retigabine, RL-81 and compound **60**, dose-response experiments (0.01-30 μM) were performed to calculate EC_{50s} using both functional parameters of $\Delta V_{1/2}$ (Figure 4.20 panel A) and maximal current increase (Figure 4.20 panel B). $\Delta V_{1/2}$ EC_{50} were 2.5±1.8 μM, 0.24±0.06 μM, and 0.15±0.03 μM for retigabine, RL-81 and compound **60** ($p<0.05$ RL-81 and **60** vs retigabine, n=5), respectively. Instead, it was not possible to define an EC_{50} for retigabine when the maximal current was taken into consideration, given the small size of the drug-induced effect, as previously reported (Li X. et al., 2021) in fact, the $I_{retigabine}/I_{control}$ was 0.99±0.15. The same experiments carried out with RL-81 (in which the $I_{RL-81}/I_{control}$ was 1.6 ± 0.2) and compound **60** (whose $I_{c60}/I_{control}$ was 2.1 ± 0.3) revealed EC_{50s} of 0.27±0.04 μM and 0.06 ± 0.01 μM ($p<0.05$, n=6-11), respectively.

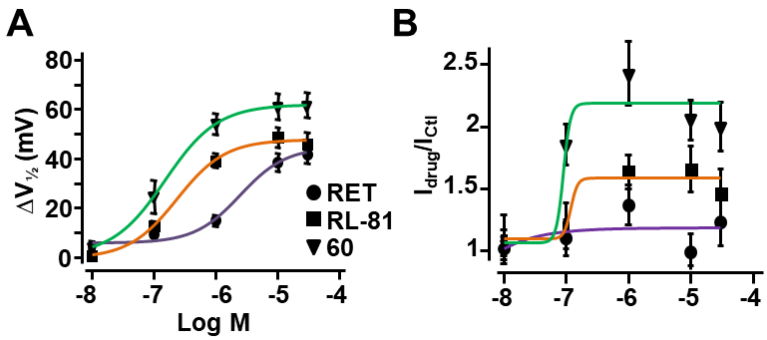

Figure 4.20 Dose-response curves reporting the effects of the 3 indicated compounds on the $V_{1/2}$ shift ($\Delta V_{½}$) in mV (**A**) and on maximal current densisty ($I_{drug}/I_{control}$; **B**) calculated at +20mV for K_v7.2/7.3 channels

Altogether, these data, while confirming the 10-fold higher potency of RL-81 over retigabine as K_v7.2/7.3 activator (Kumar et al. 2016), also revealed that compound **60** was 16 times more potent than retigabine, thus resulting about twice more potent than RL-81. Such rank-order of potency is similar to that revealed by the Tl^+-based fluorescent assay, although the absolute EC_{50} values calculated with electrophysiological methods appear generally lower than those assessed with the fluorescence assay; indeed, the EC_{50s} were 11.2 ± 1.6 μM for retigabine, 4.0 ± 1.0 μM for RL-81 ($p<0.05$ vs retigabine, n=5, see section 4.2.2, Figure 4.10), and 3.2 ± 1.7 μM for compound **60** ($p<0.05$ vs retigabine, n=5).

4.2.7 Binding site of compound 60 in $K_v7.2$

Our molecular modelling simulations for compound **60** in $K_v7.2$ predicted binding interactions shared with retigabine, such as S303 in pocket 2 and W236. Moreover, additional and specific hydrophobic interactions with residues in pocket 1 of $K_v7.2$ channel were identified. In particular, average distances between compound **60** or retigabine and the residues V225, F304 and L321 suggested these aminoacidic residues were contacted by compound **60** but not by retigabine, due to its shorter later chain in area 1. To investigate if the slight increase in potency and the markedly higher efficacy as K_v7 activator shown by compound **60** over retigabine or RL-81 was due to its ability to establish additional hydrophobic interactions with residues in pocket 1, site-directed mutagenesis was used to generate three mutants $K_v7.2$ cDNAs: V225A, F304A, and L312A. Unfortunately, when these cDNAs where expressed in CHO cells and voltage-clamp experiments were performed, $K_v7.2$ V225A, F304A, and L312A mutant channels carried currents whose size was too low to be amenable for pharmacological analysis (Figure 4.21, panel A).

Electrophysiological experiments using mutant $K_v7.2$ channels S303A and W236L were performed. Noticeably, similarly to retigabine, K_v7 opening ability of compound **60** was almost fully abolished in W236L channels, and slightly but significantly reduced in S303A channels, suggesting a marked similarity in the overall binding of compound **60** and retigabine (Figure 4.21, panel B).

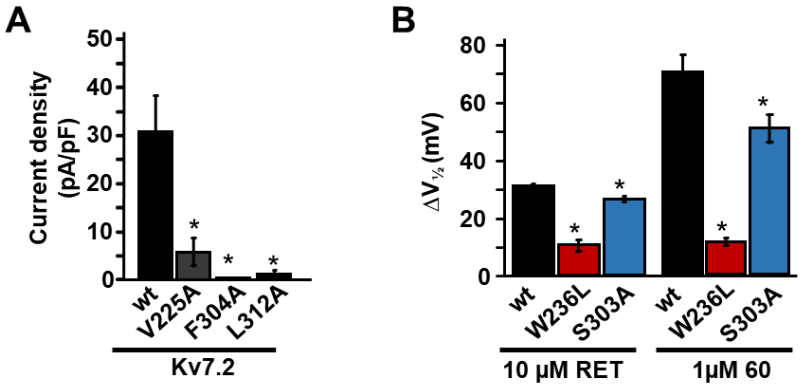

Figure 4.21 A. Current density of the indicated homomeric $K_v7.2$ channels; **B.** Effect of 10 μM RET or 1 μM **60** on the indicated homomeric $K_v7.2$ mutant channels. *indicates values significantly different ($p < 0.05$) from respective WT controls.

4.2.8 K_v7 selectivity of compound 60

In order to evaluate the effects of compound **60** on other K_v7 channels, its ability to activate $K_v7.4$ channels expressed in CHO cells was investigated. Application of

compound **60** at a concentration corresponding to the EC_{50} measured for $K_v7.2/7.3$ channels (0.1 μM), caused a $\Delta V_{1/2}$ of −29.2 ± 4.4 mV and $I_{drug}/I_{control}$ of 2.5 ± 0.3 (n= 4) on $K_v7.4$ currents; both these values were not significantly different ($p>0.05$) from those observed in $K_v7.2/7.3$ channels (Figure 4.20). These results suggested that similar to retigabine, compound **60** does not discriminate between $K_v7.2/7.3$ and $K_v7.4$ channels, a result consistent with the high degree of conservation of the amino acids involved in retigabine binding between $K_v7.2$ (Li X. et al., 2021) and $K_v7.4$ channels (Li T. et al. 2021) as well as with the structural similarity of pocket 1 likely accommodating the R1 substituents responsible for the higher potency of compound **60** as a K_v7 activator.

4.2.9 Anticonvulsant effects of compound 60 in a mouse model of acute seizures

The data described in the sections above suggested that compound **60** was a chemically-stable, highly-potent $K_v7.2/7.3$ channel activator. Since activation of $K_v7.2/7.3$ channels is known to exerts antiseizure effects *in vivo* (Rostock et al. 1996) the possible anticonvulsant activity of compound **60** was evaluated in an acute seizure model and compared to that of retigabine. To this aim, a widely used mouse model of generalized myoclonic seizures such as the acute exposure to pentylenetetrazol (PTZ) was chosen.

Convulsive behavior was triggered by a subcutaneous (s.c.) injection of 100 mg/Kg PTZ in mice, intensity of seizures was assessed and quantified according to the revised Lüttjohann's scale (see Materials and Methods) (Luttjohann et al. 2009) using a 9-points severity score ranging from 0 (wisker trembling) to 8 (wild jumping). For each animal, the maximal severity score (Figure 4.23 panel A) and the time latency required to reach such value (Figure 4.23 panel B) were recorded. To assess the antiseizure effects of retigabine and compound **60**, each mouse was pre-treated with retigabine (1 or 3 mg/Kg i.p.) or compound **60** (0.1, 0.3, or 1 mg/Kg i.p.) 30 minutes before PTZ injection. In vehicle-treated mice the seizure score and the latency to maximal seizures were 7.4 ± 0.1 and 407.6 ± 89.3 seconds, respectively (Figure 4.23 panela A and B). Retigabine failed to affect seizure severity (seizure score of 6.9 ± 0.3 and 7.3 ± 0.3 at 1 mg/kg and 3 mg/kg, respectively, Figure 4.x panel A), whereas it significantly increased the latency to maximal seizure(s) when used at 3 mg/Kg (1041.4 ± 223.2 s, Figure 4.x panel B), in agreement with literature data (Forcelli et al. 2012). By contrast, compound **60** was able to reduce both the severity and the latency of PTZ-induced seizures when used at doses 10-times lower than those of retigabine (seizure score of 6.0 ± 0.4 and latency time of 1159.7 ± 169.4 s at 0.3 mg/Kg dose, Figure 4.23 panels A and B, respectively).

To demonstrate that the antiseizure effects of retigabine and compound **60** were mediated by their K_v7 channel-opening actions, the K_v7 selective channel blocker XE991 (3 mg/Kg i.p.) was used. In these experiments, for retigabine or compound **60** the minimum effective doses calculated from previous experiments were used: 3 mg/Kg (retigabine) and 0.3 mg/Kg (compound 60), respectively. XE991 alone did not affect seizure severity score or latency; in animals pre-treated with XE991 both retigabine (3 mg/Kg) and **60** (0.3 mg/Kg) antiseizure effects were fully prevented, confirming that their effect is due to K_v7 activation Figure 4.23 panels C and D).

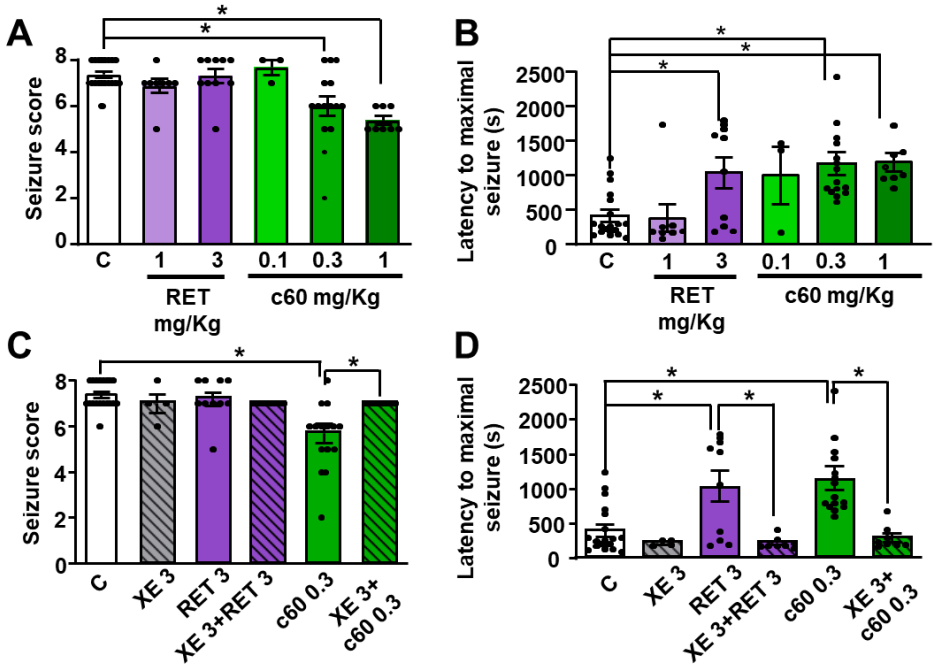

Figure 4.23 Anticonvulsant efficacy of retigabine and compound **60** (c60) in pentylenetetrazol (PTZ)-induced acute seizures in mice. **(A-B)** Average values for seizure score **(A)** and latency to onset of a maximal seizure **(B)** as a function of retigabine (RET) or compound **60** doses. Individual scores calculated in each animal are indicated by dots. **(C-D)** Effect of retigabine (RET) and compound **60**, with (hatched bars) or without (empty bars) pretreatment with XE991 (XE 3mg/Kg) on seizure score **(C)** and latency to onset of a maximal seizure **(D)**. The asterisk (*) indicates values significantly different ($p < 0.05$) from respective controls.

In our experiments, only about 37% (7/19) of vehicle-treated mice survived at the end of the 60 min observation period (Figure 4.24), this was in line with the high mortality rate observed in the PTX model (Breidenbach et al. 2020). In agreement with its strong antiseizure effect, compound **60** dose-dependently reduced mortality, with 87% (13/15) animals treated with 0.3 mg/Kg and all animals (8/8) treated with the highest dose of 1 mg/Kg surviving; instead, no protective effect on mortality was observed with the highest dose of retigabine (3mg/Kg), with only 40% (4/10) of mice surviving. Notably, compound **60**-induced pro-survival effects were largely (though not fully) abolished by XE991 pretreatment (Figure 4.24), with 75% (6/8) of mice surviving after PTZ administration.

As reported (Zaczek et al., 1998) doses higher than 3 mg/kg XE991 led to the occurrence of significant tremors, which may affect the behavioral observation of the epileptic phenotype; this might have resulted in the lower survival observed in XE-treated animals when compared to controls or retigabine-treated animals; thus, no attempt was made to use doses higher than 3 mg/kg to revert the pro-survival effect of compound **60**.

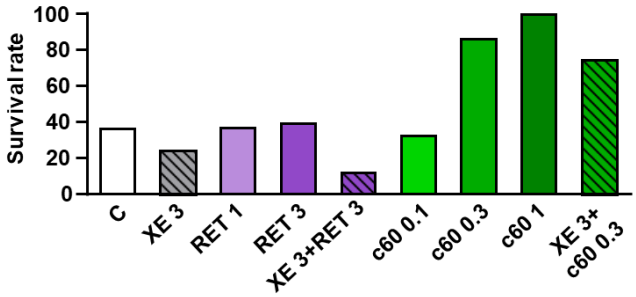

Figure 4.24 Effect of RET (1, 3 mg/Kg), **c60** (0.3-1 mg/Kg) or XE991 (3mg/Kg) on mice survival rate after PTZ exposure. The number of animals used in each group was: 19 for controls, 4 for XE (3 mg/Kg), 8 for RET (1 mg/Kg), 10 for RET (3 mg/Kg), 8 for XE+RET (3+1 mg/Kg); 3 for **c60** (0.1 mg/Kg), 15 for **c60** (0.3 mg/Kg), 8 for **c60** (1 mg/Kg), and 8 for XE+**c60** (3+0.1 mg/Kg).

4.2.10 Pharmacokinetic assessment of compound 60

Poor brain penetration and short half-life were two pharmacokinetic limits of retigabine. To investigate this aspect, brain/plasma distribution and plasma half-life of compound **60** were studied and compared to retigabine. Brain and blood samples were processed to allow UHPLC−MS/MS analysis.

The results obtained revealed that after 60 min i.p. administration of each drug at 1 mg/kg in mice, the brain and plasma concentrations were 469.2 ± 142.8 ng/mg and 202.2 ± 90.9 ng/mg for retigabine, and 726.6 ± 178.8 ng/mg and 18.2 ± 3.7 ng/mg for compound **60**, respectively (Figure 4.25). Thus, compound **60** showed a remarkable brain accumulation, with a brain/plasma ratio 18-times higher than that of retigabine (40.4 vs 2.3, respectively). This result is likely explained by the higher lipophilicity (logP 4.74) of compound **60** over that of retigabine (logP 3.08).

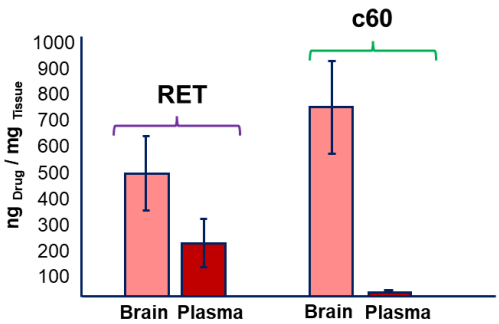

Figure 4.25 Retigabine (RET) and compound 60 (c60) brain and plasma level after 60 min i.p. administration of each drug at 1 mg/kg in mice

Blood sampling at predetermined intervals (0, 0.5, 2, 4, 8, and 24 hours) after i.p. administration of retigabine (3 mg/Kg) or compound **60** (0.3 mg/Kg) was performed to provide intial clues on time-dependent pharmacokinetics of compound **60** when compared to retigabine; these experiments required multiple blood sampling in a short time, and therefore rats instead of mice were used. The results obtained revealed that, altough the AUC normalized on the administreted dose (AUC/dose) was not significantly different between retigabine and compound **60** (0.44 for retigabine vs 0.33 for compound 60), the plasma half-life of compound **60** (16.9 hours) was about 5-times higher than that of retigabine (2.4 hours) (Figure 4.26). These results suggest that the longer plasma half-life of compound 60 might overcome another important limitation of retigabine, namely its three times a day dosing requirement.

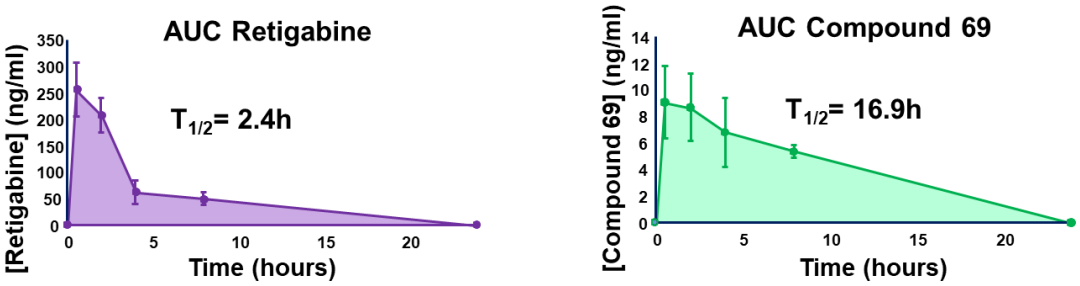

Figure 4.26 Plasma concentration-time curves after a single-dose of Retigabine (3 mg/Kg) or compound 60 (0.3 mg/Kg) injected i.p in rats. Values are represented as mean with ±SD (n=3)

4.3 Identification of novel K_v7 modulators using a Drug Repurposing Strategy

Although the rational design of a new molecule, such as compound **60**, allowed us to develop a potential new drug with an improved pharmacological profile and fewer side effects than the reference drug retigabine, we know that a new chemical entity must pass through several stages of preclinical and clinical trials before it reaches therapy. So, an alternative approach we explored to identify novel $K_v7.2/7.3$ channel activators that could reach clinical use more quickly than a newly synthesised molecule was the Drug Repurposing Strategy.

Drug Repurposing is the investigation of existing drugs for new therapeutic purposes, with the advantage of reducing time and costs involved in developing a new chemical entity as a drug. The first step to find a new use of a drug is to identify a new pharmacological target it acts on; one of the systematic approaches used to aid this step is the HTS of repurposing compounds libraries.

HTS consists of highly automated screening systems to record a biological activity at the molecular, cellular or organism level. In our work we used a cell based HTS to screen *The Fraunhofer repurposing library*, a collection of 5632 compounds deriving from the Broad

Repurposing Hub (Corsello et al. 2017), including 3400 compounds that have reached clinical use across 600 indications as well as 1582 preclinical compounds with varying degrees of validation.

The experiments described in the sections 4.3.1 and 4.3.2 were performed at the Screening-Port of the Fraunhofer Institute for Translational Medicine and Pharmacology ITMP, under the scientific direction of Dr. Philip Gribbon and in cooperation with the HTS specialist Oliver Keminer and with the bioinformatics scientist Andrea Zaliani.

4.3.1 Adaptation of the lab-scale fluorescence-based assay for a large-scale format

The lab-scale FluxOR assay described in section 4.1.2 was a valuable tool to study the effect of newly-synthesized retigabine analogues in activating K_v7 channels (see sections 4.2.2 and 4.2.3). However, the parameter used to study their K_v7 opening ability, such as the slope of the fluorescent curves, requires a kinetic measurement of the fluorescent signal lasting at least 15 seconds after the addition of Tl^+ to the external cellular solution, for each tested substance. To screen large libraries of thousands of compounds, such kinetic measurement would take an inordinate amount of time and was therefore unsuitable. To find a parameter other than the slope to query the library, and to optimize the assay to an automated handling of the tested compounds, an adaptation of the fluorescence-based assay from a lab-scale to a large-scale was necessary.

To adapt the FluxOR assay to a large-scale automated process suitable to screen large libraries of compounds and identify K_v7 channels modulators, CHO-$K_v7.2/7.3$ and CHO-$K_v7.3$* cells were seeded in 384-well plates and different assay conditions were tested.

When the “Wash method” of FluxOR assay, involving removal of medium and several buffer replacements, was applied in a 384-well plate, it caused problems affecting the reproducibility of the experiment such as incomplete removal of medium or buffers, loss of adherent cells, air bubbles in different wells (data not shown). Therefore, the “Direct method” in which buffers are added to the well without removing the medium, was used in place of the “Wash method”.

The high sensitivity of the hightrouput plate reader (Enivion 2103 multilabel Reader, PerkinElmer) produced an intense background noise, therefore *BackDrop* background suppressor (Thermofisher) was added to the Assay Buffer (detailed protocol is described in section 3.6.2 of *Materials and Methods*).

Before thallium addition, each plate was read for 3 seconds (pre-scan) in order to measure the base line rapresenting the F_0 value. The drugs to test were added using an automated

system called *EchoTM-compound transfer-system,* this step requires about 45 seconds for a whole 384-well plate. The K_v7 activator retigabine was used in CHO-K_v7.2/7.3, in CHO-K_v7.3* and in the parental cell line rapresented by non-transfected CHO cells to exclude off-target interferences with the thallium influx (Yu et al. 2016).

Experiments described in the previous sections and performed using a kinetic measurement mode, showed that the fluorescent signal starts to increase immediately after the addition of thallium (figure 4.9 panel A). Those measurement were taken using a plate reader equipped with an internal dispenser that automatically adds the thallium-containing solution one well at a time, and simultaneously reads the fluorescent signal.

Unfortunately, for the experiments performed at the Fraunhofer Institute it was not possible to automate the addition of the thallium solution to the wells since the Enivion Plate reader used does not present an internal dispenser, therefore this step was done manually with a multichannel pipet and required about one minute for a whole 384-wells plate. After thallium was added, the plate was inserted in the plate reader.

The time needed to manually add the thallium solution and to move the plate from one instrument to another produced a delay between thallium addition and plate reading, so part of the increasing fluorescent signal was lost. Therefore, to study how the delay affected the signal and how long it was stable over time, the fluorescent signal was measured for 300 seconds and the raw fluorescence was normalized to F_0 (Figure 4.27).

In non-transfected cells a slight increase in fluorescence over time was measured, likley due to the spontaneous entry of thallium into the cell through diffusion processes not mediated by K_v7 channels; this fluorescent signal was not modulated by retigabine 10 μM (Figure 4.27, panel A, curves of vehicle and retigabine overlapping). Despite the use of the background suppressor, the dinamyc range for CHO-K_v7.2/7.3 was to narrow to ensure a good assay resolution, with the signal for vehicle (negative control) and 10 μM retigabine (positive control) too close to each other (data not shown). Therefore, for the large-scale assay development the CHO-K_v7.3* cell line was used.

In CHO-K_v7.3* cells treated only with vehicle (Assay Buffer/0.1 % DMSO) the influx of thallium through the open channels produced a fluorescent signal increasing over time (Figure 4.27, panel B, gray curve); retigabine treatment (10 μM) produced a stronger signal that rose reaching a plateau after about 100 seconds (Figure 4.27, panel B, purple curve).

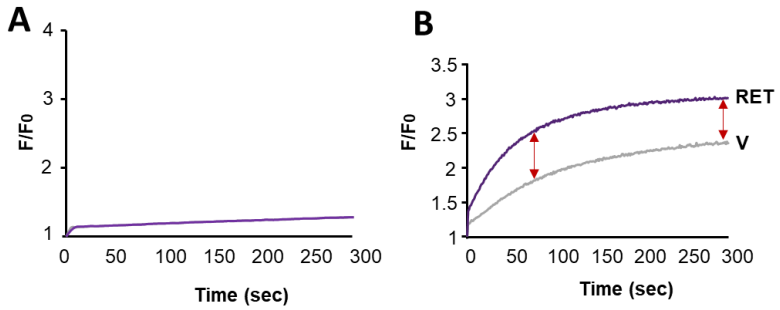

	Sec 50	Sec 300
$\frac{F_t/F_{0\ RET}}{F_t/F_{0\ Vehicle}}$	1.62 ± 0.04	1.25 ± 0.02

Figure 4.27 (A, B) FluxOR fluorescence curves generated in non-transfected CHO cells **(A)** and in CHO-K_v7.3* cells **(B)** by vehicle (V, DMSO 0.1%, gray curve) or Retigabine 10 μM (RET, purple curves). **(C)** Dynamic range of FluxOR assay in CHO-K_v7.3* cells.

As mentioned above, to obtain curves describing the increment of fluorescence over time and measure a slope, a kinetic measurement of the fluorescent signal for several seconds in each well is needed. The amount of time spent on this measurement is acceptable to study the effect of a small number of molecules, which results in a small and manageable number of experimental groups, while it is too time-consuming to screen libraries of thousands of compounds, and it is difficult to replicate in an automated system.

Therefore, to adapt the lab-scale assay to a larger scale assay, single end-point fluorescent signal measurement was used instead of the slope of the curves.

In order to estimate an appropriate time for an endpoint estimation, the time course of the dynamic range was studied: since the vehicle signal increase over time, the difference between vehicle and retigabine tended to decrease over time (Figure 4.27, panels B, red arrows), indeed the dynamic range calculated as ratio between F_T/F_0 induced by retigabine and vehicle decreased from 1.62 ± 0.04 at F_{50}/F_0 to 1.25 ± 0.02 at F_{300}/F_0 (Figure 4.9, panel C).

To evaluate if this phenomenon affected the potency of retigabine, dose-response tests were measured at different time points after thallium addition and results are shown in figure 4.28: although the basal signal increased over time, the calculated EC_{50} value for retigabine was not strongly affected: EC_{50} shifted from 0.34 μM to 0.28 μM over a period of 450 seconds (50 – 500 s). For an endpoint measurement the timepoint at 50 seconds was therefore chosen.

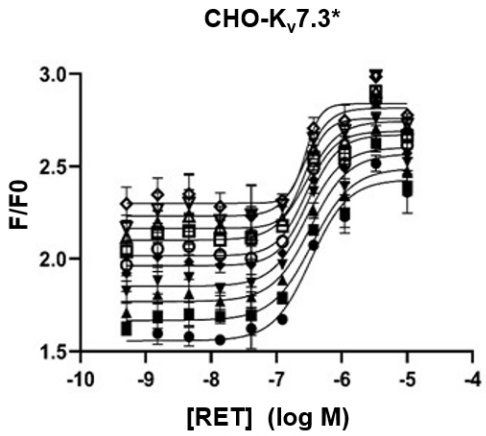

Time point (sec)	EC_{50} (µM)
50 sec,	0.33
100 sec,	0.34
150 sec.	0.33
200 sec.	0.29
250 sec.	0.30
300 sec.	0.28
350 sec.	0.29
400 sec.	0.27
450 sec.	0.27
500 sec.	0.28

Figure 4.28 Dose response curves of Retigabine detected at different time points after thallium addition in CHO-K_v7.3* cells

The last step of the assay adaptation was the assay validation consisting in a repeated test of whole 384-well plate fully loaded with testing compounds. Positive and negative controls were represented by vehicle (Assay Buffer/0.1 % DMSO), and retigabine 10 µM, respectively, and were used to calculate the Z' value as reported in literature to evaluate the robustness of the screening assay (Zhang et al. 1999). Compounds to test were part of the Fraunhofer repurposing library, were solubilized in DMSO, diluted in the Assay Buffer and tested at the concentration of 10 µM.

The end point measurement was performed recording the fluorescent signal 50 seconds after the insertion of the plate into the plate reader. The test of the same set of compounds was repeated twice (run I and run II) to determine the reproducibility of the screening mode. Endpoint measurements were expressed as the ratio F_t/F_0 and were plotted as run II against run I (Figure 4.29).

For both plates a Z' ~0.4 was calculated (run I: 0.41; run II: 0.46). Considering that a Z' ≥ 0.5 have been described as the optimal value for a robust assay (Zhang et al. 1999), the Z' ~0.4 indicated that the assay resolution we reached was not optimal. Further improvement of the assay quality was not achievable due to the fast Tl^+ influx kinetic and the unavoidable delay from the manual Tl^+ addition and the plate reading. However, despite the Z' ≤0.4, the assay validation test showed a reproducible activation of the K_v7.3* channel for most of the tested compounds, therefore the resolution was considered sufficient to perform a library screening.

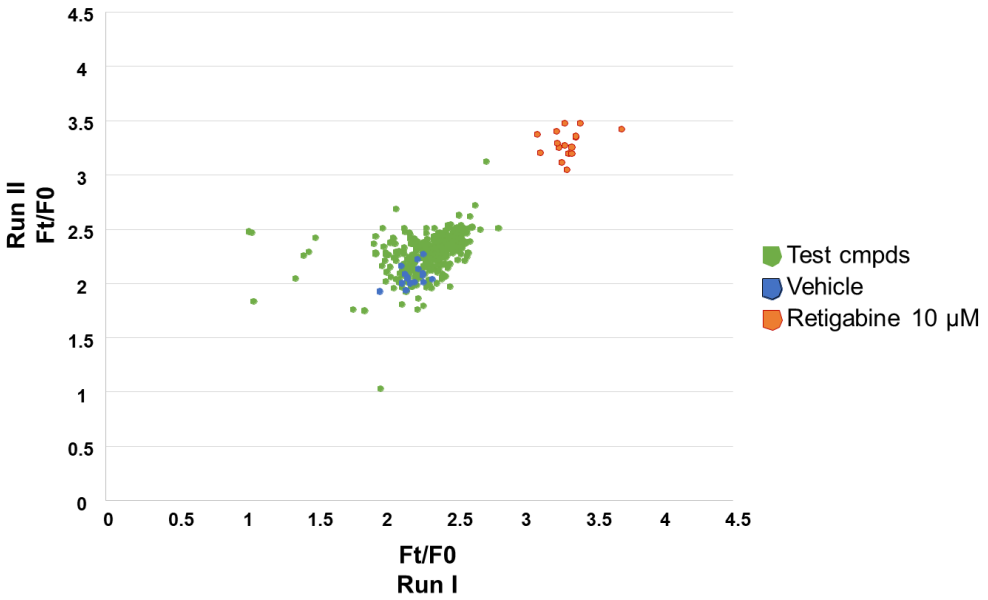

Figure 4.29 Assay validation: repeated testing of a Fraunhofer repurposing library plate. Results are expressed as the ratio F_t/F_0 and plotted as run II against run I.

4.3.2 Screening of the Fraunhofer repurposing library and hits validation

The Fraunhofer repurposing library is a collection of about 5600 compounds already characterized for their biological activity. The most (3400) of them already passed all the clinical stages of development and reached clinical use; the others are involved in pre-clinical or clinical studies.

The primary screening of the library was performed using CHO-K_v7.3* cells in the fluorescence-based assay FluxOR, as described in section 4.3.1, with the purpose to find new K_v7 channels openers. The 5632 compounds of the Fraunhofer repurposing library were divided in sixteen 384-well plates to test, on each plate positive and negative controls (retigabine10 µM and vehicle, respectively) were included according to the plate layout depicted in figure 4.30, each compound was tested at the concentration of 10 µM.

The K_v7.3* opening activity of tested compounds resulted in a fluorescent signal that was recorded in an endpoint measurement mode. The measured fluorescent signal underwent pattern correction (see section 3.8 *Data and statistical analysis*), was normalized to the positive control retigabine, and expressed as relative percentage of activation.

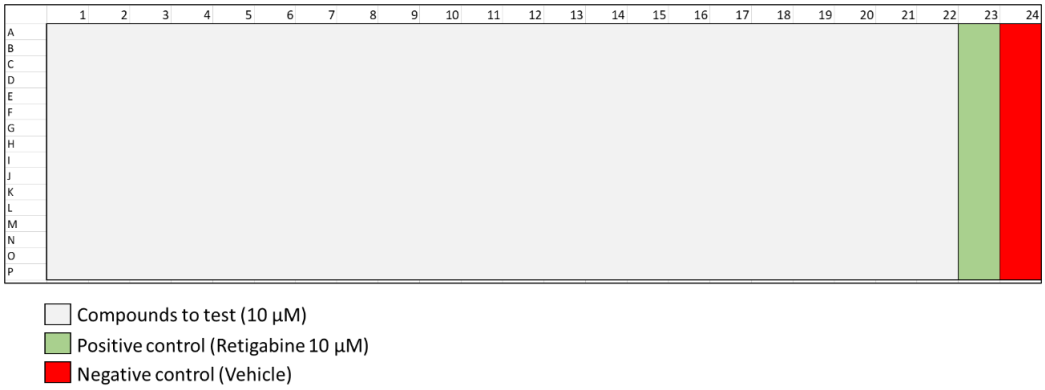

Figure 4.30 Plate Layout for the primary screening (PS). Each screening plate contains positive and negative controls and a compound area: column 1-22 = compound area; column 23 = negative control; column 24 = positive control

Among ~5600 tested compounds, 59 showed a relative percentage of activation ≥ 20% compared to retigabine and were selected as hits. Z' values of about 0.3-0.4 (Zhang et al. 1999) were calculated for most of the sixteen 384-well plates analysed, confirming the resolution capability of the assay identified in the adaptation process (section 4.3.1). However, two compounds already described as K_v7 activator were part of the library and both of them were identified as hits: one was retigabine itself, the other was ML-213 (Yu et al. 2011). These drugs were considered as internal controls for the capability of the screening assay to identify K_v7 activators among thousands of compounds.

The primary 59 hit compounds were subjected to a hit confirmation being tested at 10 µM three times in quadruplicates, using the same experimental condition of the primary screening. Among the 59 primary hits, twelve compounds showed a reproducible activity of ≥20% relative to retigabine and were confirmed as hits, other 47 primary hit compounds showed activities between 9 and 19% relative to retigabine and were considered as not confirmed hits (Table 4.6). Among not confirmed hit compounds, three compounds showing an activation just below the threshold of 20% (**C14, C26** and **C54**) were selected for their pharmacological interest to undergo a subsequent hit profiling together with the twelve confirmed hits, while the other 44 compounds were excluded from further analyses.

Table 4.6 Primary screening and hit confirmation results

Compound name	Primary Screening		Hit confirmation	
	Activity (%)	Hit	Mean activity (%) ± SEM	Confirmed
C1 ML-213	67.2	Yes	88.3 ± 29.2	**Yes**
C2 Retigabine (Library)	55.8	Yes	107.1 ± 56.9	**Yes**
C3	42.8	Yes	104.5 ± 53.0	**Yes**
C4	41.8	Yes	73.9 ± 42.7	**Yes**
C5	31.0	Yes	16.3 ± 15.4	No
C6	30.9	Yes	23.9 ± 15.7	**Yes**
C7	30.0	Yes	4.0 ± 13.6	No
C8	28.8	Yes	5.3 ± 7.2	No
C9	28.6	Yes	-8.2 ± 11.4	No
C10	26.2	Yes	-6.2 ± 7.6	No
C11	26.2	Yes	32.3 ± 19.2	**Yes**
C12	26.0	Yes	27.2 ± 3.5	**Yes**
C13	25.8	Yes	9.8 ± 8.4	No
C14	25.3	Yes	11.1 ± 15.4	No
C15	24.8	Yes	-1.3 ± 9.6	No
C16	24.8	Yes	3.5 ± 12.0	No
C17	24.8	Yes	1.6 ± 9.2	No
C18	24.5	Yes	0.2 ± 19.5	No
C19	24.5	Yes	3.0 ± 5.2	No
C20	24.4	Yes	-11.1 ± 19.4	No
C21	24.3	Yes	24.5 ± 31.0	**Yes**
C22	24.3	Yes	10.3 ± 17.1	No
C23	24.2	Yes	17.1 ± 24.9	No
C24	23.9	Yes	-0.5 ± 10.0	No
C25	23.7	Yes	-8.3 ± 12.0	No
C26	23.4	Yes	14.5 ± 10.3	No
C27	23.4	Yes	2.1 ± 11.6	No
C28	23.4	Yes	-8.5 ± 21.0	No
C29	23.3	Yes	1.9 ± 10.4	No
C30	23.3	Yes	3.7 ± 5.2	No
C31	23.3	Yes	20.3 ± 33.4	**Yes**
C32	23.0	Yes	7.5 ± 2.9	No
C33	22.7	Yes	25.9 ± 23.6	**Yes**
C34	22.3	Yes	14.8 ± 28.3	No
C35	22.3	Yes	3.9 ± 6.5	No
C36	22.2	Yes	7.7 ± 7.8	No
C37	22.2	Yes	0.9 ± 6.5	No
C38	22.1	Yes	13.1 ± 19.9	No
C39	22.1	Yes	2.2 ± 10.9	No
C40	22.0	Yes	-5.4 ± 6.8	No
C41	22.0	Yes	8.9 ± 17.0	No
C42	22.0	Yes	-0.8 ± 8.8	No
C43	21.9	Yes	7.6 ± 11.5	No
C44	21.7	Yes	5.2 ± 9.7	No
C45	21.7	Yes	13.7 ± 13.0	No
C46	21.6	Yes	4.6 ± 5.0	No
C47	21.5	Yes	3.2 ± 8.4	No
C48	21.4	Yes	6.2 ± 9.0	No
C49	21.4	Yes	-11.2 ± 1.3	No
C50	21.4	Yes	1.4 ± 13.3	No
C51	21.3	Yes	7.6 ± 3.1	No
C52	21.1	Yes	3.1 ± 8.2	No
C53	21.1	Yes	-0.9 ± 15.7	No
C54	21.1	Yes	10.5 ± 22.2	No
C55	20.9	Yes	10.4 ± 15.7	No
C56	20.7	Yes	36.3 ± 9.0	**Yes**
C57	20.7	Yes	-6.2 ± 21.4	No
C58	20.6	Yes	0.2 ± 8.4	No
C59	20.6	Yes	-8.1 ± 10.8	No

To profile the 12 confirmed hits, as well as the additional three not confirmed hits, their dose-dependent activation of $K_v7.3$* channels was studied using a ten-point dose-response curve ranging from 0.5 nM to 10 μM. On each plate retigabine (0.5 nM-10 μM) was included as positive control. Results are summarized in table 4.7. When the same dose-response tests were repeated in the parental cell line (non-trasfected CHO cells) none of the fifteen tested compounds showed activity in any tested concentrations, therefore unspecific effect (not K_v7 mediated) were excluded (data not shown).

Table 4.7 Hit profiling results. (n.a.= not applicable)

Hit Profiling		
Compound name	**EC_{50} (μM)**	**Max Activity (%)**
Retigabine (control)	0.30	120.3
C2 Retigabine (from the library)	>10	120.9
C1 ML-213	**0.24**	105.4
C3	>10	75.8
C4	**0.14**	83.8
C6	**0.27**	57
C11	n.a.	16.8
C12	**0.13**	57
C21	n.a.	~13
C31	n.a.	~13
C33	>10	28.1
C56	>10	24.5
C14	**0.23**	62.9
C26	**0.23**	24.6
C54	**0.23**	25.3

Among the fifteen profiled molecules, compounds showing an EC_{50} over the highest tested concentration of 10 μM or unmeasurable due to the flat dose-response curve were excluded from the subsequent characterization. ML-213 was excluded from the study because it was already well characterized as K_v7 activator (Yu et al., 2011).

C4, **C6**, **C12**, **C14**, **C26**, and **C54** were selected for a more in dept characterization. Unfortunately, it was not possible to study **C12** because it is no longer available on the market.

4.3.3 Electrophysiological characterization of newly-identified K_v7 activators

Five molecules were identified as new $K_v7.3$* channel activators from the screening of the Fraunhofer repurposing library (described in section 4.3.2): **C4**, **C6**, **C14**, **C26**, and **C54.** Their effect in activating $K_v7.3$* currents was further characterized by means of whole-cell patch-clamp electrophysiological experiments performed in mammalian CHO cells transiently transfected with $K_v7.3$* cDNA. Cells were clamped at -80 mV, and currents were elicited by 3-s voltage ramps from -80 mV to +20 mV (Figure 4.32, panel A, Control trace). Application of 10 μM retigabine (Figure 4.31, panel A, red trace) induced a leftward

shift in the voltage-dependence of the $K_v7.3^*$ channel and produced an increase of the current measured as ratio between current produced in presence of drug and current in control conditions ($I_{drug}/I_{control}$) of about 12-fold at -40 mV and 1.6-fold at 0 mV (Figure 4.31, panels B and C).

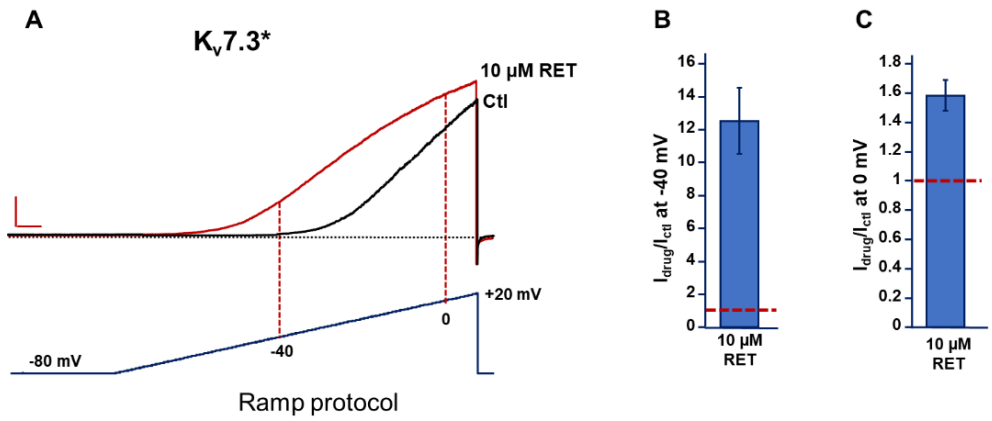

Figure 4.31 (A) Representative current traces recorded from CHO cell expressing $K_v7.3^*$ channels in response to the indicated ramp protocol before (black) and after (red) application of 10 µM RET. Current scale, 500 pA; time scale, 200 ms. **(B, C)** Increased induced by 10 µM RET on current $K_v7.3^*$ measured at -40 mV **(B)** or at 0 mV **(C).**

The effect of **C4, C6, C14, C26**, and **C54** on $K_v7.3^*$ current was studied using the same ramp protocol, each molecule was tested at 10 µM: current increase induced by **C4** was 4-fold at -40 mV and 1.4-fold at 0 mV; **C26** increased $K_v7.3^*$ current of 2-fold at -40 mV and 1.2-fold at 0 mV; the other tested compound did not significantly increased $K_v7.3^*$ current, therefore their efficacy as $K_v7.3^*$ opener was not confirmed (Figure 4.32).

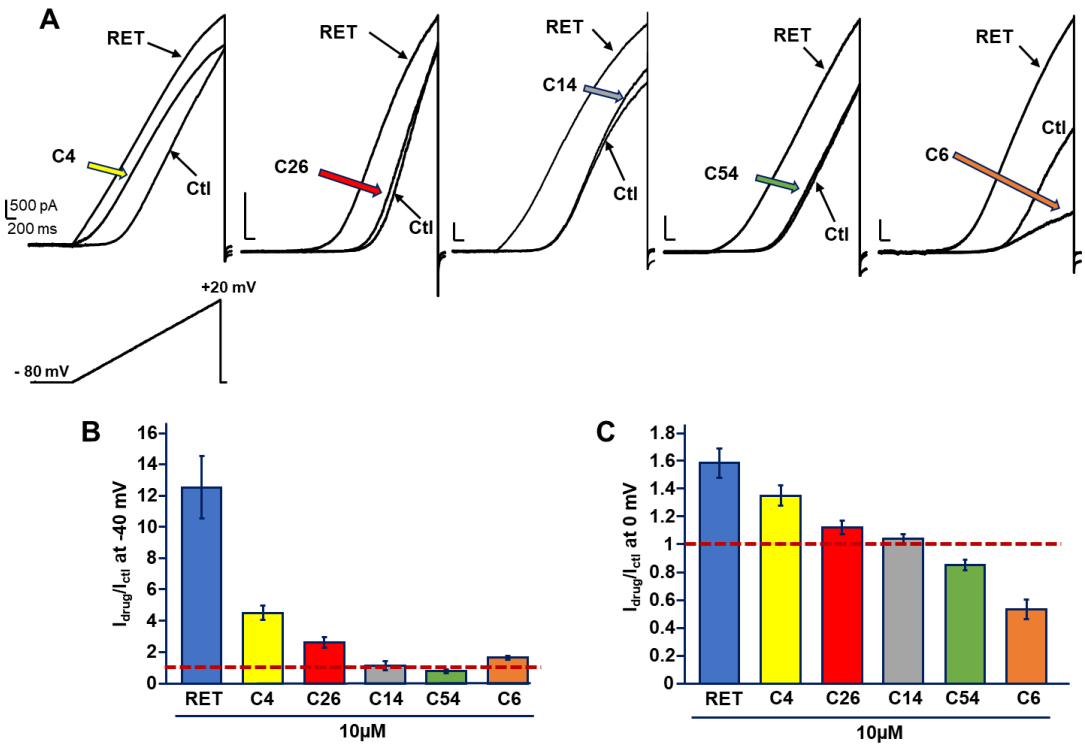

Figure 4.32 (A) Representative whole-cell current traces from $K_v7.3$* channel activated by the indicated ramp protocol recorded in control conditions (Ctl) and upon exposure to 10 μM of the indicated compounds. Current scale, 500 pA; time scale, 0.2 s. **(B, C)** $K_v7.3$* current increase induced by 10 μM retigabine (RET), C4 (JNJ), C6 (AMG), C14 (GAL), C26, and C54(BISM) calculated as ratio $I_{drug}/I_{control}$ at -40 **(B)** and 0 mV **(C)** of membrane potential.

From these experiments, **C4** emerged as the most active compound among the five newly identified, although less active than retigabine. Its activity as K_v7 opener was further studied using a voltage-clamp protocol in which $K_v7.3$* currents were activated by depolarizing steps from -140/-120/-80 to +20 mV, followed by an isopotential pulse at 0 mV (Figure 4.33, panel A).

As showed in Figure 4.33, panel A, at -40 mV the $K_v7.3$* channel started to open (red arrow). Application of 1 μM retigabine induced a leftward shift of the voltage-dependence of the channel ($\Delta V_{1/2}$) of about -40 mV, (making the channel open at -70 mV of membrane potential, Figure 4.33, panel B, red arrow) and slight increased the maximal current of about 30%. Similar effects were observed with 1 μM **C4** that increased $K_v7.3$* maximal current of about 30% but was less effective than retigabine in shifting the voltage-dependence of the channel, causing a $\Delta V_{1/2}$ of about 10 mV (Figure 4.33, panel B).

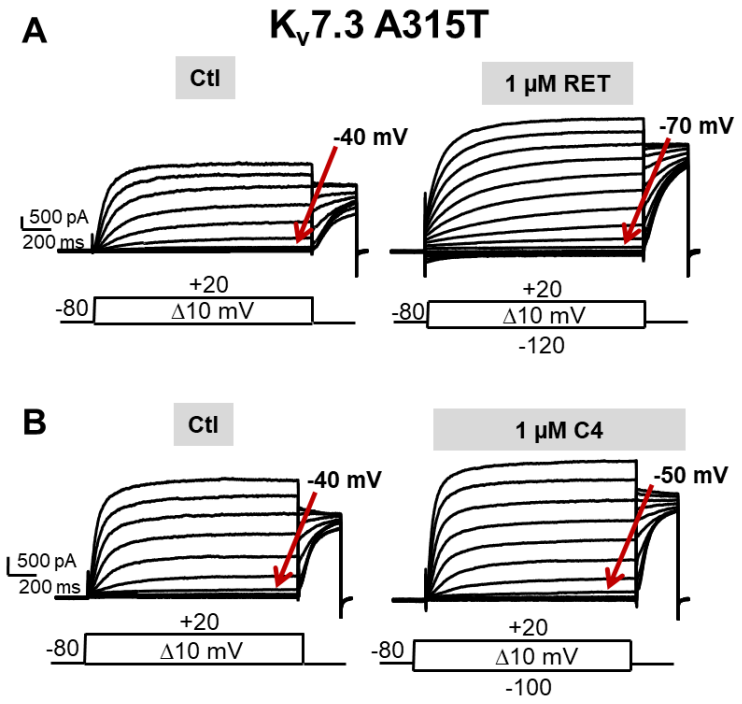

Figure 4.33 Effect of retigabine (RET) and C4 on $K_v7.3$* currents. (**A, B**) Representative macroscopic current traces recorded from a CHO cell expressing $K_v7.3$* subunit in response to the indicated voltage protocol before (Ctl) and after application of 1 μM RET (**A**) or 1 μM C4 (**B**). Current scale, 500 pA; time scale, 0.2 s.

Applying the voltage-clamp protocol described above and increasing drug concentrations from 0.01 to 30 μM, the potency of **C4** in shifting the voltage dependence of $K_v7.3$* channel was investigated and compared to that of retigabine (0.01 to 10 μM): EC_{50} calculated on $\Delta V_{1/2}$ was 2.0 ± 0.03 μM for **C4** and 0.6 ± 0.1 μM for retigabine (Figure 4.34). These data confirmed **C4** as a new $K_v7.3$* channel activator and confirmed its lower efficacy and potency in $K_v7.3$* channel compared to retigabine ($p<0.05$, = 4-8).

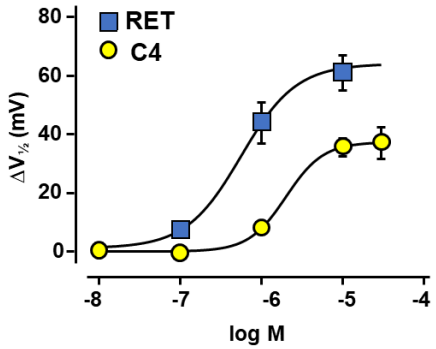

Figure 4.34 Dose-response curves of retigabine (RET, blue squares) and C4 (yellow dots) on $K_v7.3$* currents. Solid lines represent fits of the experimental data to the four-parameter logistic equation used to estimate EC_{50} values

4.3.4 Effect of C4 on $K_v7.2/7.3$ current

Experiments in sections 4.3.2 and 4.3.3 were performed in $K_v7.3$ A315T-expressing CHO cells ($K_v7.3$*) because the higher number of active channels in the cellular membrane

caused by the A315T mutation (Zaika et al. 2008) resulted in a larger dinamyc range and a better screening assay resolution compared to those obtained when K_v7.2/7.3-expressing CHO cells were used (see section 4.3.1).

A315T is an artificial tool used to enhance K_v7.3 macroscopic current size without altering other important channel characteristics, such as voltage dependence of activation, maximal open probability or PIP_2 affinity (Zaika et al. 2008; Hernandez et al. 2009). However, the K_v7 channels physiologically expressed in the CNS and mainly underlying the I_{KM} current (see section 1.3.1.4) are heteromeric K_v7.2 and K_v7.3 channels (Wang et al., 1998, Shapiro et al., 2000).

Therefore, the effect of the new identified opener **C4** was investigated on K_v7.2/7.3 current by means of whole-cell patch-clamp electrophysiological experiments performed in mammalian CHO cells transiently transfected with K_v7.2/7.3 cDNA, and its pharmacological profile was compared to that exhibited by retigabine.

When tested on K_v7.2/7.3 currents using a voltage-clamp protocol consisting in depolarizing steps from -100/-80 to +20 mV, followed by an isopotential pulse at 0 mV, **C4** had a major effect in shifting the voltage-dependence of the channel rather than enhancing the maximal currents, similar to what observed for retigabine (Miceli et al., 2008).

As showed in Figure 4.35, panel A, at -40 mV the K_v7.2/7.3 channel was closed (Ctl, red arrow). Application of 1 μM retigabine induced a leftward shift of the voltage-dependence of the channel ($\Delta V_{1/2}$), making K_v7.2/7.3 channel start to open at -50 mV. The same effect was observed upon application of 1 μM **C4**. The maximal $\Delta V_{1/2}$ measured for **C4** (30 μM) was 37.8 ± 3.6 mV, a value similar to that measured for retigabine at the same concentration ($\Delta V_{1/2}$ of 38.9 ± 3.6 mV).

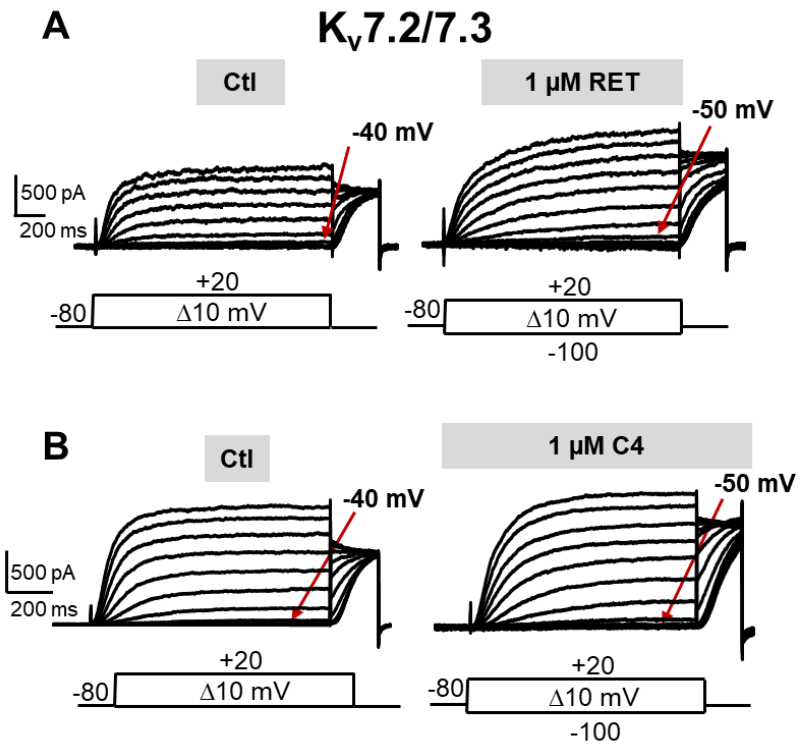

Figure 4.35 Effect of retigabine (RET) and C4 on K_v7.2/7.3 currents. (**A, B**) Representative macroscopic current traces recorded from a CHO cell expressing K_v7.2/7.3 subunit in response to the indicated voltage protocol before (Ctl) and after application of 1 μM RET (**A**) or 1 μM C4 (**B**). Current scale, 500 pA; time scale, 0.2 s.

Using the voltage-clamp protocol described above and increasing drug concentrations, the potency of C4 (0.03-30 μM) in shifting the $V_{1/2}$ of K_v7.2/7.3 channel was investigated and compared to that of retigabine (0.01-30 μM); the EC_{50}s calculated on $\Delta V_{1/2}$ was 1.2 ± 0.3 μM for **C4** and 2.5 ± 1.8 μM for retigabine ($p>0.05$, n= 4-8) (Figure 4.35, panel B). These data suggested that, although **C4** was less effective and potent than retigabine in activating K_v7.3* channel, its potency and efficacy were comparable to retigabine when tested in K_v7.2/7.3 channel (Figure 4.36).

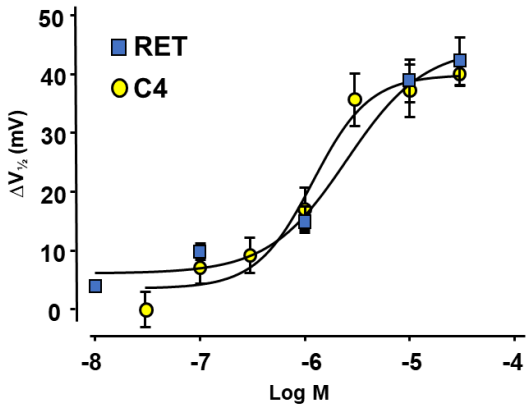

Figure 4.36 Dose-response curves of retigabine (RET, blue squares) and C4 (yellow dots) on K_v7.2/7.3 currents. Solid lines represent fits of the experimental data to the four-parameter logistic equation used to estimate EC_{50} values

4.3.5 Binding site of C4 in $K_v7.2$

A H-bonding between the carbamate group of retigabine and the indole nitrogen atom of a tryptophan (W236 in $K_v7.2$) within the S5 domain of $K_v7.2$-$K_v7.5$ channels is essential for the $K_v7.2$-$K_v7.5$ opening effect of retigabine (Wuttke et al. 2005, Schenzer et al. 2005). This tryptophan residue acts as a hydrogen bond donor (HBD) with the carbamate group of retigabine acting as a hydrogen bond acceptor (HBA) (Kim et al. 2015)

In silico simulations of **C4** docking performed using the cryo-EM structure of $K_v7.2$ (PDB ID: 7CR2; Li X. et al. 2021) showed that the nitrogen atom in the piperazine ring of **C4** could act as acceptor of an H-bond donated by W236 suggesting that **C4** binds the same pocket in $K_v7.2$ than retigabine and that its interaction with W236 could be essential for its K_v7 opening effect as it is for retigabine.

To confirm such hypothesis, electrophysiological experiments were performed in mammalian CHO cells transiently transfected with the retigabine-insensitive mutant $K_v7.2$ W236L or $K_v7.2$ WT cDNA. Cells were clamped at -80 mV, and currents were elicited by 3-s voltage ramps from -80 mV to +20 mV.

As shown in figure 4.38 panel A, upon application of **C4** (10 μM) $K_v7.2$ current was left-ward shifted (red trace) compared to the control. Conversely, K_v7 voltage-dependence shifting ability of **C4** was almost fully abolished in $K_v7.2$ W236L channels (Figure 4.37, panel B), confirming the docking simulations data and corroborating the hypothesis of a binding site for **C4** similar to that of retigabine in $K_v7.2$-5 channels.

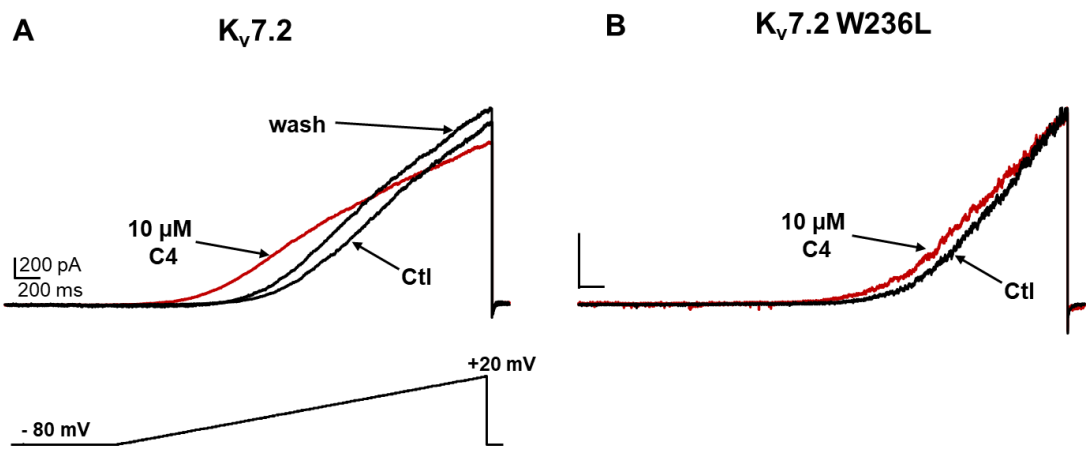

Figure 4.37 Representative whole-cell current traces from $K_v7.2$ (A) or $K_v7.2$ W236L (B) channel activated by the indicated ramp protocol recorded in control conditions (Ctl) and upon exposure to 10 μM C4 Current scale, 200 pA, time scale, 0.2 s.

5. Discussion

Epilepsy is a complex neurological disorder characterized by recurrent seizure activity. It has a high incidence rate, affecting ~50 million people worldwide in both developed and developing countries (WHO 2019).

Current management options for epilepsy include the use of anti-epileptic drugs or surgery (Anyanwu and Motamedi, 2018) or a ketogenic diet (Goswami and Sharma, 2019). However, more than 30% of patients diagnosed with epilepsy exhibit drug resistance to anti-epileptic drugs. Further, surgery and ketogenic diets do not completely alleviate the symptoms of patients with pharmacoresistant epilepsy.

Despite the development of novel anti-seizures medications (ASMs), the proportion of epilepsy patients with drug resistant epilepsies has remained stable at 30%. Thus, there is an urgent need to design newer and more effective anti-epileptic drugs and to identify new molecular targets (Chen, Brodie and Kwan, 2020).

K_v7 potassium channels represent an attractive pharmacological target for several neurologic disorder, including epilepsy (Barrese et al., 2018). The K_v7 subfamily comprises five members of volage-gated potassium channels ($K_v7.1$–$K_v7.5$) encoded by the KCNQ genes (KCNQ1–5). In neurons, tetramers containing $K_v7.2$ and $K_v7.3$, and more rarely $K_v7.5$ subunits, represent molecular components of the muscarinic-regulated (M)-current (I_{KM}).

I_{KM} activation regulates repolarization of the membrane, dampens repetitive firing, and controls neuronal excitability (Brown and Passmore, 2006), therefore, pharmacological activation of K_v7 channels appears as a rational approach to treat epilepsy as well as other disorders in which neuronal hyperexcitability plays a critical role, such as neuropathic pain (Liu et al., 2021), ischemic stroke (Bierbower et al., 2015), and amyotrophic lateral sclerosis (Wainger et al., 2021).

Retigabine, developed from the analgesic drug flupirtine, has been the first approved ASM acting on K_v7 channels. Retigabine acts on $K_v7.2$-5 channels enhancing the I_{KM} (Gunthorpe et al., 2012); this action is unique compared with the existing ASMs and highlights the advantages of exploring alternative targets for the control of seizures. Retigabine was approved in 2011 as an add-on treatment for drug-resistant partial onset seizures with or without secondary generalization in adults (Ciliberto et al., 2012). Despite its efficacy, retigabine clinical use was limited because of its long-term off-target effects of blue skin discoloration and eye abnormalities (Clark et al., 2015) with unclear consequences on vision and no information about the reversibility of these alterations upon drug

discontinuation (Brickel et al., 2020). Additionally, retigabine causes urinary retention (Brickel et al., 2012), probably because it activates $K_v7.4$ expressed in the smooth muscle of the bladder, where it regulates contractility (Malysz and Petkov, 2020). Because of limited and declining retigabine use, the manufacturer discontinued retigabine in 2017. Since retigabine has been discontinued, no ASM acting on K_v7 channels is clinically available.

In the present work, a rational *structure-based drug design* strategy and a *drug repurposing* strategy were used to identify novel K_v7 activators. For the first approach we explored the retigabine binding site in $K_v7.2$-5 channels, investigated its structure-activity relationship (SAR) and developed new analogues with improved pharmacokinetic and pharmacodynamic characteristics; for the second approach we performed a HTS screening of the Fraunhofer Repurposing Library containing 5600 bioactive compounds.

5.1 Structure-based drug design of newly synthesized retigabine analogues and its structure-activity relationship

The availability of the 3D structure of a biologically relevant target enables to exploit a rational *structure-based drug design* approach and to take advantage from *in silico* tools allowing molecular docking and molecular dynamics (MD) analysis. These techniques predict if and where a molecule binds a target and which type of interactions occur between the ligand and the aminoacidic residues within the binding site, thus helping in the analysis of the relationship between chemical-physical properties and the pharmacological activity of the molecule.

In recent years, the cryo-EM technique was used to solve many protein structures, including some K_v7 channels structures: the human $K_v7.1$, $K_v7.2$ and $K_v7.4$ channels structures, alone or in complex with ancillary subunits ($K_v7.1$/KCNE3), with endogenous modulators (PIP_2 or CaM) and with different synthetic modulators (ztz240 or retigabine as activators, linopirdine as blocker) are currently available (Sun and MacKinnon, 2020; Li X. et al., 2021; Li T. et al., 2021; Zheng et al., 2022).

To rationally design novel retigabine analogues, we investigated the chemical space at the retigabine binding site: we used the cryo-EM structure of $K_v7.2$ in complex with retigabine (Li X. et al., 2021) to perform molecular docking and MD simulations of two analogues previously described by our research group: compounds 23a and 24a, that exhibited higher potency *in vitro* in activating $K_v7.2$ channel and that shared the same binding site of retigabine, as showed by electrophysiological experiments using the retigabine insensitive $K_v7.2$ W236L mutant channel (Ostacolo et al., 2020). 23a and 24a harboured larger

substituents at the carbamate region compared to retigabine. Previously molecular docking simulations, performed using a homology $K_v7.2$ channel structure generated from the $K_v7.1$ structure (Sun and MacKinnon, 2017), suggested that these substituents were accommodated in a plastic binding pocket lined by residues L221, V225, L232, F304, L307, I311 and L312 that is not occupied by retigabine (Ostacolo et al. 2020).

In the present work, 23a and 24a were docked in $K_v7.2$ using the cryo-EM structure of $K_v7.2$ in complex with retigabine (Li X. et al., 2021). These new molecular docking and MD experiments confirmed that the larger substituents of both 23a and 24a specifically interact with residues V225, F304, and L312 lining a region that we defined *pocket 1*; these interactions are less pronounced in retigabine, given the smaller size of its amide carbonyl substituent (Figure 4.5).

In addition, two more pockets in the retigabine binding site were identified: one contributed by S303 forming an H-bond with the NH_2 at position 2 of retigabine and flanking a small hydrophobic pocket lined by T276, L299, V302, S303, F305 and A306, and another formed by F240, L243, L268, L272, L275 and F305, where F305 and F240 may interact with the fluorophenyl ring of retigabine. These two pockets were called pocket 2 and pocket 3, respectively (Figure 5.1). The three pockets identified in $K_v7.2$ also exist in $K_v7.4$, as revealed by the cryo-EM structure of $K_v7.4$ in complex with retigabine (Li T. et al., 2021), and probably in $K_v7.3$ and $K_v7.5$, as suggested by their similarities in the primary aminoacidic sequence (Figure 4.7).

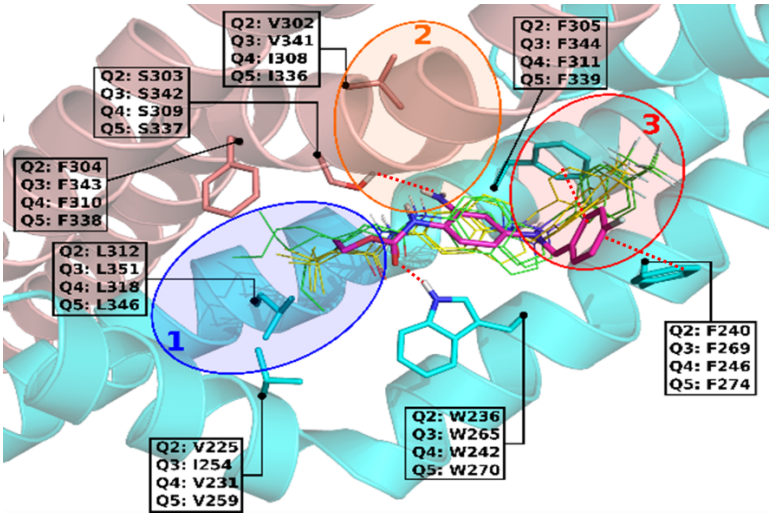

Figure 5.1 The retigabine binding site in $K_v7.2$-$K_v7.5$ channels. The three identified pockets are highlighted in blue (pocket 1), yellow (pocket 2) and red (pocket 3). For each aminoacidic residue is reported the corresponding residue in $K_v7.2$ (Q2), $K_v7.3$ (Q3), $K_v7.4$ (Q4), $K_v7.5$ (Q5). Bound conformations of retigabine (magenta), 23a (yellow) and 24a (green) are shown in thin solid sticks. Red dashed lines indicate the major interactions identified for retigabine and the indicated residues.

The identification of three pockets in the binding site of retigabine was the starting point for our *structure-based drug design.* Molecular sections of retigabine interacting in pocket 1,2

and 3 were called area 1, 2 and 3 respectively; systematic modifications in each of the three areas were introduced on the molecule to design novel retigabine analogues exploring the available chemical space in pocket 1, 2 and 3 (Figure 5.2). This synthesis exercise resulted in a small library of retigabine derivatives, whose structures are depicted in table 4.2.

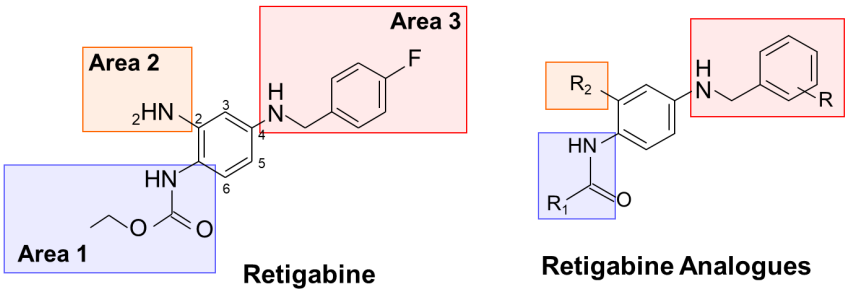

Figure 5.2 Left: retigabine structure and its three areas occupying pocket 1, 2 and 3, respectively. **Right:** Structure of retigabine analogues and modified R-groups.

To test *in vitro* the K_v7 opening activity of the newly synthesized retigabine analogues, the fluorescence-based thallium-flux assays FluxOR was used in a cellular model represented by CHO cell lines stably expressing $K_v7.2/7.3$ channels (CHO-$K_v7.2/7.3$). Upon treatment with retigabine or other K_v7 activators, the increasing CHO-$K_v7.2/7.3$ cytosolic fluorescent signal was measured for 45 seconds, obtaining fluorescence curves. The slope of the fluorescent curve between 5 and 15 seconds was selected as parameter to compare the effect of the new derivatives, each tested at 10 μM, to that of retigabine (10 μM) (Figure 4.13).

The screening results revealed the following structure-activity relationship (SAR):

Area 1:

- Linear (compounds **13**, **14**), branched (compound **17**), or cyclic (compounds **18**, **19**) lipophilic substituents increased the K_v7 opening activity when up to 7 carbon atoms are present at R1; longer side chains (compounds **15**, **16**) reduced the K_v7 opening activity; our MD simulations suggested that side chains longer than 7 atoms escape from the binding pocket (Figure 4.14, panel B) thus reducing the activity of compound **15** and impeding the binding of compound **16**.

- Hydrophilic substituents are not tolerated, indeed the ethylene glycol chain of compound **20** completely abolished the K_v7 opening activity.

- The inversion of the amide group (derivative **71**) abolished the K_v7 opening activity because impeded the H-bonding between the carbamate group of the molecule and the indole nitrogen atom of the W236, an interaction essential for the activity of retigabine and

for other K_v7 openers binding the channel pore (Wuttke et al. 2005, Schenzer et al. 2005). This observation further confirmed the hydrogen bond donor (HBD)-hydrogen bond acceptor (HBA) pattern reported in literature (Kim et al. 2015) where the carbamate group of retigabine is the HBA and the indole amino group of the W is the HBD. Recently, the inversion of the amide group was introduced also in flupirtine derivatives generated by Wurm and colleagues. Flupirtine is structurally analogue to retigabine and assumes the same binding pose in K_v7 channels. Flupirtine derivatives with the inverted amide were not active as $K_v7.2/7.3$ channel activators, consistently with our data (compound **71**) and with the literature (Kim et al. 2015). Interestingly, when an additional methyl group in position 4 of the pyridine ring (in ortho position to the amide) was added, the flupirtine derivatives were still active as $K_v7.2/7.3$ channel activators. The methyl group likely causes a rotation of the amide group out of the plane of the aromatic ring allowing it to still interact as HBA with the W residue, or induces a complete rearrangement of the molecules binding pose (Wurm et al., 2022).

Area 2:

- Replacement of $-NH_2$ in position 2 of retigabine with a hydrogen (compound **2**) did not remove the K_v7 opening activity, suggesting that the H-bond between $-NH_2$ in R_2 and S303 side chain, found in the CryoEM studies of retigabine in $K_v7.2$ (Li X. et al., 2021) is not essential for the activity; this results are in line with the observation that the retigabine derivative HN37 (Zhang et al., 2021) in which the NH_2 group at position 2 was replaced with a methyl group, was even more potent than retigabine or its structural analogue P-RET (Zhou et al., 2015).

Area 3:

- Moving the fluorine atom in position 2 of the phenyl ring (compound **52**) or its removal (compound **41**) resulted in no change in activity when compared to reference compound **13**, thus ruling out any specific halogen bond involving this fluorine atom. This was in line with our MD simulations, where the recently suggested direct contact between the retigabine fluorine atom and the carbonyl oxygen of the protein backbone at the A265 residue (Shi et al., 2020) was not found.

- The 2,6-difluoro analogue of compound **17** (compound **43**) designed to help the ligand phenyl ring to assume an optimal orientation for edge-to-face and/or face-to-face interactions with phenylalanines 240 and 305, still displayed strong activity, confirming the critical functional role of the π-π stacking interactions between F305, F240 and the retigabine benzyl ring for K_v7 opening.

- Replacement of the fluorobenzyl group with hydrophilic hydroxybenzyl (compound **57**) or pyridine (compounds **47** and **51**) groups led to a complete loss of activity, despite their ability to form π-π stacking interactions, suggesting that a critical degree of hydrophobicity at this region is required to accommodate the aromatic ring in the pocket 3 thus allowing the molecule to fit into the binding site.

- Increasing the length of the linker between the fluorobenzyl ring and the amino group at N4 of retigabine with an extra $-CH_2-$ led to a complete loss of activity (compound **42**), likely because this substitution impedes the interaction of the terminal phenyl ring of retigabine with pocket 3 residues L272 and F305 (Figure 4.15).

Among the new retigabine analogues, **13**, **14**, **17**, **19**, **23, 24, 41**, **43,** and **52** showed higher efficacy compared to retigabine when tested at 10 μM ($p<0.05$), indicating that the molecular modifications introduced in these new molecules were advantageous for K_v7 channel activation.

5.1.1 Retigabine analogues photostability and dimerization reaction

The blue discoloration observed in patients upon long-term treatment with retigabine is due to the accumulations of coloured dimers into tissues, formed upon light irradiation. A proposed four-steps dimerization mechanism is depicted in figure 4.16 and is based on: 1) the photo-induced retigabine by-products found upon UV-visible light irradiation of retigabine solution (Ostacolo et al., 2020); 2) the structure of phenazine and phenazinium dimers, such as those detected in melanin-rich eye tissues upon long-term treatment with retigabine (Groseclose and Castellino, 2019), and 3) the structure of chemical species detected as one of the process-related impurities in several batches of retigabine (Wang et al., 2012). According to the reaction mechanism, the amino groups at position 2 and 4 of the retigabine molecule are involved in, and essential for the dimerization reaction.

When the photostability and dimer-forming ability of the most active compounds in our library were addressed, dimer formation was detected for all tested compounds, except for **23** and **24**, that, in spite of that, showed an enhanced degradation when compared to retigabine (Table 4.3). The inability of compounds **23** and **24** to form dimers is likely due to the lack of the free amino group in position 2 required for the last step of the dimerization reaction to occur (Figure 4.16).

Combining the information obtained from the SAR study to that from the dimerization reaction, three additional groups of analogues were designed to block or to reduce the reactivity of the amino groups at position 2 and 4 of the retigabine molecule, and their

effect in opening K_v7.2/7.3 channels was tested using the previously described fluorescence-based assay (Figure 4.17).

The first group of retigabine analogues consisted of N4 substituted analogues, in which the tertiary amine is unavailable to form phenazine dimers (reaction 4 in figure 4.16) (compounds **25-28**). Small lipophilic substituents at N4, such as the methyl groups of **25** and **26** improved K_v7 opening activity, whereas longer lipophilic substituents, such as a propyl group of **27** did not improve activity, finally, rigid substituents, such as the acetyl group of **28** markedly reduced activity.

In the second group, the N4 was replaced with oxygen (**31**) or methylene groups (**67-68**). Unfortunately, none of these compounds were able to activate K_v7.2/7.3 channels.

The third group included derivatives replacing hydrogen atoms with electron-withdrawing fluorine atoms at position R2 of the benzene-1,2,4-triamine core scaffold (compounds **59, 60**), a strategy likely reducing the reactivity of N2 and N4. This latter approach has been profitably used before to develop potent and metabolically stable K_v7.2 activators such as RL-81 (Kumar et al. 2016) Within this series, when compared to retigabine, K_v7 opening activity was similar for **59**, and enhanced for **60**.

These results added more information about the retigabine SAR, indicating that pocket 3 displays a limited degree of plasticity, accommodating only small lipophilic substituents, and that the N4 in the retigabine structure is essential for the K_v7 opening activity, although no Cryo-EM simulation detected any interaction involving this atom.

Overall, within this novel series of molecules, three compounds (**25**, **26**, **60**) displayed efficacy as K_v7.2/7.3 channel activators higher than that of retigabine. When their photostability and dimer-forming ability were tested, we found that all of them failed to dimerize, as expected, but compounds **25** and **26** underwent extensive photodegradation, in fact, the tertiary amine in position 4 of **25** and **26,** although preventing phenazine dimers occurrence, remained prone to C-N photooxidative cleavage, the first step of retigabine photooxidation.

The reduced electron availability at N2 and N4 due to the presence of fluorine atom in position 3 of compound **60** strongly reduces also the first photooxidative step, thus conferring remarkable photostability.

Our approach, although quite conservative with only minor structural changes in the lead compound retigabine molecule, was effective in developing a new, improved derivative, the compound **60**. More dramatic chemical modifications of the retigabine structure have been used as a strategy to prevent its dimerization and formation of toxic metabolites, for

example Wurm and colleagues utilized the nicotinamide scaffold to generate safer retigabine analogues (Wurm et al., 2023). However, the resulting compounds, such as compound 18c, although unable to dimerise, presents other problems, such as poor solubility, and needs further improvement.

Radical structural changes also increase the risk of unexpected new toxicities, as in the case of ICA-105665 (also called PF-04895162), a K_v7 channel opener structurally distinct from retigabine identified by Icagen, Inc. Although ICA-105665 exerted an antiseizures affect in patients with epilepsy (Kasteleijn-Nolst Trenité et al., 2013), it failed in phase I clinical trials because of its hepatotoxic effect that was not observed when its toxicological profile was studied in rats and monkeys (Aleo et al., 2019).

5.1.2 Pharmacological characterization of compound 60: pharmacodynamic electrophysiological assessment, pharmacokinetics, and anticonvulsant effect.

Given the higher efficacy in opening $K_v7.2/7.3$ channel showed in the FluxOR assay, and the inability to form photo-induced dimers of compound **60**, it was selected for further characterization.

First, its effect on $K_v7.2/7.3$ currents was studied in electrophysiological experiments performed in mammalian CHO expressing $K_v7.2/7.3$ channels and compared to that of retigabine and its more potent analogue RL-81 (Kumar et al. 2016).

In these experiments compound **60** (1 μM) produced a large leftward shift of the voltage dependence ($V_{1/2}$) of the channel ($\Delta V_{1/2}$ ~ -60mV) with a potency in shifting the $V_{1/2}$ 16-fold higher than that of retigabine and almost 2-fold than that of RL-81.

An even more dramatic effect was observed in increasing the maximal current: 1 μM of compound **60** doubled the current density of $K_v7.2/7.3$ channel, and, when compared to RL-81, compound **60** was about 5-times more potent in increasing $K_v7.2/7.3$ maximal current (retigabine slightly affects maximal current density, therefore the EC_{50} of retigabine on this parameter was not calculated).

When compared to most previously described retigabine analogues such as SF0034, RL-81, P-RET, and NS15370, which only modestly enhanced the maximal currents (Kalappa et al., 2015; Kumar et al., 2016; Zhou et al., 2015; Dalby-Brown et al., 2013) the marked increase in current size at depolarized potentials observed with compound **60** is suggestive of a slightly different mechanism of channel activation by this drug. Thus, experiments were carried out to identify the molecular basis for such a unique mechanism.

Our molecular modelling simulations for compound **60** in $K_v7.2$ predicted some binding interactions shared with retigabine, such as H-bonds with S303 in pocket 2 (Li X. et al., 2021) and W236 in pocket 1 (Wuttke et al., 2005; Schenzer et al., 2005; Kim et al., 2015), These two interactions were experimentally confirmed: electrophysiological recordings showed that, similar to retigabine, the K_v7 opening ability of compound **60** was almost fully abolished in W236L channels and slightly but significantly reduced in S303A channels, suggesting a marked similarity in the overall binding of compound **60** and retigabine.

Moreover, additional and specific hydrophobic interactions with residues in pocket 1 of $K_v7.2$ channel were identified by our MD analysis: average distances between compound **60** or retigabine and the residues V225, F304 and L321 suggested these aminoacidic residues were contacted by compound **60** but not by retigabine, due to its shorter later chain in area 1. Unfortunately, we could not experimentally test whether the higher potency and the efficacy shown by compound **60** over retigabine or RL-81 was due to these interactions in pocket 1, in fact, $K_v7.2$ V225A, F304A, and L312A mutant channels carried currents whose size was too low to be amenable for pharmacological analysis.

Noteworthily, compound **60** and RL-81 only differ in the size and hydrophobicity of their substituents at position R1 (Figure 5.3), strongly suggesting that the small but significant potency and efficacy difference as $K_v7.2/7.3$ activators existing between these molecules can be only attributed to structural difference at this position. Moreover, substitution increasing lipophilicity in area 1 seems to have a greater impact than substitution in other areas of retigabine molecule: when a propargyl group in N4 of retigabine (area 3) was added to generate its more lipophilic analogue P-RET, this modification failed to improve potency and efficacy over retigabine although increasing the logP and therefore the brain penetration of P-RET (Zhou et al., 2015).

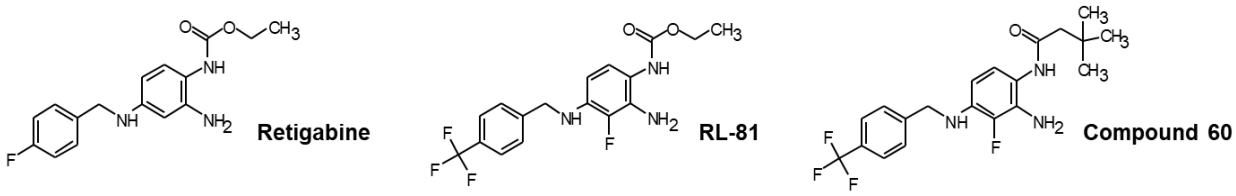

Figure 5.3 Molecular structures of retigabine, RL-81 (Kumar et al., 2016) and compound 60

Considering that the activation of $K_v7.4$ channel is correlated to the urinary retention side effect of retigabine (Malysz et al., 2020), electrophysiological experiments were performed in CHO cells expressing $K_v7.4$ channel and compound **60** was tested. Our results indicated that, similar to retigabine, compound **60** does not discriminate between $K_v7.2/7.3$ and $K_v7.4$ channels. The $K_v7.4$ activation exerted by compound **60** is consistent with the high

degree of conservation of the amino acids involved in its binding between $K_v7.2$ (Li X. et al., 2021) and $K_v7.4$ channels (Li T. et al. 2021) as well as with the structural similarity of pocket 1 accommodating the R1 substituents responsible for the higher potency of compound **60** as a K_v7 activator.

Since the amino acid residues lining the retigabine binding site are quite conserved among $K_v7.2$-5 channels, retigabine act as a pan $K_v7.2$-7.5 channels activator. Until now, none of the retigabine analogues described in the literature shows a clear selectivity among $K_v7.2$-7.5 channels, and even a compound structurally different such as ML-213, initially described as the first activator selective for $K_v7.2$ and $K_v7.4$ (Yu et al., 2011) was later found to share the retigabine binding site, being inactive in the $K_v7.2$ W236F and not selective among the $K_v7.2$-7.5 channels (Kanyo et al., 2020), pointing out how difficult it is to reach a selectivity among $K_v7.2$-5 channels working of molecules that bind the channels pore in this highly conserved site.

$K_v7.2/7.3$ channel activation is the main mechanism underlying the retigabine antiseizures effect (Main et al., 2000). Retigabine is effective in reducing seizures in different animal model of epilepsy, including the $GABA_A$ receptor antagonist pentylenetetrazol-(PTZ)-induced acute seizures model (Rostock et al. 1996) that is easy to perform and widely used to evaluate the efficacy of novel possible antiseizure medication (Breidenbach et al., 2020). This model was profitably used to study the effect of other retigabine analogues, such as HN37 (Zhang et al., 2021), or other K_v7 activators sharing the same binding site of retigabine (LuyAA4117839 by Grupe et al., 2020) or exhibiting a different structure and a binding site different from retigabine (ICA27243 by Roeloffs et al., 2008), and was therefore chosen to test the possible antiseizures effect of compound **60**.

In the PTZ mouse model, compound **60** was found to be more potent and more effective than retigabine in both reducing the severity of the seizures and increasing the latency to the maximal seizure. Both effects were abolished by the K_v7 blocker XE991, confirming that the antiseizure effect exerted by compound **60** was K_v7 mediated.

As regard the pharmacokinetics of compound **60**, we found that its metabolism was similar to that of retigabine, with a small fraction metabolized in phase I, and a larger in phase II metabolism reactions, when tested in vitro using the S9 fraction of human liver microsomes.

Poor brain penetration and short half-life were two pharmacokinetic limits of retigabine, leading to the daily administration of three doses in patients. Both features resulted improved in compound **60**: the brain/plasma distribution, measured in mice treated with 1

mg/Kg of retigabine or compound **60**, showed a remarkable brain accumulation for compound **60**, with a brain/plasma ratio 18-times higher than that of retigabine; this is likely due to the higher lipophilicity (logP 4.74) of compound **60** over that of retigabine (logP 3.08), as also observed for P-RET (logP 3.48; Zhou et al., 2015) another analogue that showed improved brain distribution over retigabine.

Moreover, compound **60** showed a much longer plasma half-life compared to retigabine (16.9 hours vs 2.4 hours), suggesting that its chronic use *in vivo* may not require multiple daily doses.

It should be highlighted that, in addition to its K_v7 opening actions, retigabine may act as a $GABA_A$ agonist, although this effect only occurs at concentrations higher than those required to activate K_v7 channels (namely, ≥10 μM) (Treven et al., 2015) and higher to those used in our *in vivo* experiments. Given its structural similarity with retigabine, and its improved brain penetration, a possible effect as $GABA_A$ agonist of compound **60** could not be excluded and will be further investigated.

5.2 Identification of C4, a novel K_v7 activator, through a Drug Repurposing HTS

Introducing a new drug on the market involves a long journey through basic research, discovery and optimization, preclinical development, human clinical trials, and regulatory approval. It takes more than a decade to get a new chemical entity to market and the entire drug developmental process costs in excess €1 billion (Hughes, 2011).

A known and well-characterized pharmacological target, such as the K_v7 channels, offers the possibility to use a powerful technique, the high-throughput screening (HTS) and the opportunity to try *drug repurposing*.

Drug repurposing is the application of an existing therapeutic to a new disease indication. Drugs that are clinically approved and repurposed can go directly to preclinical and clinical trials, reducing the lengthy amount of time and the cost for preclinical drug development.

HTS is an *in vitro* technology consisting of highly automated screening systems to record a biological activity at the model organism, cellular, pathway, or molecular level. Evaluation of molecule collections using these automated systems increases the chances to find active compounds, the so-called *"hits"* compounds. HTS can be performed using libraries of known bioactive molecules/already tested drugs to explore *drug repurposing* opportunities.

Looking for novel $K_v7.2/7.3$ channel activators among approved drugs, we used a cell based HTS to screen *The Fraunhofer repurposing library*, a collection of 5632 compounds

including 3400 compounds that have reached clinical use across 600 indications as well as 1582 preclinical compounds with varying degrees of validation. The compounds in the library derived from the Broad Repurposing Hub, a collection born from a huge systematic work done by The Broad Institute of MIT in collaboration with Harvard in Cambridge, Massachusetts. To assemble the Broad Repurposing Hub, each drug was purchased, its known activity and clinical indication were annotated, and its chemical identity and purity were experimentally confirmed (Corsello et al. 2017).

The *Fraunhofer repurposing library* has been profitably screened to identify several hits, for example six drugs counteracting the cytopathicity induced by the SARS-CoV-2 virus in Caco2 cells were identified in the library using an imaging-based screening and could be the starting point for new potential therapeutic approaches (Ellinger et al., 2021).

To screen the library looking for new K_v7.2/7.3 channel activators, we used the FluxOR assay in a cellular model consisting in CHO cells stably-expressing K_v7.3 A315T channel. As discussed in the previous section, the FluxOR assay is a fluorescence-based Tl^+-flux HTS widely used in drug discovery campaigns to identify new K_v7 modulators (Beachman et al., 2010; Li et al., 2011; Yue et al., 2016). The fluorescent signal measured by the assay is proportional to the cellular Tl^+ influx and consequently to the channel opening; the signal-to-noise ratio of this type of assay is affected by the number of channels in cellular membrane: the lower is the cellular io channel expression, the more difficult is to detect their modulation.

By the means of PiggyBAC transposon system, which ensures high transfection efficiency, we generated a CHO cell line stably expressing K_v7.2/7.3 or K_v7.3 A315T channels to be used as cellular models in the FluxOR assay (Matasci et al., 2011). K_v7.2/7.3 heteromeric channels underly the I_{KM} current that regulates neuronal excitability; A315T mutation is a tool experimentally used to increase the current density of K_v7.3 and enhance macroscopic current size without altering other important channel characteristics, such as voltage dependence of activation, maximal open probability or PIP_2 affinity (Zaika et al. 2008; Hernandez et al. 2009).

We choose to use the CHO-K_v7.3 A315T cell line (CHO-K_v7.3*) as cellular model to screen the *Fraunhofer repurposing library* because during the assay validation performed at the Fraunhofer ITMP ScreeningPort, this cell line generated a stronger fluorescent signal in the FluxOR assay upon application of the prototype K_v7 activator retigabine compared to that showed by CHO-K_v7.2/7.3 cell line, resulting in a better signal-to-noise ratio and consequently to a Z' factor sufficient to consider the screening assay robust (Zhang et al. 1999).

In the *primary screening*, compounds were tested at 10 μM of concentration and their activity was normalized on that of the positive control retigabine (10 μM), setting a threshold of 20% of activity respect to retigabine. Among 59 hits identified in the *primary screening*, 12 were confirmed in the same experimental conditions (Table 4.6). During the *hits profiling* phase, 7 compounds showed an EC_{50} lower than 10 μM in activating $K_v7.3$*channel in the FluxOR assay: ML-213, **C4, C6, C12, C14, C26**, and **C54**.

ML-213 was already well characterized as K_v7 activator (Yu et al., 2011). The fact that ML-213 was identified among ~5600 compounds is a proof of the effectiveness of our screening campaign in identifying K_v7 activators. Since it was already known and studied, ML-213 was excluded from the further electrophysiological characterization, together with **C12** that is no longer available for commercialization and difficult to source.

The subsequent electrophysiological characterization of the five selected compounds was performed through patch-clamp recordings in CHO cell expressing $K_v7.3$ A315T channel. Using a ramp protocol to enhance $K_v7.3$* currents, and applying 10 μM of each compound (**C4, C6, C14, C26**, or **C54**) we found that, at the resting membrane potential of -40 mV, retigabine induced a $K_v7.3$* current increase of 12-fold, **C4** induced an increase of 4-fold, **C26** of 2-fold, the other tested compound did not significantly increased $K_v7.3$* current, therefore their efficacy as $K_v7.3$* opener was not confirmed (Figure 4.31). This data partially confirmed the screening results, suggesting that it was effective to identify some new K_v7 activators, but it also led us to find some false-positive hits. However, a certain rate of false-positive and false-negative hits is intrinsically part of the HTS techniques (Gribbon and Sewing, 2005).

C4 activity on $K_v7.3$* currents was further studied using a voltage-clamp protocol and its dose-dependent effect was compared to that of retigabine. These experiments showed that, like retigabine, **C4** induced a shift of the voltage-dependence ($V_{1/2}$) and slight increased the maximal current of $K_v7.3$* channel. Testing **C4** at different concentrations (0.01-30 μM) we found that it was less effective and less potent that retigabine (0.01-10 μM) as $K_v7.3$* channel opener: EC_{50} calculated on $\Delta V_{1/2}$ was 2.0 ± 0.03 μM for **C4** and 0.6 ± 0.1 μM for retigabine ($p<0.05$, = 4-8) (Figures 4.33 and 4.34).

As mentioned above, introduction of the A315T mutation in $K_v7.3$ channel is an artificial tool used to increase the current amplitude of $K_v7.3$ and make it easier to be studied through electrophysiological recording. However, the K_v7 channels physiologically expressed in the CNS and mainly underlying the I_M current are the heteromeric $K_v7.2/7.3$ channels (Wang et al. 1998, Shapiro et al. 2000).

Interestingly, when tested on $K_v7.2/7.3$ currents using a voltage-clamp protocol, **C4** showed efficacy and potency comparable to those observed for retigabine in shifting the $V_{1/2}$ of the channel and enhancing the maximal current, with a maximal $\Delta V_{1/2}$ measured of 37.8 ± 3.6 mV and 38.9 ± 3.6 mV, for **C4** and retigabine, respectively (both tested at 30 μM) and EC_{50s} calculated on $\Delta V_{1/2}$ of 1.2 ± 0.3 μM and 2.5 ± 1.8 μM or **C4** and retigabine, respectively ($p>0.05$, n= 4-8) (Figures 4.35 and 4.36).

To investigate the possible binding site of **C4** in $K_v7.2$, we performed a molecular docking simulation using the cryo-EM structure of $K_v7.2$ in complex with retigabine (PDB ID: 7CR2; Li X. et al. 2021). As described in the section 4.1.2, retigabine binds the pore of $K_v7.2$ channel, in a site formed by 3 pockets. This site is quite identical among $K_v7.2$-5 channels, with only slight differences in amino acids lining the pockets (Figure 5.1). A H-bonding between the carbamate group of retigabine and the indole nitrogen atom of a tryptophan (W236 in $K_v7.2$) within the S5 domain of $K_v7.2$-$K_v7.5$ channels is essential for the $K_v7.2$-$K_v7.5$ opening effect of retigabine (Wuttke et al. 2005, Schenzer et al. 2005). This tryptophan residue acts as a hydrogen bond donor (HBD) with the carbamate group of retigabine acting as a hydrogen bond acceptor (HBA) (Kim et al. 2015).

Our in silico docking simulations of **C4** suggested that it could bind the same pocket in $K_v7.2$ than retigabine, with the nitrogen atom in the piperazine ring of **C4** acting as H-bond-acceptor and interacting with W236 as H-bond donor. Since this interaction is essential for retigabine K_v7 opening effect, we performed electrophysiological experiments in CHO cells transiently transfected with the retigabine-insensitive mutant $K_v7.2$ W236L or $K_v7.2$ WT cDNA and tested the effect of **C4** on both currents elicited by voltage ramps.

While **C4** (10 μM) was able to shift the $V_{1/2}$ of $K_v7.2$ WT channel, it was ineffective on $K_v7.2$ W236L channels (Figure 4.37), confirming the docking simulations data and corroborating the hypothesis that the binding site of **C4** was identical to that of retigabine.

All together these data indicated that **C4** is a new K_v7 opener, binding the same site of retigabine in $K_v7.2$ channel, and showing the same potency and efficacy in activating $K_v7.2/7.3$ channels *in vitro*. Further tests of **C4** *in vitro* and in animal models of epilepsy are needed to establish if it is effective in control seizures.

6. Conclusion and future directions

In conclusion, two different approaches were profitably used to identify novel K_v7.2/7.3 channels activators: the rational design of compound **60** and the repurposing of **C4**.

1. Our rational design strategy**,** combining structural modifications improving the retigabine K_v7.2-7.5 opening activity, with modifications ameliorating its safety profile, led to the identification of compound **60**. This new molecule showed improved features compared to retigabine, in fact it was more effective and more potent in activating K_v7.2/7.3 channels, less prone to form toxic photo-induced dimers and exhibits a better pharmacokinetic profile. Most importantly, compound **60** was found to be more potent than retigabine as an anticonvulsant in an acute mouse model of epilepsy, such as the PTZ-induced seizures model. Further investigations in chronic models of epilepsy are needed to provide a more detailed characterization of its mechanism of action.

In the future, if compound **60** proves to be safe in preclinical toxicology studies, it could be tested in human as new ASM, filling the clinical void left by the retigabine as only approved K_v7.2-5 opener drug.

Moreover, the SAR analysis performed in the present study added new information about the binding site and the mechanism of action of retigabine, providing provide a strong basis for future drug design.

2. From HTS of the *Fraunhofer repurposing library,* **C4** emerged as a new K_v7 opener. **C4** is a D_2 receptor antagonist developed as an atypical antipsychotic by Johnson & Johnson.

Our *in vitro* electrophysiological study showed that **C4** acts as K_v7.2/7.3 opener with efficacy and potency comparable to those of retigabine. *In silico* docking simulations, confirmed by electrophysiological experiments, indicated that **C4**, although structurally different, shares the same binding site of retigabine in K_v7.2. This could suggest that **C4** acts as a pan K_v7.2-7.5 opener, similarly to retigabine. However, its effect in the K_v7.4 and K_v7.5 potassium channels needs to be experimentally addressed, since K_v7.4 channels activation causes urinary retention, one of the side effects of retigabine.

In the future, the possible anticonvulsant effect of **C4** will be investigated using *in vitro* and *in vivo* models of epilepsy.

The *drug repurposing* approach offers the advantage of shortening the drug development process, compared to those needed for a new chemical entity. Indeed, **C4** already passed the early clinical phases of testing and resulted safe for human use, therefore if its antiseizures effect will be proven in preclinical studies, **C4** could be directly tested in a phase II clinical trial as anticonvulsant drug and could be repurposed as new ASM. It must

be said, however, that the doses used in healthy subjects and in schizophrenic patients treated with **C4** may be different from those needed to control seizures, and this aspect necessarily needs to be investigated.

The fact that the ASMs currently available are not effective in controlling seizures in about 30% of epileptic patients stresses the need to develop new antiepileptic drugs.

Retigabine has been shown to be effective in animal models predictive of drug-resistant epilepsy, suggesting that the activation of K_v7 channels, a mechanism different from that exerted by the commercially available ASMs, may be useful to treat this type of epilepsy.

Therefore, the identification of two new molecules acting as K_v7 channels activators not only opens avenues toward the development of new ASMs, but also rises the hope that these novel compounds may be useful in treating drug-resistant epilepsies.

7. References

Aaberg KM, Surén P, Søraas CL, Bakken IJ, Lossius MI, Stoltenberg C, Chin R. Seizures, syndromes, and etiologies in childhood epilepsy: The International League Against Epilepsy 1981, 1989, and 2017 classifications used in a population-based cohort. Epilepsia. **2017** 58:1880-1891.

Abbott GW The KCNE2 K+ channel regulatory subunit Ubiquitous influence, complex pathobiology. Gene **2015** 569(2),162-172.

Abbott GW, Redford KE, Yoshimura RF, Manville RW, Moreira L, Tran K, Arena G, Kookootsedes A, Lasky E, Gunnison E. KCNQ and KCNE Isoform-Dependent Pharmacology Rationalizes Native American Dual Use of Specific Plants as Both Analgesics and Gastrointestinal Therapeutics. Front Physiol. **2021** 12:777057.

Abbott GW. KCNE1 and KCNE3: The yin and yang of voltage-gated K(+) channel regulation. Gene. **2016a** 576:1-13.

Abbott GW. KCNE4 and KCNE5: K(+) channel regulation and cardiac arrhythmogenesis. Gene. **2016b** 593:249-60.

Abbott GW. KCNQs: Ligand- and Voltage-Gated Potassium Channels. Front Physiol. **2020** 11:583.

Abou-Khalil B, Auce P, Avbersek A, Bahlo M, Balding DJ, Bast T, et al. Genome-wide mega-analysis identifies 16 loci and highlights diverse biological mechanisms in the common epilepsies. Nat Commun **2018** 9:5269

Acharya C, Coop A, Polli JE, Mackerell AD Jr. Recent advances in ligand-based drug design: relevance and utility of the conformationally sampled pharmacophore approach. Curr Comput Aided Drug Des. **2011** 7:10-22.

Aiken SP, Lampe BJ, Murphy PA, Brown BS. Reduction of spike frequency adaptation and blockade of M-current in rat CA1 pyramidal neurones by linopirdine (DuP 996), a neurotransmitter release enhancer. Br J Pharmacol. **1995** 115:1163-8.

Alaimo A, Gómez-Posada JC, Aivar P, Etxeberría A, Rodriguez-Alfaro JA, Areso P, Villarroel A. Calmodulin activation limits the rate of KCNQ2 K+ channel exit from the endoplasmic reticulum. J Biol Chem. **2009** 284:20668-75.

Aleo MD, Aubrecht J, D Bonin P, Burt DA, Colangelo J, Luo L, Schomaker S, Swiss R, Kirby S, C Rigdon G, Dua P. Phase I study of PF-04895162, a Kv7 channel opener, reveals unexpected hepatotoxicity in healthy subjects, but not rats or monkeys: clinical evidence of disrupted bile acid homeostasis. Pharmacol Res Perspect. **2019** 7:e00467.

Amann B, Sterr A, Vieta E, Stampfer R, Walden J, Grunze H. An exploratory open trial on safety and efficacy of the anticonvulsant retigabine in acute manic patients. J Clin Psychopharmacol. **2006** 26:534-6.

Amato G, Roeloffs R, Rigdon GC, Antonio B, Mersch T, McNaughton-Smith G, Wickenden AD, Fritch P, Suto MJ. N-Pyridyl and Pyrimidine Benzamides as KCNQ2/Q3 Potassium Channel Openers for the Treatment of Epilepsy. ACS Med Chem Lett. **2011** 2:481-4.

Ambrosino P, Freri E, Castellotti B, Soldovieri MV, Mosca I, Manocchio L, Gellera C, Canafoglia L, Franceschetti S, Salis B, Iraci N, Miceli F, Ragona F, Granata T, DiFrancesco JC, Taglialatela M. Kv7.3 Compound Heterozygous Variants in Early Onset Encephalopathy Reveal Additive Contribution of C-Terminal Residues to PIP2-Dependent K+ Channel Gating. Mol Neurobiol. **2018** 55:7009-7024.

Angelo K, Jespersen T, Grunnet M, Nielsen MS, Klaerke DA, Olesen SP. KCNE5 induces time- and voltage-dependent modulation of the KCNQ1 current. Biophys J. **2002** 83:1997-2006.

Anyanwu C, Motamedi GK. Diagnosis and Surgical Treatment of Drug-Resistant Epilepsy. Brain Sci. **2018** 8:49.

Aronson JK. Rare diseases and orphan drugs. Br J Clin Pharmacol. **2006** 61:243-245.

Bal M, Zhang J, Zaika O, Hernandez CC, Shapiro MS. Homomeric and heteromeric assembly of KCNQ (Kv7) K+ channels assayed by total internal reflection fluorescence/fluorescence resonance energy transfer and patch clamp analysis. J Biol Chem. **2008** 283:30668-76.

Balestrini S, Sisodiya SM. Pharmacogenomics in epilepsy. Neurosci Lett **2018**; 667: 27-39.

Barrese V, Miceli F, Soldovieri MV, Ambrosino P, Iannotti FA, Cilio MR, Taglialatela M. Neuronal potassium channel openers in the management of epilepsy: role and potential of retigabine. Clin Pharmacol. **2010** 2:225-36.

Barrese V, Stott JB, Greenwood IA. KCNQ-Encoded Potassium Channels as Therapeutic Targets. Annu Rev Pharmacol Toxicol. **2018** 58:625-648.

Barton ME, Klein BD, Wolf HH, White HS. Pharmacological characterization of the 6 Hz psychomotor seizure model of partial epilepsy. Epilepsy Res. **2001** 47:217-27.

Battefeld A, Tran BT, Gavrilis J, Cooper EC, Kole MH. Heteromeric Kv7.2/7.3 channels differentially regulate action potential initiation and conduction in neocortical myelinated axons. J Neurosci. **2014** 34:3719-32.

Bayat A, Bayat M, Rubboli G, Møller RS. Epilepsy Syndromes in the First Year of Life and Usefulness of Genetic Testing for Precision Therapy. Genes (Basel). **2021** 12:1051.

Beacham DW, Blackmer T, O' Grady M, Hanson GT. Cell-Based Potassium Ion Channel Screening Using the FluxORTM Assay. Journal of Biomolecular Screening. **2010** 15:441-446.

Beghi E, Giussani G, Nichols EGBD 2016 Epilepsy Collaborators. Global, regional, and national burden of epilepsy, 1990- 2016: a systematic analysis for the Global Burden of Disease Study 2016. Lancet Neurol **2019** 18:357–375.

Ben-Ari Y, Khalilov I, Kahle KT, Cherubini E. The GABA excitatory/inhibitory shift in brain maturation and neurological disorders. Neuroscientist. **2012**18:467-86.

Bentzen BH, Schmitt N, Calloe K, Dalby Brown W, Grunnet M, Olesen SP. The acrylamide (S)-1 differentially affects Kv7 (KCNQ) potassium channels. Neuropharmacology. **2006** 51:1068-77.

Berg AT, Langfitt J, Shinnar S, Vickrey BG, Sperling MR, Walczak T, Bazil C, Pacia SV, Spencer SS. How long does it take for partial epilepsy to become intractable? Neurology. **2003** 60:186-90.

Bierbower SM, Choveau FS, Lechleiter JD, Shapiro MS. Augmentation of M-type (KCNQ) potassium channels as a novel strategy to reduce stroke-induced brain injury. J Neurosci. **2015** 35:2101-11.

Blom SM, Rottländer M, Kehler J, Bundgaard C, Schmitt N, Jensen HS. From pan-reactive KV7 channel opener to subtype selective opener/inhibitor by addition of a methyl group. PLoS One. **2014** 9:e100209.

Bloms-Funke P, Bankstahl M, Bankstahl J, Kneip C, Schröder W, Löscher W. The novel dual-mechanism Kv7 potassium channel/TSPO receptor activator GRT-X is more effective than the Kv7 channel opener retigabine in the 6-Hz refractory seizure mouse model. Neuropharmacology. **2022b** 203:108884.

Bloms-Funke P, Schumacher M, Liu S, Su D, Li J, Liere P, Rupprecht R, Nothdurfter C, Bahrenberg G, Christoph T, Habermann C, Kneip C, Schröder W, Tzschentke TM, Saunders D. A novel dual mode-of-action anti-hyperalgesic compound in rats which is neuroprotective and promotes neuroregeneration. Eur J Pharmacol. **2022a** 923:174935.

Bock C, Link A. How to replace the lost keys? Strategies toward safer KV7 channel openers. Future Med Chem. **2019**

Bock C, Surur AS, Beirow K, Kindermann MK, Schulig L, Bodtke A, Bednarski PJ, Link A. Sulfide Analogues of Flupirtine and Retigabine with Nanomolar KV 7.2/KV 7.3 Channel Opening Activity. ChemMedChem. **2019** 14:952-964.

Boehlen A, Schwake M, Dost R, Kunert A, Fidzinski P, Heinemann U, Gebhardt C. The new KCNQ2 activator 4-Chlor-N-(6-chlor-pyridin-3-yl)-benzamid displays anticonvulsant potential. Br J Pharmacol. **2013** 168:1182-200.

Bonardi CM, Heyne HO, Fiannacca M, Fitzgerald MP, Gardella E, Gunning B, Olofsson K, Lesca G, Verbeek N, Stamberger H, Striano P, Zara F, Mancardi MM, Nava C, Syrbe S, Buono S, Baulac S, Coppola A, Weckhuysen S, Schoonjans AS, Ceulemans B, Sarret C, Baumgartner T, Muhle H, Portes VD, Toulouse J, Nougues MC, Rossi M, Demarquay G, Ville D, Hirsch E, Maurey H, Willems M, de Bellescize J, Altuzarra CD, Villeneuve N, Bartolomei F, Picard F, Hornemann F, Koolen DA, Kroes HY, Reale C, Fenger CD, Tan WH, Dibbens L, Bearden DR, Møller RS, Rubboli G. KCNT1-related epilepsies and epileptic encephalopathies: phenotypic and mutational spectrum. Brain. **2021** 144:3635-3650.

Borgini M, Mondal P, Liu R, Wipf P. Chemical modulation of Kv7 potassium channels. RSC Med Chem. **2021** 12:483-537.

Börjesson SI, Hammarström S, Elinder F. Lipoelectric modification of ion channel voltage gating by polyunsaturated fatty acids. Biophys J. **2008** 95:2242-53.

Borlak J, Gasparic A, Locher M, Schupke H, Hermann R. N-Glucuronidation of the antiepileptic drug retigabine: results from studies with human volunteers, heterologously expressed human UGTs, human liver, kidney, and liver microsomal membranes of Crigler-Najjar type II. Metabolism. **2006** 55:711-21.

Bosak M, Słowik A, Kacorzyk R, Turaj W. Implementation of the new ILAE classification of epilepsies into clinical practice - A cohort study. Epilepsy Behav. **2019** 96:28-32.

Bosch DG, Boonstra FN, de Leeuw N, Pfundt R, Nillesen WM, de Ligt J, Gilissen C, Jhangiani S, Lupski JR, Cremers FP, de Vries BB. Novel genetic causes for cerebral visual impairment. Eur J Hum Genet. **2016** 24:660-5.

Boscia F, Annunziato L, Taglialatela M. Retigabine and flupirtine exert neuroprotective actions in organotypic hippocampal cultures. Neuropharmacology. **2006** 51:283-94.

Breidenbach L, Hempel K, Mittelstadt SW, Lynch JJ 3rd. Refinement of the rodent pentylenetetrazole proconvulsion assay, which is a good predictor of convulsions in repeat-dose toxicology studies. J Pharmacol Toxicol Methods. **2020** 101:106653.

Brickel N, Gandhi P, VanLandingham K, Hammond J, DeRossett S. The urinary safety profile and secondary renal effects of retigabine (ezogabine): a first-in-class antiepileptic drug that targets KCNQ (K(v)7) potassium channels. Epilepsia. **2012** 53:606-12.

Brickel N, Hewett K, Rayner K, McDonald S, De'Ath J, Daniluk J, Joshi K, Boll MC, Tiamkao S, Vorobyeva O, Cooper J. Safety of retigabine in adults with partial-onset seizures after long-term exposure: focus on unexpected ophthalmological and dermatological events. Epilepsy Behav**. 2020** 102:106580.

Brioni JD, Curzon P, Buckley MJ, Arneric SP, Decker MW. Linopirdine (DuP996) facilitates the retention of avoidance training and improves performance of septal-lesioned rats in the water maze. Pharmacol Biochem Behav. **1993** 44:37-43.

Brown DA, Adams PR. Muscarinic suppression of a novel voltage-sensitive K+ current in a vertebrate neurone. Nature. **1980** 283:673-6.

Brueggemann LI, Mackie AR, Cribbs LL, Freda J, Tripathi A, Majetschak M, Byron KL. Differential protein kinase C-dependent modulation of Kv7.4 and Kv7.5 subunits of vascular Kv7 channels. J Biol Chem. **2014** 289:2099-111.

Carver CM, Shapiro MS. Gq-Coupled Muscarinic Receptor Enhancement of KCNQ2/3 Channels and Activation of TRPC Channels in Multimodal Control of Excitability in Dentate Gyrus Granule Cells. J Neurosci. **2019** 39:1566-1587.

Castaldo P, del Giudice EM, Coppola G, Pascotto A, Annunziato L, Taglialatela M. Benign familial neonatal convulsions caused by altered gating of KCNQ2/KCNQ3 potassium channels. J Neurosci. **2002** 22:RC199.

Charlier C, Singh NA, Ryan SG, Lewis TB, Reus BE, Leach RJ, Leppert M. A pore mutation in a novel KQT-like potassium channel gene in an idiopathic epilepsy family. Nat Genet. **1998** 18:53-5.

Chen Z, Brodie MJ, Kwan P. What has been the impact of new drug treatments on epilepsy? Curr Opin Neurol. **2020** 33:185-190.

Chen Z, Brodie MJ, Liew D, Kwan P. Treatment Outcomes in Patients With Newly Diagnosed Epilepsy Treated With Established and New Antiepileptic Drugs: A 30-Year Longitudinal Cohort Study. JAMA Neurol. **2018** 75:279-286.

Cheung YY, Yu H, Xu K, Zou B, Wu M, McManus OB, Li M, Lindsley CW, Hopkins CR. Discovery of a series of 2-phenyl-N-(2-(pyrrolidin-1-yl)phenyl)acetamides as novel molecular switches that modulate modes of K(v)7.2 (KCNQ2) channel pharmacology: identification of (S)-2-phenyl-N-(2-(pyrrolidin-1-yl)phenyl)butanamide (ML252) as a potent, brain penetrant K(v)7.2 channel inhibitor. J Med Chem. **2012** 55:6975-9.

Choveau FS, Hernandez CC, Bierbower SM, Shapiro MS. Pore determinants of KCNQ3 K+ current expression. Biophys J. **2012** 102:2489-98.

Ciliberto MA, Weisenberg JL, Wong M. Clinical utility, safety, and tolerability of ezogabine (retigabine) in the treatment of epilepsy. Drug Healthc Patient Saf. **2012** 4:81-6.

Clark S, Antell A, Kaufman K. New antiepileptic medication linked to blue discoloration of the skin and eyes. Ther Adv Drug Saf. **2015** 6:15-9.

Cooper EC, Abreo T, Tran B. KCNQ channel PIP2 modulation: Two loose links, three rings, and a twist. Neuron. **2022** 110:178-180.

Coppola A, Cellini E, Stamberger H, et al. Diagnostic implications of genetic copy number variation in epilepsy plus. Epilepsia **2019** 60: 689–706.

Cormack F, Cross JH, Isaacs E, Harkness W, Wright I, Vargha-Khadem F, Baldeweg T. The development of intellectual abilities in pediatric temporal lobe epilepsy. Epilepsia. **2007** 48:201-4.

Corsello SM, Bittker JA, Liu Z, Gould J, McCarren P, Hirschman JE, Johnston SE, Vrcic A, Wong B, Khan M, Asiedu J, Narayan R, Mader CC, Subramanian A, Golub TR. The Drug Repurposing Hub: a next-generation drug library and information resource. Nat Med. **2017** 23:405-408.

Dailey JW, Cheong JH, Ko KH, Adams-Curtis LE, Jobe PC. Anticonvulsant properties of D-20443 in genetically epilepsy-prone rats: prediction of clinical response. Neurosci Lett. **1995** 195:77-80.

Dalby-Brown W, Jessen C, Hougaard C, Jensen ML, Jacobsen TA, Nielsen KS, Erichsen HK, Grunnet M, Ahring PK, Christophersen P, Strøbæk D, Jørgensen S. Characterization of a novel high-potency positive modulator of K(v)7 channels. Eur J Pharmacol. **2013** 709:52-63.

D'Andrea Meira I, Romão TT, Pires do Prado HJ, Krüger LT, Pires MEP, da Conceição PO. Ketogenic Diet and Epilepsy: What We Know So Far. Front Neurosci. **2019** 13:5.

Davoren JE, Claffey MM, Snow SL, Reese MR, Arora G, Butler CR, Boscoe BP, Chenard L, DeNinno SL, Drozda SE, Duplantier AJ, Moine L, Rogers BN, Rong S, Schuyten K, Wright AS, Zhang L, Serpa KA, Weber ML, Stolyar P, Whisman TL, Baker K, Tse K, Clark AJ, Rong H, Mather RJ, Lowe JA 3rd. Discovery of a novel Kv7 channel opener as a treatment for epilepsy. Bioorg Med Chem Lett. **2015** 25:4941-4944.

De Sarro G, Di Paola ED, Conte G, Pasculli MP, De Sarro A. Influence of retigabine on the anticonvulsant activity of some antiepileptic drugs against audiogenic seizures in DBA/2 mice. Naunyn Schmiedebergs Arch Pharmacol. **2001** 363:330-6.

Dedek K, Kunath B, Kananura C, Reuner U, Jentsch TJ, Steinlein OK. Myokymia and neonatal epilepsy caused by a mutation in the voltage sensor of the KCNQ2 K+ channel. Proc Natl Acad Sci U S A. **2001** 98:12272-7.

Delmas P, Brown DA. Pathways modulating neural KCNQ/M (Kv7) potassium channels. Nat Rev Neurosci. **2005** 6:850-62.

Dencker D, Dias R, Pedersen ML, Husum H. Effect of the new antiepileptic drug retigabine in a rodent model of mania. Epilepsy Behav. **2008** 12:49-53.

Devaux J, Dhifallah S, De Maria M, Stuart-Lopez G, Becq H, Milh M, Molinari F, Anikszteja L. A possible link between KCNQ2- and STXBP1-related encephalopathies: STXBP1 reduces the inhibitory impact of syntaxin-1A on M current. Epilepsia. **2017** 58:2073-2084.

Devaux JJ, Kleopa KA, Cooper EC, Scherer SS. KCNQ2 is a nodal K+ channel. J Neurosci. **2004** 24:1236-44.

Dilena R, DiFrancesco JC, Soldovieri MV, Giacobbe A, Ambrosino P, Mosca I, Galli MA, Guez S, Fumagalli M, Miceli F, Cattaneo D, Darra F, Gennaro E, Zara F, Striano P, Castellotti B, Gellera C, Varesio C, Veggiotti P, Taglialatela M. Early Treatment with Quinidine in 2 Patients with Epilepsy of Infancy with Migrating Focal Seizures (EIMFS) Due to Gain-of-Function KCNT1 Mutations: Functional Studies, Clinical Responses, and Critical Issues for Personalized Therapy. Neurotherapeutics. **2018** 15:1112-1126.

Drion G, Bonjean M, Waroux O, Scuvée-Moreau J, Liégeois JF, Sejnowski TJ, Sepulchre R, Seutin V. M-type channels selectively control bursting in rat dopaminergic neurons. Eur J Neurosci. **2010** 31:827-35.

Du X, Gao H, Jaffe D, Zhang H, Gamper N. M-type K+ channels in peripheral nociceptive pathways. Br J Pharmacol. 2018 175:2158-2172.

Dvir M, Peretz A, Haitin Y, Attali B. Recent molecular insights from mutated IKS channels in cardiac arrhythmia. Curr Opin Pharmacol. **2014** 15:74-82.

Ekberg J, Schuetz F, Boase NA, Conroy SJ, Manning J, Kumar S, Poronnik P, Adams DJ. Regulation of the voltage-gated K+ channels KCNQ2/3 and KCNQ3/5 by ubiquitination. Novel role for Nedd4-2. J Biol Chem **2007** 282:12135-12142.

Ellinger B, Bojkova D, Zaliani A, Cinatl J, Claussen C, Westhaus S, Keminer O, Reinshagen J, Kuzikov M, Wolf M, Geisslinger G, Gribbon P, Ciesek S. A SARS-CoV-2 cytopathicity dataset generated by high-content screening of a large drug repurposing collection. Sci Data. **2021** 8:70.

Erdem FA, Salzer I, Heo S, Chen WQ, Jung G, Lubec G, Boehm S, Yang JW. Updating In Vivo and In Vitro Phosphorylation and Methylation Sites of Voltage-Gated Kv7.2 Potassium Channels. Proteomics. **2017** 17:10.1002/pmic.201700015.

Etxeberria A, Aivar P, Rodriguez-Alfaro JA, Alaimo A, Villacé P, Gómez-Posada JC, Areso P, Villarroel A. Calmodulin regulates the trafficking of KCNQ2 potassium channels. FASEB J. **2008** 22:1135-43.

Etxeberria A, Santana-Castro I, Regalado MP, Aivar P, Villarroel A. Three mechanisms underlie KCNQ2/3 heteromeric potassium M-channel potentiation. J Neurosci. **2004** Oct 13;24(41):9146-52.

Falco-Walter J. Epilepsy-Definition, Classification, Pathophysiology, and Epidemiology. Semin Neurol. **2020** 40:617-623.

FDA Drug Safety Communication: Anti-seizure drug Potiga (ezogabine) linked to retinal abnormalities and blue skin discoloration", can be found under http://wayback.archive-it.org/7993/20170112031636/ http://www.fda.gov/Drugs/DrugSafety/ucm349538.htm, **2013**

Feng Y-CA, Howrigan DP, Abbott LE, Tashman K, Cerrato F, Singh T, et al. Ultra-Rare Genetic Variation in the Epilepsies: A Whole-Exome Sequencing Study of 17,606 Individuals. American J Hum Genet **2019** 105: 267-82.

Ferron GM, Paul J, Fruncillo R, et al. Multiple-dose, linear, dose-proportional pharmacokinetics of retigabine in healthy volunteers. J Clin Pharmacol. **2002** 42:175-182.

Fiest KM, Sauro KM, Wiebe S, et al. Prevalence and incidence of epilepsy: A systematic review and meta-analysis of international studies. Neurology **2017** 88:296-303.

Finlayson K, Turnbull L, January CT, Sharkey J, Kelly JS. [3H]dofetilide binding to transfected membranes: a potential high throughput preclinical screen. Eur J Pharmacol. **2001** 430:147-148.

Fisher RS, Acevedo C, Arzimanoglou A, Bogacz A, Cross JH, Elger CE, Engel J Jr, Forsgren L, French JA, Glynn M, Hesdorffer DC, Lee BI, Mathern GW, Moshé SL, Perucca E, Scheffer IE, Tomson T, Watanabe M, Wiebe S. ILAE official report: a practical clinical definition of epilepsy. Epilepsia. **2014** 55:475-82.

Fisher RS, Cross JH, French JA, Higurashi N, Hirsch E, Jansen FE, Lagae L, Moshé SL, Peltola J, Roulet Perez E, Scheffer IE, Zuberi SM. Operational classification of seizure types by the International League Against Epilepsy: Position Paper of the ILAE Commission for Classification and Terminology. Epilepsia. **2017** 58:522-530.

Fisher RS, van Emde Boas W, Blume W, Elger C, Genton P, Lee P, Engel J Jr. Epileptic seizures and epilepsy: definitions proposed by the International League Against Epilepsy (ILAE) and the International Bureau for Epilepsy (IBE). Epilepsia. **2005** 46:470-2.

Fitzgerald MP, Fiannacca M, Smith DM, Gertler TS, Gunning B, Syrbe S, Verbeek N, Stamberger H, Weckhuysen S, Ceulemans B, Schoonjans AS, Rossi M, Demarquay G, Lesca G, Olofsson K, Koolen DA, Hornemann F, Baulac S, Rubboli G, Minks KQ, Lee B, Helbig I, Dlugos D, Møller RS, Bearden D. Treatment Responsiveness in KCNT1-Related Epilepsy. Neurotherapeutics. **2019** 16:848-857.

Forcelli PA, Soper C, Lakhkar A, Gale K, Kondratyev A. Anticonvulsant effect of retigabine during postnatal development in rats. Epilepsy Res **2012** 101:135-40.

Frampton DJA, Choudhury K, Nikesjö J, Delemotte L, Liin SI. Subtype-specific responses of hKv7.4 and hKv7.5 channels to polyunsaturated fatty acids reveal an unconventional modulatory site and mechanism. Elife. **2022** 11:e77672.

Friedman AK, Juarez B, Ku SM, Zhang H, Calizo RC, Walsh JJ, Chaudhury D, Zhang S, Hawkins A, Dietz DM, Murrough JW, Ribadeneira M, Wong EH, Neve RL, Han MH. KCNQ channel openers reverse depressive symptoms via an active resilience mechanism. Nat Commun. **2016** 7:11671.

Gamper N, Li Y, Shapiro MS. Structural requirements for differential sensitivity of KCNQ K^+ channels to modulation by Ca^{2+}/calmodulin. Mol. Biol. Cell **2005** 16:3538–51

Gamper N, Shapiro MS. Calmodulin mediates Ca^{2+}-dependent modulation of M-type K^+ channels. J. Gen. Physiol. **2003** 122:17–31

Gamper N, Shapiro MS. KCNQ channels. In: Zheng J, Trudeau MC (eds) Handbook of ion channels. CRC Press, Boca Raton, **2015** 275–306

Gamper N, Stockand JD, Shapiro MS. The use of Chinese hamster ovary (CHO) cells in the study of ion channels. J Pharmacol Toxicol Methods. **2005** 51:177-85.

Gao Z, Zhang T, Wu M, Xiong Q, Sun H, Zhang Y, Zu L, Wang W, Li M. Isoform-specific prolongation of Kv7 (KCNQ) potassium channel opening mediated by new molecular determinants for drug-channel interactions. J Biol Chem. **2010** 285:28322-32.

Garin Shkolnik T, Feuerman H, Didkovsky E, Kaplan I, Bergman R, Pavlovsky L, Hodak E. Blue-gray mucocutaneous discoloration: a new adverse effect of ezogabine. JAMA Dermatol. **2014** 150:984-9.

Ghosh S., Nunziato, D.A., and Pitt, G.S. KCNQ1 assembly and function is blocked by long-QT syndrome mutations that disrupt interaction with calmodulin. Circ. Res. **2006** 98:1048–1054.

Goff KM, Goldberg EM. Vasoactive intestinal peptide-expressing interneurons are impaired in a mouse model of Dravet syndrome. Elife. **2019** 8:e46846.

Gómez-Posada JC, Etxeberría A, Roura-Ferrer M, Areso P, Masin M, Murrell-Lagnado RD, Villarroel A. A pore residue of the KCNQ3 potassium M-channel subunit controls surface expression. J Neurosci. **2010** 30:9316-23.

Goswami JN, Sharma S. Current Perspectives On The Role Of The Ketogenic Diet In Epilepsy Management. Neuropsychiatr Dis Treat. **2019** 15:3273-3285.

Goto A, Ishii A, Shibata M, Ihara Y, Cooper EC, Hirose S. Characteristics of KCNQ2 variants causing either benign neonatal epilepsy or developmental and epileptic encephalopathy. Epilepsia. **2019** 60:1870-1880.

Grace AA, Camm AJ. Quinidine. N Engl J Med. **1998** 338:35-45.

Greene DL, Hoshi N. Modulation of Kv7 channels and excitability in the brain. Cell Mol Life Sci. **2017** 74:495-508.

Gribbon P, Sewing A. High-throughput drug discovery: what can we expect from HTS? Drug Discov Today. **2005** 10:17-22.

Gribkoff VK, Starrett JE Jr, Dworetzky SI, Hewawasam P, Boissard CG, Cook DA, Frantz SW, Heman K, Hibbard JR, Huston K, Johnson G, Krishnan BS, Kinney GG, Lombardo LA, Meanwell NA, Molinoff PB, Myers RA, Moon SL, Ortiz A, Pajor L, Pieschl RL, Post-Munson DJ, Signor LJ, Srinivas N, Taber MT, Thalody G, Trojnacki JT, Wiener H, Yeleswaram K, Yeola SW. Targeting acute ischemic stroke with a calcium-sensitive opener of maxi-K potassium channels. Nat Med. **2001** 7:471-7.

Groseclose MR, Castellino S. An Investigation into Retigabine (Ezogabine) Associated Dyspigmentation in Rat Eyes by MALDI Imaging Mass Spectrometry. Chem Res Toxicol. **2019** 32:294-303.

Grunnet M, Jespersen T, Rasmussen HB, Ljungstrøm T, Jorgensen NK, Olesen SP, Klaerke DA. KCNE4 is an inhibitory subunit to the KCNQ1 channel. J Physiol. **2002** 542:119-30.

Grupe M, Bentzen BH, Benned-Jensen T, Nielsen V, Frederiksen K, Jensen HS, Jacobsen AM, Skibsbye L, Sams AG, Grunnet M, Rottländer M, Bastlund JF. In vitro and in vivo characterization of Lu AA41178: A novel, brain penetrant, pan-selective Kv7 potassium channel opener with efficacy in preclinical models of epileptic seizures and psychiatric disorders. Eur J Pharmacol. **2020** 887:173440.

Gunthorpe MJ, Large CH, Sankar R. The mechanism of action of retigabine (ezogabine), a first-in-class K+ channel opener for the treatment of epilepsy. Epilepsia. **2012** 53:412-24.

Hadley JK, Noda M, Selyanko AA, Wood IC, Abogadie FC, Brown DA. Differential tetraethylammonium sensitivity of KCNQ1-4 potassium channels. Br J Pharmacol. **2000** 129:413-5.

Hadley JK, Passmore GM, Tatulian L, Al-Qatari M, Ye F, Wickenden AD, Brown DA. Stoichiometry of expressed KCNQ2/KCNQ3 potassium channels and subunit composition of native ganglionic M channels deduced from block by tetraethylammonium. J Neurosci. **2003** Jun 23:5012-9

Haitin Y, Wiener R, Shaham D, Peretz A, Cohen EB, Shamgar L, Pongs O, Hirsch JA, Attali B. Intracellular domains interactions and gated motions of $I_{(KS)}$ potassium channel subunits. EMBO J **2009** 28:1994-2005.

Hansen HH, Andreasen JT, Weikop P, Mirza N, Scheel-Krüger J, Mikkelsen JD. The neuronal KCNQ channel opener retigabine inhibits locomotor activity and reduces forebrain excitatory responses to the psychostimulants cocaine, methylphenidate and phencyclidine. Eur J Pharmacol. **2007** 570:77-88.

Hansen HH, Waroux O, Seutin V, Jentsch TJ, Aznar S, Mikkelsen JD. Kv7 channels: interaction with dopaminergic and serotonergic neurotransmission in the CNS. J Physiol**. 2008** 586:1823-32.

Hebbar M, Mefford HC. Recent advances in epilepsy genomics and genetic testing. F1000Res. **2020** 9:F1000 Faculty Rev-185.

Helbig I, Heinzen EL, Mefford HC; ILAE Genetics Commission. Primer Part 1-The building blocks of epilepsy genetics. Epilepsia. **2016** 57:861-8.

Hempel R, Schupke H, McNeilly PJ, Heinecke K, Kronbach C, Grunwald C, Zimmermann G, Griesinger C, Engel J, Kronbach T. Metabolism of retigabine (D-23129), a novel anticonvulsant. Drug Metab Dispos. **1999** 27:613-22.

Hernandez CC, Falkenburger B, Shapiro MS. Affinity for phosphatidylinositol 4,5-bisphosphate determines muscarinic agonist sensitivity of Kv7 K^+ channels. J Gen Physiol **2009** 134: 437–448.

Hernandez CC, Tarfa RA, Miguel I Limcaoco J, Liu R, Mondal P, Hill C, Keith Duncan R, Tzounopoulos T, Stephenson CRJ, O'Meara MJ, Wipf P. Development of an automated screen for Kv7.2 potassium channels and discovery of a new agonist chemotype. Bioorg Med Chem Lett. **2022** 71:128841.

Hiller A, Nguyen N, Strassburg CP, Li Q, Jainta H, Pechstein B, Ruus P, Engel J, Tukey RH, Kronbach T. Retigabine N-glucuronidation and its potential role in enterohepatic circulation. Drug Metab Dispos. **1999** 27:605-12.

Hirose S, Tanaka Y, Shibata M, Kimura Y, Ishikawa M, Higurashi N, Yamamoto T, Ichise E, Chiyonobu T, Ishii A. Application of induced pluripotent stem cells in epilepsy. Mol Cell Neurosci. **2020** 108:103535.

Hoshi N, Zhang J S, Omaki M, Takeuchi T, Yokoyama S, Wanaverbecq N, Langeberg LK, Yoneda Y, Scott JD, Brown DA, Higashida H. AKAP150 signaling complex promotes suppression of the M-current by muscarinic agonists. Nat Neurosci **2003** 6: 564-571.

Housley GD, Ashmore JF. Ionic currents of outer hair cells isolated from the guinea-pig cochlea. J Physiol. **1992** 448:73-98.

Hsu HT, Lo YC, Wu SN. Characterization of Convergent Suppression by UCL-2077 (3-(Triphenylmethylaminomethyl)pyridine), Known to Inhibit Slow Afterhyperpolarization, of erg-Mediated Potassium Currents and Intermediate-Conductance Calcium-Activated Potassium Channels. Int J Mol Sci. **2020** 21:1441.

Hu H, Vervaeke K, Storm JF. Two forms of electrical resonance at theta frequencies, generated by M-current, h-current and persistent Na+ current in rat hippocampal pyramidal cells. J Physiol. **2002** 545:783-805.

Hu HN, Zhou PZ, Chen F, Li M, Nan FJ, Gao ZB. Discovery of a retigabine derivative that inhibits KCNQ2 potassium channels. Acta Pharmacol Sin. **2013** 34:1359-66.

Hughes JP, Rees S, Kalindjian SB, Philpott KL. Principles of early drug discovery. Br J Pharmacol. **2011** 162:1239-49.

Iannotti FA, Barrese V, Formisano L, Miceli F, Taglialatela M. Specification of skeletal muscle differentiation by repressor element-1 silencing transcription factor (REST)-regulated Kv7.4 potassium channels. Mol Biol Cell. **2013** 24:274-84.

Iannotti FA, Panza E, Barrese V, Viggiano D, Soldovieri MV, Taglialatela M. Expression, localization, and pharmacological role of Kv7 potassium channels in skeletal muscle proliferation, differentiation, and survival after myotoxic insults. J Pharmacol Exp Ther. **2010** 332:811-20.

Ihara Y, Tomonoh Y, Deshimaru M, Zhang B, Uchida T, Ishii A, Hirose S. Retigabine, a Kv7.2/Kv7.3-Channel Opener, Attenuates Drug-Induced Seizures in Knock-In Mice Harboring Kcnq2 Mutations. PLoS One. **2016** 11:e0150095.

Incontro S, Sammari M, Azzaz F, Inglebert Y, Ankri N, Russier M, Fantini J, Debanne D. Endocannabinoids Tune Intrinsic Excitability in O-LM Interneurons by Direct Modulation of Postsynaptic Kv7 Channels. J Neurosci. **2021** 41:9521-9538.

Ipavec V, Martire M, Barrese V, Taglialatela M, Currò D. KV7 channels regulate muscle tone and nonadrenergic noncholinergic relaxation of the rat gastric fundus. Pharmacol Res. **2011** 64:397-409.

Jespersen T, Membrez M, Nicolas CS, Pitard B, Staub O, Olesen SP, Baró I, Abriel H. The KCNQ1 potassium channel is down-regulated by ubiquitylating enzymes of the Nedd4/Nedd4-like family. Cardiovasc Res. **2007** 74:64-74.

Kalappa BI, Soh H, Duignan KM, Furuya T, Edwards S, Tzingounis AV, Tzounopoulos T. Potent KCNQ2/3-specific channel activator suppresses in vivo epileptic activity and prevents the development of tinnitus. J Neurosci. **2015** 35:8829-42.

Kalilani L, Sun X, Pelgrims B, Noack-Rink M, Villanueva V. The epidemiology of drug-resistant epilepsy: A systematic review and meta-analysis. Epilepsia. **2018** 59:2179-2193.

Kanaumi T, Takashima S, Iwasaki H, Itoh M, Mitsudome A, Hirose S. Developmental changes in KCNQ2 and KCNQ3 expression in human brain: possible contribution to the age-dependent etiology of benign familial neonatal convulsions. Brain Dev. **2008** 30:362-9.

Kanda VA, Abbott GW. KCNE regulation of K+ channel trafficking - a Sisyphean task? Front. Physiol. **2012** 3:231

Kanyo R, Wang CK, Locskai LF, Li J, Allison WT, Kurata HT. Functional and behavioral signatures of Kv7 activator drug subtypes. Epilepsia**. 2020** 61:1678-1690.

Kasimova MA, Zaydman MA, Cui J, Tarek M. PIP_2-dependent coupling is prominent in Kv7.1 due to weakened interactions between S4-S5 and S6. Sci Rep. **2015** 5:7474.

Kasteleijn-Nolst Trenité DG, Biton V, French JA, Abou-Khalil B, Rosenfeld WE, Diventura B, Moore EL, Hetherington SV, Rigdon GC. Kv7 potassium channel activation with ICA-105665 reduces photoparoxysmal EEG responses in patients with epilepsy. Epilepsia. **2013** 54:1437-43.

Kato M, Yamagata T, Kubota M, Arai H, Yamashita S, Nakagawa T, Fujii T, Sugai K, Imai K, Uster T, Chitayat D, Weiss S, Kashii H, Kusano R, Matsumoto A, Nakamura K, Oyazato Y, Maeno M, Nishiyama K, Kodera H, Nakashima M, Tsurusaki Y, Miyake N, Saito K, Hayasaka K, Matsumoto N, Saitsu H. Clinical spectrum of early onset epileptic encephalopathies caused by KCNQ2 mutation. Epilepsia. **2013** 54:1282-7.

Kavanaugh MP, Varnum MD, Osborne PB, Christie MJ, Busch AE, Adelman JP, North RA. Interaction between tetraethylammonium and amino acid residues in the pore of cloned voltage-dependent potassium channels. J Biol Chem. **1991** 266:7583-7.

Kim RY, Yau MC, Galpin JD, Seebohm G, Ahern CA, Pless SA, Kurata HT. Atomic basis for therapeutic activation of neuronal potassium channels. Nat Commun. **2015** 6:8116.
Kimitsuki T, Komune N, Noda T, Takaiwa K, Ohashi M, Komune S. Property of I(K,)(n) in inner hair cells isolated from guinea-pig cochlea. Hear Res. **2010** 261:57-62.

King CH, Lancaster E, Salomon D, Peles E, Scherer SS. Kv7.2 regulates the function of peripheral sensory neurons. J Comp Neurol. **2014** 522:3262-80.

Ko A, Jung DE, Kim SH, Kang HC, Lee JS, Lee ST, Choi JR, Kim HD. The Efficacy of Ketogenic Diet for Specific Genetic Mutation in Developmental and Epileptic Encephalopathy. Front Neurol. **2018** Jul 16;9:530.

Korsgaard MP, Hartz BP, Brown WD, Ahring PK, Strøbaek D, Mirza NR. Anxiolytic effects of Maxipost (BMS-204352) and retigabine via activation of neuronal Kv7 channels. J Pharmacol Exp Ther. **2005** 314:282-92.

Kosenko A, Kang S, Smith IM, Greene DL, Langeberg LK, Scott JD & Hoshi N. Coordinated signal integration at the M-type potassium channel upon muscarinic stimulation. EMBO J **2012** 31, 3147–3156.

Kothur K, Holman K, Farnsworth E, Ho G, Lorentzos M, Troedson C, Gupta S, Webster R, Procopis PG, Menezes MP, Antony J, Ardern-Holmes S, Dale RC, Christodoulou J, Gill D, Bennetts B. Diagnostic yield of targeted massively parallel sequencing in children with epileptic encephalopathy. Seizure. **2018** 59:132-140.

Krüger J, Schubert J, Kegele J, Labalme A, Mao M, Heighway J, Seebohm G, Yan P, Koko M, Aslan-Kara K, Caglayan H, Steinhoff BJ, Weber YG, Keo-Kosal P, Berkovic SF, Hildebrand MS, Petrou S, Krause R, May P, Lesca G, Maljevic S, Lerche H. Loss-of-function variants in the KCNQ5 gene are implicated in genetic generalized epilepsies. EBioMedicine. **2022** 84:104244.

Krzystanek K, Rasmussen HB, Grunnet M, Staub O, Olesen SP, Abriel H, Jespersen T. Deubiquitylating enzyme USP2 counteracts Nedd4-2-mediated downregulation of KCNQ1 potassium channels. Heart Rhythm. **2012** 9:440-8.

Kubisch C, Schroeder BC, Friedrich T, Lütjohann B, El-Amraoui A, Marlin S, Petit C, Jentsch TJ. KCNQ4, a novel potassium channel expressed in sensory outer hair cells, is mutated in dominant deafness. Cell. **1999** 96:437-46.

Kühnert, S., Bahrenberg, G., Kless, A., Schr¨oder, W., **2012**. Substituted 2-Oxo-And 2- Thioxo-Dihydroquinoline-3-Carboxamides as KCNQ2/3 Modulators. Patent Family Based on WO 2012/025239

Kumar M, Reed N, Liu R, Aizenman E, Wipf P, Tzounopoulos T. Synthesis and Evaluation of Potent KCNQ2/3-Specific Channel Activators. Mol Pharmacol. **2016** 89:667-77.

Kurokawa J, Bankston JR, Kaihara A, Chen L, Furukawa T, Kass RS. KCNE variants reveal a critical role of the beta subunit carboxyl terminus in PKA-dependent regulation of the IKs potassium channel. Channels (Austin). **2009** 3:16-24.

Kurokawa J, Chen L, Kass RS. Requirement of subunit expression for cAMP-mediated regulation of a heart potassium channel. Proc Natl Acad Sci U S A. **2003** 100:2122-7.

Kurokawa J, Motoike HK, Rao J, Kass RS. Regulatory actions of the A-kinase anchoring protein Yotiao on a heart potassium channel downstream of PKA phosphorylation. Proc Natl Acad Sci U S A. **2004** 101:16374-8.

Kwan P, Arzimanoglou A, Berg AT, Brodie MJ, Allen Hauser W, Mathern G, Moshé SL, Perucca E, Wiebe S, French J. Definition of drug resistant epilepsy: consensus proposal by the ad hoc Task Force of the ILAE Commission on Therapeutic Strategies. Epilepsia. **2010** 51:1069-77.

Langan Y, Nashef L, Sander JW. Case-control study of SUDEP. Neurology. **2005** 64:1131-3.

Larsson JE, Karlsson U, Wu X, Liin SI. Combining endocannabinoids with retigabine for enhanced M-channel effect and improved KV7 subtype selectivity. J Gen Physiol. **2020** 152:e202012576.

Lauritano A, Moutton S, Longobardi E, Tran Mau-Them F, Laudati G, Nappi P, Soldovieri MV, Ambrosino P, Cataldi M, Jouan T, Lehalle D, Maurey H, Philippe C, Miceli F, Vitobello A, Taglialatela M. A novel homozygous KCNQ3 loss-of-function variant causes non-syndromic intellectual disability and neonatal-onset pharmacodependent epilepsy. Epilepsia Open. **2019** 4:464-475.

Lehman A, Thouta S, Mancini GMS, Naidu S, van Slegtenhorst M, McWalter K, Person R, Mwenifumbo J, Salvarinova R; CAUSES Study; EPGEN Study, Guella I, McKenzie MB, Datta A, Connolly MB, Kalkhoran SM, Poburko D, Friedman JM, Farrer MJ, Demos M, Desai S, Claydon T. Loss-of-Function and Gain-of-Function Mutations in KCNQ5 Cause Intellectual Disability or Epileptic Encephalopathy. Am J Hum Genet. **2017** 101:65-74.

Lerche C, Scherer CR, Seebohm G, Derst C, Wei AD, Busch AE, Steinmeyer K. Molecular cloning and functional expression of KCNQ5, a potassium channel subunit that may contribute to neuronal M-current diversity. J Biol Chem. **2000** 275:22395-400.

Li H, Geng D, Zheng R, Wang R, Li Y, Liu Y, Jia Q, Zhang F. Inhibition of Kv7/M Channel Currents by Fangchinoline. Pharmacology. **2022** 14:1-9.

Li M, Santpere G, Imamura Kawasawa Y, Evgrafov OV, Gulden FO, Pochareddy S, Sunkin SM, Li Z, Shin Y, Zhu Y, Sousa AMM, Werling DM, Kitchen RR, Kang HJ, Pletikos M, Choi J, Muchnik S, Xu X, Wang D, Lorente-Galdos B, Liu S, Giusti-Rodríguez P, Won H, de Leeuw CA, Pardiñas AF; BrainSpan Consortium; PsychENCODE Consortium; PsychENCODE Developmental Subgroup; Hu M, Jin F, Li Y, Owen MJ, O'Donovan MC, Walters JTR, Posthuma D, Reimers MA, Levitt P, Weinberger DR, Hyde TM, Kleinman JE, Geschwind DH, Hawrylycz MJ, State MW, Sanders SJ, Sullivan PF, Gerstein MB, Lein ES, Knowles JA, Sestan N. Integrative functional genomic analysis of human brain development and neuropsychiatric risks. Science. **2018** 362:eaat7615.

Li P, Chen X, Zhang Q, Zheng Y, Jiang H, Yang H, Gao Z. The human ether-a-go-go-related gene activator NS1643 enhances epilepsy-associated KCNQ channels. J Pharmacol Exp Ther. **2014** 351:596-604.

Li P, Chen Z, Xu H, Sun H, Li H, Liu H, Yang H, Gao Z, Jiang H, Li M. The gating charge pathway of an epilepsy-associated potassium channel accommodates chemical ligands. Cell Res. **2013** 23:1106-18.

Li T, Wu K, Yue Z, Wang Y, Zhang F, Shen H. Structural Basis for the Modulation of Human KCNQ4 by Small-Molecule Drugs. Mol Cell. **2021** 81:25-37.e4.

Li X, Zhang Q, Guo P, Fu J, Mei L, Lv D, Wang J, Lai D, Ye S, Yang H, Guo J. Molecular basis for ligand activation of the human KCNQ2 channel. Cell Res. **2021** 31:52-61.

Li Y, Zaydman MA, Wu D, Shi J, Guan M, Virgin-Downey B, Cui J. KCNE1 enhances phosphatidylinositol 4,5-bisphosphate (PIP2) sensitivity of IKs to modulate channel activity. Proc Natl Acad Sci U S A. **2011** 108:9095-100.

Liin SI, Karlsson U, Bentzen BH, Schmitt N, Elinder F. Polyunsaturated fatty acids are potent openers of human M-channels expressed in Xenopus laevis oocytes. Acta Physiol (Oxf). **2016** 218:28-37.

Liin SI, Silverå Ejneby M, Barro-Soria R, Skarsfeldt MA, Larsson JE, Starck Härlin F, Parkkari T, Bentzen BH, Schmitt N, Larsson HP, Elinder F. Polyunsaturated fatty acid analogs act antiarrhythmically on the cardiac IKs channel. Proc Natl Acad Sci U S A. **2015** 112:5714-9.

Liin SI, Yazdi S, Ramentol R, Barro-Soria R, Larsson HP. Mechanisms Underlying the Dual Effect of Polyunsaturated Fatty Acid Analogs on Kv7.1. Cell Rep. **2018** 24:2908-2918.

Lipinski CA, Lombardo F, Dominy BW, Feeney PJ. Experimental and computational approaches to estimate solubility and permeability in drug discovery and development settings. Adv Drug Deliv Rev. **2001** 46:3-26.

Liu R, Sun L, Wang Y, Wang Q, Wu J. New use for an old drug: quinidine in KCNT1-related epilepsy therapy. Neurol Sci. **2022**

Liu R, Tzounopoulos T, Wipf P. Synthesis and Optimization of Kv7 (KCNQ) Potassium Channel Agonists: The Role of Fluorines in Potency and Selectivity. ACS Med Chem Lett. **2019** 10:929-935.

Liu S, Yu W, Lü Y. The causes of new-onset epilepsy and seizures in the elderly. Neuropsychiatr Dis Treat. **2016** 12:1425-34.

Liu W, Devaux JJ. Calmodulin orchestrates the heteromeric assembly and the trafficking of KCNQ2/3 (Kv7.2/3) channels in neurons. Mol Cell Neurosci. **2014** 58:40-52.

Liu Y, Bian X, Wang K. Pharmacological Activation of Neuronal Voltage-Gated Kv7/KCNQ/M-Channels for Potential Therapy of Epilepsy and Pain. Handb Exp Pharmacol. **2021** 267:231-251.

Lohrmann E, Burhoff I, Nitschke RB, Lang HJ, Mania D, Englert HC, Hropot M, Warth R, Rohm W, Bleich M, et al. A new class of inhibitors of cAMP-mediated Cl- secretion in rabbit colon, acting by the reduction of cAMP-activated K+ conductance. Pflugers Arch. **1995** 429:517-30.

Long SB, Tao X, Campbell EB, MacKinnon R. Atomic structure of a voltage-dependent K+ channel in a lipid membrane-like environment. Nature. **2007** 450:376-82.

Löscher W, Potschka H, Sisodiya SM, Vezzani A. Drug Resistance in Epilepsy: Clinical Impact, Potential Mechanisms, and New Innovative Treatment Options. Pharmacol Rev. **2020** 72:606-638.

Lundby A, Tseng GN, Schmitt N. Structural basis for K(V)7.1-KCNE(x) interactions in the I(Ks) channel complex. Heart Rhythm **2010** 7:708–713.

Luttjohann A, Fabene PF, van Luijtelaar G. A revised Racine's scale for PTZ-induced seizures in rats. Physiol Behav **2009** 98:579-86.

Mackie AR, Byron KL. Cardiovascular KCNQ (Kv7) potassium channels: physiological regulators and new targets for therapeutic intervention. Mol Pharmacol. **2008** 74:1171-9.

MacKinnon R, Yellen G. Mutations affecting TEA blockade and ion permeation in voltage-activated K+ channels. Science. **1990** 250:276-9.

Main MJ, Cryan JE, Dupere JR, Cox B, Clare JJ, Burbidge SA. Modulation of KCNQ2/3 potassium channels by the novel anticonvulsant retigabine. Mol Pharmacol. **2000** 58:253-62.

Malysz J, Petkov GV. Detrusor Smooth Muscle KV7 Channels: Emerging New Regulators of Urinary Bladder Function. Front Physiol. **2020** 11:1004.

Manville RW, Abbott GW. Ancient and modern anticonvulsants act synergistically in a KCNQ potassium channel binding pocket. Nat Commun**. 2018a** 9:3845.

Manville RW, Abbott GW. Cilantro leaf harbors a potent potassium channel-activating anticonvulsant. FASEB J. **2019a** 33:11349-11363.

Manville RW, Abbott GW. Gabapentin Is a Potent Activator of KCNQ3 and KCNQ5 Potassium Channels. Mol Pharmacol. **2018c** 94:1155-1163.

Manville RW, Papanikolaou M, Abbott GW. Direct neurotransmitter activation of voltage-gated potassium channels. Nat Commun. **2018b** 9:1847.

Manville RW, van der Horst J, Redford KE, Katz BB, Jepps TA, Abbott GW. KCNQ5 activation is a unifying molecular mechanism shared by genetically and culturally diverse botanical hypotensive folk medicines. Proc Natl Acad Sci U S A. **2019b** 116:21236-21245.

Martire M, Castaldo P, D'Amico M, Preziosi P, Annunziato L, Taglialatela M. M channels containing KCNQ2 subunits modulate norepinephrine, aspartate, and GABA release from hippocampal nerve terminals. J Neurosci. **2004** 24:592-7.

Martire M, D'Amico M, Panza E, et al. Involvement of KCNQ2 subunits in [3H]dopamine release triggered by depolarization and pre-synaptic muscarinic receptor activation from rat striatal synaptosomes. J Neurochem. **2007** 102:179-193.

Marx SO, Kurokawa J, Reiken S, Motoike H, D'Armiento J, Marks AR, Kass RS. Requirement of a macromolecular signaling complex for beta adrenergic receptor modulation of the KCNQ1-KCNE1 potassium channel. Science. **2002** 295:496-9.

Matasci M, Bachmann V, Baldi L, Hacker DL, De Jesus M, Wurm FM. CHO cell lines generated by PiggyBac transposition. BMC Proc. **2011** 5 Suppl 8(Suppl 8):P31.

Matthews E, Balestrini S, Sisodiya SM, Hanna MG. Muscle and brain sodium channelopathies: genetic causes, clinical phenotypes, and management approaches. Lancet Child Adolesc Health **2020** 4: 536-47.

McRae JF, Clayton S, Fitzgerald TW et al. Prevalence and architecture of de novo mutations in developmental disorders. Deciphering Developmental Disorders Study. Nature **2017** 542:433–438

McTague A, Howell KB, Cross HJ, Kurian MA, Scheffer IE. The genetic landscape of the epileptic encephalopathies of infancy and childhood. Lancet Neurol **2016** 15: 304–16.

Melman YF, Um SY, Krumerman A, Kagan A, McDonald TV. KCNE1 binds to the KCNQ1 pore to regulate potassium channel activity. Neuron **2004** 42:927–37

Miceli F, Carotenuto L, Barrese V, Soldovieri MV, Heinzen EL, Mandel AM, Lippa N, Bier L, Goldstein DB, Cooper EC, Cilio MR, Taglialatela M, Sands TT. A Novel Kv7.3 Variant in the Voltage-Sensing S4 Segment in a Family With Benign Neonatal Epilepsy: Functional Characterization and in vitro Rescue by β-Hydroxybutyrate. Front Physiol. **2020** 11:1040.

Miceli F, Soldovieri MV, Ambrosino P, Barrese V, Migliore M, Cilio MR, Taglialatela M. Genotype-phenotype correlations in neonatal epilepsies caused by mutations in the voltage sensor of K(v)7.2 potassium channel subunits. Proc Natl Acad Sci U S A. **2013** 110:4386-91.

Miceli F, Soldovieri MV, Ambrosino P, De Maria M, Migliore M, Migliore R, Taglialatela M. Early-onset epileptic encephalopathy caused by gain-of-function mutations in the voltage sensor of Kv7.2 and Kv7.3 potassium channel subunits. J Neurosci. **2015a** 35:3782-93.

Miceli F, Soldovieri MV, Joshi N, Weckhuysen S, Cooper E, Taglialatela M. KCNQ2-related disorders. In: Adam MP, Ardinger HH, Pagon RA et al (eds) **2018,** GeneReviews® [Internet]. Seattle University of Washington

Miceli F, Soldovieri MV, Martire M, Taglialatela M. Molecular pharmacology and therapeutic potential of neuronal Kv7-modulating drugs. Curr Opin Pharmacol. **2008** 8:65-74.

Miceli F, Striano P, Soldovieri MV, Fontana A, Nardello R, Robbiano A, Bellini G, Elia M, Zara F, Taglialatela M, Mangano S. A novel KCNQ3 mutation in familial epilepsy with focal seizures and intellectual disability. Epilepsia. **2015b** 56:e15-20.

Milh M, Lacoste C, Cacciagli P, Abidi A, Sutera-Sardo J, Tzelepis I, Colin E, Badens C, Afenjar A, Coeslier AD, Dailland T, Lesca G, Philip N, Villard L. Variable clinical expression in patients with mosaicism for KCNQ2 mutations. Am J Med Genet A. **2015** 167A:2314-8.

Millichap JJ, Miceli F, De Maria M, Keator C, Joshi N, Tran B, Soldovieri MV, Ambrosino P, Shashi V, Mikati MA, Cooper EC, Taglialatela M. Infantile spasms and encephalopathy without preceding neonatal seizures caused by KCNQ2 R198Q, a gain-of-function variant. Epilepsia. **2017** 58:e10-e15.

Millichap JJ, Park KL, Tsuchida T, Ben-Zeev B, Carmant L, Flamini R, Joshi N, Levisohn PM, Marsh E, Nangia S, Narayanan V, Ortiz-Gonzalez XR, Patterson MC, Pearl PL, Porter B, Ramsey K, McGinnis EL, Taglialatela M, Tracy M, Tran B, Venkatesan C, Weckhuysen S, Cooper EC. KCNQ2 encephalopathy: Features, mutational hot spots, and ezogabine treatment of 11 patients. Neurol Genet. **2016** 2:e96.

Misura KM, Bock JB, Gonzalez LC Jr, Scheller RH, Weis WI. Three-dimensional structure of the amino-terminal domain of syntaxin 6, a SNAP-25 C homolog. PNAS **2002** 99(14): 9184-9189.

Mulkey SB, Ben-Zeev B, Nicolai J, Carroll JL, Grønborg S, Jiang YH, Joshi N, Kelly M, Koolen DA, Mikati MA, Park K, Pearl PL, Scheffer IE, Spillmann RC, Taglialatela M, Vieker S, Weckhuysen S, Cooper EC, Cilio MR. Neonatal nonepileptic myoclonus is a prominent clinical feature of KCNQ2 gain-of-function variants R201C and R201H. Epilepsia. **2017** 58:436-445.

Mullen SA, Carney PW, Roten A, Ching M, Lightfoot PA, Churilov L, Nair U, Li M, Berkovic SF, Petrou S, Scheffer IE. Precision therapy for epilepsy due to KCNT1 mutations: A randomized trial of oral quinidine. Neurology. **2018** 90:e67-e72.

Nappi M, Barrese V, Carotenuto L, Lesca G, Labalme A, Ville D, Smol T, Rama M, Dieux-Coeslier A, Rivier-Ringenbach C, Soldovieri MV, Ambrosino P, Mosca I, Pusch M, Miceli F, Taglialatela M. Gain of function due to increased opening probability by two KCNQ5 pore variants causing developmental and epileptic encephalopathy. Proc Natl Acad Sci U S A. **2022** 119:e2116887119.

Nappi P, Miceli F, Soldovieri MV, Ambrosino P, Barrese V, Taglialatela M. Epileptic channelopathies caused by neuronal Kv7 (KCNQ) channel dysfunction. Pflugers Arch. **2020** 472:881-898.

Oliveras A, Roura-Ferrer M, Solé L, de la Cruz A, Prieto A, Etxebarria A, Manils J, Morales-Cano D, Condom E, Soler C, Cogolludo A, Valenzuela C, Villarroel A, Comes N, Felipe A. Functional assembly of Kv7.1/Kv7.5 channels with emerging properties on vascular muscle physiology. Arterioscler Thromb Vasc Biol. **2014** 34:1522-30.

Oprea TI, Davis AM, Teague SJ, Leeson PD. Is there a difference between leads and drugs? A historical perspective. J Chem Inf Comput Sci. **2001** 41:1308-15.

Opromolla DV, Lima LS, Marques MB. Thalidomide in acute symptoms in leprosy (erythema nodosum or multiforme). Hospital (Rio J). **1966** 69:827-844.

Orhan G, Bock M, Schepers D, Ilina EI, Reichel SN, Löffler H, Jezutkovic N, Weckhuysen S, Mandelstam S, Suls A, Danker T, Guenther E, Scheffer IE, De Jonghe P, Lerche H, Maljevic S. Dominant-negative effects of KCNQ2 mutations are associated with epileptic encephalopathy. Ann Neurol. **2014** 75:382-94.

Otto JF, Kimball MM, Wilcox KS. Effects of the anticonvulsant retigabine on cultured cortical neurons: changes in electroresponsive properties and synaptic transmission. Mol Pharmacol. **2002** 61:921-7.

Padilla K, Wickenden AD, Gerlach AC, McCormack K. The KCNQ2/3 selective channel opener ICA-27243 binds to a novel voltage-sensor domain site. Neurosci Lett. **2009** 465:138-42.

Pan Z, Kao T, Horvath Z, Lemos J, Sul JY, Cranstoun SD, Bennett V, Scherer SS, Cooper EC. A common ankyrin-G-based mechanism retains KCNQ and NaV channels at electrically active domains of the axon. J Neurosci **2006** 26:2599–2613.

Paricharak S, Méndez-Lucio O, Chavan Ravindranath A, Bender A, IJzerman AP, van Westen GJP. Data-driven approaches used for compound library design, hit triage and bioactivity modeling in high-throughput screening. Brief Bioinform. **2018** 19:277-285.

Peretz A, Degani N, Nachman R, Uziyel Y, Gibor G, Shabat D, Attali B. Meclofenamic acid and diclofenac, novel templates of KCNQ2/Q3 potassium channel openers, depress cortical neuron activity and exhibit anticonvulsant properties. Mol Pharmacol. **2005** 67:1053-66.

Peretz A, Degani-Katzav N, Talmon M, Danieli E, Gopin A, Malka E, Nachman R, Raz A, Shabat D, Attali B. A tale of switched functions: from cyclooxygenase inhibition to M-channel modulation in new diphenylamine derivatives. PLoS One. **2007** 2:e1332.

Peters HC, Hu H, Pongs O, Storm JF, Isbrandt D. Conditional transgenic suppression of M channels in mouse brain reveals functions in neuronal excitability, resonance and behavior. Nat Neurosci. **2005** 8:51-60.

Picchione KE, Inglis AM, Resnick L, Mareska DA, Bozik ME, Dworetzky S, Knopp Biosciences LLC, Discovery and Characterization of KB-3061: A Potent Kv7.2/7.3 Ion Channel Activator for the Treatment of KCNQ2-Neonatal Epileptic Encephalopathy, Abstract number : 3.045, AES **2019**

Poduri A, Lowenstein D. Epilepsy genetics--past, present, and future. Curr Opin Genet Dev. **2011** 21:325-32.

Poduri A. When Should Genetic Testing Be Performed in Epilepsy Patients? Epilepsy Curr. **2017** 17:16-22.

Pohlmann-Eden B, Weaver DF. The puzzle(s) of pharmacoresistant epilepsy. Epilepsia. **2013** 54 Suppl 2:1-4.

Postma T, Krupp E, Li XL, Post RM, Weiss SR. Lamotrigine treatment during amygdala-kindled seizure development fails to inhibit seizures and diminishes subsequent anticonvulsant efficacy. Epilepsia. **2000** 41:1514-21.

Potschka H. Animal models of drug-resistant epilepsy. Epileptic Disord. **2012** 14:226-34.

Preston P, Wartosch L, Gunzel D, Fromm M, Kongsuphol P, Ousingsawat J, Kunzelmann K, Barhanin J, Warth R, Jentsch T.J. Disruption of the K^+ channel beta-subunit KCNE3 reveals an important role in intestinal and tracheal Cl^- transport. J. Biol. Chem. **2010** 285:7165–7175.

Pushpakom S, Iorio F, Eyers PA, Escott KJ, Hopper S, Wells A, Doig A, Guilliams T, Latimer J, McNamee C, Norris A, Sanseau P, Cavalla D, Pirmohamed M. Drug repurposing: progress, challenges and recommendations. Nat Rev Drug Discov. **2019** 18:41-58.

Raol YH, Lapides DA, Keating JG, Brooks-Kayal AR, Cooper EC. A KCNQ channel opener for experimental neonatal seizures and status epilepticus. Ann Neurol. **2009** 65:326-36.

Redford KE, Abbott GW. The ubiquitous flavonoid quercetin is an atypical KCNQ potassium channel activator. Commun Biol. **2020** 3:356.

Regev N, Degani-Katzav N, Korngreen A, Etzioni A, Siloni S, Alaimo A, Chikvashvili D, Villarroel A, Attali B, Lotan I Selective interaction of syntaxin 1A with KCNQ2: possible implications for specific modulation of presynaptic activity. Plos One **2009** 4:e6586.

Richards S, Aziz N, Bale S, Bick D, Das S, Gastier-Foster J, et al. Standards and guidelines for the interpretation of sequence variants: a joint consensus recommendation of the American College of Medical Genetics and Genomics and the Association for Molecular Pathology. Genet Med **2015** 17:405-24.

Rizzo F, Ambrosino P, Guacci A, Chetta M, Marchese G, Rocco T, Soldovieri MV, Manocchio L, Mosca I, Casara G, Vecchi M, Taglialatela M, Coppola G, Weisz A. Characterization of two de novoKCNT1 mutations in children with malignant migrating partial seizures in infancy. Mol Cell Neurosci. **2016** 72:54-63.

Robbins J. KCNQ potassium channels: physiology, pathophysiology, and pharmacology. Pharmacol Ther. **2001** 90:1-19.

Rockwood K, Beattie BL, Eastwood MR, Feldman H, Mohr E, Pryse-Phillips W, Gauthier S. A randomized, controlled trial of linopirdine in the treatment of Alzheimer's disease. Can J Neurol Sci. **1997** 24:140-5.

Rode F, Svalø J, Sheykhzade M, Rønn LC. Functional effects of the KCNQ modulators retigabine and XE991 in the rat urinary bladder. Eur J Pharmacol. **2010** 638:121-7.

Roeloffs R, Wickenden AD, Crean C, Werness S, McNaughton-Smith G, Stables J, McNamara JO, Ghodadra N, Rigdon GC. In vivo profile of ICA-27243 [N-(6-chloro-pyridin-3-yl)-3,4-difluoro-benzamide], a potent and selective KCNQ2/Q3 (Kv7.2/Kv7.3) activator in rodent anticonvulsant models. J Pharmacol Exp Ther. **2008** 326:818-28.

Roepke TK, Anantharam A, Kirchhoff P, Busque SM, Young JB, Geibel JP, Lerner DJ, Abbott GW. The KCNE2 potassium channel ancillary subunit is essential for gastric acid secretion. J Biol Chem. **2006** 281:23740-7.

Rosti G, Tassano E, Bossi S, Divizia MT, Ronchetto P, Servetti M, Lerone M, Pisciotta L, Mancardi MM, Veneselli E, Puliti A. Intragenic duplication of KCNQ5 gene results in aberrant splicing leading to a premature termination codon in a patient with intellectual disability. Eur J Med Genet. **2019** 62:103555.

Rostock A, Tober C, Rundfeldt C, Bartsch R, Engel J, Polymeropoulos EE, Kutscher B, Loscher W, Honack D, White HS, Wolf HH. D-23129: a new anticonvulsant with a broad-spectrum activity in animal models of epileptic seizures. Epilepsy Res **1996**, 23:211-23.

Saganich MJ, Machado E, Rudy B. Differential expression of genes encoding subthreshold-operating voltage-gated K+ channels in brain. J Neurosci. **2001** 21:4609-24.

Saitsu H, Kato M, Koide A, Goto T, Fujita T, Nishiyama K, Tsurusaki Y, Doi H, Miyake N, Hayasaka K, Matsumoto N. Whole exome sequencing identifies KCNQ2 mutations in Ohtahara syndrome. Ann Neurol. **2012** 72:298-300.

Salzer I, Erdem FA, Chen WQ, Heo S, Koenig X, Schicker KW, Kubista H, Lubec G, Boehm S, Yang JW. Phosphorylation regulates the sensitivity of voltage-gated Kv7.2 channels towards phosphatidylinositol-4,5-bisphosphate. J Physiol. **2017** 595:759-776.

Sanders MWCB, Lemmens CMC, Jansen FE, Brilstra EH, Koeleman BPC, Braun KPJ, et al. Implications of genetic diagnostics in epilepsy surgery candidates: A single-center cohort study. Epilepsia Open **2019** 4:609-17.

Sands TT, Miceli F, Lesca G, Beck AE, Sadleir LG, Arrington DK, Schönewolf-Greulich B, Moutton S, Lauritano A, Nappi P, Soldovieri MV, Scheffer IE, Mefford HC, Stong N, Heinzen EL, Goldstein DB, Perez AG, Kossoff EH, Stocco A, Sullivan JA, Shashi V, Gerard B, Francannet C, Bisgaard AM, Tümer Z, Willems M, Rivier F, Vitobello A, Thakkar K, Rajan DS, Barkovich AJ, Weckhuysen S, Cooper EC, Taglialatela M, Cilio MR. Autism and developmental disability caused by KCNQ3 gain-of-function variants. Ann Neurol. **2019** 86:181-192.

Sanguinetti MC, Curran ME, Zou A, Shen J, Spector PS, Atkinson DL, Keating MT Coassembly of K(V)LQT1 and minK (IsK) proteins to form cardiac I(Ks) potassium channel. Nature **1996** 384:80–83.

Sarnthein J, Petsche H, Rappelsberger P, Shaw GL, von Stein A. Synchronization between prefrontal and posterior association cortex during human working memory. Proc Natl Acad Sci U S A. **1998** 95:7092-6.

Scheffer IE, Berkovic S, Capovilla G, Connolly MB, French J, Guilhoto L, Hirsch E, Jain S, Mathern GW, Moshé SL, Nordli DR, Perucca E, Tomson T, Wiebe S, Zhang YH, Zuberi SM. ILAE classification of the epilepsies: Position paper of the ILAE Commission for Classification and Terminology. Epilepsia. **2017** 58:512-521.

Schenzer A, Friedrich T, Pusch M, Saftig P, Jentsch TJ, Grötzinger J, Schwake M. Molecular determinants of KCNQ (Kv7) K+ channel sensitivity to the anticonvulsant retigabine. J Neurosci. **2005** 25:5051-60.

Schmidt D, Löscher W. Drug resistance in epilepsy: putative neurobiologic and clinical mechanisms. Epilepsia. **2005** 46:858-77.

Schrøder RL, Jespersen T, Christophersen P, Strøbaek D, Jensen BS, Olesen SP. KCNQ4 channel activation by BMS-204352 and retigabine. Neuropharmacology. **2001** 40:888-98.

Schroeder BC, Hechenberger M, Weinreich F, Kubisch C, Jentsch TJ. KCNQ5, a novel potassium channel broadly expressed in brain, mediates M-type currents. J Biol Chem. **2000** 275:24089-95.

Schroeder BC, Kubisch C, Stein V, Jentsch TJ. Moderate loss of function of cyclic-AMP-modulated KCNQ2/KCNQ3 K+ channels causes epilepsy. Nature. **1998** 396:687-90.

Schwake M, Athanasiadu D, Beimgraben C, Blanz J, Beck C, Jentsch TJ, Saftig P, Friedrich T. Structural determinants of M-type KCNQ (Kv7) K+ channel assembly. J Neurosci. **2006** 26:3757-66.

Schwake M, Jentsch TJ, Friedrich T. A carboxy-terminal domain determines the subunit specificity of KCNQ K(+) channel assembly. EMBO Rep **2003** 4:76–81

Schwake M, Pusch M, Kharkovets T, Jentsch TJ. Surface expression and single channel properties of KCNQ2/KCNQ3, M-type K+ channels involved in epilepsy. J Biol Chem. **2000** 275:13343-8.

Schwarz JR, Glassmeier G, Cooper EC, Kao TC, Nodera H, Tabuena D, Kaji R, Bostock H. KCNQ channels mediate IKs, a slow K+ current regulating excitability in the rat node of Ranvier. J Physiol. **2006** 573:17-34.

Seebohm G, Strutz-Seebohm N, Ureche ON, et al. Differential roles of S6 domain hinges in the gating of KCNQ potassium channels. Biophys J. **2006** 90:2235-2244.

Shamgar L, Ma L, Schmitt N, Haitin Y, Peretz A, Wiener R, Hirsch J, Pongs O, Attali B. Calmodulin is essential for cardiac IKS channel gating and assembly: impaired function in long-QT mutations. Circ Res. **2006** 98:1055-63.

Shapiro MS, Roche JP, Kaftan EJ, Cruzblanca H, Mackie K, Hille B. Reconstitution of muscarinic modulation of the KCNQ2/KCNQ3 K(+) channels that underlie the neuronal M current. J Neurosci **2000** 20:1710–1721

Shi L, Bian X, Qu Z, Ma Z, Zhou Y, Wang K, Jiang H, Xie J. Peptide hormone ghrelin enhances neuronal excitability by inhibition of Kv7/KCNQ channels. Nat Commun. **2013** ;4:1435.

Shi S, Li J, Sun F, Chen Y, Pang C, Geng Y, Qi J, Guo S, Wang X, Zhang H, Zhan Y, An H. Molecular Mechanisms and Structural Basis of Retigabine Analogues in Regulating KCNQ2 Channel. J Membr Biol. **2020** 253:167-181.

Shoichet BK. Virtual screening of chemical libraries. Nature. **2004** 432:862-865.

Sills GJ, Rogawski MA. Mechanisms of action of currently used antiseizure drugs. Neuropharmacology. **2020** 168:107966.

Singh NA, Charlier C, Stauffer D, DuPont BR, Leach RJ, Melis R, Ronen GM, Bjerre I, Quattlebaum T, Murphy JV, McHarg ML, Gagnon D, Rosales TO, Peiffer A, Anderson VE, Leppert M. A novel potassium channel gene, KCNQ2, is mutated in an inherited epilepsy of newborns. Nat Genet. **1998** 18:25-9.

Singhal S, Mehta J, Desikan R, Ayers D, Roberson P, Eddlemon P, Munshi N, Anaissie E, Wilson C, Dhodapkar M, Zeddis J, Barlogie B. Antitumor activity of thalidomide in refractory multiple myeloma. N Engl J Med. **1999** 341:1565-71.

Søgaard R, Ljungstrøm T, Pedersen KA, Olesen SP, Jensen BS. KCNQ4 channels expressed in mammalian cells: functional characteristics and pharmacology. Am J Physiol Cell Physiol **2001** 280:C859–C866

Soh H, Springer K, Doci K, Balsbaugh JL, Tzingounis AV. KCNQ2 and KCNQ5 form heteromeric channels independent of KCNQ3. Proc Natl Acad Sci U S A. **2022** 19:e2117640119.

Soh H, Tzingounis AV. The specific slow afterhyperpolarization inhibitor UCL2077 is a subtype-selective blocker of the epilepsy associated KCNQ channels. Mol Pharmacol. **2010** 78:1088-95.

Sokka A, Olsen P, Kirjavainen J, Harju M, Keski-Nisula L, Räisänen S, Heinonen S, Kälviäinen R. Etiology, syndrome diagnosis, and cognition in childhood-onset epilepsy: A population-based study. Epilepsia Open. **2017** 2:76-83.

Soldovieri MV, Boutry-Kryza N, Milh M, Doummar D, Heron B, Bourel E, Ambrosino P, Miceli F, De Maria M, Dorison N, Auvin S, Echenne B, Oertel J, Riquet A, Lambert L, Gerard M, Roubergue A, Calender A, Mignot C, Taglialatela M, Lesca G. Novel KCNQ2 and KCNQ3 mutations in a large cohort of families with benign neonatal epilepsy: first evidence for an altered channel regulation by syntaxin-1A. Hum Mutat. **2014** 35:356-67.

Soldovieri MV, Freri E, Ambrosino P, Rivolta I, Mosca I, Binda A, Murano C, Ragona F, Canafoglia L, Vannicola C, Solazzi R, Granata T, Castellotti B, Messina G, Gellera C, Labalme A, Lesca G, DiFrancesco JC, Taglialatela M. Gabapentin treatment in a patient with KCNQ2 developmental epileptic encephalopathy. Pharmacol Res. **2020** 160:105200.

Sorge G, Sorge A. Epilepsy and chromosomal abnormalities. Ital J Pediatr. **2010** 3;36:36.

Spear KL, Brown SP. The evolution of library design: crafting smart compound collections for phenotypic screens. Drug Discov Today Technol. **2017** 23:61-67.

Specchio N, Wirrell EC, Scheffer IE, Nabbout R, Riney K, Samia P, Guerreiro M, Gwer S, Zuberi SM, Wilmshurst JM, Yozawitz E, Pressler R, Hirsch E, Wiebe S, Cross HJ, Perucca E, Moshé SL, Tinuper P, Auvin S. International League Against Epilepsy classification and definition of epilepsy syndromes with onset in childhood: Position paper by the ILAE Task Force on Nosology and Definitions. Epilepsia. **2022** 63:1398-1442.

Spitznagel BD, Mishra NM, Qunies AM, et al. VU0606170, a Selective Slack Channels Inhibitor, Decreases Calcium Oscillations in Cultured Cortical Neurons. ACS Chem Neurosci. **2020** 11:3658-3671.

Springer K, Varghese N, Tzingounis AV. Flexible Stoichiometry: Implications for KCNQ2- and KCNQ3-Associated Neurodevelopmental Disorders. Dev Neurosci. **2021** 43:191-200.

Steinlein OK, Mulley JC, Propping P, Wallace RH, Phillips HA, Sutherland GR, Scheffer IE, Berkovic SF A missense mutation in the neuronal nicotinic acetylcholine receptor alpha 4 subunit is associated with autosomal dominant nocturnal frontal lobe epilepsy. Nat Genet **1995** 11:201-3

Stott JB, Jepps TA, Greenwood IA. K(V)7 potassium channels: a new therapeutic target in smooth muscle disorders. Drug Discov Today. **2014** 19:413-24.

Striano P, Minassian BA. From Genetic Testing to Precision Medicine in Epilepsy. Neurotherapeutics. **2020** 17:609-615.

Sun H, Lin AH, Ru F, Patil MJ, Meeker S, Lee LY, Undem BJ. KCNQ/M-channels regulate mouse vagal bronchopulmonary C-fiber excitability and cough sensitivity. JCI Insight. **2019** 4:e124467.

Sun J, MacKinnon R. Cryo-EM Structure of a KCNQ1/CaM Complex Reveals Insights into Congenital Long QT Syndrome. Cell**. 2017** 169:1042-1050.e9.

Sun J, MacKinnon R. Structural Basis of Human KCNQ1 Modulation and Gating. Cell. **2020** 180:340-347.e9.

Sundaresan L, Giri S, Singh H, Chatterjee S. Repurposing of thalidomide and its derivatives for the treatment of SARS-coV-2 infections: Hints on molecular action. Br J Clin Pharmacol. **2021** 87:3835-3850.

Surur AS, Bock C, Beirow K, Wurm K, Schulig L, Kindermann MK, Siegmund W, Bednarski PJ, Link A. Flupirtine and retigabine as templates for ligand-based drug design of KV7.2/3 activators. Org Biomol Chem. **2019** 17:4512-4522.

Svalø J, Bille M, Parameswaran Theepakaran N, Sheykhzade M, Nordling J, Bouchelouche P. Bladder contractility is modulated by Kv7 channels in pig detrusor. Eur J Pharmacol. **2013** 715:312-20.

Syeda R, Santos JS, Montal M. The Sensorless Pore Module of Voltage-gated K+ Channel Family 7 Embodies the Target Site for the Anticonvulsant Retigabine. J Biol Chem. **2016** 291:2931-7.

Syvertsen M, Koht J, Nakken KO. Prevalence and incidence of epilepsy in the Nordic countries. Tidsskr Nor Laegeforen. **2015** 135:1641-5.

Szelenyi I. Flupirtine, a re-discovered drug, revisited. Inflamm Res. **2013** 62:251-8.

Tao X, Lee A, Limapichat W, Dougherty DA, MacKinnon R. A gating charge transfer center in voltage sensors. Science. **2010** 328:67-73.

Tasic B, Menon V, Nguyen TN, Kim TK, Jarsky T, Yao Z, Levi B, Gray LT, Sorensen SA, Dolbeare T, Bertagnolli D, Goldy J, Shapovalova N, Parry S, Lee C, Smith K, Bernard A, Madisen L, Sunkin SM, Hawrylycz M, Koch C, Zeng H. Adult mouse cortical cell taxonomy revealed by single cell transcriptomics. Nat Neurosci. **2016** 19:335-46.

Tatulian L, Brown DA. Effect of the KCNQ potassium channel opener retigabine on single KCNQ2/3 channels expressed in CHO cells. J Physiol. **2003** 549:57-63.

Tatulian L, Delmas P, Abogadie FC, Brown DA. Activation of expressed KCNQ potassium currents and native neuronal M-type potassium currents by the anti-convulsant drug retigabine. J Neurosci. **2001** 21:5535-45.

Te Beek ET, Moerland M, de Boer P, et al. Pharmacokinetics and central nervous system effects of the novel dopamine D2 receptor antagonist C4. J Psychopharmacol. **2012** 26:1119-1127.

Teng JMC, Siegel DH. A new tale of thalidomide repurposing. Nat Cardiovasc Res 2022 535–536

Tinel N, Lauritzen I, Chouabe C, Lazdunski M, Borsotto M. The KCNQ2 potassium channel: splice variants, functional and developmental expression. Brain localization and comparison with KCNQ3. FEBS Lett. **1998** 438:171-6.

Tober C, Rostock A, Rundfeldt C, Bartsch R. D-23129: a potent anticonvulsant in the amygdala kindling model of complex partial seizures. Eur J Pharmacol. **1996** 303:163-9.

Treven M, Koenig X, Assadpour E, Gantumur E, Meyer C, Hilber K, Boehm S, Kubista H. The anticonvulsant retigabine is a subtype selective modulator of GABAA receptors. Epilepsia. **2015** 56:647-57.

Tsunoyama K, Amini A, Sternberg MJ, Muggleton SH. Scaffold hopping in drug discovery using inductive logic programming. J Chem Inf Model. **2008** 48:949-957.

Tykocki NR, Heppner TJ, Dalsgaard T, Bonev AD, Nelson MT. The KV 7 channel activator retigabine suppresses mouse urinary bladder afferent nerve activity without affecting detrusor smooth muscle K+ channel currents. J Physiol. **2019** 597:935-950.

Tzingounis AV, Heidenreich M, Kharkovets T, Spitzmaul G, Jensen HS, Nicoll RA, Jentsch TJ. The KCNQ5 potassium channel mediates a component of the afterhyperpolarization current in mouse hippocampus. Proc Natl Acad Sci U S A. **2010** 107:10232-7.

Tzingounis AV, Nicoll RA. Contribution of KCNQ2 and KCNQ3 to the medium and slow afterhyperpolarization currents. Proc Natl Acad Sci U S A. **2008** 105:19974-9.

Verneuil J, Brocard C, Trouplin V, Villard L, Peyronnet-Roux J, Brocard F. The M-current works in tandem with the persistent sodium current to set the speed of locomotion. PLoS Biol. **2020** 18:e3000738.

Wainger BJ, Macklin EA, Vucic S, McIlduff CE, Paganoni S, Maragakis NJ, Bedlack R, Goyal NA, Rutkove SB, Lange DJ, Rivner MH, Goutman SA, Ladha SS, Mauricio EA, Baloh RH, Simmons Z, Pothier L, Kassis SB, La T, Hall M, Evora A, Klements D, Hurtado A, Pereira JD, Koh J, Celnik PA, Chaudhry V, Gable K, Juel VC, Phielipp N, Marei A, Rosenquist P, Meehan S, Oskarsson B, Lewis RA, Kaur D, Kiskinis E, Woolf CJ, Eggan K, Weiss MD, Berry JD, David WS, Davila-Perez P, Camprodon JA, Pascual-Leone A, Kiernan MC, Shefner JM, Atassi N, Cudkowicz ME. Effect of Ezogabine on Cortical and Spinal Motor Neuron Excitability in Amyotrophic Lateral Sclerosis: A Randomized Clinical Trial. JAMA Neurol. **2021** 78:186-196.

Walsh KB, Kass RS. Regulation of a heart potassium channel by protein kinase A and C. Science. **1988** 242:67-9.

Wang AW, Yang R, Kurata HT. Sequence determinants of subtype-specific actions of KCNQ channel openers. J Physiol. **2017** 595:663-676.

Wang AW, Yau MC, Wang CK, Sharmin N, Yang RY, Pless SA, Kurata HT. Four drug-sensitive subunits are required for maximal effect of a voltage sensor-targeted KCNQ opener. J Gen Physiol. **2018b** 150:1432-1443.

Wang HS, Brown BS, McKinnon D, Cohen IS. Molecular basis for differential sensitivity of KCNQ and I(Ks) channels to the cognitive enhancer XE991. Mol Pharmacol. **2000** 57:1218-23.

Wang HS, Pan Z, Shi W, Brown BS, Wymore RS, Cohen IS, Dixon JE, McKinnon D. KCNQ2 and KCNQ3 potassium channel subunits: molecular correlates of the M-channel. Science. **1998** 282:1890-3.

Wang K, McIlvain B, Tseng E, Kowal D, Jow F, Shen R, Zhang H, Shan QJ, He L, Chen D, Lu Q, Dunlop J. Validation of an atomic absorption rubidium ion efflux assay for KCNQ/M-channels using the ion Channel Reader 8000. Assay Drug Dev Technol. **2004** 2:525-34.

Wang L, Qiao GH, Hu HN, Gao ZB, Nan FJ. Discovery of Novel Retigabine Derivatives as Potent KCNQ4 and KCNQ5 Channel Agonists with Improved Specificity. ACS Med Chem Lett. **2018a** 10:27-33.

Wang X, Zhou H, Zheng J, et al. Identification and characterization of four process-related impurities in retigabine. J Pharm Biomed Anal. **2012** 71:148-151.

Warth R, Riedemann N, Bleich M, Van Driessche W, Busch AE, Greger R. The cAMP-regulated and 293B-inhibited K+ conductance of rat colonic crypt base cells. Pflugers Arch. **1996** 432:81-8.

Watanabe H, Nagata E, Kosakai A, Nakamura M, Yokoyama M, Tanaka K, Sasai H. Disruption of the epilepsy KCNQ2 gene results in neural hyperexcitability. J Neurochem. **2000** 75:28-33.

Weckhuysen S, George Jr A. (Eds.) KCNQ2- and KCNQ3-Associated Epilepsy (Elements in Genetics in Epilepsy) **2022**. Cambridge: Cambridge University Press.

Wei AD, Wakenight P, Zwingman TA, Bard AM, Sahai N, Willemsen MH, Schelhaas HJ, Stegmann APA, Verhoeven JS, de Man SA, Wessels MW, Kleefstra T, Shinde DN, Helbig KL, Basinger A, Wagner VF, Rodriguez-Buritica D, Bryant E, Millichap JJ, Millen KJ, Dobyns WB, Ramirez JM, Kalume FK. Human KCNQ5 de novo mutations underlie epilepsy and intellectual disability. J Neurophysiol. **2022** 128:40-61.

Wells J, Swaminathan A, Paseka J, Hanson C. Efficacy and Safety of a Ketogenic Diet in Children and Adolescents with Refractory Epilepsy-A Review. Nutrients. **2020** 12:1809.

WHO Epilepsy: A public Health Initiative. Geneva: World Health Organization; **2019**

Wickenden AD, Krajewski JL, London B, Wagoner PK, Wilson WA, Clark S, Roeloffs R, McNaughton-Smith G, Rigdon GC. N-(6-chloro-pyridin-3-yl)-3,4-difluoro-benzamide (ICA-27243): a novel, selective KCNQ2/Q3 potassium channel activator. Mol Pharmacol. **2008** 73:977-86.

Williams CM, Stephens GJ. Development of cannabidiol as a treatment for severe childhood epilepsies. Br J Pharmacol. **2020** 177:5509-5517.

Wrobel E, Tapken D, Seebohm G. The KCNE Tango - How KCNE1 Interacts with Kv7.1. Front Pharmacol. **2012** 3:142.

Wu N, Nishioka WK, Derecki NC, Maher MP. High-throughput-compatible assays using a genetically-encoded calcium indicator. Sci Rep. **2019** 9:12692.

Wu YJ, Boissard CG, Chen J, Fitzpatrick W, Gao Q, Gribkoff VK, Harden DG, He H, Knox RJ, Natale J, Pieschl RL, Starrett JE Jr, Sun LQ, Thompson M, Weaver D, Wu D, Dworetzky SI. (S)-N-[1-(4-cyclopropylmethyl-3,4-dihydro-2H-benzo[1,4]oxazin-6-yl)-ethyl]-3-(2-fluoro-phenyl)-acrylamide is a potent and efficacious KCNQ2 opener which inhibits induced hyperexcitability of rat hippocampal neurons. Bioorg Med Chem Lett. **2004a** 14:1991-5.

Wu YJ, Boissard CG, Greco C, Gribkoff VK, Harden DG, He H, L'Heureux A, Kang SH, Kinney GG, Knox RJ, Natale J, Newton AE, Lehtinen-Oboma S, Sinz MW, Sivarao DV, Starrett JE Jr, Sun LQ, Tertyshnikova S, Thompson MW, Weaver D, Wong HS, Zhang L, Dworetzky SI. (S)-N-[1-(3-morpholin-4-ylphenyl)ethyl]- 3-phenylacrylamide: an orally bioavailable KCNQ2 opener with significant activity in a cortical spreading depression model of migraine. J Med Chem. **2003a** 46:3197-200.

Wu YJ, Conway CM, Sun LQ, Machet F, Chen J, Chen P, He H, Bourin C, Calandra V, Polino JL, Davis CD, Heman K, Gribkoff VK, Boissard CG, Knox RJ, Thompson MW, Fitzpatrick W, Weaver D, Harden DG, Natale J, Dworetzky SI, Starrett JE Jr. Discovery of (S,E)-3-(2-fluorophenyl)-N-(1-(3-(pyridin-3-yloxy)phenyl)ethyl)-acrylamide as a potent and efficacious KCNQ2 (Kv7.2) opener for the treatment of neuropathic pain. Bioorg Med Chem Lett. **2013** 23:6188-91.

Wu YJ, Davis CD, Dworetzky S, Fitzpatrick WC, Harden D, He H, Knox RJ, Newton AE, Philip T, Polson C, Sivarao DV, Sun LQ, Tertyshnikova S, Weaver D, Yeola S, Zoeckler M, Sinz MW. Fluorine substitution can block CYP3A4 metabolism-dependent inhibition: identification of (S)-N-[1-(4-fluoro-3- morpholin-4-ylphenyl)ethyl]-3- (4-fluorophenyl)acrylamide as an orally bioavailable KCNQ2 opener devoid of CYP3A4 metabolism-dependent inhibition. J Med Chem. **2003b** 46:3778-81.

Wu YJ, Sun LQ, He H, Chen J, Starrett JE Jr, Dextraze P, Daris JP, Boissard CG, Pieschl RL, Gribkoff VK, Natale J, Knox RJ, Harden DG, Thompson MW, Fitzpatrick W, Weaver D, Wu D, Gao Q, Dworetzky SI. Synthesis and KCNQ2 opener activity of N-(1-benzo[1,3]dioxol-5-yl-ethyl, N-[1-(2,3-dihydro-benzofuran-5-yl)-ethyl, and N-[1-(2,3-dihydro-1H-indol-5-yl)-ethyl acrylamides. Bioorg Med Chem Lett. **2004b** 14:4533-7.

Wurm KW, Bartz FM, Schulig L, Bodtke A, Bednarski PJ, Link A. Carba Analogues of Flupirtine and Retigabine with Improved Oxidation Resistance and Reduced Risk of Quinoid Metabolite Formation. ChemMedChem. **2022a** 17:e202200262.

Wurm KW, Bartz FM, Schulig L, Bodtke A, Bednarski PJ, Link A. Modifications of the Triaminoaryl Metabophore of Flupirtine and Retigabine Aimed at Avoiding Quinone Diimine Formation. ACS Omega. **2022b** 7:7989-8012.

Wurm KW, Bartz FM, Schulig L, Bodtke A, Bednarski PJ, Link A. Replacing the oxidation-sensitive triaminoaryl chemotype of problematic KV7 channel openers: Exploration of a nicotinamide scaffold. Arch Pharm (Weinheim). **2023** 356:e2200473.

Wuttke TV, Seebohm G, Bail S, Maljevic S, Lerche H. The new anticonvulsant retigabine favors voltage-dependent opening of the Kv7.2 (KCNQ2) channel by binding to its activation gate. Mol Pharmacol. **2005** 67:1009-17.

Xiong Q, Gao Z, Wang W, Li M. Activation of Kv7 (KCNQ) voltage-gated potassium channels by synthetic compounds. Trends Pharmacol Sci. **2008** 29:99-107.

Xiong Q, Sun H, Li M. Zinc pyrithione-mediated activation of voltage-gated KCNQ potassium channels rescues epileptogenic mutants. Nat Chem Biol. **2007** 3:287-96.

Xu D, Chen S, Yang J, Wang X, Fang Z, Li M. Precision therapy with quinidine of KCNT1-related epileptic disorders: A systematic review. Br J Clin Pharmacol. **2022** 88:5096-5112

Xu Parks X, Qudsi H, Braun C, Lopes CMB. The auxiliary subunit KCNE1 regulates KCNQ1 channel response to sustained calcium-dependent PKC activation. PLoS One. **2020** 15:e0237591.

Yang B, Gribkoff VK, Pan J, Damagnez V, Dworetzky SI, Boissard CG, Bhattacharjee A, Yan Y, Sigworth FJ, Kaczmarek LK. Pharmacological activation and inhibition of Slack (Slo2.2) channels. Neuropharmacology. **2006** 51:896-906.

Yang S, Lu D, Ouyang P. Design, synthesis and evaluation of novel N-phenylbutanamide derivatives as KCNQ openers for the treatment of epilepsy. Bioorg Med Chem Lett. **2018b** 28:3004-3008.

Yang S, Lu D, Ouyang P. Design, synthesis and evaluation of substituted piperidine based KCNQ openers as novel antiepileptic agents. Bioorg Med Chem Lett. **2018a** 28:1731-1735.

Yau MC, Kim RY, Wang CK, Li J, Ammar T, Yang RY, Pless SA, Kurata HT. One drug-sensitive subunit is sufficient for a near-maximal retigabine effect in KCNQ channels. J Gen Physiol. **2018** 150:1421-1431.

Yazdi S, Nikesjö J, Miranda W, Corradi V, Tieleman DP, Noskov SY, Larsson HP, Liin SI. Identification of PUFA interaction sites on the cardiac potassium channel KCNQ1. J Gen Physiol. **2021** 153:e202012850.

Ye Z, McQuillan L, Poduri A, Green TE, Matsumoto N, et al. Somatic mutation: the hidden genetics of brain malformations and focal epilepsies. Epilepsy Res**. 2019** 155:106161

Yeung SY, Pucovský V, Moffatt JD, Saldanha L, Schwake M, Ohya S, Greenwood IA. Molecular expression and pharmacological identification of a role for K(v)7 channels in murine vascular reactivity. Br J Pharmacol. **2007** 151:758-70.

Yu H, Wu M, Townsend SD, Zou B, Long S, Daniels JS, McManus OB, Li M, Lindsley CW, Hopkins CR. Discovery, Synthesis, and Structure Activity Relationship of a Series of N-Aryl- bicyclo[2.2.1]heptane-2-carboxamides: Characterization of ML213 as a Novel KCNQ2 and KCNQ4 Potassium Channel Opener. ACS Chem Neurosci. **2011** 2:572-577.

Yu HB, Li M, Wang WP, Wang XL. High throughput screening technologies for ion channels. Acta Pharmacol Sin. **2016** 37:34-43.

Yue C, Yaari Y. KCNQ/M channels control spike afterdepolarization and burst generation in hippocampal neurons. J Neurosci. **2004** 24:4614-24.

Yue JF, Qiao GH, Liu N, Nan FJ, Gao ZB. Novel KCNQ2 channel activators discovered using fluorescence-based and automated patch-clamp-based high-throughput screening techniques. Acta Pharmacol Sin. **2016** 37:105-10.

Yus-Najera E, Santana-Castro I, Villarroel A. The identification and characterization of a noncontinuous calmodulin-binding site in noninactivating voltage-dependent KCNQ potassium channels. J Biol Chem. **2002** 277:28545-53.

Zaczek R, Chorvat RJ, Saye JA, Pierdomenico ME, Maciag CM, Logue AR, Fisher BN, Rominger DH, Earl RA. Two new potent neurotransmitter release enhancers, 10,10-bis(4-pyridinylmethyl)-9(10H)-anthracenone and 10,10-bis(2-fluoro-4-pyridinylmethyl)-9(10H)-anthracenone: comparison to linopirdine. J Pharmacol Exp Ther. **1998** 285:724-30.

Zaczek R, Tinker WJ, Tam SW. Unique properties of norepinephrine release from terminals arising from the locus coeruleus: high potassium sensitivity and lack of linopirdine (DuP 996) enhancement. Neurosci Lett. **1993** 155:107-11.

Zaika O, Hernandez CC, Bal M, Tolstykh GP, Shapiro MS. Determinants within the turret and pore-loop domains of KCNQ3 K+ channels governing functional activity. Biophys J. **2008** 95:5121-37.

Zara F, Specchio N, Striano P, Robbiano A, Gennaro E, Paravidino R, Vanni N, Beccaria F, Capovilla G, Bianchi A, Caffi L, Cardilli V, Darra F, Bernardina BD, Fusco L, Gaggero R, Giordano L, Guerrini R, Incorpora G, Mastrangelo M, Spaccini L, Laverda AM, Vecchi M, Vanadia F, Veggiotti P, Viri M, Occhi G, Budetta M, Taglialatela M, Coviello DA, Vigevano F, Minetti C. Genetic testing in benign familial epilepsies of the first year of life: clinical and diagnostic significance. Epilepsia. **2013** 54:425-36.

Zaydman MA, Silva JR, Delaloye K, Li Y, Liang H, Larsson HP, Shi J, Cui J. Kv7.1 ion channels require a lipid to couple voltage sensing to pore opening. Proc Natl Acad Sci U S A. **2013** 110:13180-5.

Zhang H, Craciun LC, Mirshahi T, Rohács T, Lopes CM, Jin T, Logothetis DE. PIP_2 activates KCNQ channels, and its hydrolysis underlies receptor-mediated inhibition of M currents. Neuron. **2003** 37:963-75.

Zhang HB, Heckman L, Niday Z, Jo S, Fujita A, Shim J, Pandey R, Al Jandal H, Jayakar S, Barrett LB, Smith J, Woolf CJ, Bean BP. Cannabidiol activates neuronal Kv7 channels. Elife. **2022** 11:e73246.

Zhang J, Carver CM, Choveau FS, Shapiro MS. Clustering and Functional Coupling of Diverse Ion Channels and Signaling Proteins Revealed by Super-resolution STORM Microscopy in Neurons. Neuron. **2016** 92:461-478.

Zhang JH, Chung TD, Oldenburg KR. A Simple Statistical Parameter for Use in Evaluation and Validation of High Throughput Screening Assays. J Biomol Screen. **1999** 4:67-73.

Zhang Q, Zhou P, Chen Z, Li M, Jiang H, Gao Z, Yang H. Dynamic PIP_2 interactions with voltage sensor elements contribute to KCNQ2 channel gating. Proc Natl Acad Sci U S A. **2013** 110:20093-8.

Zhang YM, Xu HY, Hu HN, Tian FY, Chen F, Liu HN, Zhan L, Pi XP, Liu J, Gao ZB, Nan FJ. Discovery of HN37 as a Potent and Chemically Stable Antiepileptic Drug Candidate. J Med Chem. **2021** 64:5816-5837.

Zheng Y, Liu H, Chen Y, Dong S, Wang F, Wang S, Li GL, Shu Y, Xu F. Structural insights into the lipid and ligand regulation of a human neuronal KCNQ channel. Neuron. **2022** 110:237-247.e4.

Zheng Y, Xu H, Zhan L, Zhou X, Chen X, Gao Z. Activation of peripheral KCNQ channels relieves gout pain. Pain. **2015** 156:1025-1035.

Zhou P, Zhang Y, Xu H, Chen F, Chen X, Li X, Pi X, Wang L, Zhan L, Nan F, Gao Z. P-retigabine: an N-propargyled retigabine with improved brain distribution and enhanced antiepileptic activity. Mol Pharmacol. **2015** 87:31-8.

Zhou X, Ma A, Liu X, Huang C, Zhang Y, Shi R, Mao S, Geng T, Li S. Infantile seizures and other epileptic phenotypes in a Chinese family with a missense mutation of KCNQ2. Eur J Pediatr. **2006** 165:691-5.

Zhuang W, Yan Z. The S2-S3 Loop of Kv7.4 Channels Is Essential for Calmodulin Regulation of Channel Activation. Front Physiol. **2021** 11:604134.

Zuegg J, Cooper MA. Drug-likeness and increased hydrophobicity of commercially available compound libraries for drug screening. Curr Top Med Chem. **2012** 12:1500-13.

8. Appendix

Published papers:

- Musella S, **Carotenuto L**, Iraci N, Baroli G, Ciaglia T, Nappi P, Basilicata MG, Salviati E, Barrese V, Vestuto V, Pignataro G, Pepe G, Sommella E, Di Sarno V, Manfra M, Campiglia P, Gomez-Monterrey I, Bertamino A, Taglialatela M, Ostacolo C, Miceli F. *Beyond Retigabine: Design, Synthesis, and Pharmacological Characterization of a Potent and Chemically Stable Neuronal Kv7 Channel Activator with Anticonvulsant Activity*. **J Med Chem. 2022** 65:11340-11364.

- Miceli F, Millevert C, Soldovieri MV, Mosca I, Ambrosino P, **Carotenuto L**, Schrader D, Lee HK, Riviello J, Hong W, Risen S, Emrick L, Amin H, Ville D, Edery P, de Bellescize J, Michaud V, Van-Gils J, Goizet C, Willemsen MH, Kleefstra T, Møller RS, Bayat A, Devinsky O, Sands T, Korenke GC, Kluger G, Mefford HC, Brilstra E, Lesca G, Milh M, Cooper EC, Taglialatela M, Weckhuysen S. *KCNQ2 R144 variants cause neurodevelopmental disability with language impairment and autistic features without neonatal seizures through a gain-of-function mechanism*. **EBioMedicine. 2022** 81:104130.

- Nappi M, Barrese V, **Carotenuto L**, Lesca G, Labalme A, Ville D, Smol T, Rama M, Dieux-Coeslier A, Rivier-Ringenbach C, Soldovieri MV, Ambrosino P, Mosca I, Pusch M, Miceli F, Taglialatela M. *Gain of function due to increased opening probability by two KCNQ5 pore variants causing developmental and epileptic encephalopathy*. **Proc Natl Acad Sci** U S A. **2022** 119:e2116887119.

- Miceli F, **Carotenuto L**, Barrese V, Soldovieri MV, Heinzen EL, Mandel AM, Lippa N, Bier L, Goldstein DB, Cooper EC, Cilio MR, Taglialatela M, Sands TT. *A Novel Kv7.3 Variant in the Voltage-Sensing S4 Segment in a Family With Benign Neonatal Epilepsy: Functional Characterization and in vitro Rescue by β-Hydroxybutyrate*. **Front Physiol. 2020** 11:1040.

9. Ringraziamenti

Gli anni trascorsi nel dipartimento di Neuroscienze dell'Università di Napoli Federico II sono stati per me particolarmente formativi, dal punto di vista umano e professionale.

Per tutto ciò che ho imparato devo innanzitutto ringraziare il professor Taglialatela, che mi ha dato la possibilità di toccare con mano il mondo della ricerca, ha guidato il mio percorso formativo credendo in me come futura ricercatrice.

Il professore mi ha mostrato un eccellente esempio di passione per il proprio lavoro, competenza e instancabile dedizione. Il tempo che mi ha dedicato è stato prezioso.

Un ringraziamento doveroso va al dott. Miceli e al dott. Barrese i quali mi hanno insegnato cosa vuol dire vivere il laboratorio, trasformare le idee in esperimenti, analizzare i dati e soprattutto interpretarli nel modo corretto.

Infine, un ringraziamento va a tutti i colleghi del quindicesimo piano che mi hanno arricchita con i loro consigli (scientifici e non) e con la loro compagnia hanno alleggerito anche le giornate più dure. Grazie di cuore.

Lidia